Chapter 3: FLAME SUPPRESSION CHEMISTRY

Gregory T. Linteris, Ph.D.
National Institute of Standards and Technology

TABLE OF CONTENTS

3.1 INTRODUCTION

This chapter describes NGP research agents which work primarily through chemical means. As a prelude to this, it is useful to delineate the different terminology often used to describe the extinguishing of a flame. *Flame inhibition* usually refers to a weakening of a flame, i.e., a lowering of the overall exothermic reaction rate in the flame. This weakening may or may not lead to extinguishment, depending upon the flow field in which the flame exists. In contrast, the terms *fire suppression*, *flame extinguishment*, or *flame extinction* are often used to refer to the case in which the flame has been weakened to the point where it can no longer stabilize in the relevant flow field. Flame quenching refers to flame extinguishment for which heat losses to a surface was a precipitating factor.

The first three sections of the chapter group the research according to the active moiety in the chemical agent: halogens, metals, or phosphorus.

- The section on halogens starts with a description of what was known about the flame inhibiting action of CF_3Br prior to NGP research, and follows with research describing some alternative agents based on fluorine.
- The section on metals also first gives some background, and then provides extensive data on flame inhibition by iron-containing compounds - primarily because these agents have been shown to be the strongest flame inhibitors ever found. Detailed results for the effect of iron (and other agents) on flame radicals are also presented, followed by results for tin and manganese. Since most of the metals in these previous studies were added as toxic organometallic agents, the next section describes work to investigate metal moieties in various forms which are non-toxic. Since it was discovered fairly early in NGP research that metal compounds lose their effectiveness due to the formation of particles, additional research was aimed at finding other metals which were effective but did not suffer that same consequence. The remaining parts of that section describe the potential of other metals to be effective yet not to lose their effectiveness.
- The third section describes extensive research to characterize the potential and effectiveness of phosphorus-containing compounds. It starts with a description of a new experimental approach in counterflow diffusion flames which is helpful with aspirated samples of trimethyl phosphate (TMP) and dimethyl methylphosphonate (DMMP). Following that is a description of how varying the agent transport rates into the flame (through changes to the stoichiometric mixture fraction and the location of agent addition) changes the effectiveness of DMMP. In this section, a temperature dependence of the effectiveness is also described, which is further explored in the following section which describes spectroscopic measurements of OH and numerical modeling of counterflow diffusion flames of methane and air with DMMP added. The numerical model is further validated in the final subsection, where experiments and calculations are performed for premixed flat flames of methane and air with added DMMP.

The final section of the present chapter discusses studies aimed at finding unified principles to describe the fire suppression effectiveness of alternative chemical moieties:

- Comparison of spectroscopically measured reductions in the concentration of the chain-carrying radical OH and in peak temperature in opposed flow, atmospheric pressure, propane/air flames brought to near-extinction conditions through addition of several agents (CF_3Br, N_2, $Fe(CO)_5$, C_3F_7H, $C_3F_6H_2$, DMMP, and PN (cyclo-$P_3N_3F_6$).
- Description of additional spectroscopic tests to delineate the reduction in [OH] with addition of $Fe(CO)_5$ (and, for comparison, CF_3Br) to low-pressure methane-air flames.
- Discussion of the merits of using CF_3Br as a benchmark for comparison of other fire suppressants.
- A discourse on the use of inhibitor molecule bond energies as a criterion by which the flame inhibition efficiency can be predicted and understood.
- Examination of the regions of a premixed flame which are most susceptible to chemical inhibition.

The NGP research described here has moved the science of flame inhibition and suppression chemistry forward in very large measure. Entirely new, detailed, comprehensive chemical kinetic mechanisms were developed specifically for the NGP, and the use of these kinetic mechanisms in detailed numerical simulations for the present investigations has led to great insight into the action of chemically acting agents in fire suppression. New experimental techniques were developed, as well as new methods of using existing approaches. In fact, much of the present work has been cited in fields external to fire research due to their utility beyond the present needs. The work presented below will provide an outstanding basis for those future researchers who will continue the search for new fire-fighting materials. The new unified insights on fire suppression developed through NGP research are summarized at the end of this chapter.

3.2 HALOGEN-CONTAINING COMPOUNDS

3.2.1 Previous Understanding of the Inhibition Mechanism of CF_3Br (as of 1995)

In previous studies, CF_3Br (and related compounds) have been the subject of much fundamental research, for example in flow reactors,[1,2] premixed flames,[3-11] co-flow diffusion flames,[12-14] and counterflow diffusion flames.[9,15-20] Much recent research has been aimed at finding both short-[21,22] and long-term[23] replacements for CF_3Br. As a result, CF_3Br itself has been the continuing subject of many studies[24-27] since an improved understanding of its mechanism of inhibition will help in the search for alternatives, and nearly all assessments of new agents use CF_3Br as a baseline for comparison of the new agents.

As outlined above, the flame configurations used to study flame inhibition mechanisms have tended to be premixed and counterflow diffusion flames. Premixed flames have been selected mainly because the overall reaction rate, heat release, and heat and mass transport in these flames can be described with a single fundamental parameter - the laminar burning velocity, and because over certain regions, the flow field can be considered one-dimensional (greatly simplifying data collection and numerical simulation). Similarly, counterflow diffusion flames can be considered one-dimensional along the centerline, and the extinction strain rate has been commonly used as the characteristic suppression parameter. In principle, such fundamental parameters can ultimately be used to relate the behavior of the agent in the laboratory flame to its behavior in suppressing a large-scale fire[28], although this scaling is difficult in practice.

Premixed Systems

Early studies of the inhibitory effects of halogenated hydrocarbons on flames were conducted in premixed systems. Numerous research groups[12,29-31] determined the influence of halogenated methanes on the flammability limits of hydrocarbon-air mixtures. The magnitude of the inhibitory effect and its dependence on halogen type and stoichiometry generally indicated a chemical rather than thermal mechanism. Simmons and Wolfhard[12] studied the flammability limits of methane-air mixtures with bromine and methyl bromide inhibitors and showed that methyl bromide influenced the limits of flammability in the same manner as equivalent amounts of bromine and methane, indicating that the decomposition products of the halogenated methanes were responsible for the action. Garner et al.,[32] Rosser et al.,[33] Lask and Wagner[34] and Edmondson and Heap[35] measured the reduction in burning velocity of various burner − stabilized hydrocarbon-air flames with addition of several halogenated methanes, halogen acids and halogen dimers. In later work, Niioka *et al*.[36] experimentally investigated the effect of CF_3Br on the extinction velocity of opposed premixed C_2H_4 flames. The inhibitory effect was found to be more effective in rich flames than in lean flames. Mitani[37] used experimental results on the decrease of flame propagation speeds of premixed H_2-O_2-N_2 and C_2H_4-O_2-N_2 flames with CF_3Br addition to derive overall activation energies for the inhibition reactions, which correlated well with measured energies for key inhibition steps. All studies were in consensus that the magnitude of the inhibition was related to the number and type of halogen atoms present in the reactants, the concentration of the inhibitor, and the equivalence ratio, ϕ, and that the effect was generally too large to be accounted for by thermal dilution effects. This conclusion was based on supporting calculations or measurements showing that the final temperatures in the inhibited flames were not low enough to account for the burning velocity reductions observed.

Detailed information on the inhibition mechanism of brominated species has been provided by flame structure measurements. Mass spectrometric measurements of stable species concentrations in premixed flames of methane and air were conducted by several investigators: Levy et al.[38] used HBr to inhibit a Bunsen flame and found that HBr inhibited methane consumption but not CO oxidation; Wilson[4] and Wilson et al.[39] performed low-pressure inhibited premixed flame studies with methyl bromide, HCl, HBr, Cl_2, and concluded that both CH_3Br and HBr act to reduce radical concentrations in the preheat region of the flame by competing with the chain branching reaction $H + O_2 = OH + O$, and that CH_3Br lowers the peak OH concentration to near equilibrium values, while uninhibited flames have the characteristic super-equilibrium OH concentrations. Biordi et al.[5,40] used a molecular-beam mass spectrometer to obtain stable and radical species concentrations as a function of position in low-pressure premixed flat flames of methane and air with and without addition of CF_3Br, and Safieh et al.[7] performed similar experiments with a low-pressure CO-H_2-O_2-Ar flame. The data and analyses of these researchers provided detailed kinetic information on the mechanisms of Br and CF_3 inhibition under low-pressure premixed, burner-stabilized conditions. Day et al.[41] and Dixon-Lewis and Simpson[42] studied the burning velocities and the rich flammability limits of H_2-O_2-N_2 and H_2-O_2-N_2O flames. Their experiments and numerical modeling showed that the thermodynamic equilibrium relationship for the reaction $H + HBr = H_2 + Br$ together with recombination steps involving bromine atoms are primarily responsible for the inhibition effect of HBr compared to HCl and HF, rather than competition of the H atom-hydrogen halide reaction with the branching reaction $H + O_2 = OH + O$. Westbrook[8,43] developed a detailed chemical kinetic mechanism for HBr, CH_3Br, and CF_3Br inhibition and performed numerical calculations of flame structure, testing the mechanism using experimental burning velocity reductions and, to some extent, using measured species concentration profiles.

Diffusion Flames

Early investigations of the effects of chemical inhibitors on diffusion flames used the co-flow configuration. Creitz[44] determined the blow-off limits with CH_3Br and CF_3Br added to either the fuel or oxidizer stream for various oxygen volume fractions, and found that oxygen volume fractions approaching 0.30 required over 20 % CF_3Br in the oxidizer for flame detachment. Simmons and Wolfhard[12] found the blow-off limits for CH_3Br addition to the fuel and air streams for alkane and hydrogen flames, and showed that blow-off required different amounts of inhibitor for different burner geometries. Their measurements, as well as more recent ones with CF_3Br,[45,46] have shown that lower gas velocities require greater amounts of inhibitor. Simmons and Wolfhard[12] also performed accompanying spectroscopic measurements in a slot-burner with CH_3Br added to the air stream and found enhanced C_2 formation as well as a secondary reaction zone (observed via Br_2 emission) on the air side with either CH_3Br or ethane and bromine added to the air stream.

The above jet diffusion flame studies have all shown that a higher volume fraction of the brominated agent was required when it was added to the fuel stream rather than the air stream. Friedman and Levy[15] were the first to use the extinction of counterflow diffusion flames to assess the inhibitory effect of CF_3Br and CH_3Br added to the methane stream. Milne et al.[16] added CF_3Br to either the fuel or air stream of several hydrocarbon-air flames, again showing that addition to the air stream extinguished the flames at lower volume fraction than addition to the fuel stream. Ibiricu and Gaydon[47] made spectroscopic measurements with addition of CH_3Br and other inhibitors to flames of various fuels. They found OH emission to be decreased, while C_2 and HCO emission were increased. Niioka et al.[36] correlated the extinction conditions of counterflow diffusion flames of ethylene inhibited by CF_3Br in the air or fuel stream with the estimated mass flux of inhibitor to the reaction zone.

The first measurements of inhibited counterflow flames with liquid fuels were made by Kent and Williams[17,48] for CF_3Br in the oxidizer stream against a heptane pool. These were followed by extensive measurements for the same agent with numerous condensed-phase fuels by Seshadri and Williams.[49] Among other results and analyses, these investigations characterized the extinction flow velocity as a function of the oxygen mass fraction in the oxidizer stream, found the extinction flow with added inhibitor, and measured stable species mass fractions with gas chromatography. The amount of inhibitor required for flame extinction was found to increase with decreasing air flow velocity (i.e. strain) and the results were highly fuel dependent. In later work, Seshadri and co-workers [50] determined the extinction strain rate for a large number of fluorinated agents in a similar counterflow heptane-air pool burner.

Some of the above diffusion flame studies also show increased soot production with addition of halogenated inhibitors. The laser-induced incandescence and fluorescence measurements of Smyth and Everest[51] have quantified both the increased soot and decreased peak OH in such flames, although the mechanism of higher soot formation for CF_3Br was not resolved.

Mechanism of Inhibition

The basic mechanism of halogen flame inhibition was suggested by Rosser et al.[33] and further justified and refined by Butlin and Simmons,[31] Dixon-Lewis and co-workers,[41,42] Westbrook,[8,13,43] and Babushok and co-workers.[52] The reaction mechanism is:

$$H\alpha + X \rightarrow HX + \alpha$$

$$\beta + HX \rightarrow H\beta + X$$

in which X is a halogen, α is a hydrocarbon, and β is a reactive radical such as H, O, or OH. The hydrogen atom is typically affected most by the catalytic radical recombination cycles above, and its decrease leads to a lowering of the chain-branching reaction $H + O_2 \rightarrow OH + O$ and the CO consumption reaction $CO + OH \rightarrow CO_2 + H$. It was demonstrated fairly early[41] that for Br and Cl, the equilibrium condition of the first reaction was key, as was the necessity of the regeneration steps (in the form of the second reaction or some alternatives).

As described above, there has been fairly extensive past research on CF_3Br itself, as well as some simple small hydrofluorocarbon (HFC) short-term replacements. These include phenomenological tests with cup burners as well as fundamental studies. Nonetheless, tests with larger HFCs appear less frequently in the literature, with very little fundamental data from diffusion flames. The following work remedies that deficiency.

3.2.2 Suppression of Nonpremixed Flames by Fluorinated Ethanes and Propanes

Introduction

The need for environmentally acceptable substitutes for bromine-containing halons (halogenated hydrocarbons) has led to a number of studies on alternative fire suppression agents encompassing a variety of experimental geometries and scales,[21,53] as well as to the development of chemical kinetic models for these agents.[54-56] Models are instrumental in guiding the search for effective halon replacements in that they facilitate the identification of mechanisms key to suppression. Such models must be validated using experimental data. Data sets that can directly be compared to numerical results are therefore particularly valuable. For models of suppression in particular, the usefulness of experimental and numerical studies depends on how well they capture the characteristics of real fire scenarios. Most experimental studies on hydrofluorocarbons (HFCs), used as near-term halon replacements, have focused on inhibited premixed flames, usually with methane fuel, measuring parameters such as flame speed[57,58] or profiles of intermediate species.[59-61] However, most fire-fighting scenarios involve higher hydrocarbon fuels, non-premixed flames, and aim to achieve extinction rather than inhibition. In order to extend laboratory results to more realistic situations, a broad range of data sets is needed to provide adequate model validation for suppression by both HFCs and other classes of alternative agents now being identified.

Research by Williams and co-workers[62] focused on the suppression effectiveness of HFCs in extinguishing non-premixed flames. Although less effective fire suppressants than brominated halons, these agents are currently used as near-term replacements. They possess many of the same favorable physical properties as brominated halons, but do not destroy the stratospheric ozone layer.[21,50] Previously, the Naval Research Laboratory (NRL) investigated non-premixed counterflow methane/air and propane/air flames suppressed by CF_4, CHF_3, and CF_3Br.[63] The NGP extended the methane/air and propane/air extinction studies to include all fluorinated ethanes containing at least four fluorine atoms, and ten fluorinated propanes containing at least five fluorine atoms. The fluorinated ethane and fluorinated propane data sets were generated to provide additional input to validate chemical kinetic models such as those developed recently for HFCs.[54-56, 59] Also tested were sulfur hexafluoride (SF_6,

largely inert[13]), nitrogen, three bromine-containing halons, and one iodine-containing halon. All compounds investigated are listed in Table 3-1.

Table 3-1. Agents Tested.

Agent	Chemical Formula	$C_p^{300\ K}$ (J/mol.K)[a]	$H^{1600\ K}-H^{300\ K}$ (kJ/mol)[b]	Flames[e]
HFC-134	CHF_2CHF_2	90.9	183[31]	M,P,H
HFC-134a	CF_3CH_2F	87.2	186[31]	M,P,H
HFC-125	CF_3CHF_2	95.9	195[31]	M,P,H
FC-116	CF_3CF_3	107.7	206[31]	M,P,H
HFC-245ca	$CHF_2CF_2CH_2F$	123.7	244[c]	M,P
HFC-245cb	$CF_3CF_2CH_3$	123.0	242[c]	M,P
HFC-245eb	CF_3CHFCH_2F	123.0[c]	242[c]	M
HFC-245fa	$CF_3CH_2CHF_2$	122.0[35]	241[35]	M
HFC-236cb	$CF_3CF_2CH_2F$	130.0[c]	256[c]	M,P,H
HFC-236ea	$CF_3CHFCHF_2$	129.8	256[c]	M,P,H,A
HFC-236fa	$CF_3CH_2CF_3$	128.1	253[c]	M,P,H,A
HFC-227ca	$CF_3CF_2CHF_2$	140.0[c]	276[c]	M,P,H
HFC-227ea	CF_3CHFCF_3	139.8	275[38]	M,P,H,A
FC-218	$CF_3CF_2CF_3$	150.6	289[c]	M,P,H
Halon 1301	CF_3Br	70.5	125[36]	P,H,A
Halon 13001	CF_3I	61.3[36]	126[36]	P,H
Halon 1211	CF_2ClBr	74.6[d]	133[39]	P,H
Halon 1201	CHF_2Br	58.7[d]	120[39]	P,H
Sulfur Hexafluoride	SF_6	97.4[36]	185[36]	M,P,H
Tetrafluoromethane	CF_4	61.2	122[36]	H,A
Nitrogen	N_2	29.1[36]	42[36]	M,P,H,A

[a] Specific heat at 300 K. The numerical superscripts in square brackets indicate reference numbers. If no superscript is present, the value is from Reference 64.

[b] Sensible enthalpy required to raise the agent's temperature from 300 K to 1600 K. The sources for the data used to derive the sensible enthalpy values are indicated by the numerical superscripts in square brackets.

[c] Estimated.

[d] From Reference 65, evaluated at 298 K.

[e] Flames in which given agent was tested: M, methane counterflow; P, propane counterflow; H, n-heptane cup burner; A, methanol cup burner.

An experimental geometry that captures many characteristics of pool fire threats is that of the cup burner, which is described more fully in Chapter 6. Bench-scale co-flow burners operated with a liquid fuel, cup burners are widely used for estimating agent concentrations required to combat fires.[66] Hamins et al. [50] compared a number of HFC agents in cup burner tests using five different fuels: n-heptane, two types of jet fuel, and two types of hydraulic fluid. For nearly all agents tested, the concentrations required to

extinguish the n-heptane flame exceeded those required for the other fuels by less than 10 %. Thus, n-heptane cup burner studies provide extinction data applicable to many hydrocarbon flames.

For validation of kinetic models, treating detailed chemical mechanisms in the two-dimensional model required to describe cup burner flames is computationally difficult. An alternative to cup burners for suppression mechanism studies is provided by non-premixed counterflow flames. This configuration is computationally tractable since it can be modeled quasi-one-dimensionally, along the axis of symmetry of the flame, by invoking a similarity transform.[67] Experimentally, it is also advantageous in that it allows control of the strain rate imposed on the flame. In this paper, the strain rate in a counterflow burner is defined as the maximum axial gradient in axial velocity on the oxidizer side of the flame zone. The strain rate is easily adjusted by changing the gas flows. The effects of suppression agents can then be quantified over a range of flame conditions by measuring the extinction strain rate as a function of agent concentration. Hamins et al.[50] and Saso et al.[68] found that HFC extinction concentrations for low strain rate n-heptane counterflow flames were similar to those obtained in n-heptane cup burners. Since the cup burner configuration is relevant to many fire scenarios, the results of Hamins *et al.* and Saso *et al*. suggest that agent extinction concentrations in low strain rate non-premixed counterflow flames are pertinent to these same scenarios.

The choice of a model fuel compound for suppression studies involves a trade-off between representative extinction properties and computational tractability. Gaseous fuels including methane, ethane, and propane are attractive to use from both experimental and modeling standpoints, but their relevance to fires involving long chain hydrocarbons needs to be determined. Furthermore, no model fuel is representative of all fire threats. Indeed, alcohol fires, methanol fires in particular, are very difficult to extinguish, even with CF_3Br.[69] The extinction behavior of methane/air counterflow, propane/air counterflow, n-heptane cup burner and methanol cup burner flames are compared in this study to identify systematic trends in the suppression effectiveness of selected agents as a function of the fuel used. In addition to providing experimental data for HFC model validation, another objective of the current investigation is to assess whether methane or propane counterflow burner extinction studies are appropriate models for HFC suppression of liquid hydrocarbon fires.

Tanoff et al. [70] recently computed the extinction strain rate of methane/air counterflow flames suppressed by several C_1 and C_2 HFCs. One of their major conclusions was that most HFCs investigated, with the exception of CHF_3, would be better suppressants in methane flames if they were chemically inert. Also, agents predicted to form CF_2O in the counterflow flame, principally from CF_3 radicals, were found to be better suppressants than those that do not. The chemical contribution to suppression of the CF_3 group was reported by Sheinson et al.,[13] who attributed 25 % of CF_3Br's suppression ability to this moiety. The present study further investigates the impact of CF_3 groups in an agent on suppression by comparing the performance of four sets of HFC isomers.

In counterflow burners, flows at extinction are apparatus dependent. Comparisons between results obtained from different experimental and numerical counterflow flame studies must therefore be made through extinction strain rates. While flows are easily determined, velocity profile measurements are required to determine local extinction strain rates. Here, a burner-specific relationship between local strain rate and flow conditions was obtained. All strain rates quoted herein are therefore traceable to an experimental determination of the local velocity field.

Experiment

The counterflow burner and experimental methodology have been described previously.[63] The burner consisted of two vertically-mounted open straight tubes, approximately 50 cm long, having an inner diameter of 1 cm. The tube exits were spaced 10.0 mm ± 0.5 mm apart. The gap size was determined by translating the burner assembly with respect to a laser beam perpendicular to the tube axis, and measuring the height at which the beam was blocked by the tubes. The top tube was equipped with a cooling jacket to prevent the hot combustion products from preheating the upper reactant stream. The tubes were housed in a Plexiglas chamber, which was continuously purged with nitrogen to dilute combustion products and unburned reactants before they entered the exhaust.

For experiments with methane, the fuel was introduced through the top tube while air/agent mixtures were introduced through the bottom. For experiments with propane, air/agent mixtures were delivered from the top, fuel from the bottom. These configurations were used because they produced the most stable flames at low strain rates. For propane, inverting the reactant streams did not significantly affect the extinction strain rate of the uninhibited flame. Flows of all gases were regulated by mass flow controllers (Sierra Instruments), which were calibrated using a piston flowmeter (DC-2, Bios International). All flow conditions were laminar, with tube Reynolds numbers never exceeding 2100.

During extinction measurements, the flows of fuel and air were set to obtain a flame midway between the tubes. The agent flow was then slowly increased at intervals of 30 s to 45 s, with periodic adjustments of the fuel and air flows to maintain the flame's position, until the flame extinguished. The flame's position was determined by monitoring its image on a video screen. The stagnation plane was always slightly toward the fuel tube from the flame zone. In experiments with methane, the flame typically extinguished completely. For propane, local extinction typically occurred along the centerline, leaving a ring-shaped flame with a hole along the burner axis, similar to that described by Potter and Butler.[71] In all tests, the agent was added to the air stream. This mode of application most closely resembled actual situations, in which an agent is introduced into the air around the fire, with the fuel burning in a non-premixed flame.

The cup burner apparatus and methodology have been described in detail elsewhere.[13] The design was virtually identical to that of Hamins et al.[50] The piston flow meter was used to measure the agent and air flows after each extinction measurement. The total flow of air + agent was 20 L/min ± 1 L/min for all extinction measurements, giving a flow velocity, averaged over the 105 mm inner diameter chimney, of 4.1 cm/s ± 0.2 cm/s past the 28 mm outer diameter cup. Experiments were conducted on both n-heptane and methanol flames. The fuel level was kept within 0.5 mm of the top of the cup without overflowing, as low liquid levels led to attachment of the flame to the heated rim of the Pyrex cup, resulting in anomalously high extinction values.

The agents listed in Table 3-1 were obtained from the following suppliers: HFC-245eb and halon 13001, Flura; HFC-245fa, AlliedSignal; HFC-236ea and HFC-236fa, Dupont; HFC-227ea and halon 1201, Great Lakes; FC-218, Scott Specialty Gases; halon 1301 and CF_4, Matheson. The nitrogen was obtained from the Naval Research Laboratory's in-house supply. The remaining agents were from PCR. The stated purity of the agents was at least 97 %. All agents were used as supplied, with the exception of HFC-245ca, HFC-245eb and HFC-245fa. These pentafluoropropanes have boiling points close to room temperature: 25 °C, 23 °C, and 15 °C, respectively. They were therefore premixed with air in a 1:3 ratio before being tested. The pressure increase ensured that stable flows of these agents were delivered to the

burners. Extinction data was also collected with HFC-245fa unmixed with air. These data were consistent with those obtained using the agent/air mixture.

All of the agents in Table 3-1 were tested in the propane counterflow flame with the exception of HFC-245eb, HFC-245fa, and CF_4. All of the agents were tested in the methane counterflow flame with the exception of halon 1301, halon 13001, halon 1211, halon 1201, and CF_4. All of the agents with the exception of the pentafluoropropanes were tested with n-heptane in the cup burner. HFC-236ea, HFC-236fa, HFC-227ea, halon 1301, CF_4, and nitrogen were tested with methanol in the cup burner.

Extinction Strain Rate Determination

Many researchers performing studies in counterflow burners have characterized extinction conditions in terms of global or imposed parameters, such as flow rates and gap size,[72] or global strain rates calculated from these parameters.[50,73] These global parameters representing the imposed flow conditions can be compared to the same parameters obtained from numerical calculations of extinction conditions.[74] Because the local flow field near the flame determines extinction, the comparison of global parameters is valid only as long as the relationship between the local strain rate and the global conditions are the same for the experiment and the calculations. Recent measurements[67,75] have cast doubts on the adequacy of representing counterflow experimental boundary conditions by either plug or potential flow in numerical calculations. Comparisons of measured and numerical local strain rates in the vicinity of the flame should show less sensitivity to boundary conditions than comparisons of measured and numerical global strain rates.

The most direct approach in determining strain rate is to measure the local velocity fields. As velocities cannot be measured at extinction, determination of local extinction strain rate involves a series of velocity measurements in increasingly strained flames, and extrapolation to extinction.[63] This sequence of measurements must be repeated for each fuel/oxidizer/additive system and each additive loading, requiring large numbers of velocity profile measurements.

In the present study, air stream local strain rates were determined by measuring the centerline axial velocity as a function of axial position by an LDV system (QSP Digital). The oxidizer stream was seeded with 0.3 μm alumina particles (Buehler). The velocity profile on the oxidizer side of the flame was fit to a 6^{th} order polynomial, and the relevant local strain rate was taken to be the maximum value of the derivative of this function. Velocity profiles were measured for propane/air, methane/air, methane/(air + HFC-227ea), and propane/(air + SF_6) flames.

Based on these measurements, an empirical, burner-specific relationship to convert global parameters into local strain rates was determined. Figure 3-1 shows the data used in obtaining this correlation. Measured local strain rate is plotted versus the plug flow global strain rate parameter derived by Seshadri and Williams[76], and restated by Chelliah et al. [67] in Equation 3-1.

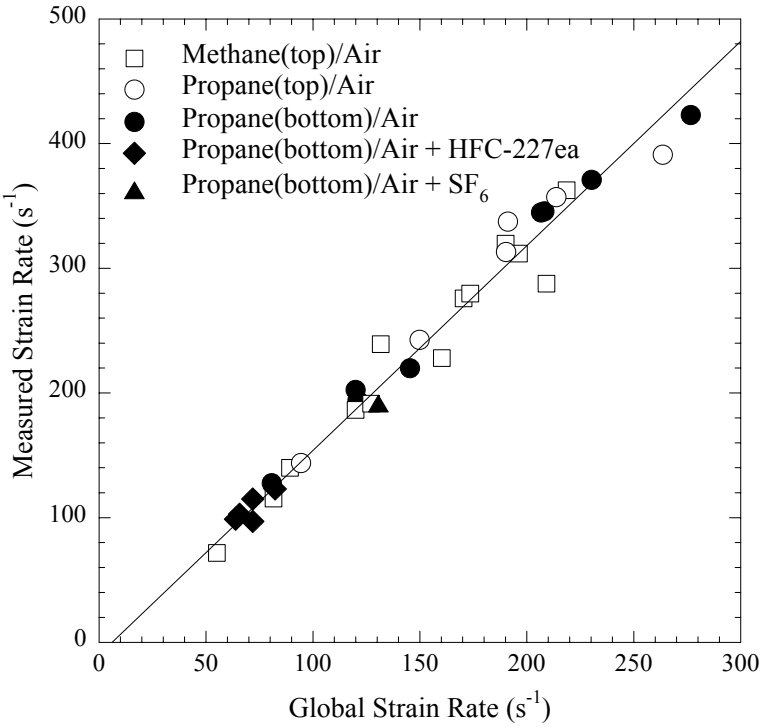

Figure 3-1. Comparison of Local Strain Rates Measured by Laser Doppler Velocimetry in Non-premixed Counterflow Flames and Global Strain Rates Calculated from Equation 3-1. (The solid line corresponds to the linear regression given in Equation 3-2.)

$$K_{global,plug} = \frac{2|V_o|}{L}\left(1+\left(\frac{\rho_f V_f^{\,2}}{\rho_o V_o^{\,2}}\right)^{0.5}\right), \tag{3-1}$$

where L is the gap size (1 cm), and $\rho_{f,o}$ and $V_{f,o}$ are the densities and velocities of the fuel and oxidizer streams, respectively. V is as the *average* velocity across the tube exit. Measured local strain rates for all flame conditions, including those with suppressants present, were proportional to $K_{global,\,plug}$ from Equation 3-1,

$$K_{local} = (1.57 \pm 0.02)\, K_{global,plug}\ , \tag{3-2}$$

where the velocities used in the global expression are averages based on measured volumetric flows. The local extinction strain rates discussed in the present study were obtained using Equations 3-1 and 3-2.

Seshadri and Williams' plug flow global strain rate expression is for the axial gradient in axial velocity at the stagnation plane calculated for inviscid non-reacting flow, with plug flow boundary conditions imposed at the burner exits. The current apparatus, with straight burner tubes, has velocity boundary conditions significantly different from plug flow. Measurements near the tube exits indicated a nearly parabolic profile for an individual tube in isolation, with some flattening of the profile when the opposing flow from the second tube was introduced. The centerline velocity of a parabolic profile in tube flow was twice the average velocity determined from the volumetric flow and the cross-sectional area. At a given flow, the tube exit centerline velocities in the current apparatus were therefore expected to be between once and twice the plug flow values. Hence, the coefficient relating K_{local} and $K_{global,plug}$ was predicted to lie between 1 and 2. The factor of 1.57 obtained was consistent with this prediction. Pellett et al. [77] also determined that local and global strain rates were linearly related in their opposed-tube burners: local

strain rates were found to be 3 times larger than their global counterparts. Pellett et al. used burners with a ratio of gap size to tube diameter equal to 2. For the burner considered here, this ratio was equal to 1.

Non-Premixed Counterflow Flame Experiments

Figure 3-2 and Figure 3-3 show how local extinction strain rate varied with agent molar concentration for methane and propane non-premixed counterflow flames, respectively. Figure 3-2a and Figure 3-3a show the suppression effects of the fluorinated ethanes, SF_6 and N_2. The N_2 extinction concentrations have been divided by two for presentation in the figures. Figure 3-2b and Figure 3-3b show results for the fluorinated propanes. Figure 3-3c shows the effects of halon 1301, halon 13001, halon 1211 and halon 1201 on the extinction strain rate of a propane flame. The error bars shown in Figure 3-2a and Figure 3-3a for the HFC-134 data are at the 99.7 % (3σ) confidence level. Horizontal error bars represent uncertainties in air and agent flows. Vertical error bars represent uncertainties in air, agent and fuel flows, gap size, room temperature and pressure, and the constant of proportionality between local and global strain rates (Equation 3-2). At comparable concentrations or extinction strain rates, uncertainties in the data for the other agents are similar to those shown for HFC-134. The N_2 extinction concentration uncertainties are similar to those for HFC-134 at comparable loadings. They increase to ± 1.7 mole % at the highest concentrations.

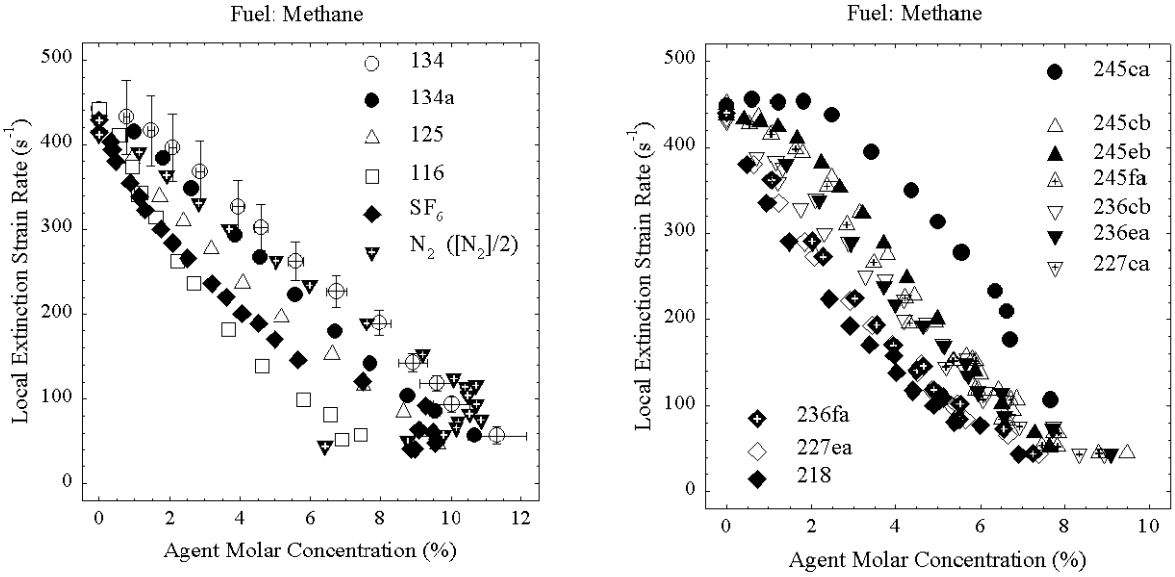

Figure 3-2. Extinction Strain Rate vs. Agent Molar Concentration for Non-premixed Methane-air Flames Suppressed by: a) Fluorinated Ethanes, SF_6, and N_2; and b) Fluorinated Propanes.

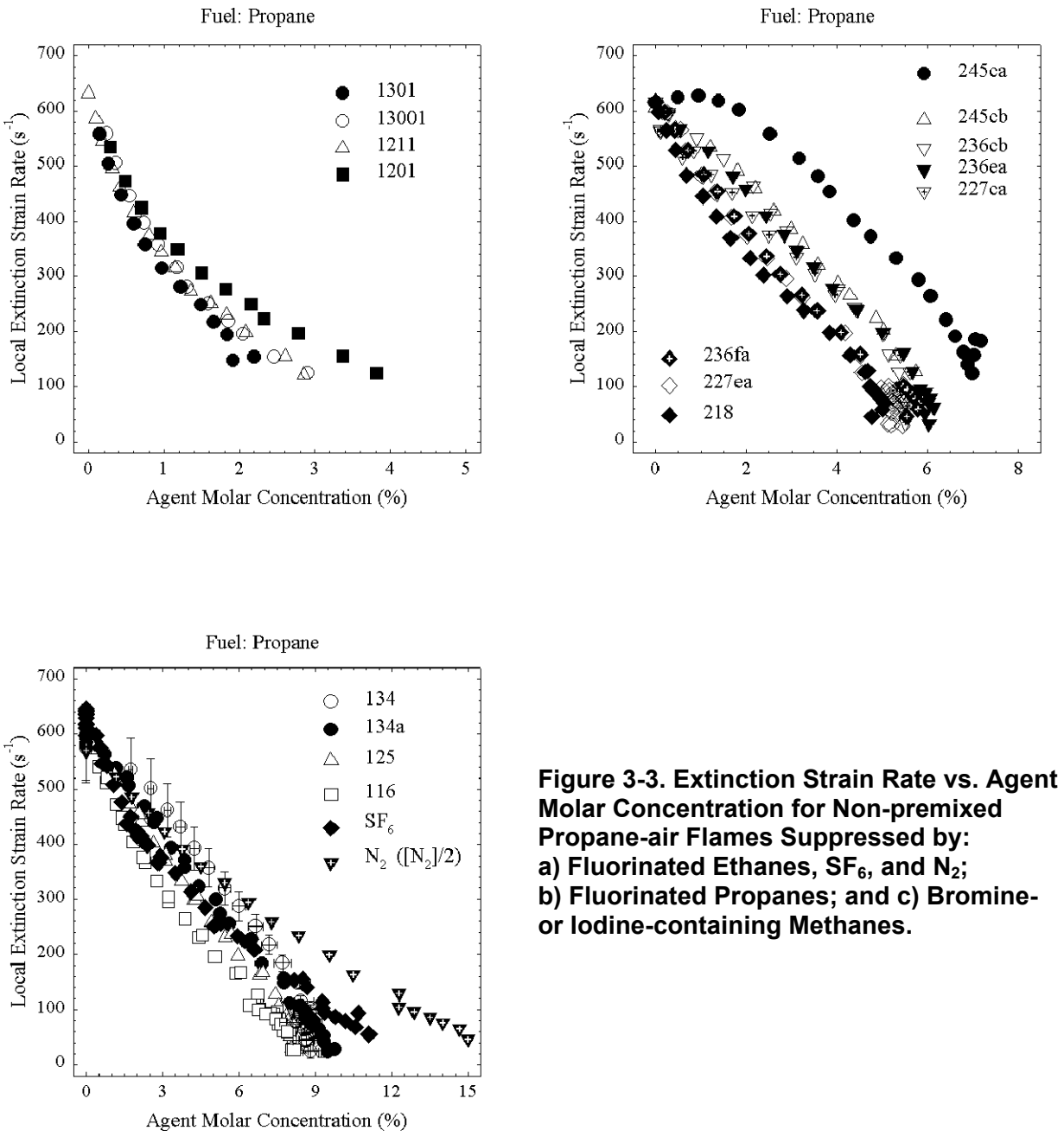

Figure 3-3. Extinction Strain Rate vs. Agent Molar Concentration for Non-premixed Propane-air Flames Suppressed by: a) Fluorinated Ethanes, SF_6, and N_2; b) Fluorinated Propanes; and c) Bromine- or Iodine-containing Methanes.

Extinction of Uninhibited Methane and Propane Flames

The average uninhibited non-premixed counterflow methane/air and propane/air flame local extinction strain rates were compared to values found in the literature. Pellett et al.[77] used two different opposed-nozzle burners to obtain extinction strain rates of 384 s^{-1} and 396 s^{-1} for methane/air flames. Furthermore, Chelliah et al.[67] measured the local extinction strain rate of their non-premixed counterflow methane/air flame to be 380 s^{-1}. Yang and Kennedy[78] measured theirs to be 340 s^{-1}. Both of these values were obtained for flames having strain rates below that required for extinction. They correspond to lower

bounds for the values that would be calculated from an extrapolation to extinction, and are consistent with the results of the present study. Yang and Kennedy indicated that the strain rate they report is approximately 10 % lower than that which would be obtained through extrapolation; and that the uncertainty in their critical strain rate is approximately +10 % and -5 %.

Global extinction strain rates for uninhibited counterflow non-premixed methane/air and propane/air flames have also been reported. MacDonald et al.[79] reported a global extinction strain rate of 296 s^{-1} for methane. The corresponding global value obtained in the present study was 273 s^{-1}. Since the experimental geometries in both studies are similar, the values are expected to be comparable. MacDonald et al. indicate that variations of up to 80 s^{-1} were observed in their uninhibited global extinction strain rates, due to variations in their air's oxygen content. The global methane extinction number collected in the present study is thus consistent with theirs. Puri and Seshadri[80] report global extinction values, but for a different experimental geometry. The results cannot be directly compared.

Agent Suppression Effectiveness

Figure 3-2 and Figure 3-3 show that, in general, the extinction strain rate of both methane and propane flames decreased as agent loading increases. Thus, the agents inhibited the flames. For HFC-245ca, however, the extinction strain rates at concentrations below 2 % are higher than those for the uninhibited flames. At these loadings, this agent increased flame strength. Nevertheless, above 2 %, extinction occurred at strain rates below the uninhibited values, and extinction strain rates decreased with increases in concentration: in larger quantities, HFC-245ca acted like a suppressant. The extinction data presented in Figure 3-2 and Figure 3-3 are limited to strain rates above 70 s^{-1}. Below this value, considerable scatter was observed and, for several agents, extinction concentrations began to decrease with diminishing strain rate. At low strain rates, the flames became more susceptible to both conductive and radiative heat losses to the burner, and to fluctuations in the flow currents present in the surrounding chamber gases.

A secondary flame zone about 1 mm on the air side of the principal non-premixed flame was observed in tests with HFC-245ca, particularly at high loadings. Hamins et al.[50] also found separate agent and fuel consumption zones in their numerical investigation of the structure of halon 1301 inhibited n-heptane/air non-premixed counterflow flames. In the current study, the secondary flame zone appeared to be caused by the agent burning in the air in a premixed fashion. Yang et al.[81] predicted this phenomenon for CH_3Cl addition to the oxidizer stream of a methane/air counterflow flame. Although HFC-245ca is non-flammable at ambient temperature and pressure, heat release from the non-premixed flame was apparently sufficient to support its premixed combustion. Grosshandler et al.[82] investigated the flammability of HFC-245ca, and concluded that a stoichiometric mixture of HFC-245ca and air could sustain combustion if preheated 100 K above ambient temperature. A secondary flame zone was also observed in tests with a more effective suppressant, HFC-245cb, but was less pronounced than in the HFC-245ca case.

The relative suppression effectiveness of the fluorinated propanes can be assessed from Figure 3-2b and Figure 3-3b. The most effective fluorinated propanes were FC-218, HFC-227ea, and HFC-236fa, all of which contain two CF_3 groups. HFC-227ca, HFC-236ea, HFC-236cb, and HFC-245cb, along with HFC-245fa and HFC-245eb in the methane case, were less effective and contain one CF_3 group. HFC-245ca has no CF_3 groups and was clearly less effective than the other fluorinated propanes tested. The extinction strain rate curves clustered together in terms of the number of CF_3 groups present in the agent.

Among agents with the same number of CF_3 groups, compounds with higher fluorine to hydrogen atom (F:H) ratios were slightly more effective agents, particularly at low concentrations: FC-218 was slightly more effective than HFC-227ea and HFC-236fa; and HFC-227ca, HFC-236ea and HFC-236cb were more effective than the pentafluoropropanes. At higher concentrations, agent suppression effectiveness was not as affected by the F:H ratio. The impact on suppression of substituting an F atom for an H atom in the agent molecule is both chemical and physical in nature. F atoms can scavenge H atoms in flames to form HF, reducing the number of H's that participate in flame propagation reactions.[61] Furthermore, as shown in Table 3-1, substituting one F for one H in a fluorinated propane led to a 5 % to 8 % increase in its specific heat at 300 K, enhancing the molecule's sensible enthalpy. Higher F:H ratios were therefore expected to increase the physical suppression effectiveness of fluorinated propanes. However, as the data show, the effect of substituting one H for an F was minor compared to that of arranging the fluorine atoms to provide a CF_3 group: HFC-236fa was more effective than HFC-227ca, which has one more fluorine atom but one less CF_3 group.

The impact of CF_3 groups on suppression is further illustrated by the fluorinated ethane results shown in Figure 3-2a and Figure 3-3a. FC-116, which has two CF_3 groups, was more effective than HFC-125 and HFC-134a, which only have one. HFC-134, which contains no CF_3 groups, was the least effective of the fluorinated ethanes for most flame conditions. The presence of additional fluorine atoms in FC-116 and HFC-125 could explain their enhanced effectiveness relative to HFC-134a and HFC-134. However, the tetrafluoroethanes have the same number of fluorine atoms. At strain rates above 100 s^{-1}, HFC-134a was more effective than HFC-134, which correlates with the presence of a CF_3 group in the former. At lower strain rates, the extinction concentrations of these two agents were comparable.

The presence or absence of a CF_3 group also influenced the suppression effectiveness of the halons shown in Figure 3-3c. This figure shows that halon 1201 (CHF_2Br) was less effective than both halon 1301 (CF_3Br) and halon 13001 (CF_3I), particularly at higher loadings; and halon 1211 (CF_2ClBr) was slightly less effective than halon 1301. Sheinson et al.[13] investigated the chemical suppression effectiveness of the CF_3Y and SF_5Y (Y = F, Cl, Br, I) series in an n-heptane cup burner. They concluded that, for CF_3Cl, the CF_3 moiety made a greater chemical contribution to suppression than the Cl atom. This conclusion is consistent with the greater effectiveness of halon 1301 relative to halon 1211 observed here.

Fluorinated Ethanes vs. Fluorinated Propanes

The effectiveness of the fluorinated ethanes relative to that of the fluorinated propanes can be assessed by comparing Figure 3-2a to Figure 3-2b, and Figure 3-3a to Figure 3-3b. At strain rates below 100 s^{-1}, fluorinated ethanes extinguished methane flames at concentrations between 5 % and 10 %. Loadings between 4 % and 8 % were required for the fluorinated propanes. In the case of propane flames, below 100 s^{-1}, extinction concentrations for the fluorinated ethanes ranged from 6 % to 10 %. For the fluorinated propanes, they ranged from 4 % to 8 %. The steeper extinction strain rate curves for the fluorinated propanes indicate that, as a group, they were more effective agents on a molar basis than the fluorinated ethanes. Table 3-1 shows that the specific heats at 300 K of the fluorinated propanes range from 122.0 to 150.6 J-mol^{-1}-K^{-1}, as opposed to 87.2 to 107.7 J-mol^{-1}-K^{-1} for the fluorinated ethanes. The greater effectiveness of the fluorinated propane agents is consistent with their greater sensible enthalpy relative to the fluorinated ethanes.

Methane Flames vs. Propane Flames

Figure 3-2 and Figure 3-3 can also be compared to assess the differences between suppression of methane and propane non-premixed counterflow flames. The uninhibited propane flame was more difficult to extinguish, requiring an average strain rate of 583 s^{-1} vs. 415 s^{-1} for methane. However, the extinction strain rates of flames fueled with propane decreased more rapidly with increases in suppressant loading such that, at strain rates below 100 s^{-1}, methane and propane flames were extinguished by similar fluorinated agent loadings. If the extinction strain rates are normalized by the corresponding uninhibited strain rates and compared, the sensitivity of both methane and propane flames to agent addition is found to be similar. The propane flames were slightly more sensitive to the suppressants. Figure 3-2 and show that extinction strain rate curve shapes are different for the two fuels.

Numerical Investigation of Tetrafluoroethane Isomer Effectiveness

The kinetic model developed at NIST[83] for fluorinated hydrocarbons has been used to numerically investigate the effects of halogenated compounds on C1 and C2 organic flames. [52,54,58,70] With this model, Tanoff et al.[70] predicted extinction strain rates for methane/air counterflow flames suppressed by CF_4, CHF_3, CF_3CF_3 (FC-116), CF_3CHF_2 (HFC-125), and CF_3CH_2F (HFC-134a). The NIST model was also used by Linteris et al.[57], who reported both experimental and computational flame speeds for methane/air mixtures containing FC-116, HFC-125, and HFC-134a. Reaction pathway analyses of agent decomposition showed that CF_2O was an important intermediate for FC-116, which initially decomposes to form two CF_3 radicals. The numerical calculations predicted that as the hydrogen content of the fluorinated ethane increased, less CF_2O was produced. To our knowledge, no previous modeling studies have compared different isomers. In the present form of the kinetic mechanism, only fluoroethane isomers may be compared, because the fluorocarbon kinetic mechanism, in its original form, does not include C3 species. Recently, the mechanism has been extended to cover HFC-227ea. [55,56,84] Kinetic mechanisms for other fluoropropanes have not yet been developed.

In the present study, calculations were conducted using the NIST model to predict flame speeds of stoichiometric methane/air mixtures doped with 3.81 mole % of either HFC-134 or HFC-134a. The goal of these calculations was to determine if the current kinetic model predicts isomeric differences between the two agents, and why these differences may exist. Although extinction strain rate predictions, such as those performed by Tanoff et al., are more relevant to the measurements of Figure 3-2a and Figure 3-3a, they are computationally more demanding. It is generally acknowledged that flame speed is closely related to extinction strain rate.[71] The current calculations, which predict isomeric differences in suppression, should therefore carry over to non-premixed flames.

The flame speed calculations were performed on a domain extending 25 cm from the flame into the cold reactants, and 60 cm into the hot products. The calculations used multicomponent viscosities, thermal diffusivities for H and H_2, and windward differencing for the convective terms. The initial temperature of the reactants was set to 298.2 K. The ultimate solutions were obtained on meshes having 150 grid points.

The kinetic mechanism used was essentially that developed by NIST, modified according to L'Espérance et al.[61] The reactions

$$FCO + CHF_2 \Leftrightarrow CF_2{:}CO + HF \quad \text{(R3-1)}$$

$$CF_3CHF + H \Leftrightarrow CHF{:}CF_2 + HF \quad \text{(R3-2)}$$

$$CF_3CHF + H \Leftrightarrow CH_2F + CF_3 \quad \text{(R3-3)}$$

$$HCO + CF_3 \Leftrightarrow CF_2{:}CO + HF \quad \text{(R3-4)}$$

were taken from Linteris et al. [57] Furthermore, the reactions

$$CH_2F + CF_3 + M \Leftrightarrow CH_2FCF_3 + M \quad \text{(R3-5)}$$

$$CH_2F + CF_3 \Leftrightarrow CHF{:}CF_2 + HF \quad \text{(R3-6)}$$

were also added. These latter two reactions were not present in the NIST mechanism, although the analogous reactions for all other pairs of fluorinated methyl radicals were included. The kinetic rates of reactions R3-5 and R3-6 were estimated by taking the geometric mean of the rates of the analogous reactions for $CH_3 + CF_3$ and $CHF_2 + CF_3$. R3-5 represents an additional destruction pathway for HFC-134a not considered in the modeling of Reference 57.

Finally, the thermal decomposition reaction

$$CF_3\text{-}CHF\ (+ M) \Leftrightarrow CF_2{:}CHF + F\ (+ M) \quad \text{(R3-7)}$$

was added using the high pressure kinetic expression from Reference 56 and estimated low pressure kinetics from Reference 84. This reaction proved very important in modeling suppression by HFC-227ea, in which the CF_3-CHF radical is formed from the parent agent by C-C bond dissociation. From HFC-134a, this radical is produced by hydrogen abstraction.

The predicted flame speeds for the mixtures containing HFC-134 and HFC-134a were 18.9 cm/s and 15.5 cm/s, respectively, or 48 % and 39 % of the calculated uninhibited methane/air flame speed of 39.4 cm/s. For the HFC-134a case, the experimental measurement and numerical prediction of Linteris et al.[57] were 38 % and 29 %, respectively. Flame speed measurements for methane/air/HFC-134 mixtures have not been reported. Thus, the kinetic model predicted a substantial difference in inhibition effectiveness between the two tetrafluoroethane isomers. The refinements in the kinetic mechanism greatly improved agreement with the experimental flame speed measurement for HFC-134a.

Reaction pathway diagrams for HFC-134 and HFC-134a are shown in Figure 3-4a and Figure 3-4b. The major removal pathway for CHF_2-CHF_2 is thermal dissociation of the C-C bond. For CH_2F-CF_3, the major removal pathways are hydrogen abstraction by H and OH, and HF elimination. Sensitivity analysis indicated that these initial reaction steps had the greatest influence on the difference in flame speed between the two isomers. This may be a consequence of the major removal pathways for HFC-134a consuming H or OH and generating less reactive species, while the dominant HFC-134 pathway generates radicals.

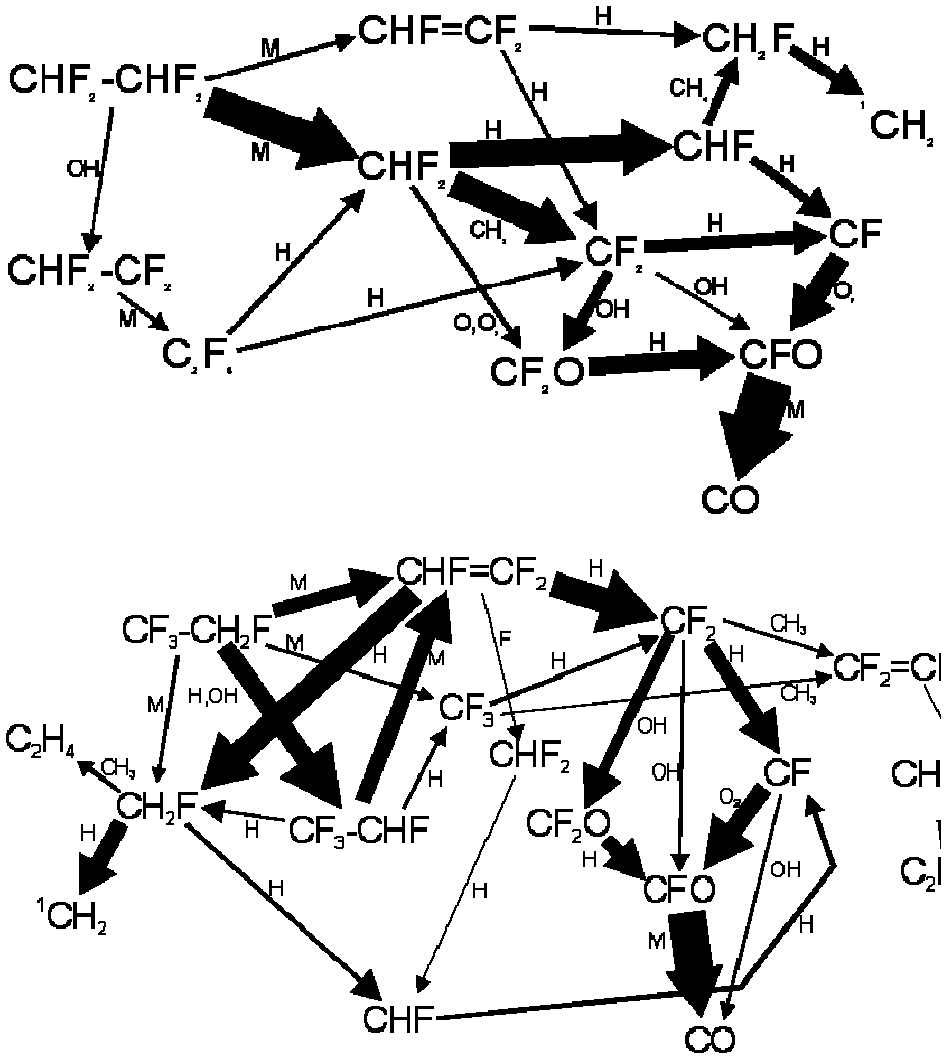

Figure 3-4. Reaction Pathways for Premixed Methane/air Flames Doped with 3.81 Volume % of: (a) HFC-134 and (b) HFC-134a.

The reaction pathways associated with HFC-227ea should be representative of those of other fluorinated propanes. HFC-227ea, under most conditions, is consumed by thermal decomposition, not radical attack. The decomposition pathways are HF elimination and C-C bond removal. The latter process dominates in near-stoichiometric, high temperature flames.[84] For asymmetric isomers, more than one product channel exists for most agent destruction reactions. If a fluorinated ethyl radical is produced by thermal decomposition, it is likely to decompose through H atom elimination from the methyl group, if one is present. Otherwise, F atom elimination will be the dominant process.[84] H and F are both reactive species. However, H has a higher diffusivity and participates in the H + O_2 chain branching reaction, while F reacts primarily in a chain propagating reaction with H_2O. These considerations provide one possible explanation for the observed isomeric differences among fluoropropanes. Kinetic mechanisms for these agents must be developed and validated before a more definitive analysis can be conducted.

Cup Burner Experiments

The n-heptane and methanol cup burner extinction concentrations obtained in Reference 62 are provided in Table 3-2. Concentrations based on both volumetric and molar proportions are included. The two sets of values are not identical as several of the agents deviate from ideal gas behavior at ambient conditions. Each concentration represents the average of at least 3 runs. At the 99.7 % confidence level (3σ), the uncertainties associated with the cup burner values were estimated to be ± 0.6 mole %, with the exception of those for CF_4 and N_2, estimated to be ± 1.5 mole %. Table 3-2 also shows the n-heptane cup burner data (vol. %) of Hamins et al.[50] Extinction concentrations from the two data sets are within 7 % of each other for all agents except HFC-236fa, for which they differ by 11.5 %.

Table 3-2. Cup Burner Extinction Concentrations.

Agent	n-Heptane Cup Burner (Present Study)		n-Heptane Cup Burner (Reference 50)	Methanol Cup Burner (Present Study)	
	Vol. %	Mol. %	Vol. %	Vol. %	Mol. %
Halon 1301	3.1[a]	3.1	3.0	6.3	6.4
Halon 13001	3.2[a]	3.2			
Halon 1211	3.6	3.7			
Halon 1201	4.1	4.1			
FC-218	6.1[b]	6.3	6.4		
HFC-236fa	6.1	6.3	6.8	8.0	8.2
HFC-227ea	6.4	6.6	6.3	8.9	9.2
HFC-227ca	6.9	7.1			
HFC-236ea	7.2	7.5		9.9	10.3
HFC-236cb	7.4	7.7			
FC-116	7.9[a]	8.0	8.4		
HFC-125	8.8	8.9	8.8		
HFC-134a	10.0	10.2	10.2		
Sulfur Hexafluoride	10.6	10.9			
HFC-134	10.9	11.1			
Tetrafluoromethane	16.0[a]	16.0		22.0	22.1
Nitrogen	30.0[a]	30.0	31.8	41.6	41.6

[a] From Reference 13.
[b] From Reference 13, but corrected for typographical error.

Hamins et al.[50] and Saso et al.[68] compared cup burner values to extinction data collected in liquid n-heptane counterflow flames. Both studies found that counterflow extinction concentrations at low strain rates were similar to those obtained in a cup burner. To assess the impact of fuel type on extinction loadings, methane and propane counterflow values at low strain rates were compared in the present study

to n-heptane and methanol cup burner values. An appropriate counterflow extinction strain rate must be selected to make the comparison. Hamins et al. used a global strain rate of 50 s^{-1}. Saso et al. used a global strain rate of 30 s^{-1}, but defined their global strain rate as half that used by Hamins et al. In this investigation, a local strain rate of 80 s^{-1} was chosen.

Figure 3-5a, b, c, and d show n-heptane cup burner, methanol cup burner, methane counterflow, and propane counterflow extinction results, respectively. For each fuel, the agents are presented in decreasing order of effectiveness, with the most effective agent being the top bar. The methane and propane counterflow extinction values for N_2 were divided by two for presentation in the figure. The counterflow extinction concentrations for agents not tested at strain rates as low as 80 $^{s-1}$ were extrapolated from the curves of Figure 3-2 and Figure 3-3. The predicted agent extinction concentrations represent the loadings that would be required to suppress the given flames assuming that the agents were inert, and that they extinguished the flames at the same sensible enthalpy per mole of oxygen as CF_4 and SF_6.

Physical Versus Chemical Contributions to Suppression

Physical versus chemical contributions to suppression for different agents are compared following the formalism of Tucker et al.[69] and Sheinson et al.[13] Physical contributions attributed to agent addition include increased thermal mass, oxygen dilution, and increased conductive heat losses for agents with high thermal conductivities such as helium. Sheinson et al. found that the dominant physical effect of most fluorinated agents is to add thermal mass. CF_4 and SF_6, essentially inert, both extinguish n-heptane cup burner flames when the amount of agent added is such that the energy required to raise the temperature of the nitrogen and agent present, from 300 K to 1600 K, exceeds a critical value. This critical value is proportional to the amount of oxygen supplied, and is similar for CF_4 and SF_6. It is lower for non-fluorinated agents such as Ar, He, N_2, and CO_2, due to greater contributions of thermal conductivity and oxygen dilution to suppression for these agents.

In the present study, the extinction concentration for CF_4 was used to estimate the sensible enthalpy per mole of oxygen required to extinguish a methanol flame. The estimated extinction sensible enthalpy for this flame was found to be 322 kJ/mol O_2. Similarly, SF_6 extinction concentrations were used to obtain extinction sensible enthalpies for methane and propane flames of 254 kJ/mol O_2 and 258 kJ/mol O_2, respectively. In the case of n-heptane, both CF_4 and SF_6 extinction concentrations were available. The SF_6 data led to a sensible enthalpy value 1 % lower than that estimated from the CF_4 data. The average of the two values, 267 kJ/mol O_2, was chosen as the extinction sensible enthalpy for the n-heptane flame.

Physical contributions to suppression of other compounds can be estimated by assuming that they are inert and that they extinguish a given flame at the same sensible enthalpy per mole of oxygen as CF_4 and SF_6. The method is valid for compounds with physical contributions to suppression dominated by thermal mass addition, as they are for SF_6 and CF_4. Physical predictions for the extinction concentrations of the agents tested in this study are shown in Figure 3-5. The sensible enthalpies required to raise agent temperature from 300 K to 1600 K are provided in Table 3-1. A comparison of the measured and predicted extinction data reveals that the bromine- and iodine-containing compounds suppress flames mostly through chemical means, with physical contributions to suppression not exceeding 30 % regardless of fuel type. For all of the other agents, the chemical contribution to suppression does not exceed 35 %. The differences between the measured and predicted values for N_2 are consistent with the findings of Sheinson et al. For HFC-134 and HFC-245ca in methane, the actual extinction concentrations

are larger than the sensible enthalpy predictions. The net effect of fluorocarbon chemistry for these agents, which do not contain CF_3 groups, is to promote combustion.

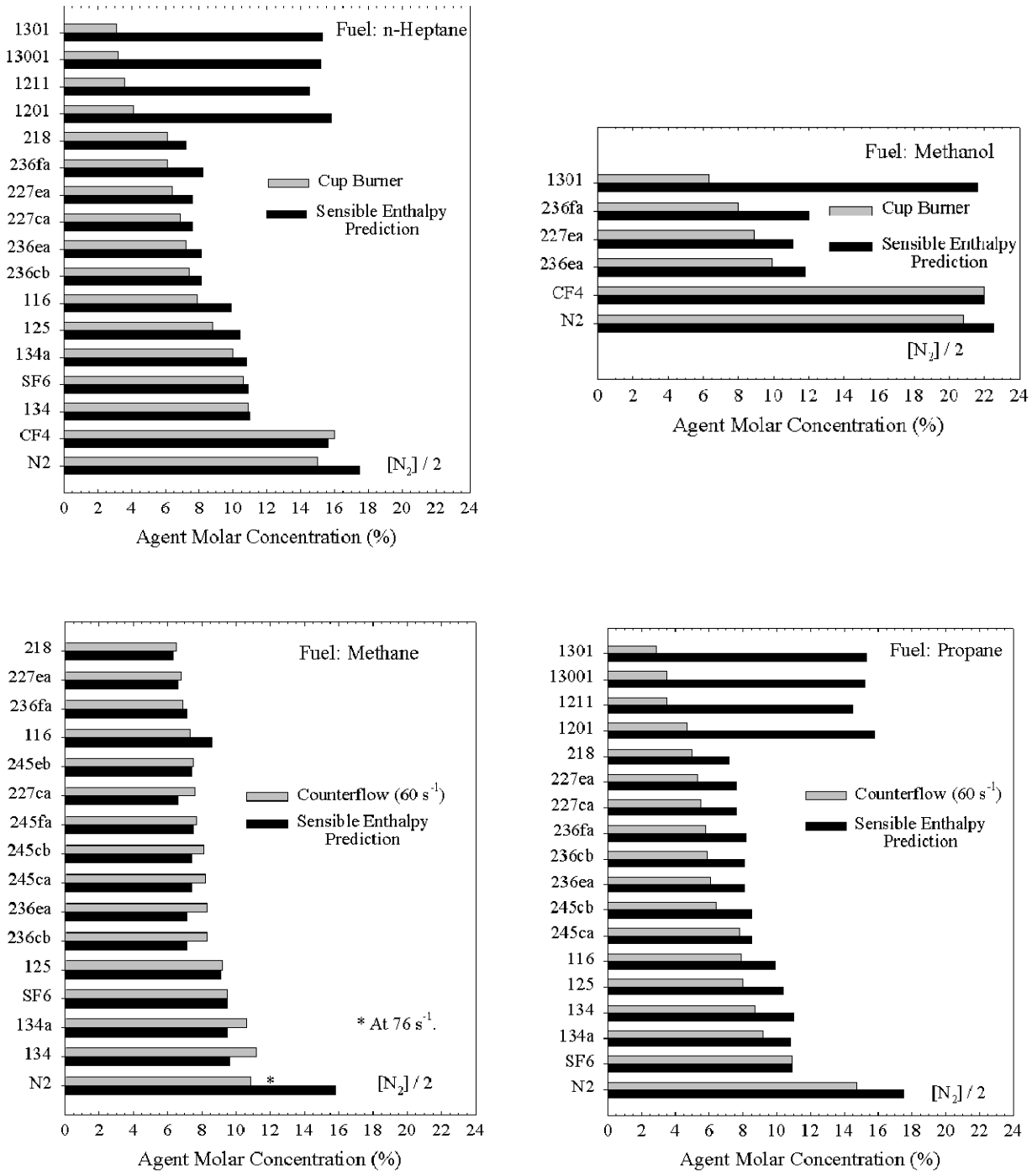

Figure 3-5. Extinction Concentrations for Agents Suppressing: (a) n-heptane/air Cup Burner Flames; (b) Methanol/air Cup Burner Flames; (c) Methane/air Counterflow Flames at a Strain Rate of 80 s^{-1}; (d) Propane/air Counterflow Flames at a Strain Rate of 80 s^{-1}.

Effect of Fuel Type on Suppression Effectiveness Ranking

The extinction data of Figure 3-5 show that agent effectiveness rankings were similar for the fuels tested. The bromine- or iodine-containing agents formed the most effective group of suppressants. FC-218, HFC-227ea, HFC-227ca and HFC-236fa constituted the next most effective group, followed by the remaining hexafluoropropanes and the pentafluoropropanes. HFC-245ca was the least effective of the fluorinated propanes tested, but was more effective than FC-116 and HFC-125. The tetrafluoroethanes and SF_6 were only more effective than CF_4 and N_2. The effectiveness ranking for methane, although similar to that of the other fuels, did exhibit some peculiarities. First, FC-116 appeared more effective than most of the fluorinated propanes. Second, within the 3σ experimental uncertainty of $\pm$ 0.8 mole %, all of the fluorinated propanes tested containing less than two CF_3 groups were equal in their ability to suppress methane flames at 80 s^{-1}.

Although the relative effectiveness of the various suppressant groups was similar for all the fuels tested, the exact ranking within a group depended on the fuel. Furthermore, the rankings extracted from the counterflow data were somewhat strain rate dependent. The position of the SF_6 extinction strain rate curve relative to those of the fluorinated ethanes illustrates this dependence.

Figure 3-3a shows that at strain rates between 400 s^{-1} and 500 s^{-1}, in a propane flame, SF_6 was more effective than HFC-125. Below 100 s^{-1}, it was less effective than both HFC-134 and HFC-134a. These extinction concentrations are all expressed on a molar basis. On a mass basis, the bromine- and iodine-containing agents were still the most effective suppressants, with all of the other agents tested, including N_2, exhibiting similar effectiveness.

Effect of Fuel Type on Agent Extinction Concentrations

Figure 3-5 shows that fuel type had an impact on the magnitude of the extinction concentrations, but not on the effectiveness ranking of the agents tested. The extinction concentrations obtained in the four different fuels are compared for several agents in Figure 3-6. Included are all of the agents tested in the n-heptane cup burner, with the exception of halon 13001, halon 1211, and halon 1201. The agents are ranked in order of decreasing n-heptane effectiveness, with the most effective agent as the top bar.

Figure 3-6 shows that, for the agents tested, methanol flames were more difficult to extinguish than the alkane flames. This was due in part to methanol's high sensible enthalpy of extinction relative to that of the alkanes. For all agents except halon 1301, between 30 % and 40 % more agent was required to suppress methanol flames relative to the n-heptane flames. For halon 1301, the required amount doubled. The greater reduction in the effectiveness of halon 1301 was attributed to a decrease in its chemical contribution to suppression. For n-heptane, chemical factors contribute 80 % to halon 1301's effectiveness. For methanol, they contribute 70 %.

Extinction concentrations for methane and propane non-premixed counterflow flames at 80 s-1 were similar to those for n-heptane cup burner flames. All 12 of the agents tested in both n-heptane and methane flames were more effective against the latter. The largest deviations between the two fuels occurred with N_2, 28 %, and HFC-116, 20 %. For 8 out of the 12 agents, the deviations were less than 10 %. In the case of propane, the largest deviations from the n-heptane values occurred with HFC-236cb, 25 %, and HFC-134, 22 %. For 4 out of the 13 agents tested in both fuels in Figure 3-6, the deviations were less than 10 %, with all 13 agents more effective in propane. Halon 1201 and halon 13001 were the

only agents more effective in n-heptane: 10 % more halon 1201 and 3 % more halon 13001 were required for propane flames. Counterflow experiments with both methane and propane at low strain rates yield extinction concentrations, in addition to effectiveness rankings, applicable to n-heptane cup burners.

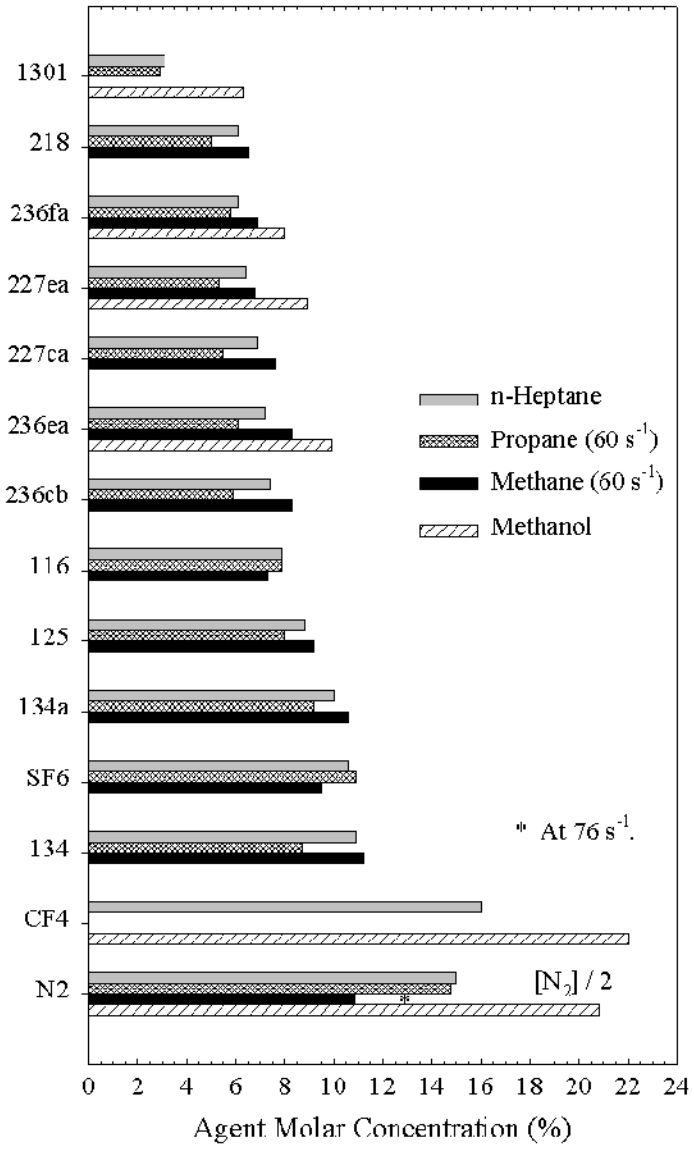

Figure 3-6. Effect of Fuel Type on Agent Extinction Concentration. The n-heptane and Methanol Data were Collected in a Cup Burner. The Methane and Propane Data were Collected in a Counterflow Burner at a Strain Rate of 80 s^{-1}.

Conclusions

Curves relating extinction strain rate to agent molar concentration were obtained for a variety of suppressants in methane/air and propane/air non-premixed counterflow flames. The list included four fluorinated ethanes, ten fluorinated propanes, four bromine- or iodine-containing halons, CF_4, SF_6 and N_2.

- The relative effectiveness of the fluorinated propanes correlated with the number of CF_3 groups in the agent's molecular structure. Effectiveness did not correlate significantly with any other structural feature.

- For agents with the same number of CF_3 groups, compounds with higher fluorine to hydrogen atom ratios were slightly more effective, particularly at low concentrations.
- The presence of CF_3 groups also correlated with an enhanced suppression performance of agents that contain bromine.
- Numerical predictions of the flame speed of doped methane/air mixtures indicated that HFC-134a, with one CF_3 group, caused a greater reduction in flame speed than HFC-134. Chemical kinetic analysis indicated that a difference in the major pathway for removal of the parent compound was primarily responsible.
- Overall, the fluorinated propanes were found to be more effective on a molar basis than the fluorinated ethanes. This was consistent with the greater sensible enthalpy of the former. For all the HFCs studied, the chemical contributions to suppression did not exceed 35 %.
- Bromine- or iodine-containing agents were more effective than compounds that contained fluorine as the sole halogen. These bromine- and iodine-containing agents suppressed flames mainly through chemical means, with physical contributions to suppression not exceeding 30 %.
- Fuel type did not affect agent effectiveness ranking, but did affect the magnitude of the extinction concentrations. Methanol flames were more difficult to extinguish than either methane, propane, or n-heptane flames, which were similar to each other. For halon 1301, the agent concentration required to extinguish a methanol cup burner was more than double the amount required to extinguish an n-heptane flame. For HFC-236fa, HFC-227ea, HFC-236ea, CF_4, and N_2, 30 % to 40 % more agent was required.

3.3 METAL-CONTAINING COMPOUNDS

3.3.1 Background

The NGP also conducted research to identify new, non-halocarbon suppressants and to understand the mechanisms of inhibition of known, effective agents.[85-87] Metal-containing compounds were of particular interest. Prior to the NGP, the behavior of metal compounds in flames had been studied with regard to several flame phenomena and had been found to be up to several orders of magnitude more effective flame inhibitors than the halogens.[34] While research had been conducted to understand metals in hydrocarbon fames, and progress had been made, a thorough description of the mechanisms of inhibition provided by these agents had yet to be delineated.

In the most obviously relevant work, metal-containing compounds have been added to flames in a number of screening tests, aimed specifically at assessing their potential as fire suppressants. Results from these tests have helped understand the compounds' influence on flame speed (premixed flames) and extinction (diffusion flames), as well as their effect on ignition. Flame studies have also been used to understand the detailed mechanism of inhibition by metal agents, either by providing direct experimental data on species present in the flame zone, or by validating numerical models which are then used to calculate the flame structure; either of these approaches are then used to develop an understanding of the relevant chemical kinetic mechanisms.

Studies of engine knock suppression by metal-containing compounds provided much early data on metals in flames. Since engine knock is known to occur from the rapid pressure rise (and subsequent detonations) inside an engine cylinder caused by too fast reaction of the homogeneous charge of fuel and air, the mechanisms of engine knock reduction may have clear relevance to fire suppression—in which the goal is again to reduce the overall reaction rate with the addition of the suppressing agent. In engines—as well as in heating applications—research has also been directed at understanding their efficacy at soot reduction. Although both soot formation and the overall reaction rate of flames are known to be related to the location and concentration of radicals in the flame, the effects of metals on soot formation are not reviewed here.

Other systems have been used to understand metal chemistry in flames. A large amount of fundamental work has been done with premixed, atmospheric pressure flat flames. The flat flame provides a nearly one-dimensional system, and the region above the flame (i.e., downstream of the main reaction zone) provides a long residence time, high temperature region for radical recombination. The H-atom concentration typically is measured with the Li-LiOH method (described later in this chapter), and the additive's effect on the radical recombination rate is determined. In addition, much detailed fundamental understanding has come from shock tube studies and flash photolysis studies in reaction vessels. Some studies of fire retardants are also relevant to fire suppression mechanisms of metals, such as when the fire retardant works by suppressing the gas phase reactions (and the subsequent heat release and heat feedback to the solid sample). Finally, after-burning in rocket nozzles provided motivation to understand metal-catalyzed radical recombination reactions, and modeling studies have been performed for those systems.

From these studies, it was clear that metals can have a profound effect on flame chemistry. Further, their effectiveness in these varied applications may well be related. In any event, data from each of the applications can provide insight into possible metals for application to fire suppression as well as provide fundamental data useful for predicting their performance in a range of applications. Work investigating the effect of metals for each of the applications is described in the remainder of this subsection.

The remainder of this section provides background on the current understanding of metal inhibition of flames, identifying metals with fire suppression potential, and presents fundamental data which can be used in future comparison with modeling results.

In particular, iron pentacarbonyl, $Fe(CO)_5$, has been found to be one of the strongest inhibitors, up to two orders of magnitude more effective than CF_3Br at reducing the burning velocity of premixed hydrocarbon-air flames.[88,89] Despite past research, a thorough description of its mechanism of inhibition had not been delineated. Iron pentacarbonyl forms particulates upon passing through a flame. Interestingly, other very effective inhibitors also involve a condensed phase. These inhibitors include those which form the particulates after passing through the flame as well as those which are initially added as a condensed phase. The former category includes other organometallics compounds such as lead tetraethyl and nickel carbonyl and the halometallic compounds $TiCl_4$ and $SnCl_4$,[34] as well as a new class of fire suppressants, pyrotechnically generated aerosols,[90] which may work similarly. The latter category includes the widely used alkali metal salt powders $NaHCO_3$ and $KHCO_3$,[91] other metal salts,[92] and a new type of suppressant, non-volatile organic precursors.[93] These condensed phase agents have many similarities, in particular, their strong inhibiting action and the lack of a complete understanding of their modes of inhibition.

Because $Fe(CO)_5$ is so effective, it was selected first for further study under the NGP. Although its toxicity prevents it from being used as a flame suppressant, an understanding of its inhibition mechanism was expected to help in developing new agents, and the experimental and analytical tools being developed would be useful for the study of other heterogeneous inhibitors. The approach was to use simple laboratory flames, both premixed Bunsen-type and counterflow diffusion, to obtain fundamental information on the action of iron pentacarbonyl. The burning velocity and extinction strain rate, both of which provide a measure of the overall reaction rate, were determined with addition of $Fe(CO)_5$, while varying the stoichiometry, oxygen mole fraction, flame temperature, and flame location. These experiments allowed control of the chemical environment, the location where the metal-containing species were formed, and the transport of these species to the reaction zone.

Studies of the inhibition mechanism of the iron are described, and are followed by a description of the reasons why it losses its effectiveness in some flame systems. The equivalent flame inhibiting species of other metal agents are then discussed, and evidence for any potential loss of effectiveness for these other metals is assembled.

Engine Knock

Agents that reduce engine knock may also be effective flame inhibitors, and it was useful to examine the literature of engine knock to search for possible moieties. Engine knock is the onset of detonation waves in an engine cylinder brought about by the homogeneous ignition of the end-gas region of highly compressed and heated fuel and air. The effect of some agents in reducing knock has been known since the 1920s, including compounds of bromine, iodine, tellurium, tin, selenium, iron, and lead, as well as aniline.[94] Tetraethyl lead (TEL) very early became the anti-knock agent of choice. While much subsequent research was performed to understand its mechanism of knock reduction, the exact mechanism for this agent remains an unsolved problem in combustion research (perhaps because leaded fuels were later banned due to their poisoning effect on exhaust catalytic converters). Although much progress was made, the researchers divided into two camps: those endorsing a heterogeneous mechanism[95] and those promoting a homogeneous radical recombination mechanism.[96]

Several known effects of lead in engines support the heterogeneous mechanism. Muraour[97] appears to have been the first to propose chain-breaking reactions on the surface of a colloidal fog formed from TEL. The particle cloud was subsequently shown to be composed of PbO, which is the active species.[98] Since a strong influence of PbO coatings on reaction vessel walls has also been observed,[98] a heterogeneous mechanism of PbO was assumed. Although other results support the heterogeneous mechanism, the evidence is somewhat circumstantial. The known *metallic* antiknock compounds (tetraethyl lead, tellurium diethyl, iron pentacarbonyl, nickel tetracarbonyl[95]) all produce a fog of solid particles. The alkyls of bismuth, lead, and thallium are anti-knocks, but those of mercury (which does not form particles) are not.[99] Richardson et al.[100] showed that carboxylic acids increase the research octane number of TEL in engines, and argued that they reduced agglomeration of the PbO particles in the engine end-gas, but acknowledged that their arguments were qualitative. Zimpel and Graiff[101] sampled end gases in a fired engine for transmission electron microscopy (TEM). They claimed that 1000 nm diameter particles formed prior to the arrival of the flame, proving that the effect of TEL was heterogeneous. Commenters to the paper pointed out, however, that the particles could be forming in the sampling system, that the effect of lead extenders was not captured in the particle morphology, and that even if particles form, the gas phase species can also be present, and it is thus not precluded that they are doing the inhibition.

Based on the work of Rumminger and Linteris,[102] even if particles form, they can re-evaporate in the hot region of the flame if they are small enough. Finally, as described by Walsh,[95] a major shortcoming in the work with TEL is that it is easily absorbed on the way to the reaction vessel, so that it is difficult to know how much TEL actually makes it to the flame. As subsequently described by Linteris and co-workers, the efficiency[103-107] and particle formation[102,108] of organometallic agents are strongly affected by the volume fraction of the metal compound.

In later work, Kuppo Rao and Prasad[109] claimed to prove the heterogeneous mechanism of lead anti-knock agents. They inserted copper fins coated with PbO into the cylinder of an engine, or injected 30 μm particles into the air stream, and found antiknock effects. They interpreted these results as evidence that the mechanism is heterogeneous. Nonetheless, they did not measure for the presence of gas phase lead compounds, so a homogeneous mechanism cannot be ruled out. For the eleven lead compounds tested, they found the effectiveness to vary by a factor of about six, and found similarly sized particles of CuO_2, CuO, $CuCl_2$, $NiCl_2$, and $SnCl_2$ to have equal effectiveness which was less than any of the lead compounds.

The early and strong evidence for a homogeneous gas phase inhibition mechanism of TEL was developed by Norrish.[96] Using flash photolysis of mixtures of acetylene, amyl nitrite, and oxygen in a reaction vessel, with and without TEL, the absorption and emission spectra of amyl nitrate, OH, Pb, PbO, NO, CN, CH, and TEL were obtained as a function of reaction progress. The reactants were chosen since, in the absence of anti-knock compounds, they showed the strong homogeneous detonation characteristic of engine knock. The researchers found that the induction time increased linearly with TEL addition at low TEL partial pressures, but that the effectiveness dropped off at higher pressures. This result was described subsequently for the flame inhibitors $Fe(CO)_5$,[88,103] $SnCl_4$[34,107] and $CH_3C_5H_4Mn(CO)_3$ (MMT).[107] After decomposition of TEL, Pb was present in low concentration, followed by large amounts of PbO and OH, which subsequently dropped off. With TEL addition, the formation of OH was retarded, and the increase in OH emission was smoother and better behaved. No particles were reported. Norrish et al. described the action of TEL as a two-stage homogeneous gas phase reaction mechanism. In the first stage, TEL reacts with the peroxide and aldehyde intermediates (characteristic of the end of the cool flame regime of alkane combustion), thus reducing the availability of these species for initiating the well-known second stage of the combustion. Gas phase PbO from the TEL then reacts with the chain-carrying intermediates to reduce the rate of heat release, slow the temperature rise, and reduce detonation. It is noteworthy that many of the features subsequently described by Linteris and Rumminger[110] as necessary for flame inhibition by iron compounds (effectiveness in the absence of particles, decreasing effectiveness with higher inhibitor concentration, key role of the metal monoxide species, and the necessary coexistence of OH and metal monoxide species) were shown in the 1950s by Norrish and co-workers to be necessary for effective knock reduction by TEL. Although it was of the highest quality, the findings of Norrish and co-workers were discredited by the engine community largely because the tests were not done in engines or with typical fuels. This work predated most of the important flame inhibition work of the 1970s by 20 years.

Flame Screening Tests

Papers describing the results of screening tests clearly demonstrated the superior effectiveness of some metal-containing compounds as flame inhibitors. The seminal work of Lask and Wagner[34] investigated the efficiency of numerous compounds for reducing the burning velocity of premixed Bunsen-type

hexane-air flames stabilized on a nozzle burner. They found the metal halides $SnCl_4$ and $TiCl_4$ to be quite effective at low volume fraction (and $GeCl_4$ about a factor of two less then these). In unpublished work, cited by others,[111] Lask and Wagner provide the measured flame speed reduction with addition of $SbCl_3$ to hexane-air flames, showing it to be about twice as effective as CF_3Br. They tested $Fe(CO)_5$, $Pb(C_2H_5)_4$, and CrO_2Cl_2 and found these to be spectacularly effective, with volume fractions of only 170 μL/L and 150 μL/L required for the first two to reduce the burning velocity by 30 %. (Although not quantified, they believed the effectiveness of CrO_2Cl_2 to be even higher.) They categorized the active species in the compounds they tested into two classes: the halogens, and the much more effective transition metals. Skinner and coworkers,[112] using a burner which produced conical flames, tested 80 compounds for reducing the burning velocity of premixed hydrogen-air flames (fuel-air equivalence ratio ϕ of 1.75). They found the most effective to be: tetramethyl lead TML $Pb(CH_3)_4$, $Fe(CO)_5$, $TiCl_4$, $SnCl_4$, $SbCl_5$, and TEL (in that order), with TEL only slightly better than CF_3Br, and TML about 11 times better. A limitation of this work, however, was that the agents were tested at only a single volume fraction. Since the efficiency of many agents is known to vary with their concentration,[103] such an approach can skew the relative performance rankings. Also, in the hotter, faster-burning hydrogen flames, the propensity to form particles from the metal oxides and hydroxides is less than in the slower, cooler hydrocarbon-air flames of other studies (see Rumminger et al.[102]). An additional flame screening test was performed by Miller,[113] who tested 15 compounds added to low-pressure (1.01 kPa) premixed and diffusion flames, and found $SnCl_4$, $POCl_3$, $TiCl_4$, $Fe(CO)_5$), WF_6, and CrO_2Cl_2 to have some promise.

Two screening tests involved the inhibition of propagating premixed flames through clouds of small solid particles of inhibitor. Rosser et al.[91] added metal salts as dispersions of fine particles (2 μm to 6 μm diameter) to premixed methane-air flames. They used the reduction in upward flame propagation rate through a vertical tube as a measure of the inhibition effect. They correctly described the effects of flame speed and particle diameter on the particle heating rate, and together with the volatilization rate for each compound, assessed the fraction of the particle which was vaporized. They quantified the effect of particle size on inhibition effectiveness, and showed that while additional agent decreased the flame speed, the effectiveness eventually saturated (i.e., beyond a certain additive mass fraction, additional inhibitor had a greatly reduced effect on the flame speed). They postulated a homogeneous gas phase inhibition mechanism involving H, O, and OH radical recombination reaction with the metal atom and its hydroxide. This mechanism had many of the features of subsequently described mechanisms[107,114-116] which are now believed to be correct. They also correctly understood that catalytic radical recombination relies upon a super-equilibrium concentration of radicals (commonly present in premixed flames and diffusion flames at higher strain), and that this provides an upper limit to the chemical effect of catalytically acting agents. Finally, they suggested that adding an inert compound as a co-inhibitor can overcome this limitation. A number of alkali metal sulfates, carbonates, and chlorides were tested, as well as cuprous chloride CuCl, which was found to be about twice as effective as Na_2CO_3 (after correcting for the larger size of the CuCl particles).

A later study involving premixed flames with particles was performed by deWitte et al.[117] In it, relatively large particles (100 μm diameter) were electrostatically suspended in a tube and then injected into a downward facing premixed Bunsen-type flame, and their effect on the flame temperature, burning velocity, and extinction condition was measured. Various barium, sodium, and potassium compounds were tested, as well as $AlCl_2$, $CuCl_2$, and PbO. The authors noted a thermal and chemical effect of the particles, and assumed that the chemical effect was due to recombination of chain-carrying radicals on the particle surfaces. The authors estimated that for these large particles, little of the particles could be

vaporized. Nonetheless, it is not possible to separate the heterogeneous and homogeneous inhibition effects from their data. The authors found particles of $CuCl_2$ and PbO to be about two and eight times as effective as particles of Na_2CO_3, and surprisingly, found $AlCl_3$ to be about three times as effective.

Flame screening tests of many compounds were performed by Vanpee and Shirodkar[92] to test the relative effectiveness of metal salts. The metal acetonates and acetylacetonates were dissolved in ethanol, and fine droplets of the metal salt solutions were sprayed into the air stream of a counterflow diffusion flame over an ethanol pool. The inhibition effect was quantified, at a given air flow velocity (i.e., strain rate) as the change in the oxygen volume fraction at extinction caused by addition of the inhibitor, normalized by the inhibitor volume fraction (Mole merit number = $(X_{O_2,ext} - X_{O_2,ext,i})/X_i$, in which $X_{O_2,ext,i}$ and $X_{O_2,ext}$ are the oxygen volume fractions required for extinction, with and without added inhibitor, and Xi is the volume fraction of inhibitor in the oxidizer stream). Their results are depicted in Figure 3-7, which shows the metal compounds tested, listed from most effective to least. The maximum and minimum values of the mole merit number are listed for the range of oxidizer velocities of the tests (50 cm/s to 60 cm/s).

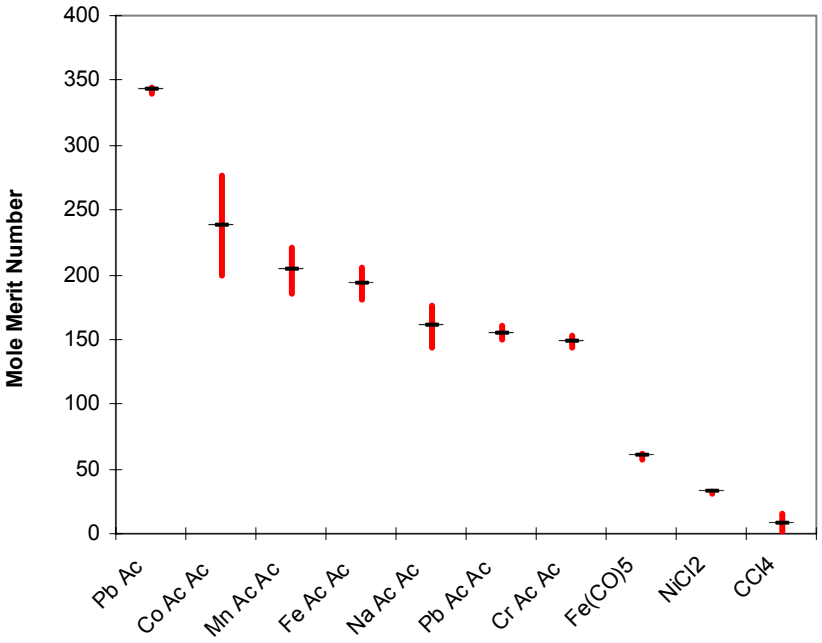

Figure 3-7. Mole Merit Number of Metal-containing Compounds for the Oxidizer Velocities in the Range of 50 cm/s to 60 cm/s.[92]

As the figure shows, the metal salts of Pb, Co, Mn, Fe, and Cr all showed some inhibition effect. Interestingly, $Fe(CO)_5$ was not as effective as iron acetylacetonate, and for lead, the acetonate was about twice as effective the acetylacetonate. It should be noted, however, that the interpretation of the present data are complicated by several effects. First, changing the oxygen mole fraction changed the temperature, which can change the effectiveness of an agent, as subsequently described in References 103-105, 118, and 119. Since the air stream velocity was changed while holding the nebulizer flow constant, the ethanol concentration changed in these partially premixed diffusion flames. Adding changing amounts of a fuel species (i.e., the carrier ethanol) in the air stream, changed the flame location and the scalar dissipation rate for a given strain rate (i.e., air flow velocity), so that the extinction condition was modified (as discussed in References 73 and 120). The size of the residual particle (which will vary from agent to agent) could affect its ability to vaporize in the flame, affecting the indicated efficiency. Finally, for metal agents that condense, their marginal effectiveness was a very strong

function of the concentration at which they are added. Hence, without knowing what the additive mole fraction was, it is difficult to cross compare the effectiveness of the different agents. For these reasons, the results shown in Figure 3-7 are considered qualitative, rather than quantitative. For example, subsequent studies[121] have rated iron as about 10 times as effective as sodium, in contrast to the results of Vanpee and Shirodkar, which show the acetylacetonate of iron to be only about 20 % more effective than that of sodium.

Radical Recombination above Premixed Flames

Much of the understanding of the homogeneous gas phase flame inhibition by metals came from studies of H-atom recombination rates above premixed, fuel rich, H_2-O_2-N_2 burner-stabilized premixed flames. The techniques, pioneered by Sugden and co-workers,[122-124] involve absorption spectroscopy for OH, and the Li/LiOH technique for H atom. (In the latter technique, the strong absorption lines of Li and Na are simultaneously measured above a flat flame. With the assumptions that Na is present in the flame only in atomic form and that Li is present only as Li and LiOH, the measured ratio of the Li to Na absorption together with the known equilibrium constant for the reaction Li + H_2O = LiOH + H provides [H].) In some of their early relevant work they determined the dominant metal species in H_2-O_2-N_2 premixed flames above Meker burners with added dilute sprays from aqueous salts of copper and manganese. Copper was found to exist mostly as Cu in the flame, and the dissociation constants of CuH[125] and CuOH[124] were determined from their concentrations above the flame at different temperatures.

The copper-containing species present above a Meker burner supplied with H_2-N_2-O_2 mixtures with added copper salts were found to be Cu, CuO, CuOH, and CuH.[124,125] Their concentrations were related by the balanced reactions:

$$Cu + H_2O \leftrightarrow CuOH + H$$

$$Cu + OH + X \leftrightarrow CuOH + X$$

$$Cu + H_2 \leftrightarrow CuH + H$$

$$Cu + H + X \leftrightarrow CuH + X\,.$$

In a detailed study of chromium, Bulewicz and Padley[126] added μL/L levels of Cr (from either chromium carbonyl or aqueous sprays of chromium salts) to a premixed, fuel-rich, flat-flame burner of H_2+O_2+N_2, and measured the catalytic radical recombination by the chromium compounds. They identified the active chromium species as Cr, CrO, CrO_2, and $HCrO_3$ and also detected solid particles, which appeared to have equivalent black-body temperatures up to 500 K higher than the gas. They estimated an *upper limit* for the rate of heterogeneous radical recombination on the particle surfaces, and estimated that, at an upper limit, it was the same order as the natural un-catalyzed recombination rate in the flame. They also found that Cr showed measurable catalytic radical recombination even when added at volume fractions of about 1μL/L, at which heterogeneous particle catalysis cannot be contributing. They cited Jenkins (1969, personal communication) as first showing the catalytic effect of metals (Ca, Sr, Ba) on radical recombination in flames. Interestingly, their data showed a saturation effect in the catalytic radical recombination by Cr species, and their analyses showed that it is due, not to condensation of the active gas phase Cr-containing species to particles, but to reduction in the available radicals to recombine.

Bulewicz and Padley proposed that the following balanced reactions are important in chromium inhibition, but did not develop an explicit mechanism:

$$Cr + OH \leftrightarrow CrO + H$$

$$CrO + OH \leftrightarrow CrO_2 + H$$

$$CrO_2 + H_2O \leftrightarrow HCrO_3 + H\ .$$

Further, they speculated that at very low additive concentrations, the following gas phase reactions might be important:

$$CrO + H + X\ => CrOH^* + X$$

$$CrOH^* + H\ => CrO + H_2\ .$$

In continuing work, Bulewicz and coworkers[115,116] studied the catalytic effects of 21 metal species for recombining chain-carrying flame radicals present at super-equilibrium levels above premixed, fuel rich, flat flames of H_2+O_2+N_2 at 1860 K. Table 3-3 shows the ratio of the catalyzed to uncatalyzed recombination rate for H atom caused by each of the metals, added at 1.3 μL/L.

Table 3-3. Catalytic Efficiency of Different Metals in Promoting Radical Recombination.
Values of k_{obs}/k_{uncat} (T = 1860 K; X[M] = 1.3 μL/L; $H_2/O_2/N_2$ = 3/l/6)

Strong Effect		Some Effect		No Effect	
Cr	2.8	Co	1.1	V	1
U	1.82	Pb	1.1	Ni	1
Ba	1.75	Zn	1.07	Ga	1
Sn	1.6	Th	1.06	Cl	1
Sr	1.35	Na	1.04		
Mn	1.3	Cu	1.04		
Mg	1.25	La	1.04		
Ca	1.25				
Fe	1.2				
Mo	1.16				

The cut-off value for this ratio was arbitrarily set to 1.1, and those above that value were described as having a strong catalytic effect. The possibility of heterogeneous recombination on particles was admitted, but at these low volume fractions, the authors argued primarily for a homogeneous gas phase mechanism involving H or OH reaction with the metal oxide or hydroxide (attributed to Jenkins).

$$H + MO + (X) = HMO + (X)$$

$$HMO + OH\ (\text{or } H) = MO + H_2O\ (\text{or } H_2),$$

in which M is a metal, and X is a third body.

Concurrent with the alkaline earth metals, Cotton and Jenkins[114] showed that Ca, Sr, and Ba added as a fine mist of a salt solution to premixed H_2+N_2+O_2 flat flames catalyzed the radical recombination for additive volume fractions in the range of 1 μL/L to 10 μL/L. By estimating the reaction rates in possible recombination mechanisms, they recommended the radical recombination mechanism to be:

$$MOH + H \Rightarrow MO + H_2$$

$$MO + H_2O(+X) \Rightarrow M(OH)_2(+X)$$

$$M(OH)_2 + H \leftrightarrow MOH + H_2O.$$

Jenkins and co-workers extended their studies of metal-catalyzed radical recombination in premixed flames to study soot formation in diffusion flames. The strong effect of metals on soot formation in flames is well-known.[127] Cotton et al.[128] added 40 metals to co-flow diffusion flames of propane and N_2/O_2 mixtures and measured their effect on soot emissions and the smoke point. They postulated a mechanism for soot reduction whereby the catalytic reaction scheme listed above ran backwards, dissociating H_2O and H_2 into OH and H, which then oxidized the soot particles.

The question of heterogeneous versus homogeneous gas phase chemistry was investigated by Bulewicz et al.[129] Through examination of the variation of the intensity of emitted radiation as a function of wavelength from particles formed above a premixed H_2+O_2+N_2 flat flame with added spray of aqueous uranium salt, they determined that the particles (presumably uranium oxide) were up to 500 K above the gas temperature. They interpreted the particle temperature rise to be caused by the catalytic recombination of H and OH on the particle surfaces. Nonetheless, Tischer and Scheller[130] pointed out that the spectral variation of the particle emissivity was unknown, and the gray-body assumption of Bulewicz was probably unjustified. They also argued that the excess temperature may have been due to surface reactions other than radical recombination.

In similar work with premixed, fuel rich, flat flames of H_2+O_2+N_2, Jensen and Jones[131] extended the classic $Li + H_2O \leftrightarrow LiOH + H$ photometric method to include the equilibrium for the reaction

$$Sr^+ + H_2O \leftrightarrow SrOH^+ + H\ ,$$

in which $[SrOH^+]/[Sr^+]$ was measured mass spectrometrically. Using both this new technique as well as the LiOH photometric method, they studied the catalytic flame radical recombination by tungsten and molybdenum, as well as once again confirming the strong effect of tin. Using flames at temperatures of 1800 K to 2150 K, and with metal addition at 1 μL/L to 110 μL/L, they collected data on the rates of radical recombination in the presence of the metallic catalysts (added as tetramethyl tin, or hexacarbonyls of tungsten or molybdenum), and measured the major species present in flames inhibited by W and Mo. By analogy with the mechanisms they developed for calcium[114] and iron[132] in flames, they then postulated reaction mechanisms for W and Mo, and estimated the rates for the reactions in the catalytic cycles. For the conditions of their flames, the radical recombination cycles, for either W or Mo, were about five times faster then those of tin. (Using the results of Linteris et al.,[107] this translates to an effectiveness about 10 times that of CF_3Br, or about one-fifth that of $Fe(CO)_5$). For tungsten and molybdenum, the cycles are:

$$HWO_3 + H \leftrightarrow WO_3 + H_2$$

$$WO_3 + H_2O \leftrightarrow H_2WO_4$$

$$H_2WO_4 + H \leftrightarrow HWO_3 + H_2O$$

$$\text{(net: } H + H \leftrightarrow H_2\text{)}$$

and

$$HMoO_3 + H \leftrightarrow MoO_3 + H_2$$

$$MoO_3 + H_2O \leftrightarrow H_2MoO_4$$

$$H_2MoO_4 + H \leftrightarrow HMoO_3 + H_2O$$

$$\text{(net: } H + H \leftrightarrow H_2\text{)}.$$

Jensen and Jones[131] found the dominant species in tungsten and molybdenum inhibition to be WO_3, HWO_3, and H_2WO_4, and MoO_3, H MoO_3, and H_2MoO_4.

In continuing work, Jensen and Jones[133] used similar techniques to study the radical recombination by cobalt added to a premixed, fuel rich, flat flame of H_2-N_2-O_2. With Co added as cyclopentadienylcobalt dicarbonyl at volume fractions of about 0.03 □L/L to 145 □L/L, and flame temperatures ranging from 1800 K to 2615 K, they spectroscopically identified the dominant cobalt-containing species to be Co, CoO, CoOH, and $Co(OH)_2$, with most of the cobalt being present in the flame as free Co atoms. Again by analogy with the Ca and Fe mechanisms, the Co mechanism was postulated to be:

$$Co + OH \Rightarrow CoO + H$$

$$CoOH + H \leftrightarrow Co + H_2$$

$$CoO + H_2O \leftrightarrow Co(OH)_2$$

$$Co(OH)_2 + H \leftrightarrow CoOH + H_2O$$

$$\text{(net: } H + H \leftrightarrow H_2\text{)},$$

with the first step added since Co is the dominant Co-containing species. The rates of these catalytic steps were again inferred from the experimental data. Cobalt appeared to be about 2/3 as effective as tin in these flames.

Gas phase Flame Retardants

Insight into mechanisms of metal flame inhibition was gleaned from studies of metal species added to materials as fire retardants (when their mode of action has been found to be in the gas phase). One such system is the antimony - halogen combination. Although they did not unravel the detailed mechanism, Fenimore and coworkers[134-137] showed that the relevant species act in the gas phase; they believed that the antimony moieties poisoned the flame, much as do brominated species. Similarly, Martin and Price[138] observed that the addition of triphenylantimony to certain polymer substrates provided fire retardancy, even in the absence of halogen, and believed the mechanism involved antimony species in the gas phase.

In a series of detailed experiments, Hastie and co-workers determined the mechanism of flame inhibition in the antimony-halogen system. Using a Knudsen effusion cell containing Sb_2O_3 over which passed HCl, they showed that $SbCl_3$ was evolved through a series of halogenation steps involving successive oxychloride phases.[139] Using a molecular beam mass spectrometer, they studied both the pyrolysis products of polyethylene retarded by antimony-oxide/halogen, as well as intermediate species profiles in premixed $CH_4/O_2/N_2$ flames with added $SbCl_3$ and $SbBr_3$.[140] For the pyrolysis studies, the major effused species from the polymer were $SbCl_3$ and SbOCl. In the flame studies,[141] they found that $SbCl_3$ reacted readily to SbOCl, which then reacted with H to form SbO. They measured the major intermediate species

of $SbBr_3$ flame inhibition to be SbO, Sb, HBr, and Br. They also measured the decrease in the hydrogen atom volume fraction with addition of $SbBr_3$, and developed a reaction sequence for the formation of the intermediate species, as well as for the gas phase inhibition reactions. They argued strongly that the inhibition effect of antimony-oxide/halogen system was predominantly from the reaction sequence:

$$\begin{aligned} SbO + H &\rightarrow SbOH^* \\ SbOH + H &\rightarrow SbO + H_2 \\ \hline \text{net: } H + H &\rightarrow H_2 \end{aligned}$$

with a smaller effect from the usual bromine sequence, and an even smaller contribution from the equivalent chlorine cycle.

Ignition Studies

The effect of metals on ignition has been studied in both shock tubes and flames. Morrison and Scheller[111] investigated the effect of twenty 20 inhibitors on the ignition of hydrocarbon mixtures by hot wires. They found that $SnCl_4$ was the most effective inhibitor tested for increasing the ignition temperature, whereas the powerful flame inhibitors CrO_2Cl_2 and $Fe(CO)_5$ had no effect on the ignition temperature. Dolan and Dempster[142] studied the effect of small particles (5 μm to 10 μm diameter) of metal compounds on suppressing the spark ignition of premixed natural gas-air mixtures in a vertical 7 cm diameter tube. They found that barium hydroxide octahydrate, barium chloride, and copper acetate monohydrate were each about three times less effective than sodium bicarbonate particles, while cuprous oxide and cobaltous chloride hexahydrate were each about 20 % less effective than $NaHCO_3$. Several studies have shown that metals can actually speed the ignition process in some chemical systems. In shock-tube studies, Matsuda and co-workers[143] found that $Cr(CO)_6$ *reduced* the initiation time for reaction of CO or C_2H_2 with O_2 in shock-heated gases. The metal carbonyl was present at 0 μL/L to 50 μL/L, so the presence of any particles was precluded. The mode of action was believed to be gas phase reactions involving CrO, CrO_2, and CrO_3. In later shock-tube work with $Fe(CO)_5$ in mixtures of CO-O_2-Ar, Matsuda[144] found that a volume fraction of $Fe(CO)_5$ of few hundred μL/L greatly accelerated the consumption of CO_2. They postulated the effect to be due to oxidation of CO by metal oxides via: FeO + CO => Fe + CO_2, and noted that these reactions may be of importance since the mixtures were quite dry ($X_{OH} \approx 5$ μL/L). Interestingly, such accelerating oxidation pathways were also found to be important in the dry reaction of CO with N_2O in flames.[145] In recent shock tube studies of CH_4-O_2-Ar mixtures, Park et al.[146] found that with (500, 1000, or 2000) μL/L of $Fe(CO)_5$, the ignition time was shorter than without the additive, again indicating a promotion effect of the metal additive; however, they did not determine the cause of the promotion for this moist system. Finally, in flash photolysis studies many years ago, Erhard and Norrish[96] found that unlike $Pb(C_2H_5)_4$ and $Te(CH_3)_2$ which retarded hydrocarbon combustion, $Ni(CO)_4$, $Fe(CO)_5$, and $Cr(CO)_6$ all greatly accelerated the combustion.

Radical Recombination in Rocket Nozzles

Jensen and co-workers were motivated to study combustion inhibition by metal compounds largely by the desire to suppress afterburning in rocket nozzle exhausts. Using mechanisms developed for K, Ba, Fe, Mo, W, Cr, and Sn, Jensen and Webb[147] calculated the amount of inhibitor required to suppress afterburning in the exhaust plume of a double-base propellant (unspecified composition, but usually a

homogeneous mixture consisting of nitrocellulose and nitroglycerine). The products of the propellant reactions consisted of a fuel rich mixture, principally CO and H_2, much like the recombination region above the fuel-rich premixed H_2-O_2-N_2 laboratory flames used to study the metal-catalyzed radical recombination. Their calculations (which did not include the effects of condensation to particles) indicated that W and Mo were about a factor of five less effective than Fe, Cr was about a factor of six less effective, and Sn was more than seven times less effective. These results are consistent with those of the flat flame measurements described above.

Jensen and Webb did not measure particles or calculate the degrading effects of particle formation on the suppression of afterburning in rocket motors, but they did estimate the upper limit for radical recombination by the heterogeneous reactions on the particle surfaces. Their calculations indicated that although significant, the heterogeneous reactions could not suppress the afterburning, even for the smallest particle diameters assumed (10 nm). They also estimated that although the inhibiting species were probably volatilized in the combustion chamber, the characteristic times for condensation were probably of the same order as the residence time in the nozzle, indicating the potential for condensation. Their conclusions were that the metals held good promise for afterburning suppression in rocket motors, and that further work was necessary to estimate the rates of the catalytic cycle reactions and of the condensation rates of the metal derivatives under the conditions in their system.

Other Relevant Investigations of Metal Compounds in Combustion Systems

There have been a number of recent papers dealing with metals in flames. Crosley and co-workers[148] added MMT to premixed flames with the purpose of studying its effect on NO formation. Adding MMT at volume fractions of about 0.5 μL/L to near-stoichiometric premixed low-pressure (522 Pa) propane-air flat flames in a McKenna burner, they measured the temperature and the relative concentrations of OH, H, O, CH, NO, and CO through the flame. While they observed no discernable effect of the MMT, this may have been due either to the low concentration of the additive, or the low pressure, both of which could limit the influence.[89,107] They did, however, start to develop a mechanism for manganese which served as a basis for future efforts.[107]

Chromium reaction in a atmospheric pressure, premixed hydrogen-air flat flame was studied by Yu et al.[149] Using microprobe gas sampling in the region downstream from the main reaction zone, they collected chromium species in the gas and condensed phase. The particle size distribution and the fraction of Cr as Cr(VI) was determined as a function of position. In addition, they assembled a kinetic mechanism for Cr reaction in flames through analogy with boron and aluminum combustion, and used the mechanism, together with the measured temperature profile, to calculate the fraction of hexavalent Cr in the downstream region from the flame zone. They also modeled the growth (but not the reaction) of the particle phase. For both particle growth and Cr(IV) formation, the calculations were able to predict the experimental trends. They concluded that further kinetic model development was necessary for accurate treatment of Cr speciation in flames. In later work, Kennedy et al.[150] studied the morphology of the particles formed in a hydrogen–air–nitrogen co-flow diffusion flame with added chromium nitrate or chromium hexacarbonyl. They found that the morphology of the particles varied with the temperature of the flame and the source of the chromium.

Kellogg and Irikura[151] performed theoretical calculations to predict the heats of formation as well as the enthalpies and free energies of reaction for the FeO_xH_y species thought to be important in iron inhibition.

They found that nearly all of the reactions involving these species and potentially contributing to flame inhibition are exergonic at 1500 K. Hence, they suggested that further refinement of the inhibition mechanisms of iron would require knowledge of the actual kinetic rates of the inhibition reactions to improve upon the preliminary estimates of Rumminger et al.[104]

In a comprehensive review of possible chemicals for use as halon alternatives, Tapscott et al.[152] suggested that of the metals, Cu, Fe, Mn, and Sn, were worthy of further study. Since that time, premixed[107] and co-flow diffusion flame[153] studies have been performed for compounds containing Fe, Mn, and Sn. No additional work has been reported for copper compounds as fire suppressants.

Detailed Studies with Iron

After the potential effectiveness of iron as a flame inhibitor was indicated,[34,95,99] the behavior of iron pentacarbonyl was investigated in detail in several old investigations. The extraordinary flame inhibiting effectiveness of iron was first identified by Lask and Wagner[34] in their screening study involving methane-, hexane-, and benzene-air premixed Bunsen-type flames with numerous additives. In continuing work,[89] Wagner and co-workers described the superior effectiveness of $Fe(CO)_5$ for reducing the burning velocity of hydrocarbon-air flames in nozzle burners. They found that an $Fe(CO)_5$ volume fraction of 100 μL/L reduced the burning velocity by 25 % when added to stoichiometric methane-air flames at atmospheric pressure. With oxygen as the oxidizer, or at reduced pressure, they found the effectiveness to be lowered. For hydrogen-air flames, $Fe(CO)_5$ was again much more effective than Br_2. They noted that at low volume fractions, the decrease in the burning velocity was proportional to the concentration of $Fe(CO)_5$, whereas for increasing concentrations of $Fe(CO)_5$, the relative influence seemed to decrease. They postulated a homogeneous radical recombination mechanism at low volume fraction, and a heterogeneous one at higher.

To understand the detailed mechanism of $Fe(CO)_5$, Bonne et al.[89] spectroscopically investigated premixed flat flames of methane with air or O_2. Unfortunately, at the low pressures for which the flame zone was expanded sufficiently to optically probe the flame (800 kPa), the kinetic effect of $Fe(CO)_5$ was very small. Nonetheless, for $Fe(CO)_5$ volume fractions up to 100 μL/L they observed that (1) the peak OH volume fraction X_{OH} was unchanged, but shifted slightly downstream from the burner, and (2) the decay rate of X_{OH} was increased in the presence of $Fe(CO)_5$, clearly indicating the effect of $Fe(CO)_5$ on radical concentrations in the flame. They measured FeO and Fe emission, as well as Fe absorption, and found that Fe and FeO emission peaked in the main high-temperature reaction zone, implicating these species in the radical recombination reactions. Although FeO had a double peak, with a minimum at the location where the rate of OH recombination was greatest, the authors did not feel that the decrease in FeO emission was correlated with a decrease in FeO concentration. They noted that solid particles were forming, that they were attempting to measure them, and said that the results of these measurements would be reported in the future (but no publications subsequently appeared).

In later work, the high effectiveness of iron was confirmed for methane-air premixed Bunsen-type flames, and extended to counterflow diffusion flames, by Reinelt and Linteris.[103] Their work indicated clearly that iron was very effective at low concentration, but that the effectiveness leveled off at higher concentration. Further studies with premixed flames of $CO\text{-}O_2\text{-}N_2$ and$CO\text{-}N_2O\text{-}N_2$ confirmed the effectiveness of $Fe(CO)_5$ in other systems.

3.3.2 Metals with Demonstrated Flame Inhibition Potential

Based on the above, Table 3-4 presents a list of metals whose compounds have demonstrated inhibitory effects in flame systems. The type of flame system used to determine the effectiveness is listed across the top (Note: FR denotes Fire Retardant). Under each category of flame system, the individual reference is listed. The elements are listed in the approximate order of demonstrated or expected effectiveness. Note, however, that there is large uncertainty in this ranking.

Table 3-4. Metals Which Have Shown Flame Inhibiting Properties.

	Detailed Flame Studies					Engine Knock					Flame Screening Tests						Flat Flame Radical Recombination						Ignition			FR
Element	89	103	107	106	153	99	94	109	96	95	34	92	112	113	117	91	116	115	126	133	131	132	142	111	96	139
Cr											x	x		x			x	x	x							
Pb						x	x		x	x	x	x	x		x		x									
Fe	x	x		x	x	x	x			x	x	x	x	x			x					x				
Mn			x		x																					
Ni								x		x																
W														x							x					
Mo																	x				x					
Cu								x							x	x	x						x			
Te							x		x	x																
Tl						x																				
Bi						x																				
U																	x	x								
Zn																		x								
La																		x								
Th																		x								
Se							x																			
Sn			x		x		x	x			x		x	x			x	x			x		x	x		
Ti											x		x	x												
Co												x					x			x			x			
Ge											x															
Sb											x		x													x

3.3.3 Flame Inhibition by Iron-containing Compounds

Recent results provide convincing evidence that the strong flame inhibition by iron is due to a homogeneous gas phase mechanism, which is described below. Following that, the experimental data showing iron's loss of effectiveness is described, along with a discussion of the parameters which most affect the particle formation which is believed to cause the loss of effectiveness.

Gas Phase Mechanism

A detailed mechanism for the gas phase iron-catalyzed radical recombination in flames was developed by Jensen and Jones,[132] and later, expanded by Rumminger et al.[104] In both, the main catalytic cycle leading to radical recombination was postulated to be:

$$\begin{aligned} FeOH + H &\leftrightarrow FeO + H_2 \\ FeO + H2O &\leftrightarrow Fe(OH)_2 \\ Fe(OH)_2 + H &\leftrightarrow FeOH + H_2O \\ \hline (\text{net: } H + H &\leftrightarrow H_2). \end{aligned}$$

This mechanism is shown schematically in Figure 3-8.

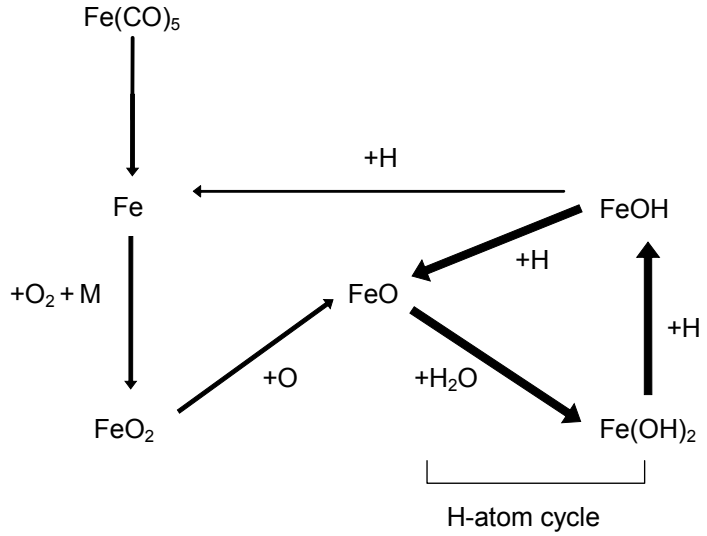

Figure 3-8. Main Catalytic Radical Recombination Cycle of Iron Found to be Important for Methane-air Flames.

Although the mechanism described in Rumminger et al. also included other catalytic cycles, they were not found to be particularly important in methane-air flames, premixed or diffusion.[105] In work with premixed CO-N_2-O_2 flames, however, the following additional catalytic cycle was found to be much more important than the H-atom cycle:

$$\begin{aligned} Fe + O_2 + M &\leftrightarrow FeO_2 + M \\ FeO_2 + O &\leftrightarrow FeO + O_2 \\ FeO + O &\leftrightarrow Fe + O_2 \\ \hline (\text{net: } O + O &\leftrightarrow O_2) . \end{aligned}$$

This new O-atom cycle together with the H-atom cycle are shown in Figure 3-9. Thicker arrows correspond to higher reaction flux. Reaction partners are listed next to each arrow.

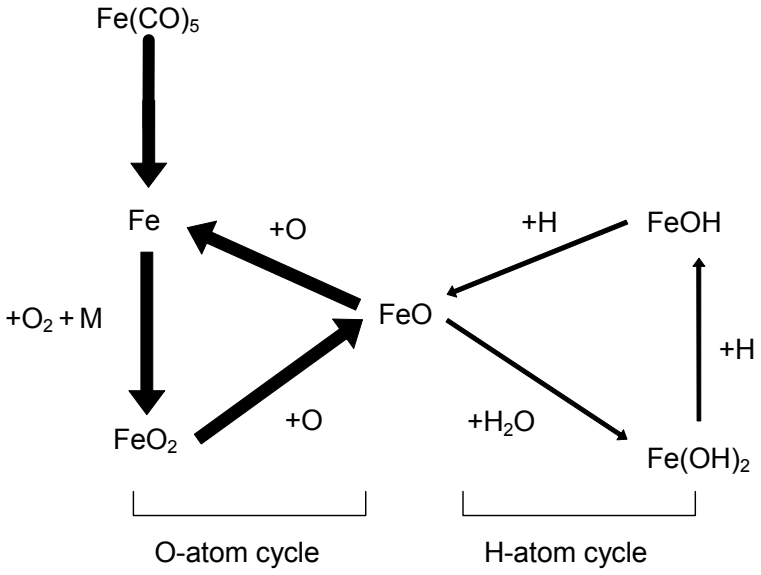

Figure 3-9. Radical Recombination Reaction Pathways Found to be Important for CO-H_2-O_2-N_2 Flames.[118]

Further, more recent computations of the thermochemistry of iron compounds at flame conditions support the possibility of many more radical recombination cycles.[151] In that study, seven iron species thought to exist at flame temperature were considered: Fe, FeH, FeO, FeOH, FeO_2, FeO(OH), $Fe(OH)_2$,[104] and the heat of reaction at 0 K, and the change in Gibbs free energy at 1500 K were calculated. Based on the results, however, very few of the considered reactions and cycles could be eliminated based on the thermodynamics. The complexity of the situation is illustrated in Figure 3-10, (Kellogg and Irikura[151]), which shows schematically the possible inhibition cycles of iron. (Note that in the figure there are on the order of 50 possible *cycles* since [Fe] can be replaced by Fe, FeH, FeO, or FeOH.)

It is important to observe that even for iron, for which the most research has been performed, the mechanism is in very early stages of development. For example, the rates of the most important reaction steps in the mechanism were selected (within the uncertainty bounds suggested by Jensen and Jones[132]) so as to provide the best agreement with experiments. The mechanism has been tested only for near stoichiometric premixed CH_4-N_2-O_2 , CO-N_2-O_2, and CO-N_2O premixed flames, CH_4-O_2-N_2 counterflow diffusion flames, and CH_4-air cup burner flames. Although at low Fe additive mole fraction the agreement was usually good, there were some conditions for which the predicted inhibition was off significantly. These cases include lean premixed CH_4-air flames (ϕ=0.9), CH_4-O_2-N_2 flames with an oxygen volume fraction in the oxidizer of 0.20, and the cup burner flames with added CO_2 (at very low $Fe(CO)_5$ volume fraction).

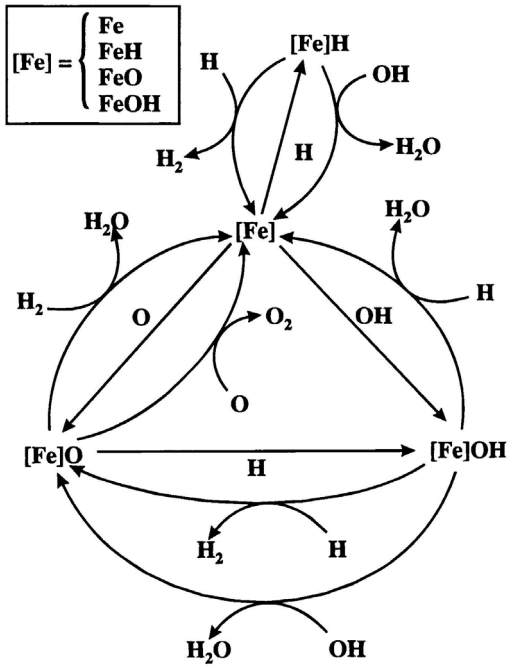

Figure 3-10. Different Classes of Reactions Which May Contribute to Iron's Super-efficient Flame Suppression Ability through the Catalytic Recombination of Radical Species.[151]

The main ramification of the above gas phase inhibition mechanism for fire suppression is that lowering radical concentrations lowers the overall reaction rate in the flame, weakening it. In laboratory flames, radical concentrations typically go above equilibrium levels, to super-equilibrium levels. This is particularly true for both premixed and high and moderate strain counterflow diffusion flames. At low strains, however, the radical super-equilibrium is less. (See Figure 3-11.) Radical concentrations in actual fires have not been measured. Nonetheless, recent research using cup burner flames[154] (which, to some extent, resemble small-scale fires) has shown that a stabilization region at the flame base, called the flame kernel, resembles a near-stoichiometric low-temperature premixed flame. Hence, the gas phase *catalytic* radical recombination cycles should be as important in the stabilization of fires as they are for laboratory flames. This is partially confirmed since other gas phase catalytic agents (for example, CF_3Br) are effective in both laboratory flames and full-scale fires.

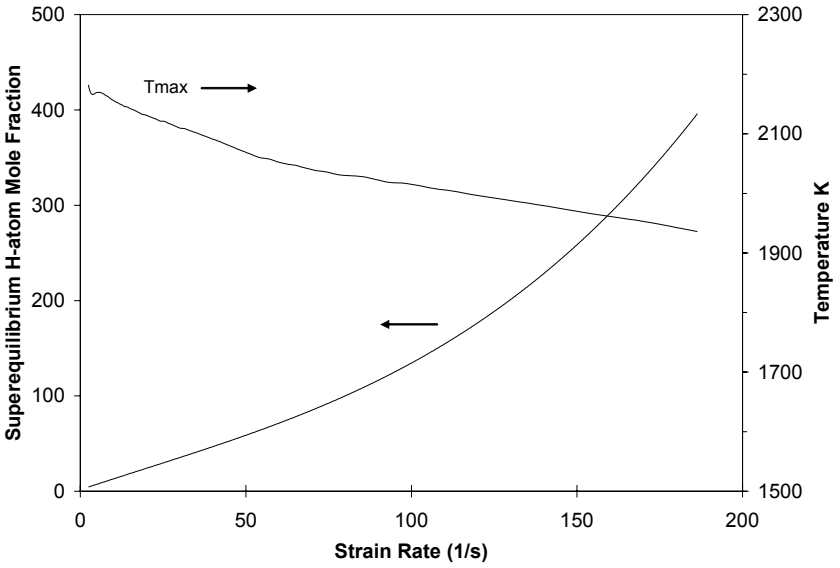

Figure 3-11. Calculated H-atom Super-equilibrium Ratio and Peak Temperature in a Counterflow Diffusion Flame as a Function of Strain Rate.

Inhibition of Low Pressure Opposed-flow Methane-air Flames by $Fe(CO)_5$

Introduction

For premixed and non-premixed flames, measurements of radical concentrations (O, H, OH) serve as useful indicators of the chemical rates that are being affected, because chemical inhibiting agents act to reduce the super-equilibrium concentration of radicals. Radical concentrations reach their maximum concentrations in the flame reaction zone and then decay toward equilibrium values. Thus, if an inhibitor were present, it would reduce the maximum radical concentrations toward equilibrium values and show the amount of chemical inhibition present.[155] Radical measurements are thus directly related to burning velocity and extinction strain rate measurements.

Prior to the NGP, there had been no laboratory measurements of the change in the concentration of radical species with increasing addition of $Fe(CO)_5$ to non-premixed flames. In fact, only limited measurements of radical species in non-premixed flames inhibited by CF_3Br existed.[36,51,156] McNesby and co-workers[157] examined the influence that $Fe(CO)_5$ had on the structure of a low pressure, opposed flow, CH_4-air flames. OH radical profiles were measured as the concentration of inhibitor was increased, approaching extinguishment. Flames inhibited by N_2 or CF_3Br were included for reference.

Apparatus

Figure 3-12 presents a schematic diagram of the experimental arrangement. The opposed flow burner apparatus was contained within a 200 L combustion chamber. The combustion chamber was a six-armed stainless steel cross, with the four horizontal arms being 25.4 cm in diameter and the two vertical arms being 30.48 cm in diameter. The opposed jet ducts were mounted in the vertical arms with each head having two axes of motion under computer control. The opposed jet duct diameters were 7.68 cm and the active burner surface was approximately 7.6 cm in diameter. Laminar flow was established in the jet ducts, with the initial gases impinging on a 0.32 cm thick, porous, stainless steel, sintered disk. The gases flowed through a 2.54 cm region before passing through a second, 0.32 cm thick, porous, stainless steel, sintered disk. The second porous disk opened to the combustion chamber. Schlieren images of the gases showed laminar flow from both ducts. The gases and cooling water were fed to the burner ducts via stainless tubing.

Optical access to the chamber was provided on the vertical arms of the chamber through 10.16 cm diameter windows. There were also four additional ports in the horizontal plane, each located between two of the window arms. These ports served as access for pressure monitoring, thermocouple manipulation, and electrical connections. Also mounted on the top and bottom of each window arm were vacuum ports to remove the combustion gases. These eight ports were joined to a single 5.08 cm I.D. tube which fed the gas to a scrubber mounted on a high volume vacuum pump. The scrubbed exhaust gases were then vented to the atmosphere. All flames were studied at a pressure of 6.6 kPa (50 torr), the oxidizer flow consisted of 10 L/min synthetic air (79 % N_2 + 21 % O_2, Matheson UHP Grade) flowing from the upper duct, and the fuel flow was 10 L/min of methane (Matheson UHP Grade) flowing from the lower duct. The gases were regulated and monitored by a gas handling manifold system constructed from a series of flow controllers (Tylan General).

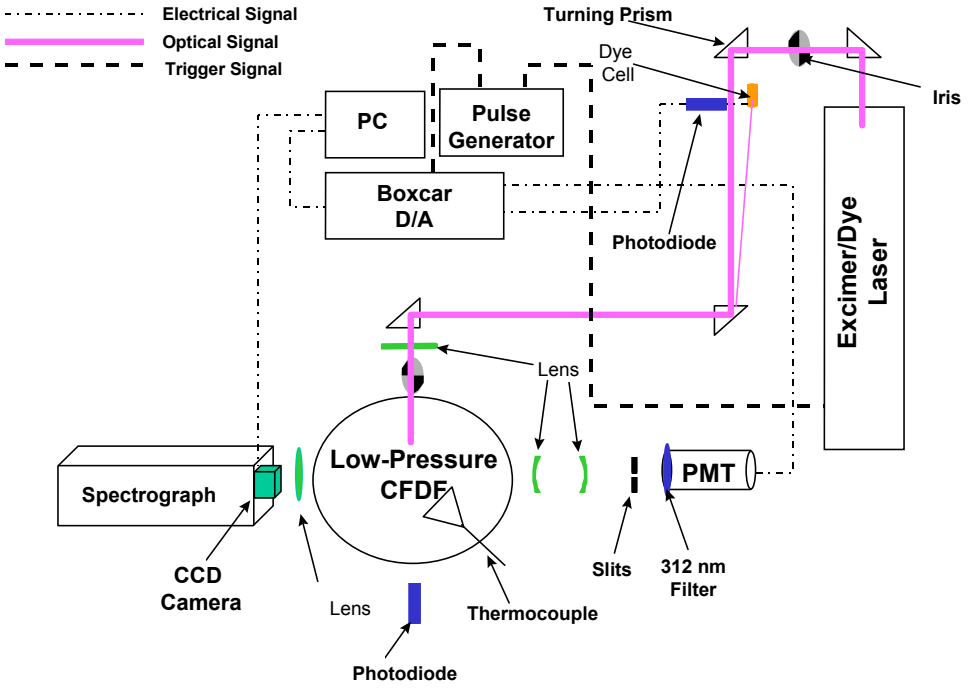

Figure 3-12. Schematic Diagram of the Low Pressure Burner and Optical Measurement Arrangement.

The oxidizer and fuel ducts were separated 3.8 cm. For the flow conditions and flow duct separation, the luminous flame zone was located on the oxidizer side of the stagnation plane, and the global strain rate was calculated to be 50.2 sec^{-1}.[76] The inhibitors were added to the oxidizer flow for delivery to the flame zone.

$Fe(CO)_5$ is a liquid at room temperature and its introduction into the flame was accomplished by bubbling argon (Ar) through a flask containing 25 ml of $Fe(CO)_5$ that was immersed in a constant temperature bath maintained at 13 °C. The resulting Ar/ $Fe(CO)_5$ mixture consists of ≈ 2 % $Fe(CO)_5$ and ≈ 98 % Ar. The maximum flow of Ar through the bubbler was 0.41 L/min. At this flow, the effect of Ar on the flame was minimal. The gaseous output of the bubbler apparatus passed through a 5 L/min mass flow meter to monitor the Ar/$Fe(CO)_5$ mixture being delivered to the oxidizer stream. The mass flow meter was calibrated for the Ar/$Fe(CO)_5$ mixture using a standard soap bubble technique.

Diagnostics

Flame emission spectra were measured using a Princeton Instruments ICCD camera (Model 120) coupled to a 0.75 m SPEX spectrograph (Model 1702) with a 1200 gr/mm grating controlled by an external Compudrive. A 50 cm focal length lens collected light from the center of the flame and focused it onto the entrance slits (0.05 mm) of the spectrograph. The determined field of view of this optical arrangement was 1 cm^2. The ICCD camera, which had an active area of 384 x 576 pixels, was operated in a CW manner and each image recorded was acquired with 50 total accumulations on the camera.

Laser induced fluorescence excitation spectra in the flame were measured using a Lambda Physik excimer/dye laser system. The system consists of a Lambda Physik Compex 102 XeCl excimer laser, a Scanmate 2 dye laser (Rhodamine 6g), and a Second Harmonic Generator (SHG). The fundamental output of the dye laser (580 nm wavelength) was frequency doubled in the SHG unit with a BBO crystal to around 290 nm. The UV laser radiation was tuned to the peak of the $P_2(8.5)$ transition at 286.566 nm

((1,0) $A^2\Sigma^+ \leftarrow X^2\Pi$) (References 158-160). The intensity of this transition was slightly temperature dependent,[161] varying by approximately 12 % over the range of maximum temperatures for the flames studied here. The selected transition varied linearly with input energy. Low laser energies were used and the laser was operated in the linear regime. The UV light output of the SHG unit was focused to the center of the burner chamber using a 50 cm focal length fused silica lens and had a vertical and horizontal beam waist of 0.4 mm and 0.5 mm, respectively. Fluorescence was collected at 90 º to the direction of the excitation laser beam, focused through 0.75 mm horizontal slits to define the collection volume, passed through a band pass filter centered at 312 nm with an 11 nm bandwidth, and detected by a photomultiplier tube (PMT) (Phillips Model XP2018B). Fluctuations in laser power were detected by a photodiode that monitored laser induced fluorescence from a cell containing Rhodamine 6g dye.

The output signals from the PMT and monitor photodiode were directed to gated integrator/boxcar averagers (SRS Model SR-250) operating in a 10 shot average mode. The boxcar gate widths were set to 3 ns. The trigger pulses to the excimer laser and boxcars were supplied by a digital delay pulse generator (SRS Model DG535) at a rate of 10 Hz. Spatially resolved OH LIF profiles were measured by tuning the excitation laser to the peak of the $P_2(8.5)$ transition and, with the beam location fixed, vertically translating the burner assembly.

Results

Table 3-5 lists the inhibitor agent concentrations at extinction and the average uncertainties due to measurement variance.

Table 3-5. Inhibitor Concentrations (µL/L) and Uncertainty (± µL/L) at Flame Extinction.

Inhibitor	N_2	CF_3Br	$Fe(CO)_5$
Extinction Concentration	9426	3735	451
Uncertainty	566	672	77

The large degree of variance was due to changes in the burner cooling. The flow of cooling water to the burner ducts was not monitored precisely, and thus the burner performance probably changed slightly from day-to-day operation. This deficiency was perhaps significant because the burner was operated in a quasi-adiabatic condition, and thus heat losses from the flame to the burner ducts caused decreases in extinction concentrations observed experimentally. Preliminary numerical calculations of extinction concentrations for CF_3Br and $Fe(CO)_5$ were 4000 µL/L and 271 µL/L, respectively.[162]

The numerical calculations for both CF_3Br and $Fe(CO)_5$ were performed using kinetic models.[52,104] Preliminary numerical calculations by Babushok[163] using the kinetic model for $Fe(CO)_5$ inhibition of Rumminger et al.,[104] but corrected for the pressure dependence of the $FeO + H_2O \leftrightarrow Fe(OH)_2$ reaction, demonstrated an extinction concentration of 612 µL/L.

All three inhibited flames extinguished in the flat region directly between the opposed flow fuel and oxidizer ducts. Addition of N_2 or CF_3Br to the 6.6 kPa CH_4-air flame did not significantly alter the visual appearance of the flat, axisymmetric, blue disk flame. Addition of $Fe(CO)_5$ to the flame caused an orange/yellow luminous zone to appear above the blue luminous zone, similar to what was observed by Reinelt and Linteris.[164] As the $Fe(CO)_5$ inhibited flame approached extinction, the blue and the

orange/yellow luminous zones gradually merged, and the flame assumed a uniform bright orange/yellow color. The orange/yellow luminosity in the $Fe(CO)_5$ inhibited flame was believed to be caused by iron oxide emission.[89] The dual flame zone observation, which has been observed in previous $Fe(CO)_5$ studies,[89] was further characterized using emission spectroscopy.

For the compositional analysis of the solid particles formed in the flame, particle samples were collected and analyzed using a scanning electron microscope (SEM) and X-ray fluorescence (XRF) techniques. Particle samples were taken from the upper cooled burner duct, where large deposits were found, and from an uncoated, 0.2 mm diameter Pt/Pt-10 % Rh wire thermocouple inserted into the visible center of a $Fe(CO)_5$ inhibited flame. The collected particulate material appeared as a ruddy orange powder. The XRF showed the elemental composition of the particles to be iron and oxygen. An exact ratio of iron to oxygen was not determined, but the SEM analysis indicated that the size of the particles ranged from 1 μm to 10 μm, with most being 1μm to 2 μm and quasi-spherical in morphology.

Emission Spectroscopy

Emission spectroscopy was used to qualitatively examine the behavior of OH for each inhibited flame as well as the decomposition of $Fe(CO)_5$ upon introduction into the flame. For OH, images were collected at increasing concentrations of inhibitor. Images indicated that for approximately equal inhibitor concentrations added to the flame, the flame to which $Fe(CO)_5$ had been added demonstrated the smallest relative OH emission intensity. These observations illustrated that addition of $Fe(CO)_5$ to the flame had the greatest effect on the OH population. However further quantification of the results was risky because ground state populations and temperatures calculated from OH emission in flames using a Boltzmann distribution can be misleading. That is, nascent OH that is responsible for the chemiluminescence may not be in thermal equilibrium with ground electronic state OH and other combustion gases.

Figure 3-13 shows a representative emission image collected in the 554 nm wavelength region from the centerline of a flame with 10 % of the experimentally determined extinction concentration of $Fe(CO)_5$ added to the oxidizer flow. The addition changed the molecular emission spectra to include iron species such as FeO and FeOH as well as atomic iron lines.[165] These modifications to the molecular emission spectra altered the flame's emission intensity, which is illustrated in Figure 3-13. The spatial mapping indicated that some of the $Fe(CO)_5$ had decomposed prior to the luminous flame region at approximately 10.4 mm ± 1 mm from the oxidizer duct with a majority of the emission in this spectral region attributed to FeO.[166] The lower continuum, at approximately 14.8 mm ± 1 mm from the oxidizer duct, was due to the broadband luminosity of the hydrocarbon flame. Earlier emission images[165] of CH emission from similar low pressure CH_4-air flames seeded with $Fe(CO)_5$ showed an additional region of emission intensity closer to the oxidizer duct which was not observed in both uninhibited and inhibited flames seeded with N_2 or CF_3Br. The additional intensity was identified as iron lines not present in the uninhibited flame.

Recognition of iron oxide particle formation invoked suggestions of heterogeneous chemistry occurring. Work by Babushok et al.,[167] who modeled the effect of an ideal gas phase flame inhibitor using gas kinetic rate constants for a set of radical scavenging and inhibitor-regenerating reactions, indicated otherwise. Calculations were conducted for a premixed flame containing $Fe(CO)_5$ and a premixed flame with the ideal gas phase flame inhibitor. The calculations showed that the burning velocities, which were very non-linear as inhibitor concentrations increased, for both flame systems were nearly equal for the

same inhibitor quantities. This result showed that the $Fe(CO)_5$ inhibition mechanism was dominated by homogeneous gas phase chemistry when the inhibitor is added in small concentrations.[167]

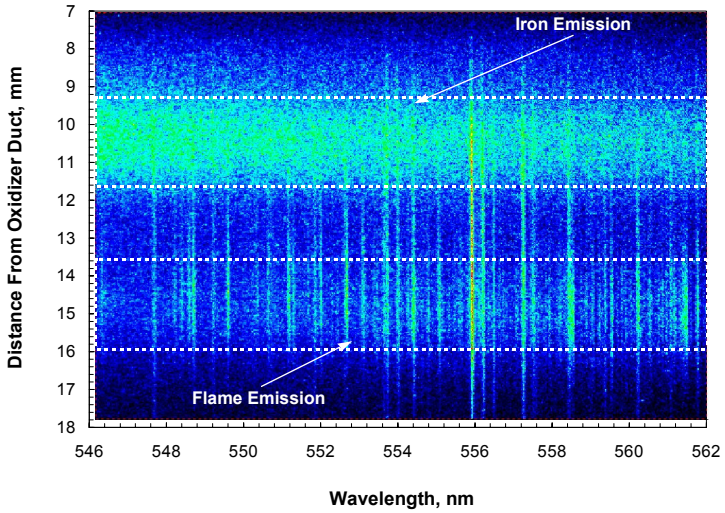

Figure 3-13. Emission Image Collected from the Centerline of the Low Pressure, Opposed Flow, CH_4-air flame with 10 % of the $Fe(CO)_5$ Concentration Required to Extinguish the Flame.

Laser Induced Fluorescence

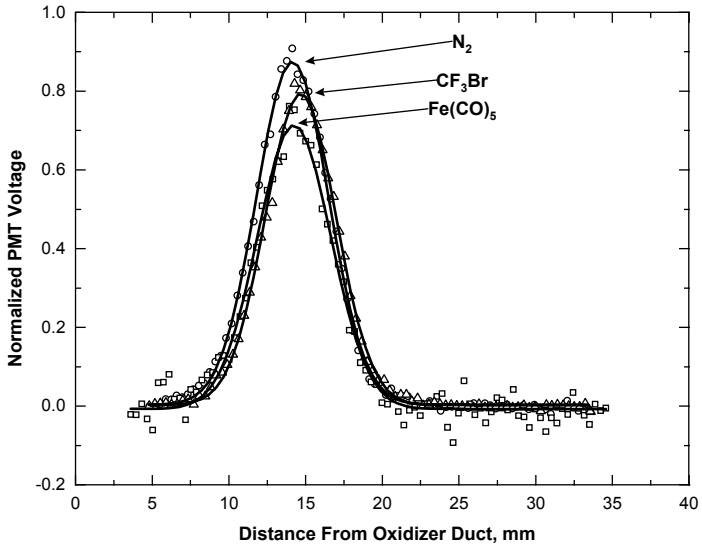

Figure 3-14 shows representative OH LIF profiles measured in flames to which $Fe(CO)_5$, CF_3Br, or N_2 had been added.

Figure 3-14 LIF [OH] Profiles Collected from Inhibited CH_4-air Flames Containing Nominally Half of the Concentration Required for Extinguishment. N_2: O; CF_3Br: Δ; $Fe(CO)_5$: □.

The inhibitor concentrations and percents of the concentration required for extinguishment were N_2 (4721 µL/L, 50 %), CF_3Br (1996 µL/L, 53 %), and $Fe(CO)_5$ (229 µL/L, 51 %). The data had been normalized to the peak intensity of the OH LIF profile in an uninhibited flame. The N_2 doped flame had the smallest effect (leaving the highest intensity), followed by CF_3Br and $Fe(CO)_5$.

The addition of an inhibitor to the flame can also change the nature of the flame's reaction zone.

- Location: For the uninhibited flame, the location of the average OH LIF maximum from the oxidizer duct was 14.34 mm ± 0.05 mm. The addition of $Fe(CO)_5$ had a negligible effect on the OH LIF maximum position. The addition of CF_3Br or N_2 to the flame slightly shifted the position of the OH LIF maximum toward the oxidizer duct to locations of 14.12 mm and 13.65 mm, respectively. The shifts were small and were largest for the weakest inhibitor, each added at 50 % of its extinguishing concentration. Preliminary numerical calculations[163] using the kinetic model for $Fe(CO)_5$ inhibition of Rumminger et al.,[104] but corrected for the pressure dependence of the $FeO + H_2O \leftrightarrow Fe(OH)_2$ reaction, predicted the position of the OH maximum concentration at 13.0 mm from the oxidizer duct.
- Width: Previous studies[168-173] had shown that a decrease in the flame's reaction zone width indicated increased localized strain, which could cause local quenching or flame extinction. The width of the flame's reaction zone may be characterized by the width of a radical profile (Miller, 1996). For the analysis of the radical profile shape modifications, the profiles were fit to a Gaussian function. The width of the flame zone was defined as the distance of one half of the maximum intensity of the Gaussian OH profile, i.e., Full Width Half Maximum (FWHM). The determined [OH] profile width for the uninhibited flame was 5.67 ± 0.08 mm. Addition of N_2 did not change the profile width. The addition of CF_3Br or $Fe(CO)_5$ narrowed the profile width to 5.50 mm and 5.22 mm respectively. Thus, reduction of the profile widths was small and was largest for the strongest inhibitor, the opposite of the location effect described above.
- Intensity Trend: Figure 3-15 presents normalized OH LIF peak intensities vs. inhibitor concentrations. For normalization, the OH maximum intensity from the uninhibited flame was used. The presented data were uncorrected for collisional quenching and temperature dependence, and the major source for error in the peak OH LIF intensities was the laser shot-to-shot variation. The shot-to-shot variance occurred as the laser energy was scanned over the spectral region of interest. The shot-to-shot uncertainty averaged ± 1.5 % which contributed to the overall measurement uncertainty of 4 %.

Flames inhibited by $Fe(CO)_5$ and CF_3Br demonstrated decreases in OH populations that were quasiproportional to the inhibitor concentrations. Flames inhibited by N_2 demonstrated non-linear behavior, with initially small changes in [OH] and more rapid decreases as extinction was approached. The final measurable [OH] data points, which were near each flame's extinction point concentration, were approximately the same for all three inhibitors: 0.73 to 0.67. Thus, there was an approximately 30 % decrease in the normalized OH intensity at extinction for each inhibitor. The same model used to calculate the peak OH location gave a normalized OH maximum concentration at extinction of 0.73 for $Fe(CO)_5$. The ratio of each inhibitors' concentration relative to CF_3Br near extinction was N_2:CF_3Br:$Fe(CO)_5$ = 2.5:1:0.11, indicating that the $Fe(CO)_5$ flame inhibition effectiveness was approximately a factor of 10 greater than CF_3Br. These results were similar to Reinelt and Linteris[103] who observed that 500 μL/L of $Fe(CO)_5$ added to the air stream of an atmospheric pressure, CH_4/-air, counterflow flame reduced the strain by ≈ 30 %, while addition of 5000 μL/L of CF_3Br reduced the strain about 20 %.

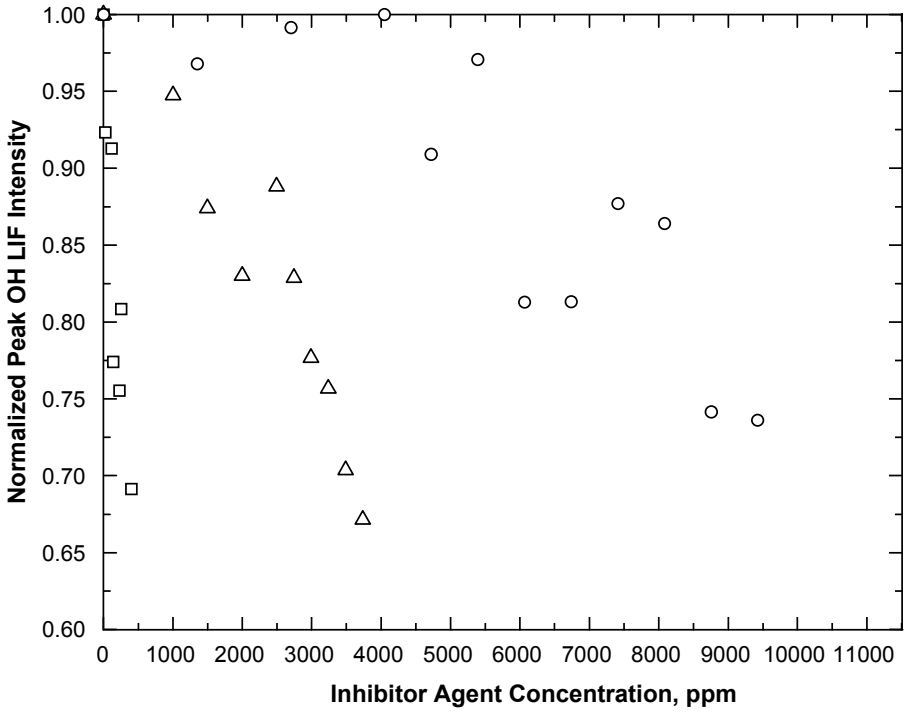

Figure 3-15. Dependence of Normalized Maximum OH LIF Intensity on Inhibitor Concentration. ◊: N_2; Δ: CF_3Br; □: $Fe(CO)_5$. The lowest experimental measurements of OH intensity correspond to near-extinction conditions.

[OH] measurements[156] in non-premixed atmospheric pressure hydrocarbon flames have also shown decreasing OH concentrations with increasing CF_3Br concentrations.[51] The observed quasimonotonic decrease of [OH] in the current flames with increasing of CF_3Br and $Fe(CO)_5$ concentrations was similar to decreases of chain carrier concentrations in the reaction zone of simulated premixed C1-C2 flames with CF_3Br, CF_3I, CF_4, C_2F_6, and C_2F_5H additives.[52] Uncorrected OH absorption profile measurements by Bonne and co-workers[89] showed a slight decrease in the integrated OH concentrations, i.e., area under curves, with increasing $Fe(CO)_5$ concentrations for a low pressure (8 kPa), premixed, stoichiometric methane/air flame.

The saturation effect (leveling), which was observed for burning velocities in atmospheric pressure, premixed methane flames seeded with $Fe(CO)_5$,[103,104,174] was not observed in this work. Two types of saturation have been discussed in the literature: (1) saturation of chemical influence[52], and (2) saturation due to condensation processes.[103] Both result in a decrease in inhibitor efficiency with increased inhibitor concentration, but the latter was believed to dominate for $Fe(CO)_5$ inhibited flames.

The current low pressure, non-premixed flame results show some similarities to the premixed CH_4-O_2 flame of Bonne et al.[89] at pressures from 101 kPa to 10 kPa. At 101 kPa , addition of 0.03 % $Fe(CO)_5$ to the Bonne flame decreased the burning velocity ≈ 7.5 %, while at 50 kPa, addition of 0.03 % $Fe(CO)_5$ decreased the burning velocity ≈ 6 %. In premixed CH_4-air flames, addition of 0.01 % $Fe(CO)_5$ at 101 kPa caused the burning velocity to decrease 24 % while at 50 kPa the decrease in burning velocity was only 8 % to 9 %. Obviously, $Fe(CO)_5$ had a more pronounced effect in the CH_4-air flames, but for both systems the decreases in burning velocities were observed to be linear at all pressure conditions and the inhibitor influence of $Fe(CO)_5$ diminished with decreasing pressure.

Conclusions

The first LIF measurements of [OH] in the reaction zone of inhibited low pressure, opposed flow flames approaching extinction showed:

- There was a two-zone (blue and orange) luminous flame structure for a $Fe(CO)_5$ inhibited flame.
- [OH] levels decreased with increasing $Fe(CO)_5$ and CF_3Br concentrations added to the flames.
- $Fe(CO)_5$ was about 10 times as effective a suppressant as CF_3Br.
- Addition of both chemically active and physically active inhibitors had relatively small effects on the locations of the OH maximum intensities and on the width of the [OH] distribution in the flame front. The weakest inhibitor had the largest effect.
- The addition of $Fe(CO)_5$ and CF_3Br slightly narrows the width of the flame reaction zone. The strongest inhibitor had the largest effect.
- Close to extinguishment, flames inhibited with both physically active and chemically active agents showed a 30 % reduction in peak OH concentration.

Iron's Loss of Effectiveness through Particle Formation

If the gas phase inhibition mechanism of iron were the only consideration, it should be a very effective agent for extinguishing fires. However, NGP research with premixed flames[102] and counterflow diffusion flames[108] indicated that particle formation would limit the effectiveness of iron to those situations in which it was added at high concentration. Subsequent work showed that iron pentacarbonyl at low concentrations was much less effective in cup burner flames than was expected based on the results in premixed or counterflow diffusion flames.[153]

The effectiveness of iron as a flame inhibitor declines as the mole fraction at which it is added is increased. This lower effectiveness had been mentioned briefly by Jost and co-workers,[88] who surmised that a particle inhibition mechanism may be at work at high concentration. They also said that work was underway to understand the role of particle formation; however, subsequent papers did not appear. Many other flame inhibitors also showed lower effectiveness as their concentration increased.[175] However, the loss of effectiveness of iron is much more dramatic. Reinelt and Linteris[103] quantified the loss of effectiveness of iron for premixed and diffusion flames. Rumminger et al.[104] described a gas phase kinetic mechanism for iron inhibition, and showed that the loss of effectiveness was not predicted by a gas phase mechanism (ruling out low radical concentration as the reason for the loss of effectiveness). Linteris et al.[107] have recently described the performance of iron, tin, and manganese in cup burner flames. The loss of effectiveness of iron in each of these flame systems is described below.

Based on the encouraging results for the powerful flame inhibition properties of iron compounds, extinction experiments of ferrocene together with an inert compound generated by a solid propellant gas generator (SPGG) were conducted in an enclosure containing a spray flame.[176] The combination did not have the expected high efficiency. Although it was not possible to extract fundamental information concerning the lack of effectiveness for their flame configuration, the results of Holland and co-workers provided evidence for a loss of effectiveness for iron, and motivated a search for an explanation.

Premixed Flames

For premixed flames, Figure 3-16 shows that the gas phase mechanism predicts a continuing decrease in the normalized burning velocity ($S_L/S_{L,\ uninhibited}$) as [$Fe(CO)_5$] increases, whereas the experiments show a leveling off. (Uncertainties in any experimental data cited throughout this chapter are discussed in the source publication.)

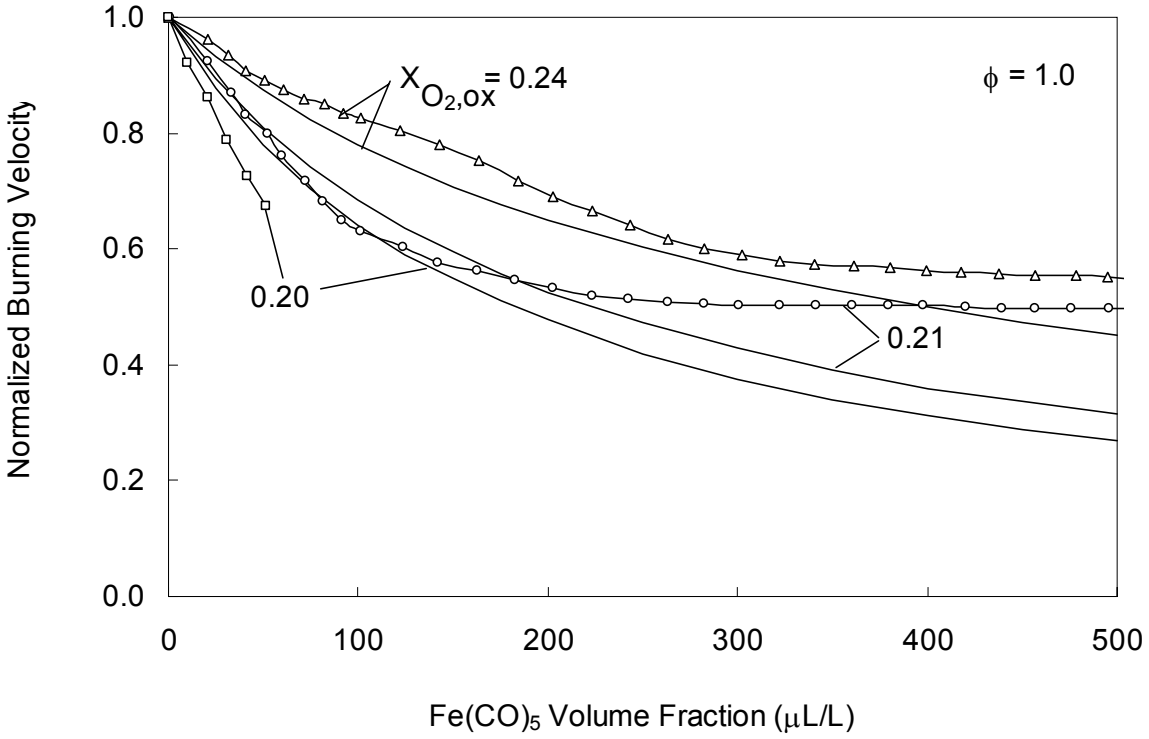

Figure 3-16. Calculated and Measured Normalized Burning Velocity of Premixed $CH_4/O_2/N_2$ Flames with $X_{O_2,ox}$ = 0.20, 0.21, and 0.24 for ϕ = 1.0.[104]

Subsequent measurements of particles in the premixed flames showed that the loss of effectiveness of the iron was correlated with formation of particles (as illustrated in Figure 3-17 and Figure 3-18), and the scattering from the particles was correlated with the residence time in the flame (necessary for condensation to occur), as shown in Figure 3-19. In addition to measuring the particles with thermophoretic sampling and quantifying their size and agglomeration characteristics with transmission electron microscopy, they also calculated the maximum effect that the particles could have on the burning velocity. Constructing a "perfect heterogeneous inhibitor" model (in which any collision of a radical with a particle recombines the radical to a stable species), they showed that heterogeneous reactions cannot account for the measured flame speed reduction of $Fe(CO)_5$.

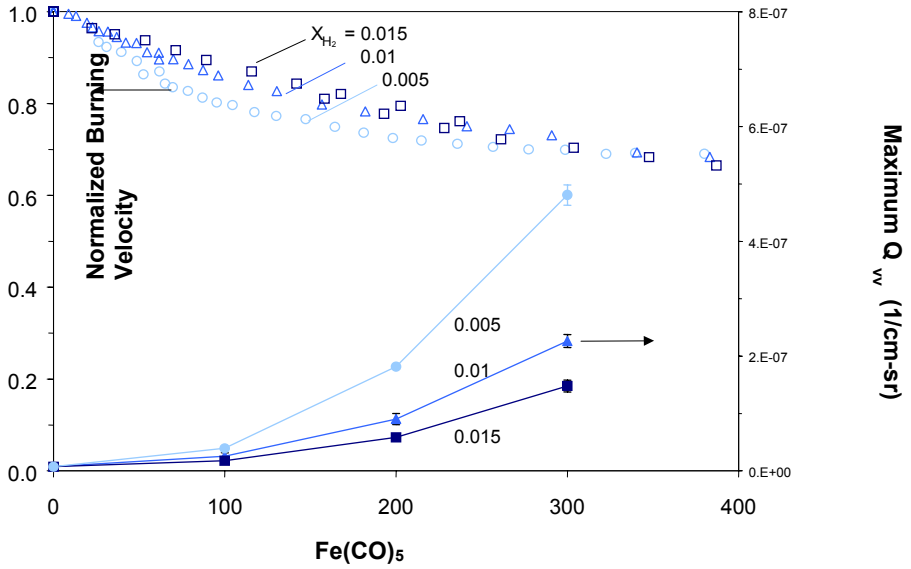

Figure 3-17. Normalized Burning Velocity[103] and Maximum Measured Scattering Signal Q_w[102] for ϕ=1.0 CH_4 Flame with $X_{O_2,ox}$ = 0.21 and 0.24.

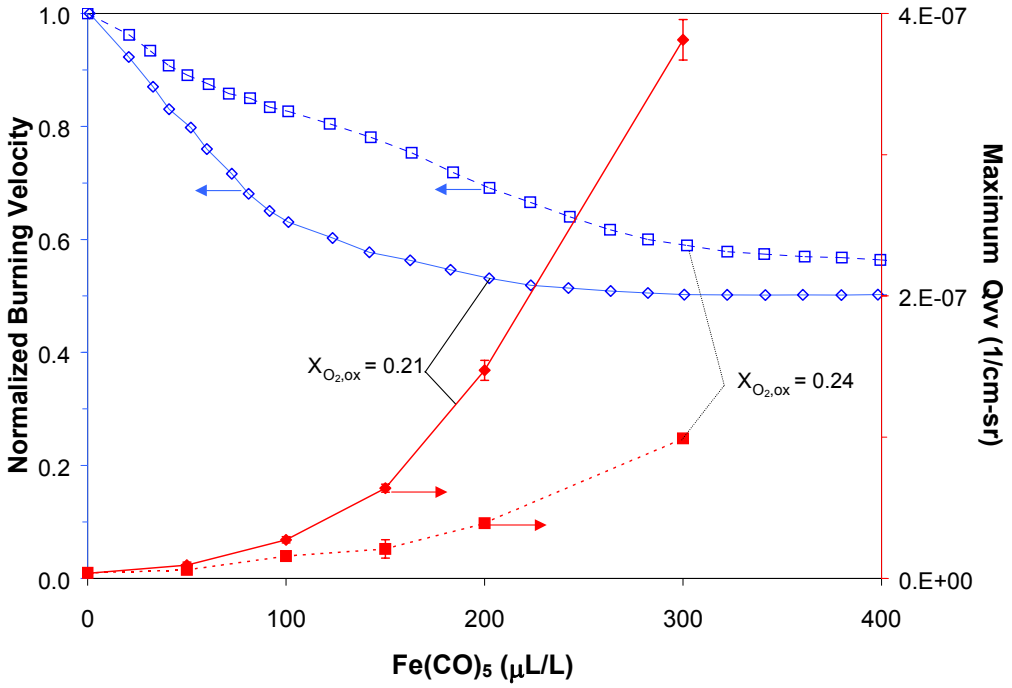

Figure 3-18. Maximum Scattering Signal and Normalized Burning Velocity[118] for CO-H_2 Flames as $Fe(CO)_5$ Concentration Varies.[102]

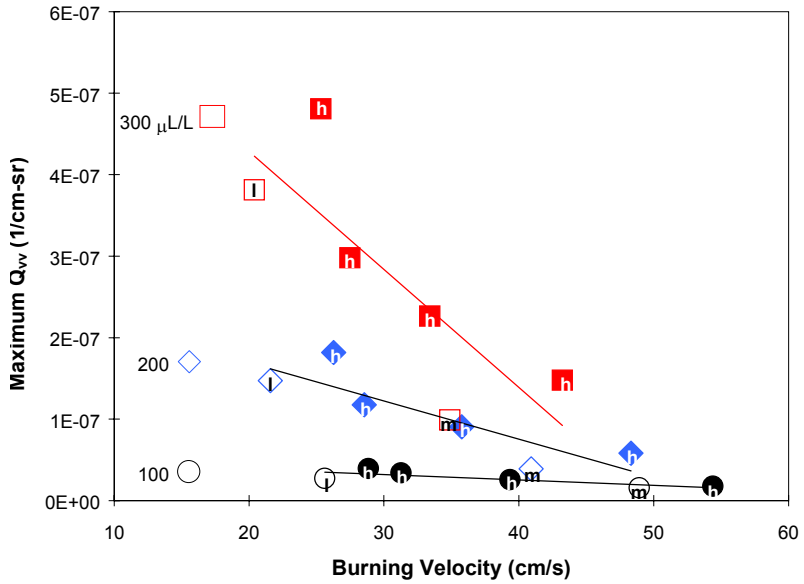

Figure 3-19. Maximum Q_{vv} for Flames of CH_4 (open symbols) and CO (closed symbols) as a Function of the Burning Velocity. The letters correspond to the adiabatic flame temperature (l = 2220 K, m = 2350 K, h = 2470 K); the symbol shape (square, diamond, and circle) corresponds to the loading of $Fe(CO)_5$.[102]

Figure 3-20 shows the experimental data for normalized flame speed reduction by $Fe(CO)_5$ along with the prediction for the perfect gas phase inhibitor and perfect heterogeneous inhibitor (for different assumed particle diameter sizes). As shown, the perfect gas phase inhibitor mechanism shows burning velocity reductions fairly close to that of $Fe(CO)_5$; whereas, the perfect heterogeneous mechanism does not show enough inhibition, about a factor of eight too low, even for perfect collisions with 10 nm particles. Interestingly, the slope of the $Fe(CO)_5$ curve in Figure 3-20 in the "flattening out" region is of the same order as that of the perfect 10 nm diameter particles. Hence, Jost et al.'s[88] postulate that the region of lower effectiveness may be due to radical recombination on particles surfaces may be true. Note also that the slope in the flat region is of the same order as that for CF_3Br in these premixed flames.

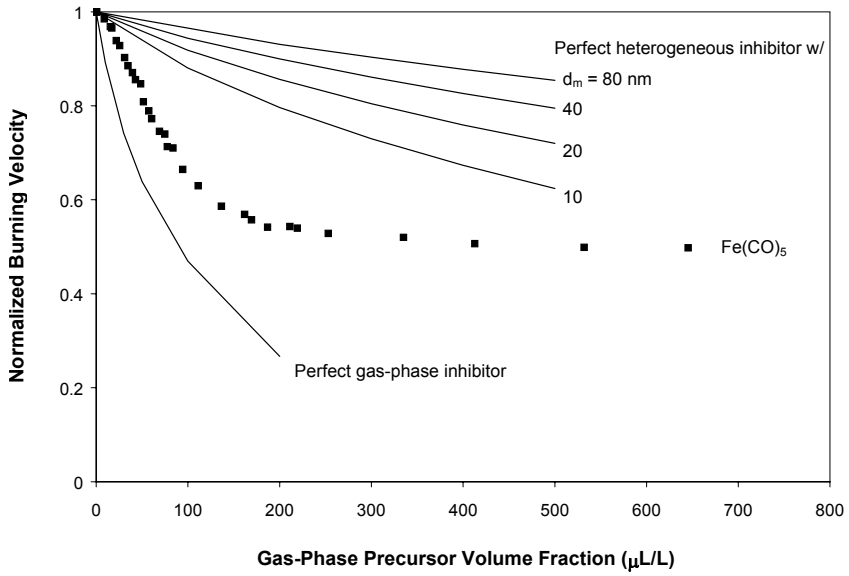

Figure 3-20. Calculated Normalized Burning Velocity for Several Diameters, d_m, of Ideal Heterogeneous Inhibitor, $Fe(CO)_5$ data[103], and Calculated Normalized Burning Velocity using the Perfect Gas Phase Inhibitor Mechanism.[102,167]

Counterflow Diffusion Flames

Similar experimental and modeling results were described for counterflow diffusion flames. As shown in Figure 3-21, the gas phase model predicts more inhibition at higher [$Fe(CO)_5$] than do the experiments. Measured particle scattering signals again showed that the loss of effectiveness (and discrepancy between the measured and gas phase predicted inhibition) increased as particle scattering signal increased; i.e., particle formation was correlated with loss of effectiveness of the $Fe(CO)_5$ (Figure 3-22). It is important to note that in the counterflow diffusion flames, the propensity to form condensed-phase iron particles *in the flame region* was not the only mechanism shown to be correlated with loss of effectiveness of iron. If particles formed in one part of the flame, but were unable (due to entrainment or thermophoresis) to be transported to the reaction zone, the active iron species could be sequestered from the region in which they must be present to inhibit the flame. By adding the $Fe(CO)_5$ to either the fuel or air stream, and changing the flame location relative to the stagnation plane (by diluting the fuel or oxidizer with N_2), Rumminger et al. clearly showed the effect of drag and thermophoretic forces on reducing particle (and hence iron) transport to the region of radical chain branching.

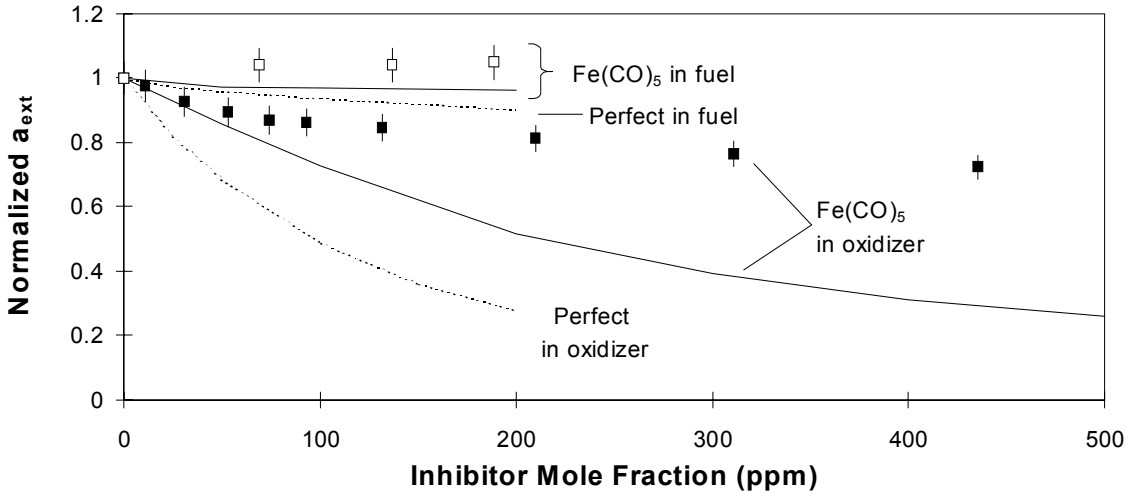

Figure 3-21. Normalized Extinction Strain Rate for Counterflow Diffusion Flames. Closed symbols: measurements with the $Fe(CO)_5$ in the oxidizer; open symbols: measurements with $Fe(CO)_5$ in the fuel; solid lines: calculations with $Fe(CO)_5$; dashed lines: calculation with perfect inhibitor.[105]

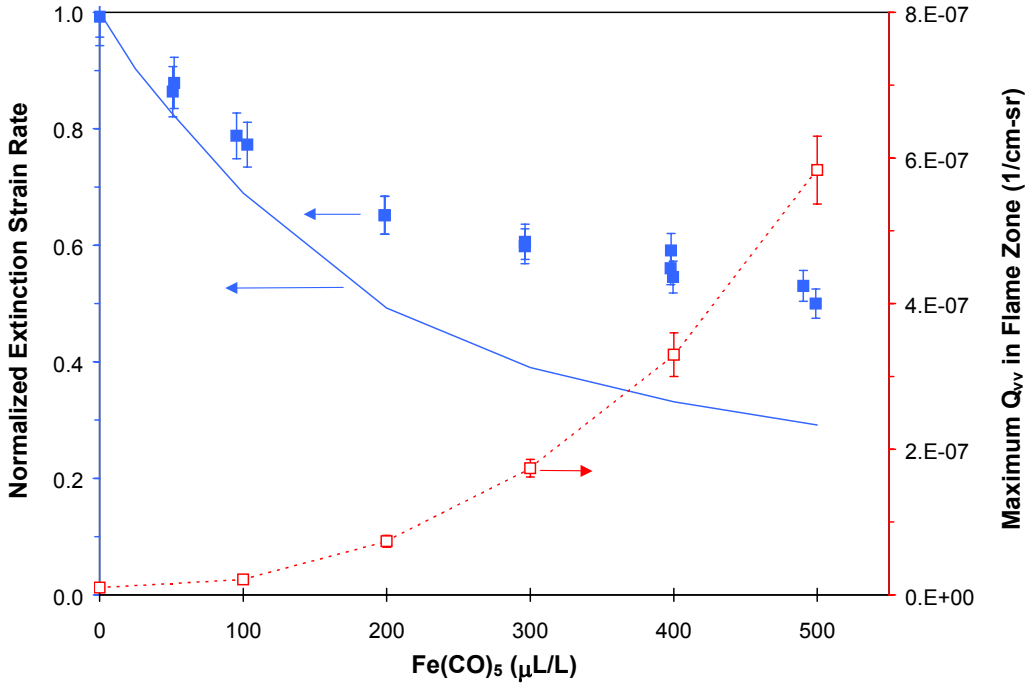

Figure 3-22. Correlation between Inhibition Effect in Counterflow Diffusion Flames and Maximum Measured Scattering Signal Q_{vv} . Filled points are experimental normalized a_{ext}, solid line is calculated a_{ext}.[105] Open symbols connected by dotted lines are maximum measured Q_{vv}. Particle data were collected at 75 % of a_{ext}.[108]

Cup Burner Flames

Linteris et al. tested $Fe(CO)_5$, TMT, and MMT in cup burner flames.[85,86,153] Based on the loss of effectiveness at higher $Fe(CO)_5$ concentrations that was demonstrated in premixed and diffusion flames, it was not expected that iron pentacarbonyl alone would be effective in cup burner flames. However, several publications had suggested that a combination of a good catalytic agent and an inert agent would prove to be effective.[14,91,118,175,177,178] The premise was that the overall reaction rate would be lowered in part through radical recombination by the catalytic agent, and in part through the lower temperature caused by the added diluent. To test these suggestions, Linteris et al. added $Fe(CO)_5$, MMT, or TMT to a cup burner of methane and air, and measured the amount of CO_2 required for extinction.[153] This approach is conceptually the same as the classic oxygen index test used for assessing material flammability.[135] In that test, the oxygen volume fraction in the air stream at blowoff (i.e., the oxygen index) is determined for solid, liquid, or gaseous fuels with chemical additives in either the fuel or oxidizer.

Unfortunately, the effectiveness of CO_2 combined with any of the metal agents was much less than anticipated. Figure 3-23 shows the measured CO_2 volume fraction required for extinction as a function of the catalytic agent volume fraction in the air stream. Data are presented for Br_2, CF_3Br, $Fe(CO)_5$, MMT, and TMT. As shown, although the metals are still more effective than CF_3Br at low concentration, they are not nearly as effective as expected from the results in premixed and counterflow diffusion flames. The reasons for this loss of effectiveness are described below.

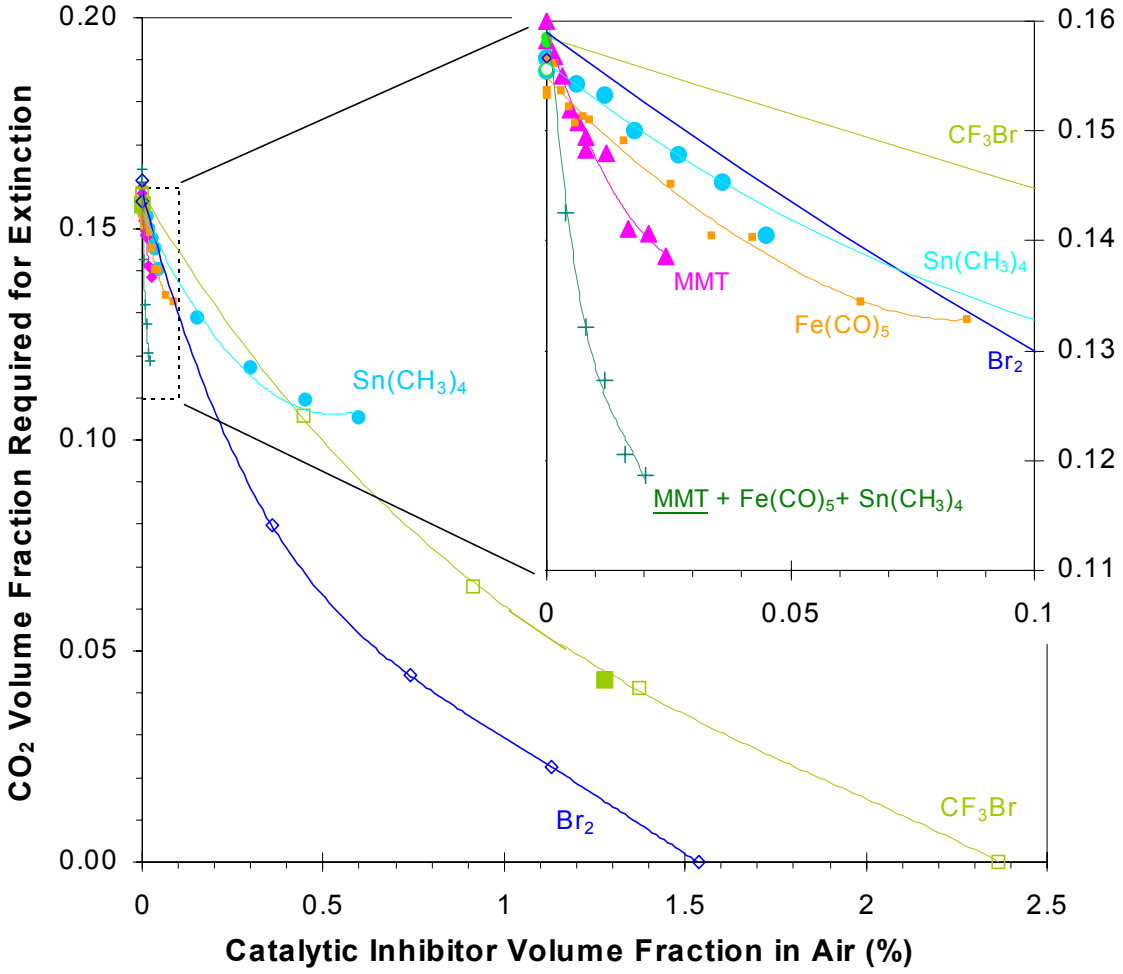

Figure 3-23. Volume Fraction of CO_2 Required for Extinction ($X_{CO_2,ext}$) of Methane-air Cup Burner Flames as a Function of the Volume Fraction of Catalytic Inhibitor Added to the Air Stream. Inset shows region in dotted box with expanded scales.[153]

In order to understand the lower effectiveness of metals in cup burner flames compared to premixed and counterflow diffusion flames, several steps were taken. First, particle measurements were made in cup burner flames inhibited by $Fe(CO)_5$. Shown in Figure 3-24 are scattering cross sections for laser light at 488 nm as a function of radial position and height above the burner in a methane-air cup burner flame with 8 % CO_2 and $Fe(CO)_5$ in air at four volume fractions.[153] The dotted lines show flame location from a digitized video image of the uninhibited flame. The figures indicated that particles were present both inside and outside (but not coincident with) the luminous flame zone, and that higher $Fe(CO)_5$ loadings produced higher particle scattering signals.

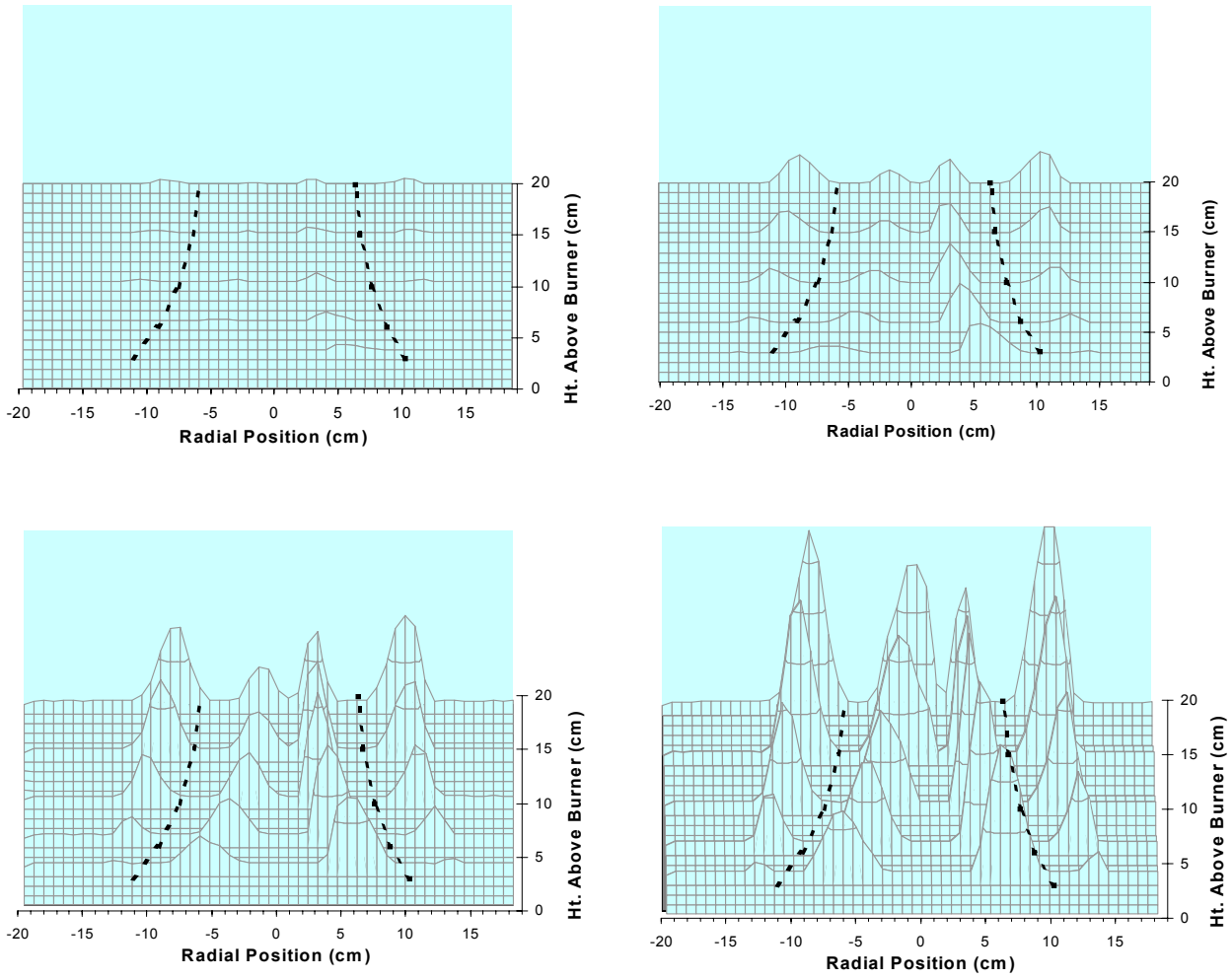

Figure 3-24. Particle Light Scattering as a Function of Radial Position and Height above Cup Burner for Four Loadings of $Fe(CO)_5$. [153] Top left: 100 μL/L, top right: 200 μL/L, bottom left: 325 μL/L, bottom right: 450 μL/L.

In order to understand the particle formation and chemical inhibition, numerical modeling of the cup burner flames inhibited by $Fe(CO)_5$ were performed,[153] using the gas phase only numerical model developed previously. This model has predicted the blow-off condition of methane and air cup burner flames with added CO_2 [154] and CF_3H.[179] The temperature field and the velocity vectors for methane-air cup burner flames with 10 % CO_2, and 0 μL/L and 100 μL/L of $Fe(CO)_5$ are shown in Figure 3-25, while Figure 3-26 shows the calculated blow-off behavior.

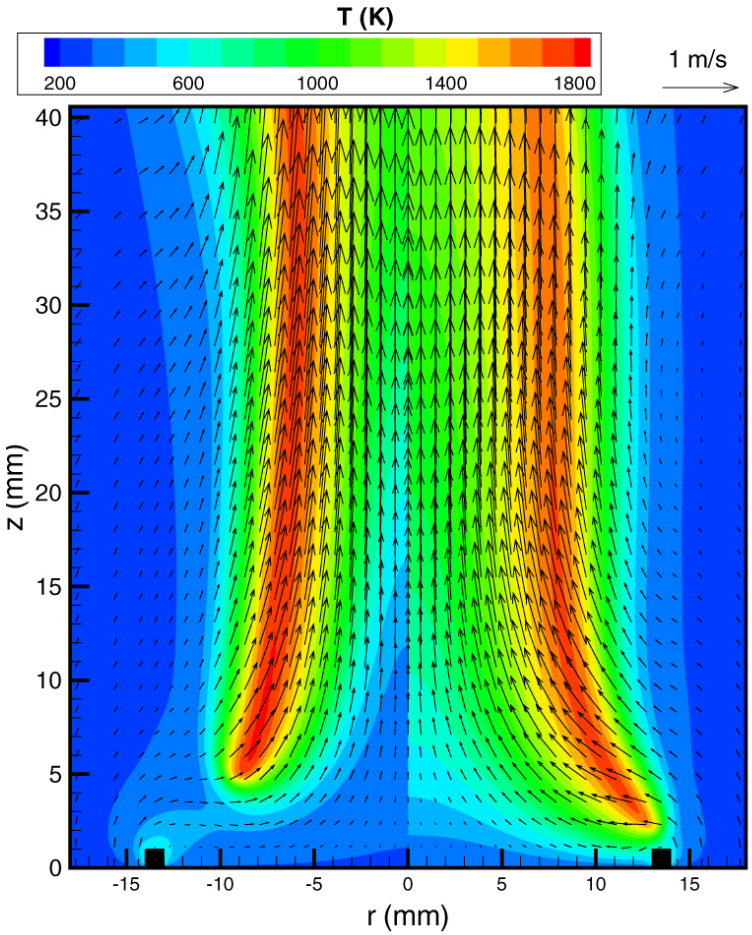

Figure 3-25. Calculated Temperature (color scale) and Velocity Vectors (arrows) for Methane-air Cup Burner Flame with an Oxidizer Stream CO_2 Volume Fraction of 0.1, with (left) and without (right) an Added $Fe(CO)_5$ Volume Fraction of 100 μL/L.[153]

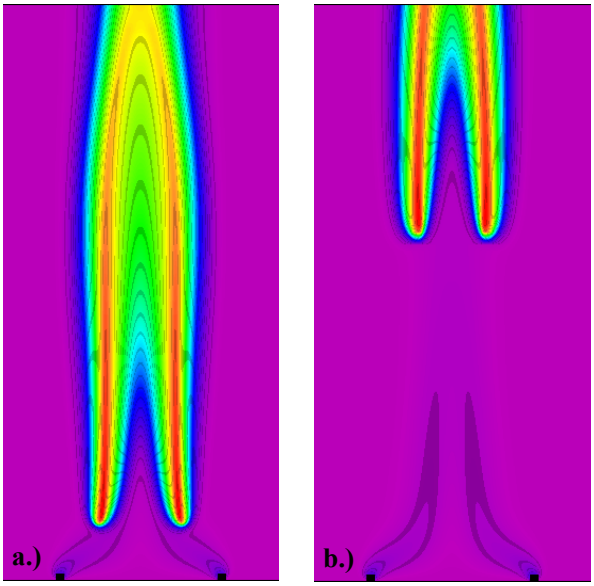

Figure 3-26. Map of Calculated Temperatures in Cup Burner Methane-air Flames with 10 % CO_2 in the Oxidizer Stream and (a) 0.011 and (b) 0.012 $Fe(CO)_5$ Volume Fraction in the Air Stream, Illustrating the Blowoff Phenomenon.[153]

As in other flame configurations, the loss of effectiveness of iron and a discrepancy between predicted (gas phase model) and measured effectiveness were both correlated with the formation of particles, as shown in Figure 3-27.

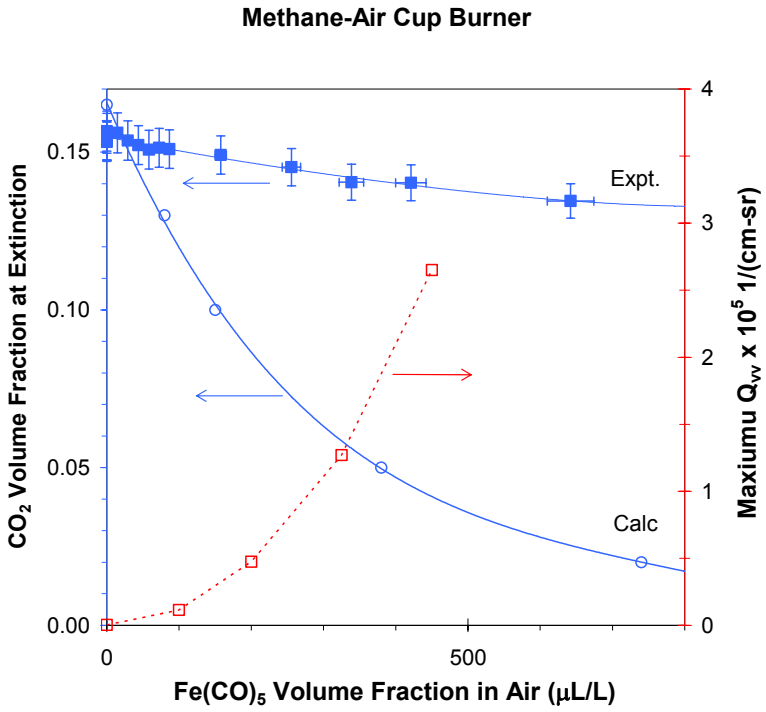

Figure 3-27. Experimental and Calculated Extinction Volume Fraction of CO_2 (left axis) and Peak Measured Scattering Cross Section (right axis), as a Function of the Volume Fraction of $Fe(CO)_5$ in the Air Stream.[85,153]

To understand the propensity for particle formation, the degree of supersaturation of some of the iron-containing intermediates was calculated through the flame, using the detailed flame structure obtained from the model, together with vapor pressure data available from the literature. For a height above the cup burner which passes through the flame kernel (i.e., the stabilization region), Figure 3-28 shows the radial profile of temperature and volume fractions of iron species and radicals, as well as the supersaturation ratio (which is the ratio of the calculated species partial pressure to the planar vapor pressure at the local conditions). The supersaturation ratio is highest for FeO, followed by Fe and $Fe(OH)_2$, and the values decrease as the radial location of peak temperature is approached. Note that vapor pressure data for FeOH, FEOOH, and FeO_2 are not available, so their condensation potential has not been assessed. The condensation potential is strong since the temperature of the flame kernel is much lower than the relevant regions of premixed or counterflow diffusion flames.

Finally, the numerical model was extended to include calculation of the particle trajectory for inert particles added to the flame, including the effects of gravity, drag, and thermophoretic forces. This was done since early estimates[180] were that thermophoresis may have been driving the particles away from the flame region. The results of the calculations (Figure 3-29) show that near the flame base, there was some deviation of the particles both up and down around the reaction kernel; however, examination of the estimated radial and axial thermophoretic velocities shows them to have been much less than the gas velocity. Consequently, the particles still passed directly into the reaction kernel, so the effect of thermophoresis near this region is expected to be minor. Nonetheless, the other results described above provided evidence that the loss of effectiveness was due to particle formation.

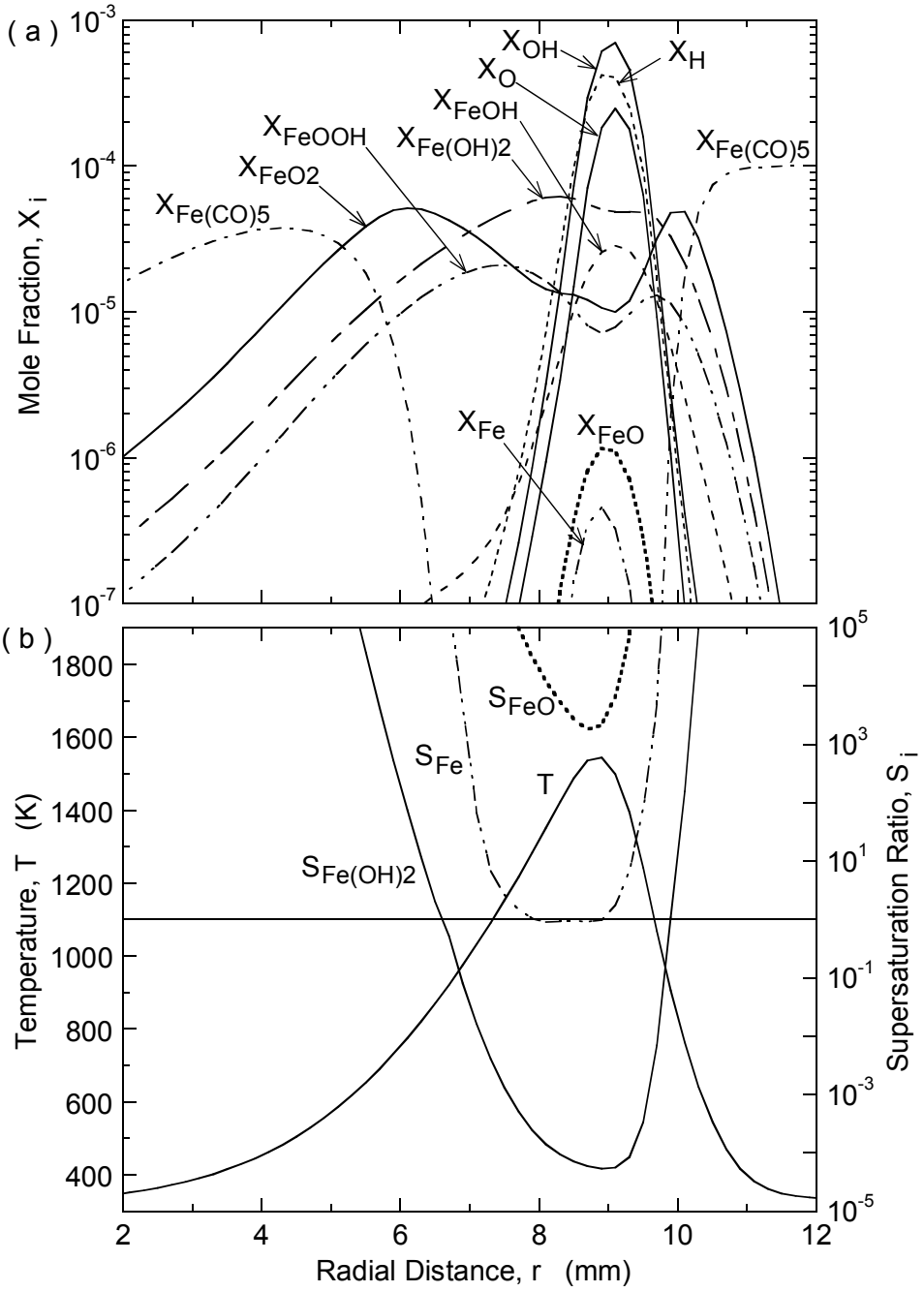

Figure 3-28. (a) Calculated Volume Fractions, Xi, of Iron-containing and Other Major Species as a Function of Radial Position at 4.8 mm above the burner (corresponding to the location of the reaction kernel in the flame base); and (b) the Supersaturation Ratio, Si, for Fe, FeO, and $Fe(OH)_2$.[153]

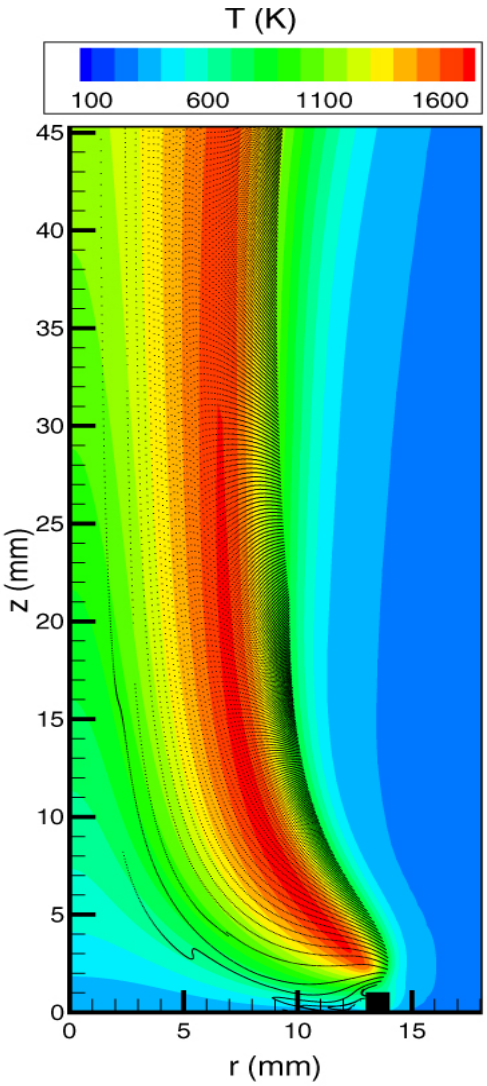

Figure 3-29. Calculated Particle Trajectories for Free Molecular Regime Particles in a CH_4–air Flame with 10 % CO_2 in the Oxidizer Stream.[153]

A review of the results from previous work with particle formation in premixed, counterflow diffusion, and cup burner flames inhibited by $Fe(CO)_5$ outlined the importance of the following physical effects with respect to effective chemical inhibition:

- Gas phase transport of the active iron-containing species to the region of high H-atom concentration is necessary for efficient inhibition.
- Particle formation near the location of peak [H] can act as a sink for the iron-containing intermediate species and reduce the catalytic effect.
- The volume fraction of inhibitor influences condensation, since at low values, it may be below its saturation value.
- The available residence time affects particle growth.
- If the particles are small enough, they can re-evaporate upon passing into the high temperature region of the flame.
- Thermophoretic forces can be large in the flame and re-distribute particles away from peak [H].

- Convection and drag forces combined with the existing flow field in the flame can prevent particles from reaching the region of peak [H].
- The flame temperature of the stabilization region of cup burner flames is much lower than in premixed or counterflow diffusion flames, exacerbating the condensation potential.

In order to assess the condensation potential of other flame inhibiting metals, it is necessary to know their concentrations in the flame, as well as their local vapor pressure. The availability of these data for the metals listed in Table 3-4 is discussed below.

3.3.4 Flame Inhibition by Tin and Manganese

Introduction

Faced with the finding that the highly effective flame inhibitor iron pentacarbonyl loses its effectiveness due to condensation of the active species to particles, it became important for the NGP to determine if other metal-containing compounds caused similar strong flame inhibition while not suffering from the loss of effectiveness. Since there had been evidence that manganese- and tin-containing compounds were of high flame inhibition efficiency and since these compounds typically have higher vapor pressures than the corresponding iron compounds, these two families became a subject of NGP research.

Tin compounds are used as fire retardant additives for polymers, and as agents to reduce smoke and CO formation.[127,181] The mechanism of flame inhibition has been attributed to both the promotion of condensed phase char and gas phase flame inhibition.[181,182] Lask and Wagner[34] found $SnCl_4$ to be about 1/34 as effective as $Fe(CO)_5$ at reducing the burning velocity of premixed n-hexane–air flames by 30 %, and Miller et al.[112] found it to be about 2/3 as effective as $Fe(CO)_5$ at reducing the flame speed of hydrogen-air flames by 80 %. Miller[113] measured the amount of inhibitor required to lift-off a premixed $CH_4/O_2/N_2$ flat flame at low pressure, and found that tetramethyltin ($Sn(CH_3)_4$, TMT) and $SnCl_4$ required a mole fraction of 1.7 % and 1.1 %, respectively; whereas $Fe(CO)_5$ and Br_2 required 0.23 % and 2.3 %, respectively. Morrison and Scheller[111] investigated the effect of 20 flame inhibitors on the ignition of hydrocarbon mixtures by hot wires, and found that $SnCl_4$ was the most effective inhibitor tested for increasing the ignition temperature; whereas the powerful flame inhibitors CrO_2Cl_2 and $Fe(CO)_5$ had no effect on the ignition temperature. As a result of these studies, $SnCl_4$ was recommended as a compound deserving further study.[183]

The effects of manganese compounds on flames had also been studied. Vanpee and Shirodkar[92] investigated the influence of many metal chlorides and metal acetates and acetylacetonates on the limiting oxygen index at extinction in a partially premixed counterflow pool burner of ethanol and air. In their experiments, the inhibitor was dissolved in ethanol, which was aspirated into the air stream. They found manganese acetylacetonate to be more effective than acetylacetonates of iron or chromium. Westblom et al.[148] analyzed the consequence of trace amounts of methylcyclopentadienylmanganese tricarbonyl ($CH_3C_5H_4Mn(CO)_3$, MMT) on the flame structure of a premixed propane-air flame at 5.33 kPa, but found no measurable effect. They suggested a kinetic model for the influence of MMT on those flames.[148] In a review article, Howard and Kausch[127] reported that manganese-containing compounds were among the most effective soot-reducing fuel additives. Finally, MMT is a known antiknock agent for gasoline,[184] and an NGP panel[185] suggested manganese compounds as agents for further consideration in studies of fire suppression performance.

This section presents NGP data on flame inhition by manganese- and tin-containing compounds. The additive influence was analyzed through the effects on the laminar burning velocity of methane-air mixtures for different equivalence ratios and oxygen mole fractions. The kinetic mechanisms of flame inhibition were analyzed by comparing simulation results with experimental data. The relative inhibition efficiencies of TMT, MMT, $Fe(CO)_5$, and CF_3Br were deduced and analyzed. While the manganese and tin compounds tested are too toxic to be used directly as fire suppressants, they provide convenient means for introducing Mn and Sn to a flame, so that the inhibition mechanisms of these elements can be studied.

Experimental Apparatus

Premixed flames were used for the first tests of new metallic inhibitors. The premixed burning velocity is a fundamental parameter describing the overall reaction rate, heat release, and heat and mass transport in the flame. Furthermore, the inhibitor reaches the reaction zone by convection, so that the amount which enters is unambiguous. The experiments are rapid and relatively straightforward, allowing tests over a wide range of conditions. The flames are easily modeled with existing numerical codes, so that detailed information on the mechanism of chemical inhibition can be determined. There is also a very large data base on the effectiveness of other chemical and inert inhibitors in premixed flames for comparison.

The laminar flame speed S_L in a premixed flame provides a measure of an agent's reduction of the global reaction rate. While good techniques exist which allow measurement of burning velocity under conditions of controlled stretch rates,[186] they require seeding with particles for determination of the local gas velocity. Since the presence of particles would influence the condensation rates of metallic species, these tests instead employed the total area method with a Bunsen-type flame.[187] The experimental arrangement, described in detail elsewhere,[57,102,106,118,164] was modified to accommodate new evaporators for TMT and MMT. A Mache-Hebra nozzle burner (1.0 cm ± 0.05 cm diameter) produced a premixed Bunsen-type flame about 1.3 cm tall with a straight-sided schlieren image that was captured by a video frame-grabber board in a PC. Digital mass flow controllers held the oxygen mole fraction in the oxidizer stream $X_{O2,ox}$, the equivalence ratio ϕ, and the flame height constant while maintaining the inlet mole fraction of the inhibitor (X_{in}) at the desired value. The average burning velocity was determined from the reactant flows and the schlieren image using the total area method. The fuel gas was methane (Matheson UHP, 99.9 %), and the oxidizer stream consisted of nitrogen (boil-off from liquid N_2) and oxygen (MG Industries, H_2O less than 50 μL/L, and total hydrocarbons less than 5 μL/L). The inhibitors used were $Fe(CO)_5$ (Aldrich), TMT (Alfa Aesar), MMT (Alfa Aesar), CF_3Br (Great Lakes), N_2 (boil-off), and CO_2 (Airgas). The catalytic agents were liquids at laboratory conditions. Since they were required in low mole fraction, they were added to the flame in gaseous form rather than as droplets. The $Fe(CO)_5$ was added to the carrier gas using a two-stage saturator in an ice bath.[118] Nitrogen was the carrier gas for all agents. The TMT was added using an identical two-stage saturator, with a volume of liquid TMT in each stage greater than 50 cm^3 for all tests. The ice bath was maintained at (0 ± 0.2) °C with a maximum carrier gas flow 0.40 L/min. Because of the toxicity of the agents, the $Fe(CO)_5$ and TMT saturators, as well as the premixed flame burner, were located in fume hoods. For the MMT, the saturator had three stages, each 20 cm long, 2.36 cm I.D. stainless steel tube, and the entire apparatus was submerged in a controlled temperature bath (Neslab), and vented. The bath temperature was typically (79.2 ± 0.1) °C, and the carrier gas flow for this saturator was always <0.5 L/min. The mole fraction of the organometallic inhibitors in the air stream was calculated based on the measured air flow, measured carrier gas flow, and vapor pressure of the agent at the bath temperature, assuming saturated carrier gas. The parameters in the Antoine equation, $\log_{10}(P)=A-B/(T+C)$ (T in °C, P in bar), were (A,B,C): (6.77273, 4.0932, 7.2283),

(1258.22, 1286.16, 1882), and (211.587, 235.846, 200) for $Fe(CO)_5$, [188] TMT, [189] and MMT, [190] respectively. Since the vapor pressure of MMT is much lower than that of the other agents, experiments with MMT were conducted at a slightly elevated temperature, with the transfer lines and inlet gases maintained at (80 ± 3) °C and the burner tube maintained at (80 ± 1) °C. For the experiments with TMT and $Fe(CO)_5$, the inlet gas temperature T_{in} was (294.2 ± 1) K. Although the absolute value of the burning velocity is quite sensitive to the inlet temperature, comparisons of agent performance across this range of differing gas inlet temperatures is valid, since the *reduction* in the *normalized* burning velocity with agent addition was relatively insensitive in T_{in}. For example, calculations for inhibition by TMT (discussed below), and calculations and experiments with CO_2 (unpublished data of Reference 106) showed that changing the inlet gas temperature from 294 K to 353 K provided nearly identical curves of normalized burning velocity versus inhibitor mole fraction, differing from each other by less than 2 % for the two inlet temperatures.

Tests were performed for ranges of equivalence ratio and oxygen mole fraction in the oxidizer stream $X_{O_2,ox}$. The agent mole fraction was calculated relative to the total reactant flow. The test conditions are listed in Table 3-6. The inhibitor for which each of the test conditions was used is included for reference; the values in the table are for uninhibited flames only. Note that while the inlet temperature for the $Fe(CO)_5$ and TMT experiments was 294 K, the experimental and numerically calculated burning velocities in the table have been converted to equivalent values at 298 K to facilitate comparison with other values available in the literature.

Table 3-6. Uninhibited Laminar Burning Velocities S_L and Adiabatic Flame Temperatures T_{AFT} from 1-D Planar Numerical Calculations, Together with the Average Burning Velocity Measured in the Bunsen-type Flames.

Inhibitor(s)	ϕ	$X_{O_2,ox}$	T_{in} K	T_{AFT} K	$S_{L,calc}$, cm/s	$S_{L,exp}$ cm/s
TMT	0.9	0.21	298	2159	35.3	33.9 ± 1.3
	1.0	"	"	2235	39.6	38.0 ± 2.3
	1.1	"	"	2193	39.8	38.0 ± 1.5
	1.0	0.20	"	2185	34.7	33.6 ± 1.4
	"	0.244	"	2377	57.0	58.0 ± 3.4
MMT	0.9	0.21	353	2177	48.0	47.2 ± 1.5
	1.0	"	"	2264	53.2	52.9 ± 2.9
	1.1	"	"	2251	53.6	52.8 ± 2.0
	1.0	0.19	"	2167	41.3	39.9 ± 1.6
	"	0.2	"	2220	47.4	45.5 ± 1.7
	"	0.244	"	2396	74.3	74.7 ± 4.1
MMT and $Fe(CO)_5$	1.0	0.244	353	2396	74.3	75.9 ± 4.9

The burning velocity in Bunsen-type flames is known to vary at the tip and base of the flame; however, these effects are most important over a small portion of the flame. Several steps were taken to minimize the influence of curvature and stretch on interpretation of the action of the chemical inhibitor.

- Use of the schlieren image for the flame area, which was maintained at a constant size (1.3 cm tall) for all tests.
- Normalization of the burning velocity of inhibited flames, i.e., the burning velocity of the inhibited flame divided by the burning velocity of the uninhibited flame, in order to reduce the error caused by flame curvature and stretch.
- Limiting interpretation of the data to inhibitor loading which produced less than 40 % reduction in flame speed.

Determination of the uncertainties in the experimental data using the present apparatus has been described in detail elsewhere.[118] For the present data, the uncertainty (expanded uncertainties with a coverage factor of 2) in the normalized burning velocity were less than ± 5 % for all cases. The uncertainty in the equivalence ratio was 1.4 %. Neglecting the uncertainties (unspecified) in the vapor pressure correlation for $Fe(CO)_5$, TMT, and MMT, uncertainties in the bath temperature, ambient pressure and carrier gas flow rate yielded an inhibitor mole fraction uncertainty of 6.5 %.

Kinetic Mechanisms and Numerical Modeling

There are few data on the chemical kinetics of tin compounds at flame temperatures, although kinetics studies of tin have been conducted for chemical vapor deposition. Studies with H_2-O_2-N_2 flames by Bulewicz and Padley[191] indicated that tin was present as Sn, SnO, and SnOH, with SnO overwhelmingly predominant. Recent spectroscopic data also indicated that tin was present in flames as Sn, SnO, and SnOH,[192] with SnO accounting for approximately 97 % by volume of all tin species.

The present kinetic model for flame inhibition by tin compounds contains reactions of the species Sn, SnO_2, SnO, SnH and SnOH. The reaction set was based on the consideration of possible reactions of tin-containing species with the radical pool and with the main species of methane combustion. The mechanism, listed in Table 3-7, consists of 37 reactions of tin-containing species. Rate constants were obtained from the literature when available, or otherwise estimated using empirical procedures and analogies with similar reactions. The reverse rates of the reactions in Table 3-7 were calculated from the forward rate and the equilibrium constant. It was assumed that tin (and manganese) species are non-reactive with hydrocarbon molecules. In the model development, estimates of rate constants were first made, and then the rates of the most important reactions were adjusted (based on sensitivity analysis) to provide agreement with the experimental results. The decomposition of TMT was described by the overall step listed in Table 3-7, but using the rate constant for the reaction $Sn(CH_3)_4 \rightarrow Sn(CH_3)_3 + CH_3$.[193] Enthalpies of formation for the tin-containing (and manganese-containing) species are presented in Table 3-8. Enthalpies of formation for SnOH and SnH were estimated based on bond energies from References 191 and 194.

Table 3-7. Reaction Rate Data for Tin Inhibition of Premixed Methane-air Flames.
($k = A\ T^b\ \exp(-E/RT)$, mole, s, cm, kJ)

No.	Reaction	A	b	E	Reference
1	$SnC_4H_{12} => Sn+C_2H_6+C_2H_6$	7.94E+13	0.0	230.	193
2	$Sn+H+M = SnH+M$	1.00E+15	0.0	0.0	a
3	$Sn+OH+M = SnOH+M$	5.36E+18	-0.45	0.0	*
4	$Sn+OH = SnO+H$	1.00E+13	0.0	27.2	a
5	$Sn+O+M = SnO+M$	1.00E+17	0.0	0.0	a
6	$Sn+O_2 = SnO+O$	3.07E11	0.79	3.63	195
7	$Sn+O_2 (+M) = SnO_2 (+M)$	2.00E+13	0.0	0.0	a
	Low pressure limit:	1.5E+18	0.0	16.7	
8	$Sn+HCO = SnH+CO$	3.00E+13	0.0	0.0	a
9	$Sn+CH_3O = SnO+CH_3$	2.00E+13	0.0	0.0	a
10	$Sn+CO_2 = SnO+CO$	1.39E+14	0.0	75.6	195
11	$Sn+HO_2 = SnO+OH$	1.00E+13	0.0	0.0	a
12	$SnO+H+M = SnOH+M$	5.50E+17	0.0	0.0	a
13	$SnO+O+M = SnO_2+M$	1.00E+20	-1.0	0.0	a
14	$SnO+HCO = SnOH+CO$	9.30E+13	0.0	0.0	a
15	$SnO+HO_2 = SnOH+O_2$	3.00E+13	0.0	29.3	a
16	$SnO_2+H = SnO+OH$	1.00E+14	0.0	8.37	a
17	$SnO_2+OH = SnOH+O_2$	3.00E+12	0.0	31.4	a
18	$SnO_2+OH = SnO+HO_2$	3.00E+12	0.0	46.0	a
19	$SnO_2+O = SnO+O_2$	3.00E+13	0.0	8.37	a
20	$SnO_2+CH3 = SnO+CH_3O$	3.00E+12	0.0	18.8	a
21	$SnO_2+CO = SnO+CO_2$	2.00E+12	0.0	20.9	a
22	$SnOH+H = Sn+H_2O$	1.20E+12	0.0	12.6	a
23	$SnOH+H = SnO+H_2$	7.10E+13	0.0	4.18	a
24	$SnOH+OH = SnO+H_2O$	6.30E+13	0.0	0.0	a
25	$SnOH+O = SnO+OH$	3.00E+13	0.0	0.0	a
26	$SnOH+O = SnO_2+H$	5.00E+12	0.0	37.7	a
27	$SnOH+CH_3 = SnO+CH_4$	2.00E+13	0.0	4.18	a
28	$SnH+H = Sn+H_2$	5.00E+13	0.0	4.18	a
29	$SnH+OH = Sn+H_2O$	3.00E+13	0.0	0.0	a
30	$SnH+OH = SnOH+H$	5.00E+12	0.0	20.9	a
31	$SnH+O+M = SnOH+M$	1.00E+15	0.0	0.0	a
32	$SnH+O = Sn+OH$	5.00E+13	0.0	4.18	a
33	$SnH+O = SnO+H$	8.00E+12	0.0	4.18	a
34	$SnH+CH_3 = CH_4+Sn$	5.00E+13	0.0	4.18	a
35	$SnH+HCO = Sn+CH_2O$	2.00E+12	0.0	18.8	a
36	$SnH+O_2 = SnO+OH$	3.00E+12	0.0	29.3	a

a Estimates
* By analogy with reactions of K species in Reference 196

Table 3-8. Thermodynamic Properties of Tin- and Manganese-containing Species (298 K).

Species	Enthalpy of Formation kJ/mol	Entropy J/(mol K)	Heat Capacity J/(mol K)	Reference
Mn	283.6	173.6	20.8	197
MnO	161.7	236.0	31.7	197
MnO_2	23.01	269.3	42.2	197
MnOH	17.32	250.3	45.8	197
$Mn(OH)_2$	-373.2	291.2	67.1	e, 198
MnOOH	-116.3	283.3	53.9	e, 198
MnH	197.9	213.6	29.6	197
MMT	-439.3	401.7	149.9	198
Sn	301.2	168.4	21.3	197
SnO	21.91	232.1	31.8	197
SnO_2	11.69	251.5	49.5	197
SnOH	-15.06	244.8	46.0	*e*, 191
SnH	268.2	214.7	29.7	*e*, 194
$Sn(CH_3)_4$	-17.70	361.2	137.8	199,178
Sn_2	425.4	267.2	42.1	197

a Estimates

The kinetic mechanism for studying the influence of manganese additives in premixed methane-air flames is presented in Table 3-9. The list of possible Mn-containing species participating in inhibition reactions includes Mn, MnH, MnO, MnOOH, MnHOH, MnOH, MnO, MnO_2 and $Mn(OH)_2$. All species except MnH and MnHOH were considered in the mechanism of Smith.[198] The role of MnOH and MnO in radical recombination was discussed by Bulewicz and Padley[116], and the species MnO and Mn were recently measured in a low pressure propane flame doped by MMT.[148] Hildenbrand and Lau[200] used mass spectrometry to identify the species MnO_2, MnOH, and $Mn(OH)_2$. MnH was included in the current model since equilibrium calculations showed it to be present in significant quantities in MMT-inhibited flames.

The manganese inhibition reaction set was reduced from an initial list of approximately 160 reactions to 61 reactions based on thermochemical considerations and preliminary calculations. The decomposition of MMT followed the overall description suggested in References 148 and 198, and used their rate constants for the Mn-species reactions whenever possible. Rate constants for the remaining reactions were estimated by analogy and based on thermochemical estimates. The main assumptions were the formation of MnO_2 through the reaction of Mn atom with oxygen molecule and the formation of $Mn(OH)_2$ via reaction of MnO with water (both by analogy to reactions of iron-containing species[104]).

The transport parameters of tin- and manganese-containing species were estimated through analogy with similar metallic species, or based on molecular weight correlations for similar species.

Kinetic models for highly effective flame inhibitors can be considered to consist of two sub-models. The first sub-model includes reactions for the agent decomposition and formation of the active inhibiting species, and the second includes the inhibition reactions. In previous work, it was shown that for the phosphorus-containing compound DMMP and for ferrocene, the decomposition reactions have a small influence on the predicted inhibitor efficiency as long as the overall activation energy of decomposition is less than 250 kJ/mol to 335 kJ/mol.[106,201] In the present work, this was also found to be true for TMT and MMT decomposition.

Table 3-9. Reaction Rate Data for Manganese Inhibition of Premixed Methane-air Flames.
($k = A\ T^b \exp(-E/RT)$, mole, cm, s, kJ)

No.	Reaction	A	b	E	Reference
1	Mn+H+M = MnH+M	1.00E+15	0.0	0.0	a
2	Mn+OH+M = MnOH+M	8.00E+22	-2.2	0.0	198
3	Mn+O+M = MnO+M	1.00E+15	0.0	0.0	a
4	$Mn+O_2 = MnO+O$	2.50E+14	0.0	125.5	198
5	$Mn+O_2$ (+M) = MnO_2 (+M)	2.00E+13	0.0	0.0	a
	Low pressure limit:	1.50E+18	0.0	12.6	
6	Mn+HCO = MnH+CO	3.00E+13	0.0	0.0	a
7	MnO+H+M = MnOH+M	7.00E+15	0.0	0.0	198
8	$MnO+O+M = MnO_2+M$	2.00E+19	-1.0	0.0	198
9	MnO+H = Mn+OH	1.00E+14	0.0	16.7	a
10	MnO+OH+M = MnOOH+M	3.00E+17	0.0	0.0	a
11	$MnO+CH_3 = Mn+CH_3O$	1.00E+14	0.0	29.3	a
12	$MnO+H_2 = Mn+H_2O$	3.00E+12	0.0	20.9	202
13	$MnO+H_2O = MnO_2H_2$	5.40E+12	0.0	0.0	202
14	$MnO+CO = Mn+CO_2$	3.00E+11	0.0	0.0	198
15	MnO+HCO = MnOH+CO	2.40E+13	0.0	0.0	198
16	$MnO+CH_2OH = MnOH+CH_2O$	2.40E+13	0.0	0.0	198
17	MnO_2+H+M = MnOOH+M	2.00E+22	-1.5	0.0	198
18	MnO_2+H = MnO+OH	1.00E+14	0.0	29.3	a
19	MnO_2+OH = $MnOH+O_2$	3.00E+12	0.0	29.3	a
20	MnO_2+O = $MnO+O_2$	5.00E+13	0.0	8.37	a
21	MnO_2+CO = $MnO+CO_2$	2.00E+12	0.0	20.9	a
22	MnOH+H = $Mn+H_2O$	1.20E+12	0.0	2.09	198
23	MnOH+H = $MnO+H_2$	3.00E+13	0.0	4.18	a
24	MnOH+OH+M = MnO_2H_2+M	1.00E+23	-2.0	0.0	198
25	MnOH+OH = $MnO+H_2O$	1.00E+13	0.0	6.28	198
26	MnOH+O+M = MnOOH+M	1.00E+18	0.0	0.0	a
27	MnOH+O = $Mn+HO_2$	3.00E+13	0.0	71.1	a
28	MnOH+O = MnO+OH	3.00E+13	0.0	0.0	198

No.	Reaction	A	b	E	Reference
29	$MnOH+O = MnO_2+H$	5.00E+12	0.0	37.7	a
30	$MnOH+CH_3 = MnO+CH_4$	2.00E+13	0.0	12.6	a
31	$MnOOH+H+M = MnO_2H_2+M$	1.00E+16	0.0	0.0	a
32	$MnOOH+H = MnO+H_2O$	2.00E+13	0.0	0.0	a
33	$MnOOH+H = MnOH+OH$	3.00E+13	0.0	20.9	a
34	$MnOOH+H = MnO_2+H_2$	1.00E+13	0.0	16.7	a
35	$MnOOH+OH = MnO_2+H_2O$	6.00E+12	0.0	6.28	198
36	$MnOOH+O = MnOH+O_2$	2.00E+13	0.0	10.5	a
37	$MnOOH+O = MnO+HO_2$	3.00E+12	0.0	66.9	a
38	$MnOOH+O = MnO_2+OH$	3.00E+13	0.0	18.8	a
39	$MnOOH+CH_3 = MnO+CH_3OH$	3.00E+12	0.0	31.4	a
40	$MnOOH+CH_3 = MnOH+CH_3O$	1.00E+13	0.0	46.0	a
41	$MnOOH+CO = MnOH+CO_2$	2.00E+12	0.0	20.9	a
42	$MnO_2H_2+H = MnOH+H_2O$	6.60E+13	0.0	4.18	a
43	$MnO_2H_2+H = MnOOH+H_2$	5.00E+13	0.0	79.5	a
44	$MnO_2H_2+OH = MnOOH+H_2O$	1.00E+13	0.0	37.7	a
45	$MnO_2H_2+O = MnOOH+OH$	2.00E+13	0.0	83.7	a
46	$MnO_2H_2+CH_3 = MnOOH+CH_4$	1.00E+13	0.0	87.9	a
47	$MnH+H = Mn+H_2$	5.00E+13	0.0	12.6	a
48	$MnH+OH = Mn+H_2O$	1.00E+14	0.0	0.0	a
49	$MnH+O+M = MnOH+M$	1.00E+15	0.0	0.0	a
50	$MnH+O = Mn+OH$	1.00E+14	0.0	8.37	a
51	$MnH+CH_3 = CH_4+Mn$	1.00E+14	0.0	8.37	a
52	$MnH+O_2+M = MnOOH+M$	1.00E+16	0.0	0.0	a

a Estimates

The laboratory flames inhibited by TMT and MMT were numerically modeled as one-dimensional, freely-propagating flames. Solutions were obtained using the Sandia flame code Premix,[203] and the CHEMKIN[204] and transport property[205] subroutines. (Solutions were obtained for values of GRAD and CURV of 0.17 and 0.25 in PREMIX.) The kinetic mechanism for methane combustion was GRIMech 3.0, [206] with the nitrogen chemistry removed. The methane sub-mechanism contained 36 species and 219 reactions.[i] The calculations were for 1-D planar flames, while the experiments determined the average flame speed of Bunsen-type flames which can be influenced by curvature and stretch. To minimize these effects, both the experimental and calculated data are presented as normalized flame speed reduction.

[i] The reaction mechanisms used for the present calculations for flames with manganese or tin compounds should be considered only as a starting point. Numerous changes to both the rates and the reactions incorporated may be made once a variety of experimental and theoretical data are available for testing the mechanism.

Results

Observations

The appearance of the flames with added organometallic inhibitors is shown in Figure 3-30. Flames with iron pentacarbonyl were bright orange, with tetramethyltin they were bright pale blue, and with MMT, yellow-green. The intensity of the visible emission increased with inhibitor mole fraction. As the loading of metallic inhibitor increased, there became visible a luminous outer shroud as seen clearly in the last two images on the right in Figure 3-30. These were regions of high particle concentration from inhibitor condensation, leading to broad-band black body radiation, visible here in the orange part of the spectrum. For the TMT-inhibited flames, a white-colored powder (presumably tin oxide) formed on the rim of the quartz burner tube during the tests, especially at high TMT loading. This deposit was removed between collection of each data point. For MMT and $Fe(CO)_5$, a dark red or an orange deposit was formed, respectively. The rate of deposition for these inhibitors, however, was much lower than for the TMT, which was added to the flames at mole fractions about ten times higher.

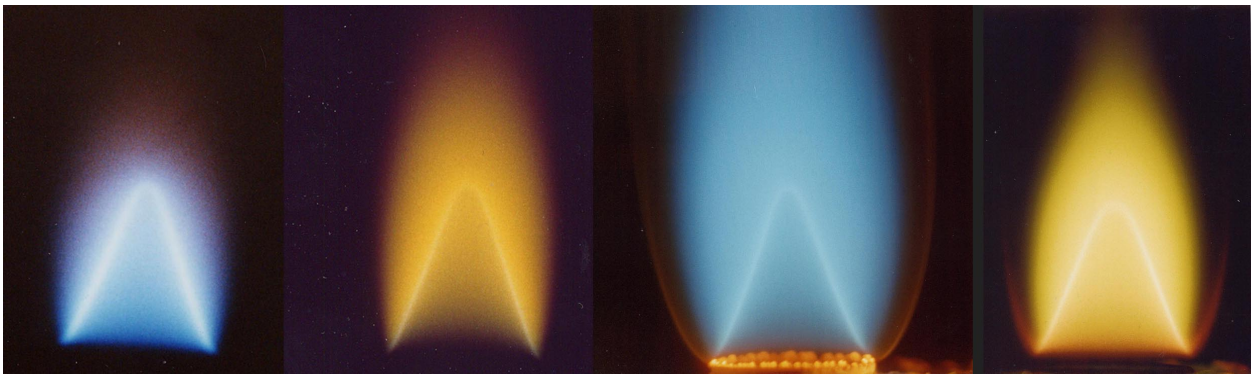

Figure 3-30. Visible Images of Methane-air Premixed Flames. (From left to right: no inhibitor, 50 µL/L of $Fe(CO)_5$, 4000 µL/L of TMT, and 400 µL/L of MMT).

Inhibition by Tetramethyltin

Figure 3-31 shows the relative burning velocity reduction with addition of TMT to methane-air flames ($X_{O_2,ox}$ =0.21) for values of equivalence ratio of 0.9, 1.0, and 1.1. The dotted lines are curve fits to the experimental data, and the solid lines are the results of the numerical calculations described above (and discussed below). Data are plotted as normalized burning velocity, which is the burning velocity of the inhibited flame divided by the value for the same flame in the absence of inhibitor. The calculated and experimental burning velocities, along with the calculated adiabatic flame temperatures of the uninhibited flames used for the normalization are listed in Table 3-6. For the uninhibited flames, the experimentally determined average burning velocities for the Bunsen-type flames were within about 4 % of the calculated values for 1-D planar flames. In Figure 3-31 (as well as Figure 3−32, Figure 3−33, Figure 3−34, and Figure 3−36 described below), the last data point shown represents the highest volume fraction of inhibitor for which flames could be stabilized on the present burner (i.e., they extinguished at higher volume fractions). The experimental results in Figure 3-31 demonstrate that for stoichiometric flames, 3000 µL/L of TMT reduced the flame speed by about 41 %, which is about a factor of two better than CF_3Br. The data also showed that, unlike $Fe(CO)_5$, the richer flames were inhibited more strongly by TMT than the leaner flames. (Additional numerical tests with SnO as the inhibitor showed that the poorer

inhibition of lean flames was due to the fuel effect from the hydrocarbon portion of the relatively large amounts of $Sn(CH_3)_4$ added to the flames.)

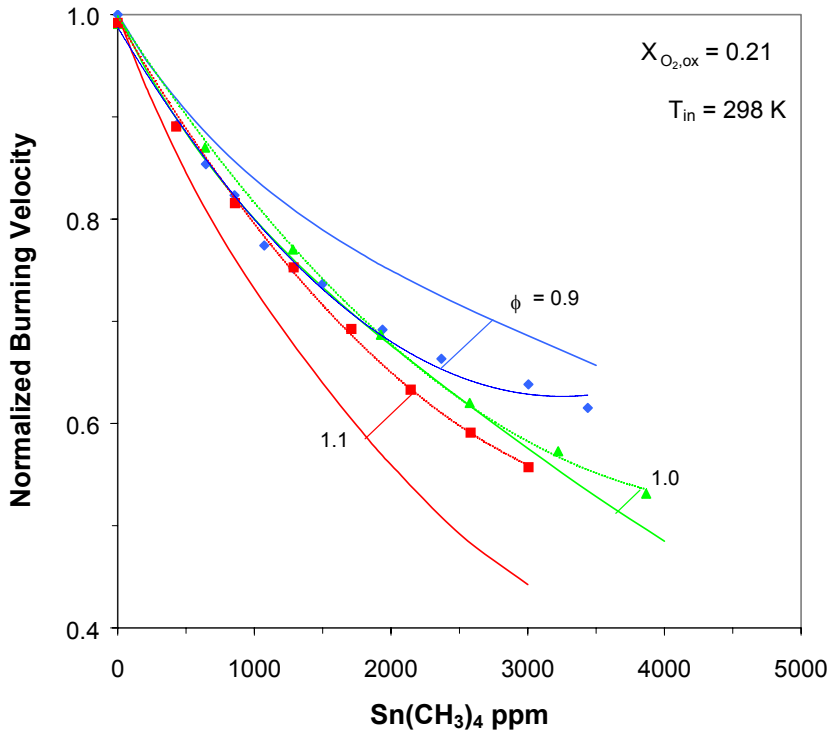

Figure 3-31. Normalized Burning Velocity of Premixed $CH_4/O_2/N_2$ Flames Inhibited by TMT for $X_{O2,ox}$=0.21 and ϕ=0.9, 1.0, and 1.1 (Dotted lines: curve fits to data; solid lines: numerical predictions.)

As described below, the burning velocity reduction caused by tin species was most sensitive to the rates of the reactions: SnO + H + M ↔ SnOH + M, and SnOH +H ↔ SnO + H_2. Consequently, the pre-exponential factors were adjusted in those rates to provide agreement with the experimental results for stoichiometric mixtures of methane with air. Note, however, the relatively high level of the rate constant for the reaction H + SnO + M ↔ SnOH + M. Bulewicz and Padley[116] also found that a high rate was required for this process to provide agreement with their experimental data on hydrogen atom recombination in the products of a hydrogen flames. As Figure 3-31 shows, the numerical model predicted the amount of inhibition well for stoichiometric flames. For rich and lean flames, however, the model over- and under-predicted the burning velocity, respectively. For the reaction set considered, reasonable adjustments to the rate constants did not provide better agreement.

Figure 3-32 shows the measured and calculated flame speeds for TMT in stoichiometric flames $X_{O_2,ox}$ equal to 0.20, 0.21, and 0.244. The experimental data and calculations (with adjusted rate constants) show good agreement for the three values of $X_{O_2,ox}$; however, for the hottest flames ($X_{O_2,ox}$ = 0.244), the mechanism slightly overpredicted the inhibition at low mole fraction, and underpredicted it for higher mole fraction. The experimental data show that for the slower and cooler flames (e.g., equivalence ratio is 0.9 or 1.0 and $X_{O_2,ox}$ = 0.20 or 0.21), the TMT started to lose its effectiveness above a certain value. For $Fe(CO)_5$ inhibited flames, such behavior was shown to be due to condensation of the iron-containing intermediates.[102]

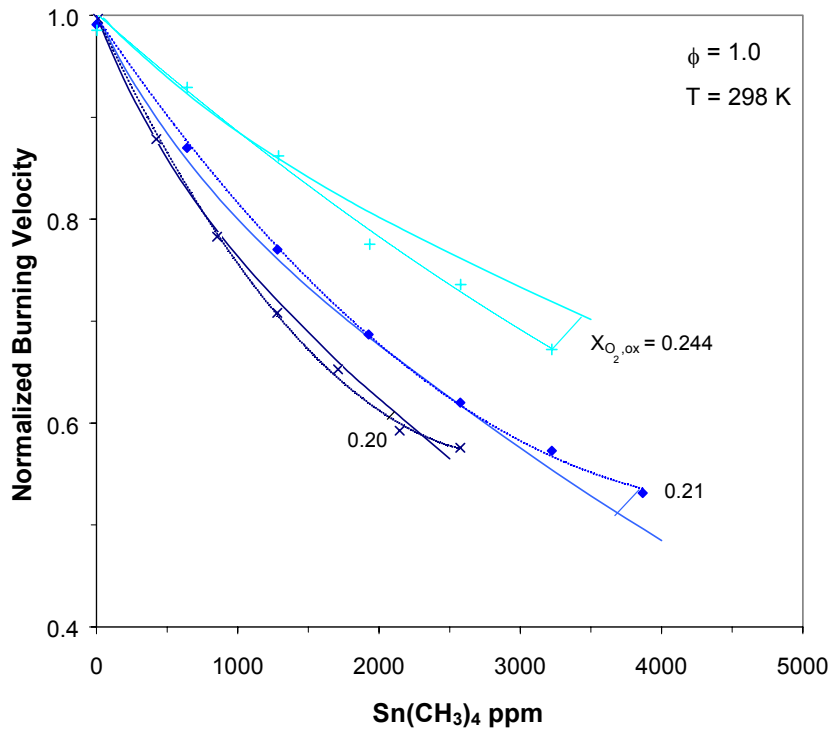

Figure 3-32 – Normalized Burning Velocity of Premixed $CH_4/O_2/N_2$ flames Inhibited by TMT for ϕ=1.0 and $X_{O_2,ox}$=0.20, 0.21, and 0.244. (Dotted lines: curve fits to the data; solid lines: numerical predictions)

Inhibition by MMT

The premixed flames inhibited by the Mn-containing compound MMT were slightly preheated (T_{in} = 80 °C). The values of the calculated and experimental uninhibited burning velocities, and the adiabatic flame temperatures are shown in Table 3-6. The normalized burning velocities of MMT-inhibited flames with variation in equivalence ratio and $X_{O_2,ox}$ are shown in Figure 3−33 and Figure 3−34. MMT was about 13 times more efficient at flame inhibition than TMT; however, it too started to lose its effectiveness for flame speed reductions near 50 %. Based on the sensitivity of the burning velocity to the reaction rates, the pre-exponential factors of the reactions $Mn(OH)_2 + H \leftrightarrow MnOH + H_2O$ and $MnO + H_2O \leftrightarrow Mn(OH)_2$ were adjusted to provide agreement with experimental data for these methane-air flames at ϕ=1.0. Using the rates shown in Table 3-9, the model predicted the burning velocity reduction quite well. Nonetheless, for the hottest flames ($X_{O_2,ox}$ = 0.244) this mechanism also overpredicted the inhibition slightly at low inhibitor mole fraction, and underpredicted the inhibition somewhat at intermediate mole fractions. Also, this gas phase mechanism did not capture the decrease in inhibitor effectiveness which occurred with increasing inhibitor initial mole fraction, likely a result of condensation of Mn-containing species.

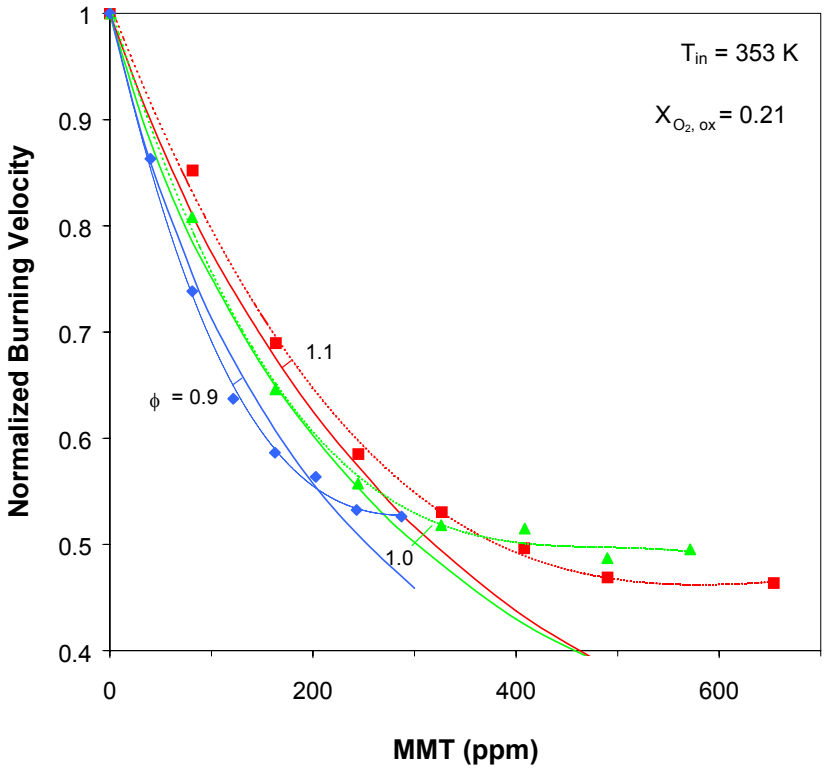

Figure 3-33. Normalized Burning Velocity of Premixed $CH_4/O_2/N_2$ Flames Inhibited by MMT with $X_{O2,ox}$=0.21 and ϕ=0.9, 1.0, and 1.1. (Dotted lines: curve fits to data; solid lines: numerical predictions)

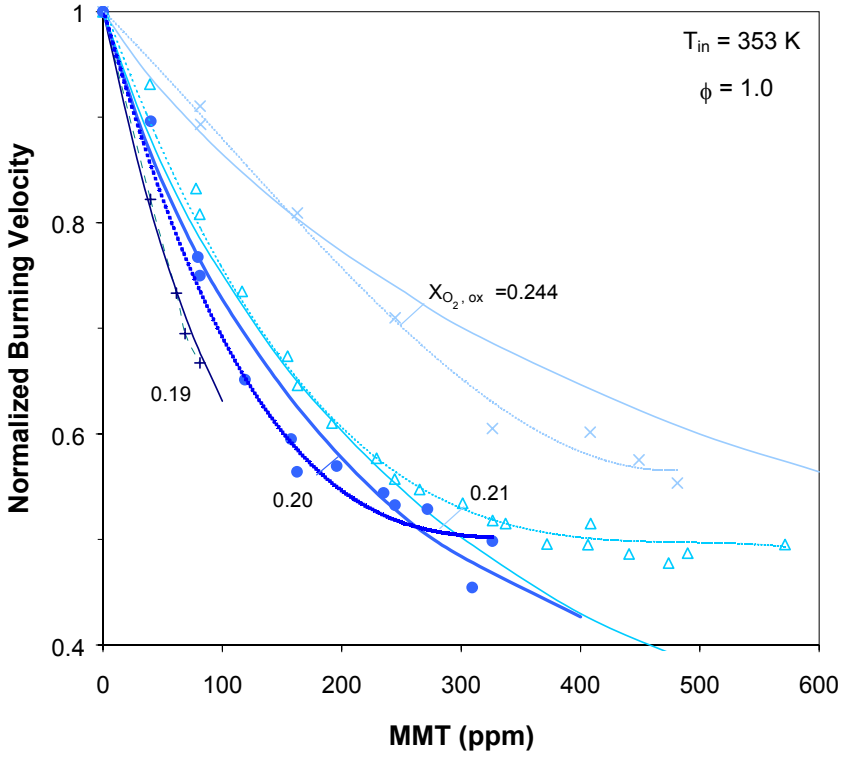

Figure 3-34. Normalized Burning Velocity of Premixed $CH_4/O_2/N_2$ Flames Inhibited by MMT, with ϕ=1.0 and $X_{O2,ox}$=0.19, 0.20. 0.21, and 0.244. (Dotted lines: curve fits to the data; solid lines: numerical predictions)

Comparative Performance of Metals

Figure 3-35 compares the inhibition effectiveness of $Fe(CO)_5$, MMT, TMT, $SnCl_4$, CF_3Br, and CO_2. The data for $SnCl_4$ inhibition from Reference 34 show tin tetrachloride was as effective in n-hexane/air flames as TMT was in methane/air flames. Although the experimental data shown for TMT and $SnCl_4$ are not for an elevated inlet temperature of 80 °C, numerical calculations showed that the reduction in the *normalized* flame speed caused by TMT addition with T_{in}=298 K differs from that with T_{in}=353 K by less than 1 %. $Fe(CO)_5$ is significantly more effective than any of the other agents, and all of the metal-based inhibitors had greatly reduced effectiveness for burning velocity reductions greater than 50 %. When the inhibitor mole fractions are re-scaled in Figure 3-35 to provide overlap at 30 % reduction in burning velocity, the normalized burning velocity curves of all inhibitors are nearly coincident for flame speed reductions less than 40 % (i.e., the curves are roughly linear up to this degree of normalized flame speed reduction). Such re-scaling of the experimental data shows that at low mole fraction, $Fe(CO)_5$ was about 80 times, MMT 40 times, and TMT three times as effective as CF_3Br at reducing the overall reaction rate of stoichiometric, premixed methane-air flames. For flame speed reductions greater than 40 %, the curves for these five agents diverged. As discussed previously,[175,207] most inhibitors lose their marginal effectiveness at higher mole fractions, but the decrease in inhibition effectiveness is much more dramatic for the organometallic compounds, as was found previously for $Fe(CO)_5$.

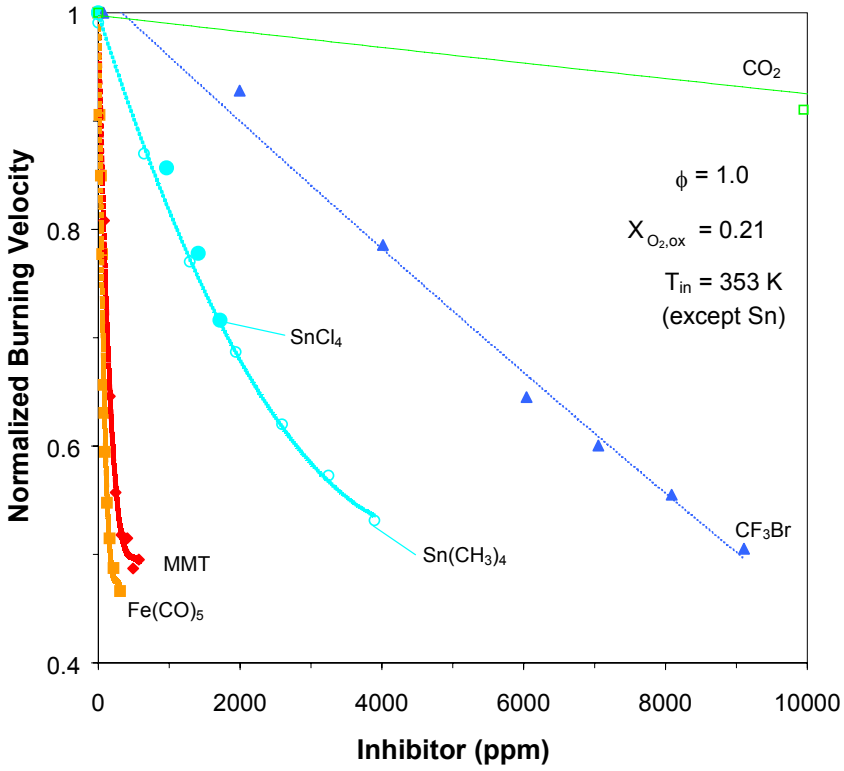

Figure 3-35. Normalized Burning Velocity of Premixed $CH_4/O_2/N_2$ Flames Inhibited by CO_2, CF_3Br, $Sn(CH_3)_4$, $SnCl_4$ [34], MMT, and $Fe(CO)_5$. T_{in} = 353 K for all data except $Sn(CH_3)_4$ and $SnCl_4$ which are at 298 K. Lines are curve fits to data.

Blends of Metals

One approach for overcoming the loss of effectiveness is to add non-condensing amounts of several inhibitors. To test this approach in premixed flames, Linteris and co-workers performed tests with a blend of MMT and $Fe(CO)_5$, added at a molar ratio of 2:1, respectively. Data for pure MMT, pure $Fe(CO)_5$, and their combination are shown in Figure 3-36 (T_{in} = 353 K, phi=1.0, and $X_{O_2,ox}$=0.244). The experimental data are represented by the points with a curve fit (dotted line), while the results of the numerical calculations are shown by the solid lines. (The data for the combination of MMT and $Fe(CO)_5$ are plotted as a function of the mole fraction of the abundant agent, MMT). The numerical model, which includes both the reactions of manganese-containing species and the iron-containing species from Reference 104 predicts well the normalized flame speed reduction. As the figure shows, adding 0.5 moles of $Fe(CO)_5$ for each mole of MMT added did provide additional flame speed reduction over that from MMT alone. This is significant since, as discussed previously,[102] the loss of effectiveness of the metals at higher concentration could be caused either by condensation of active species, or by the loss of radical population by catalytic recombination. Since the addition of iron to the manganese-inhibited flame caused significant additional inhibition, the *strong* loss of effectiveness in the MMT-inhibited flames was likely due to condensation rather than radical depletion. If the cause was radical depletion, addition of $Fe(CO)_5$ to the flames already inhibited by high amounts of MMT would have yielded no additional inhibition, since few radicals would be left to recombine. The gas phase kinetic model captured the *mild* reduction of effectiveness of either agent or their blend acceptably well (for flame speed reductions of less than 40 %).

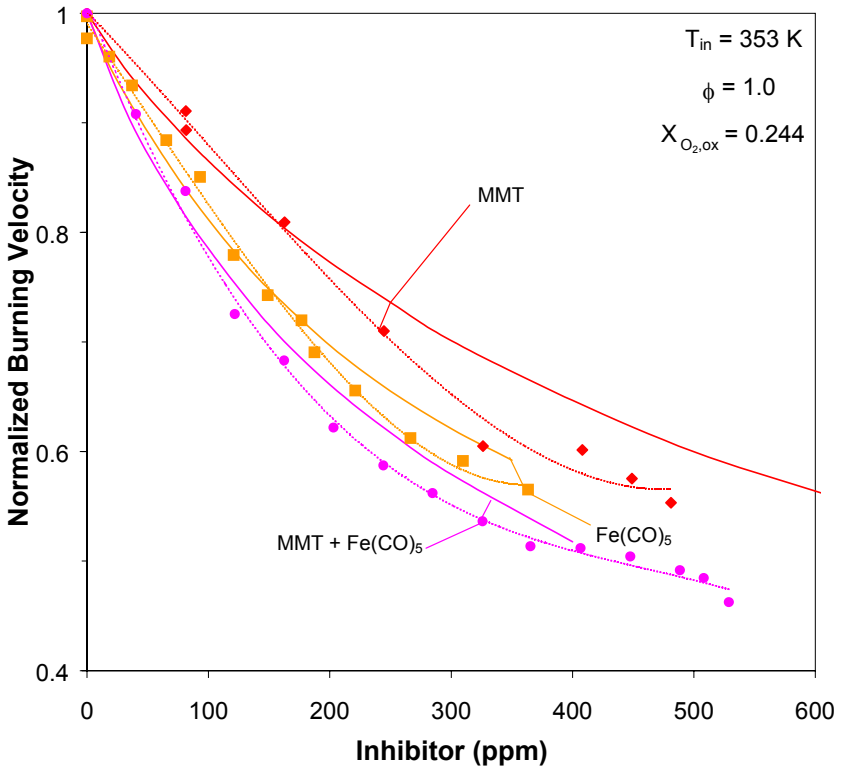

Figure 3-36. Normalized Burning Velocity of Premixed $CH_4/O_2/N_2$ Flames Inhibited by Pure MMT and $Fe(CO)_5$, and by a Blend of the Two. Dotted lines are curve fits to the data; solid lines are numerical model calculations.

Discussion

One of the benefits of numerical modeling of the flame structure of inhibited flames is that the results of the calculations provide detailed insight into the actual reasons for the strong inhibition. Further, the results for different inhibitors can be used to understand why they each demonstrate a different effectiveness. In the sections below, the inhibition mechanisms of tin and manganese are discussed and compared to that for iron. The difference in efficiency for these systems are shown to be related to the formation reaction and equilibrium relationships for the intermediate metal di-hydroxide species $Fe(OH)_2$ and $Mn(OH)_2$.

Inhibition Mechanisms of Tin and Manganese

Examination of species profiles, reaction fluxes, and sensitivity coefficients from the numerically predicted flame structure allows investigation of the mechanisms of inhibition of these metallic compounds. The calculations show that TMT decomposes quickly in the flame, with 90 % consumption at 1000 K. A diagram showing the important reactions for tin inhibition is shown in Figure 3-37 (which also shows in parallel format the reaction paths for MMT, and $Fe(CO)_5$ inhibition). In the calculations used to prepare Figure 3-37, TMT, MMT, or $Fe(CO)_5$ were present at (1963, 128, or 105) μL/L, respectively, in the premixed methane-air flames (ϕ=1.0, T_{in}=353 K, and X_{ox} =0.21); these volume fractions produced a 30 % reduction in flame speed.

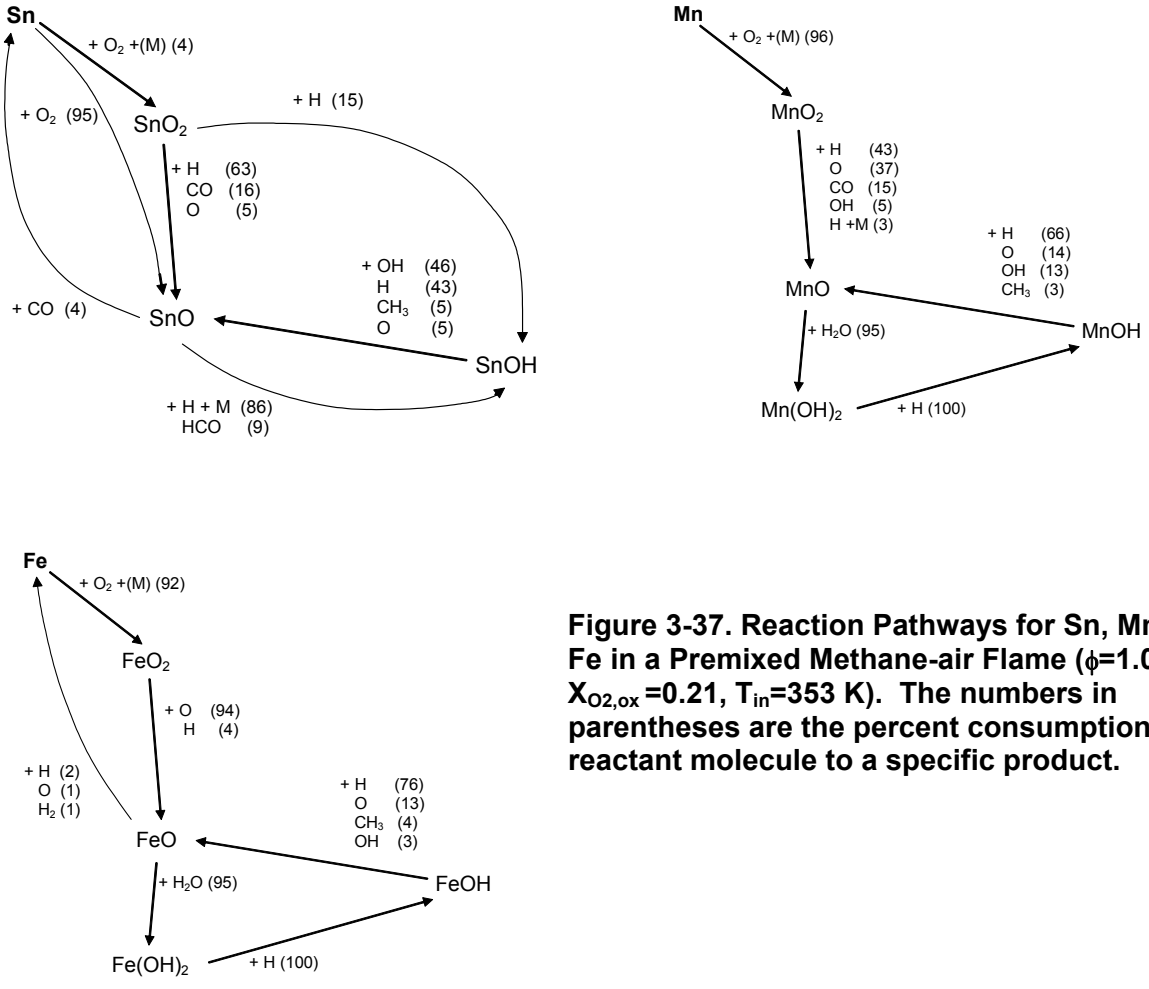

Figure 3-37. Reaction Pathways for Sn, Mn, and Fe in a Premixed Methane-air Flame (ϕ=1.0, $X_{O2,ox}$ =0.21, T_{in}=353 K). The numbers in parentheses are the percent consumption of the reactant molecule to a specific product.

The determination of the important reactions was based on consideration of both the reaction flux and sensitivities. The reaction flux represents the production or consumption of a species by chemical reaction. For a particular reaction, it is defined as the integral of that reaction rate per unit volume over the entire flame domain. The total reaction flux for a species is defined as the sum of the reaction fluxes for the individual reactions which produce or consume it. In Figure 3-37, the pathway for consumption of each species is shown, with arrows connecting the relevant reactant and product species. The number next to each arrow represents the fraction of the total consumption flux for that species which proceeds through that particular reaction.

The tin atom formed as a result of TMT decomposition quickly reacts with O_2 through the reactions Sn + O_2 (+M) $\leftrightarrow$ SnO_2, and Sn + O_2 $\leftrightarrow$ SnO + O. The former reaction leads to SnO from the reaction of SnO_2 with CO, H, or other radicals. Conversely, the latter reaction forms SnO directly, and is fast at room temperature as compared to the analogous reaction of iron atom. Formation of SnO leads to the following reactions with H and HCO radicals:

$$SnO + H + M \leftrightarrow SNOH + M$$

$$SnO + HCO \leftrightarrow SnOH + CO$$

which, together with the radical scavenging reactions of SnOH, complete the catalytic radical recombination cycle of tin:

$$SnOH + H \leftrightarrow SnO + H_2$$

$$SnOH + OH \leftrightarrow SnO + H_2O$$

$$SnOH + CH_3 \leftrightarrow SnO + CH_4$$

$$SnOH + O \leftrightarrow SnO + OH\ .$$

The net effect of the dominant inhibition reactions can be shown as:

$$SnO + H + M \leftrightarrow SnOH + M$$

$$SnOH + H \leftrightarrow SnO + H_2$$

$$\text{net: } H + H \leftrightarrow H_2$$

Equilibrium calculations show that SnO is the major tin species in the products of a stoichiometric methane–air flame with added TMT. Figure 3-38 presents the sensitivity coefficients of the burning velocity to the rate constants (after adjustment) of tin-containing species for methane/air mixtures with equivalence ratios of 0.9, 1.0, and 1.1. In general, the burning velocity was sensitive to the rates of the catalytic cycle reactions with high fluxes: SnO reaction with H or HCO, and SnOH reaction with H, OH, CH_3, or O. The burning velocity was most sensitive to the rate of the reaction SnO + H + M $\leftrightarrow$ SnOH + M, which had a sensitivity about four times less than the chain-branching reaction H + O_2 $\leftrightarrow$ OH + O. As was found for DMMP and ferrocene additives,[106,201] the burning velocity of flames inhibited by TMT was not particularly sensitive to the rate of the decomposition reaction. Numerical tests showed that changes in the overall activation energy of TMT decomposition in the range 170 kJ/mol to 335 kJ/mol had little effect on the burning velocity with up to 2000 μL/L of TMT. Hence, the inhibition effectiveness of tin compounds is likely to be independent on the parent molecule, as long as rapid decomposition occurs.

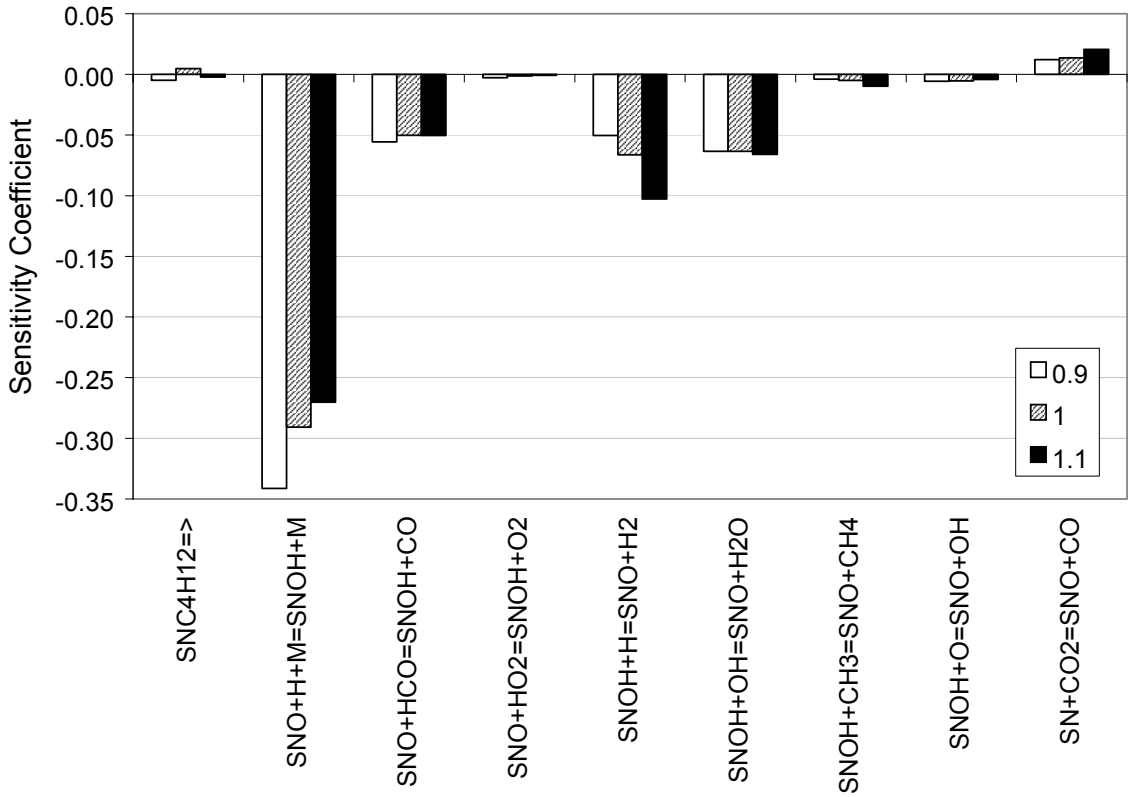

Figure 3-38. First-order Sensitivity Coefficient of the Burning Velocity to the Specific Reaction Rate Constant for Reactions with Tin-containing Species (1963 μL/L of TMT).

The reaction SnO + CO ↔ Sn + CO_2 (which is followed by Sn+O_2=SnO+O) is an additional route for CO consumption, and is chain-branching (net: CO+O_2=CO_2+O), which reduced the inhibiting effect of SnO in these flames. Similar behavior was found for CO – N_2O flames inhibited by $Fe(CO)_5$.[145] Changes in these rates affected the calculated inhibition efficiency of TMT; nevertheless, the mechanism was dominated by the rate of reaction SnO + H + M ↔ SnOH + M.

Analysis of the numerical results for inhibition by MMT showed that the behavior of manganese in premixed methane-air flames was similar in many details to that of iron pentacarbonyl. The reaction pathway for manganese species is also shown in Figure 3-37, and the pathway for iron species from $Fe(CO)_5$ is shown for comparison. As with iron pentacarbonyl, Mn reacts with O_2 to form MnO_2 , which reacts primarily with radicals to form MnO. The catalytic radical recombination cycle consists of:

$$MnO + H_2O \leftrightarrow Mn(OH)_2$$

$$Mn(OH)_2 + H \leftrightarrow MnOH + H_2O$$

$$MnOH + H \text{ (or OH, O)} \leftrightarrow MnO + H_2 \text{ (or } H_2O, OH)$$

$$\text{net: } H + H \leftrightarrow H_2$$

$$\text{(or: } H + OH \leftrightarrow H_2O, H + O \leftrightarrow OH)$$

Although flame equilibrium calculations showed that the species MnH was present at relatively large concentrations, the contribution of reactions of this species to the inhibition effect was relatively small. Figure 3-39 shows the highest absolute values of the sensitivity coefficients of burning velocity to the rate constants (after adjustment) for reactions of manganese-containing species. The burning velocity was sensitive to the rates of the three reactions in the catalytic cycle above, with the rate of the reaction $Mn(OH)_2 + H \leftrightarrow MnOH + H_2O$ having the greatest absolute value. The burning velocity was also somewhat sensitive to the rates of the reactions forming MnO_2 and MnO. The reaction $MnO + H \leftrightarrow Mn + OH$ has a positive sensitivity; i.e., increasing its rate increased the burning velocity. This chain propagating reaction temporarily removed MnO from the catalytic cycle above, thus weakening the inhibition.

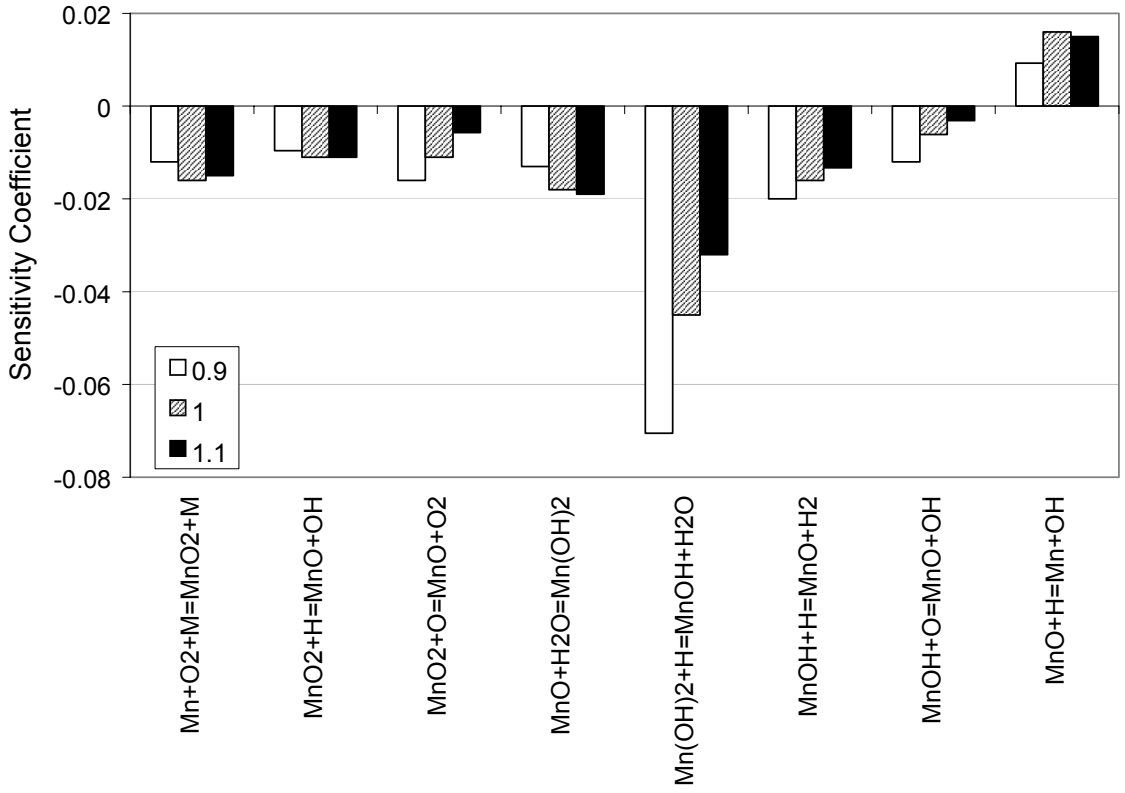

Figure 3-39. First-order Sensitivity Coefficient of the Burning Velocity to the Specific Reaction Rate Constant for Reactions with Manganese-containing Species (150 μL/L of MMT).

Comparison of inhibition by $Fe(CO)_5$, MMT, and TMT

In order to evaluate the inhibition mechanisms under comparable conditions, the numerical calculations (for ϕ=1.0, $X_{O_2,ox}$ =0.21, and T_{in}=353 K) were performed, as above, for initial values of TMT, MMT, and $Fe(CO)_5$ which provided an equivalent reduction (30 %) in the normalized burning velocity. These volume fractions were found to be 1963 μL/L, 128 μL/L, and 105 μL/L, respectively. While suppression of a fire would probably require higher agent concentration than that which provides a 30 % flame speed

decrease, this degree of flame speed reduction was selected for two reasons. It provided a significant reduction in overall reaction rate (a factor of two) and kept the agent concentration far enough above the values at which the model and experiments start to diverge (possibly due to condensation). For these flames, the structures were quite similar and the flame speed was the same (37.3 cm/s), allowing straightforward comparison of the inhibition mechanisms.

Based on the calculated results, TMT was required at a mole fraction which was about 17 times greater than iron or manganese compounds for a similar reduction in overall reaction rate. This occurred because the reactions to form SnOH from SnO were rate-limiting and slow. Further, the reverse of the reaction $SnO + H + M \leftrightarrow SnOH + M$ was relatively fast at the location of peak catalytic cycle activity because SnO was a dominant equilibrium product in the high temperature region.

In order to further compare the performance of TMT, MMT, and $Fe(CO)_5$, it was useful to plot the relevant species mole fractions as a function of temperature through the flame. Figure 3-40 shows the mole fractions of the metal species in the inhibition cycles, and the radical species H, OH, and O. The vertical line shows the location of the maximum rate of the $H+O_2$ branching reaction. Note that the locations of the peak fluxes of the inhibition reactions (not shown) were very close to the peak flux of the $H+O_2$ reaction and to the maximum concentrations of H, OH, and O. The bottom figure for TMT inhibition clearly shows the preponderance of SnO as the sink for tin atoms (note the rescaling), hence requiring a large initial TMT mole fraction to achieve both fast reaction of SnO with H atom, and appreciable mole fraction of SnOH for radical scavenging. In Figure 3-40, consider the Mn-containing species at the location of peak H-atom flux. MnO was present in higher mole fraction than FeO. This occurred from the significant backward reaction of $MnO + H_2O \leftrightarrow Mn(OH)_2$, which provided a lower $Mn(OH)_2$ concentration for the rate-limiting step $Mn(OH)_2 + H \leftrightarrow MnOH + H_2O$.

The importance of constraints on equilibrium concentrations as they relate to inhibitor efficiency is illustrated in Figure 3-41, which shows the fraction of all metal species in the flame. For these equilibrium calculations, the metallic element (Sn, Mn, or Fe) was present at a mole fraction or 1.0×10^{-4}, and methane and air were present at stoichiometric proportions. For TMT inhibition, the Sn appeared overwhelmingly as SnO (note the scale change on Sn and SnOH), thus higher levels of TMT were required to yield the required levels of SnOH reaction with H atom, and for the required rates of the slow reaction $SnO + H + M \leftrightarrow SnOH + M$. Note that since the flames of Figure 3-40 all had equivalent levels of inhibition, the flux of each radical recombining catalytic cycle was about the same; e.g., SnOH, MnOH, and FeOH must have been present at about the same mole fraction since their rates of reaction with H-atom were close, and the rates of reactions forming the hydroxide were approximately the same. Comparing $Mn(OH)_2$ and $Fe(OH)_2$ in Figure 3-41, in the MMT-inhibited flames, the concentration of $Mn(OH)_2$ for temperatures above 1800 K dropped off rapidly, whereas in the $Fe(CO)_5$-inhibited flames, $Fe(OH)_2$ did not. Since the reaction of $Mn(OH)_2$ with H atom was rate-limiting (Figure 3-39), decreases in the $Mn(OH)_2$ mole fraction made MMT less effective as an inhibitor than $Fe(CO)_5$.

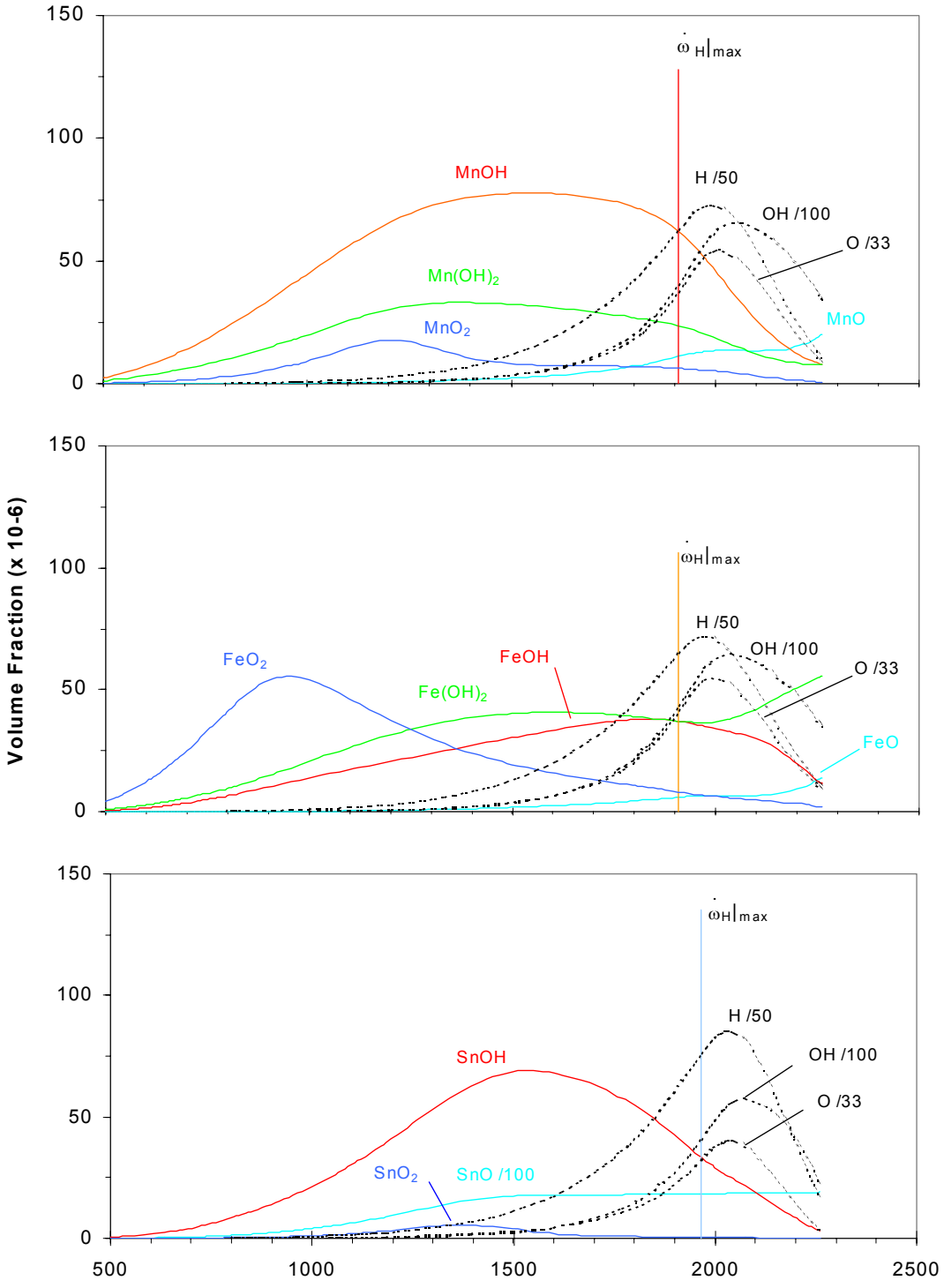

Figure 3-40. Volume Fractions of O, and OH Radicals and Metal Species Intermediates as a Function of Temperature in Flame for $Fe(CO)_5$, MMT, and TMT Added at 105 μL/L, 128 μL/L, and 1963 μL/L (corresponding to a 30 % reduction in flame speed). T_{in}=353 K, ϕ=1.0, $X_{O_2,ox}$ =0.21.

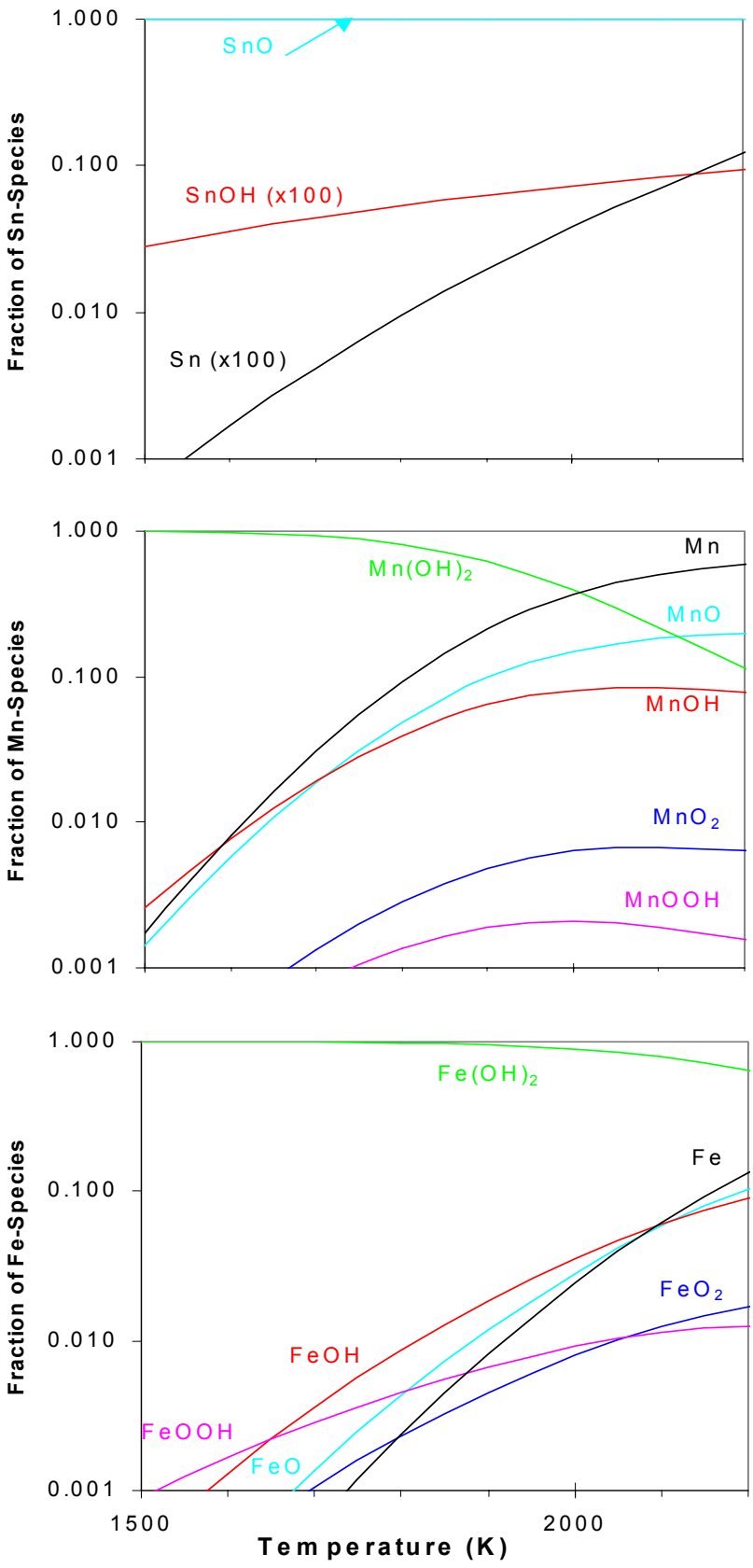

Figure 3-41 Fractions of Sn-, Mn-, and Fe-species at Equilibrium in Methane-air Flames as a Function of Temperature.

Conclusions

This section described the first experimental measurements of the influence of manganese- and tin-containing compounds (MMT, TMT) on the burning velocity of methane/air flames. Comparisons with the agents $Fe(CO)_5$ and CF_3Br demonstrated that manganese and tin-containing compounds are effective inhibitors. The inhibition efficiency of MMT was about a factor of two less than that of iron pentacarbonyl. TMT was about 26 times less effective, although it was still about twice as effective as CF_3Br. There were conditions for which both MMT and TMT showed a loss of effectiveness beyond that expected due to radical depletion, and the cause is believed to be particle formation. Kinetic models describing the inhibition mechanisms of MMT and TMT additives were suggested. Simulations of MMT- and TMT-inhibited flames showed reasonable agreement with experimental burning velocity data. The decomposition of the parent molecule for the tin and manganese species was found to have a small effect on the inhibition properties for the range of concentrations used in this work. Calculations confirmed that the main tin-containing species in the flame zone was SnO, while the concentrations of SnO_2, SnOH and Sn were relatively small. The inhibition effect of TMT was determined mostly by the rate of the association reaction $H+SnO + M \leftrightarrow SnOH + M$, and the catalytic recombination cycle was completed by the reactions $SnOH + H \leftrightarrow SnO + H_2$ and $SnOH + OH \leftrightarrow SnO + H_2O$. The inhibition mechanism of manganese-containing compounds was similar, in many details, to the inhibition mechanism for iron pentacarbonyl: $MnO + H_2O \leftrightarrow Mn(OH)_2$; $Mn(OH)_2 + H \leftrightarrow MnOH + H_2O$, and $MnOH + OH$ (or H) $\leftrightarrow MnO + H_2O$ (or H_2). The burning velocity was most sensitive to the rate of $Mn(OH)_2 + H \leftrightarrow MnOH + H_2O$ reaction. Comparison of the mechanisms of inhibition of TMT and MMT to $Fe(CO)_5$ showed that the manganese was not as efficient an inhibitor as iron: due to equilibrium constraints, the mole fraction of the intermediate species $Mn(OH)_2$ drops off at higher temperature (in comparison to $Fe(OH)_2$), slowing its rate-limiting reaction with H atom in the catalytic cycle. This result illuminated the role of equilibrium constraints on species concentrations in the efficiency of catalytic cycles.

3.3.5 Complexation/Matrix Absorption of Super-effective Agents

Introduction

While the high flame inhibition effectiveness of these types of compounds would appear to encourage their pursuit as potential fire suppressants, their high toxic potency is a severe deterrent. (See Chapter 6.) To overcome this limitation, the NGP examined means to absorb or adsorb such compounds into an inert matrix for transport to and release in the flame zone. Alternatively, perhaps other, non-toxic compounds of these metals existed which are also superb inhibitors and which maintain their action up to higher mole fractions. Iron-containing compounds, and in particular $Fe(CO)_5$, were the initial focus of the research. They had been found to be the most efficient metallic flame inhibitors, and thus would be most able to overwhelm the additional mass of the matrix material or complexing moiety and contend with halon 1301 in flame suppression efficiency.

Absorption Tests of $Fe(CO)_5$ into Matrix Materials

The objectives of this research[85] were to develop a system for introducing the inhibitor into matrix materials, quantify the absorption and desorption processes of the inhibitor into and out of the matrix, and investigate the thermal stability of the matrix-inhibitor combination.

Matrix Materials and Super Agents Considered

The selection of matrix material had to consider several key factors:

- Since the primary purpose of the matrix was safe storage and transport of the superagent, it needed to be inert. Porous silica and aerogel fit these criteria well. Zeolite particles have Na^+ imbedded in the structure and could influence the flame inhibition. Porous carbon particles were not considered, since they could promote flame propagation through oxidation of carbon.
- For efficient loading of agent, the matrix needed to have a high surface area to mass ratio. Zeolite particles have a high ratio of about 800 m^2/g, while crystalline sodium bicarbonate particles have a very low value. The porous silica particles considered had an intermediate value of 550 m^2/g. Aerogel particles have high pore volume to mass, but offer lower agent adsorption surface area.
- The matrix particles had to be seedable into flames. Submicron particles were hard to seed in a steady, consistent manner as opposed to particles above 5 μm. In this regard, zeolite particles with a mean diameter of 2 μm were on the borderline, and the maximum mass loading of seeded zeolite particles did not exceed 0.6 %. In comparison, porous silica particles in the size range of 15 μm to 40 μm were well behaved in the seeder, and a mass loading as high as 6 % was attained in flame experiments.
- The desorption rate of the agent from the pore structure had to be favorable.
- The matrix material had to be stable during the heating and desorption process. A sample of zeolite particles collected after passing through a premixed flame indicated spherical particles greater than the initial size. This perhaps indicated that the matrix material had melted and, through agglomeration, formed large spherical particles.

Because of the superior flame inhibition properties of $Fe(CO)_5$, most of the absorption effort was devoted to this compound. For safety, some experiments were conducted with molecular iodine as a surrogate material for testing the performance of an absorbed agent.

$Fe(CO)_5$ Absorption Method

Iron pentacarbonyl was absorbed into particles of zeolite-NaX, zeolite-NaY, silica aerogel, and porous silica, as well as $NaHCO_3$ and Na_2CO_3. The system developed for introducing the $Fe(CO)_5$ into the various matrix materials is shown in Figure 3-42. The technique is a standard method for absorbing compounds into matrix materials. The apparatus was evacuated to a pressure of 7 Pa. In the initial absorption studies, about 1 g of solid support material was first inserted into one of the tubes. This sample was then heated under vacuum for 3 h to 4 h to remove the absorbed gases from the internal pore structure. The support material was then allowed to return to room temperature. The $Fe(CO)_5$ to be absorbed was poured into the second tube, with the interconnecting valve closed. While keeping the $Fe(CO)_5$ close to its freezing temperature, the valve in the interconnecting tube was opened briefly to remove the gas-$Fe(CO)_5$ mixture. Finally, the valve to the suction pump was closed and the interconnecting valve was left open, allowing the $Fe(CO)_5$ vapor to diffuse and absorb into the pore structure. This process typically took about one to two days.

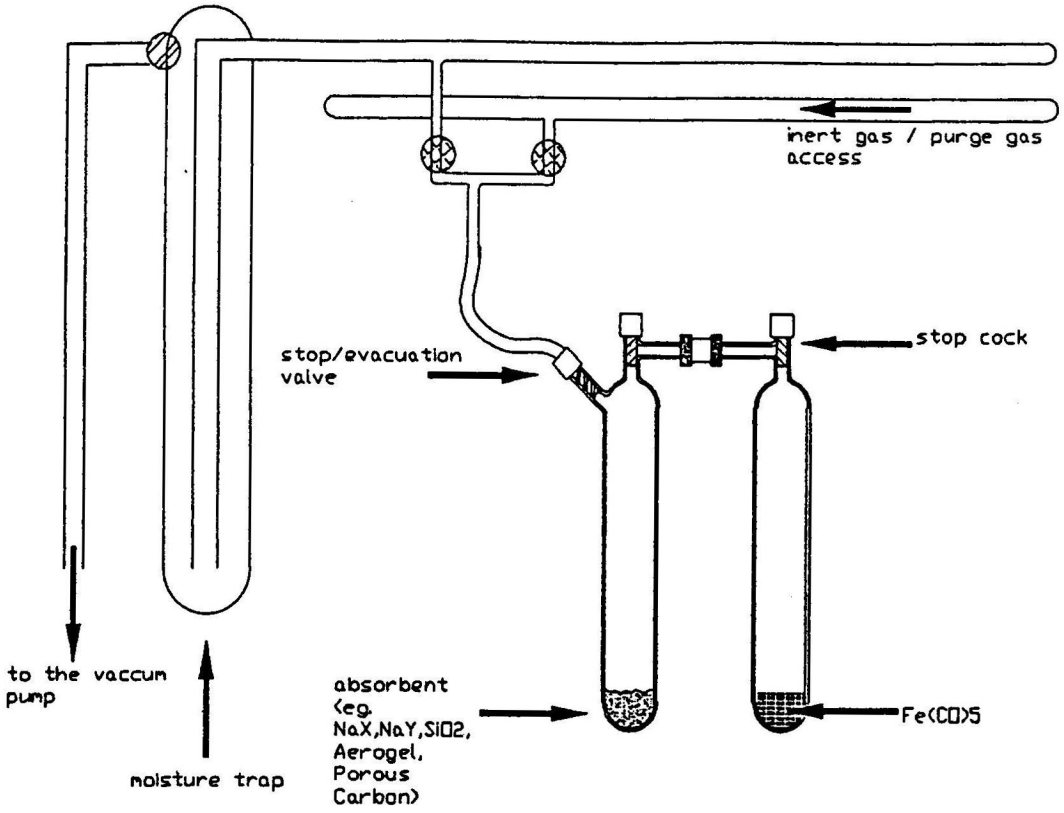

Figure 3-42. Schematic of the Experimental Setup for $Fe(CO)_5$ Absorption.

$Fe(CO)_5$ Absorption Results

For zeolite-NaX with pore volume of 0.3 cm^3/g,[208] the estimated mass of $Fe(CO)_5$ required to completely saturate the internal pore volume was about 0.3 g/g of zeolite-X. About 10 % of additional $Fe(CO)_5$ was generally poured into the glass tube to ensure complete absorption. Based on the mass increase of the tube containing zeolite-NaX, about 33 % increase in gross mass of the particles was observed, which was consistent with the estimate based on the internal pore volume. This implied that the particles of zeolite-NaX *ab*sorb the $Fe(CO)_5$ into their pore structure, as opposed to just *ad*sorbing the agent onto the external surface. This amount of mass uptake was encouraging, since only 100 μL of $Fe(CO)_5$ added to one L of reaction zone volume should reduce the overall reaction rate by a factor of four. Thus, adding a mass loading of particles of 1 % should provide sufficient $Fe(CO)_5$ to yield an observable burning velocity or extinction strain rate reduction in our apparatus.

After the $Fe(CO)_5$ was absorbed into the zeolite-NaX, the particles changed color to a faint brown/yellow. Based on the color change, the absorption appeared to be uniform in the zeolite particle sample. In addition, a very faint coating (presumably $Fe(CO)_5$) was observed on the tube walls. When the absorption process was allowed to take place with the chemical hood light on, the color of the $Fe(CO)_5$-absorbed zeolite particles was a darker shade of brown. This was believed to be caused by the decomposition of $Fe(CO)_5$ to $Fe_2(CO)_9$ (iron nonacarbonyl) in the presence of light.

When the $Fe(CO)_5$-absorbed zeolite-NaX was exposed to air by opening the valve, a reaction front propagated rapidly across the sample, sometimes with a bright orange-colored emission (apparently a flame inside the absorption tube). Hence, it appears that the iron pentacarbonyl reacted pyrophorically with air. Additional experiments were conducted by exposing the $Fe(CO)_5$-impregnated zeolite-NaX particles to either pure oxygen or nitrogen. In oxygen, the particles showed even more violent reaction, whereas in nitrogen, there was no reaction. These tests showed that the decomposition process was related to the oxygen concentration. While these observations were qualitative, this unexpected result indicated that zeolite-NaX may not be an appropriate support matrix for delivering unreacted $Fe(CO)_5$ to a flame, and other support materials were pursued.

There is a theoretical basis for believing that zeolite-NaY would be a more desirable support material than would be zeolite-NaX. The surface physical-chemical properties of the zeolite likely have an important role in the $Fe(CO)_5$ decomposition process. The general formula for a unit cell of zeolite is given by $Na_xAl_xSi_{192-x}O_{384}{\cdot}yH_2O$, where x ranges from 48 to 74 for zeolite Y and from 74 to 96 for zeolite X. While the cage structures of zeolite-NaX and -NaY are similar, the difference between them is in the content of cation Na^+ in the solid matrix. The lower NA^+ content of zeolite-NaY leads to weaker internal electric fields than in zeolite-NaX, and hence a lower propensity for decomposition of the $Fe(CO)_5$ in zeolite-NaY. When exposed to air, the $Fe(CO)_5$-absorbed zeolite-NaY also indicated $Fe(CO)_5$ decomposition, but the intensity of the observed reaction was much slower than with zeolite-NaX. Tests with porous silica particles gave weak indication of $Fe(CO)_5$ decomposition.

Besides porous silica particles, aerogel particles synthesized at University of Virginia were also tested as a possible support material. These particles were formed by hydrolysis of tetraethyl orthosilicate ($Si(OC_2H_5)_4$) in ethanol, followed by drying to remove extra ethanol and water, leaving behind a solid matrix which was 96 % porous. Three $Fe(CO)_5$ absorption experiments were conducted with the aerogel particles produced using the apparatus in Figure 3-42. Prior to absorbing $Fe(CO)_5$, the aerogel particles were heated to 200 °C to 250 °C to remove as much moisture as possible. The first sample indicated a particle mass increase of about 200 %. Two subsequent absorption experiments with aerogels, however, indicated $Fe(CO)_5$ absorption of 14 % and 101 % of the aerogel particle mass. (Note that the second sample was from the same batch of aerogel as the first, while the third sample was from a newly synthesized batch of aerogel.) Furthermore, both the second and third samples reacted after about 5 min to 10 minutes exposure to air, while the first sample with substantially larger increase in mass did not react when exposed to air for a long period of time.

The decreased uptake of $Fe(CO)_5$ in the second and third aerogel samples and the subsequent reaction when exposed to air led to the hypothesis that either water or ethanol in the aerogel (from the synthesis process described above) was not completely removed. Since $Fe(CO)_5$ is known to react violently with water, the absorbed water was perhaps the most likely cause for the above discrepancy in $Fe(CO)_5$ absorption and its decomposition.

Quantification of $Fe(CO)_5$ Absorption/Desorption

A standard technique for measuring the desorption or the decomposition properties of materials is thermogravimetric analysis TGA. In these tests, the sample is continuously weighed, while its temperature is increased. Zeolite, silica, and aerogel samples were heated to about 500 °C in steps of 5 °C/min, while $NaHCO_3$ and Na_2CO_3 were heated only to 150 °C because of their propensity to decompose. The TGA analyses required transferring of the $Fe(CO)_5$ absorbed particles from the

absorption flask to the weighing pan of the TGA. During this process, some fraction of the particles could react with ambient air, so the transfer time was strongly minimized. TGA analyses were performed for all of the absorbed particles. The $Fe(CO)_5$-absorbed aerogel particles did not react immediately when exposed to air, hence the desorption of $Fe(CO)_5$ from these particles measured via TGA was probably the most reliable. However, the desorption from aerogels showed a great variation from sample to sample, ranging from 5 % to 200 %.

The data in Table 3-10 help understand the desorption loss from the various types of $Fe(CO)_5$-laden particles following exposure to air. The elemental analyses (by Southern Testing and Research Laboratories) quantify the amount of Fe and Na remaining in the particles.

- The second column lists the Fe remaining in the sample, based on the weight loss of the sample in the TGA measurements.
- The third and fifth columns provide the Fe and Na remaining in the samples following exposure of the specimens to air at ambient temperature.
- The fourth and sixth columns show the Fe and Na remaining following heating at 500 °C in air for several hours to ensure that $Fe(CO)_5$ was fully decomposed.

Table 3-10. Summary of the Fe and Na Mass Loadings in Unheated and Heated Particles.

Support Material	From TGA	From Elemental Analysis			
	Fe (% by Mass)	Fe (% by Mass)		Na (% by Mass)	
	Heated	Unheated	Heated	Unheated	Heated
Zeolite-NaX	7.1 ± 0.7	8.9 ± 0.9	7.1 ± 0.7	11.0 ± 1.1	9.8 ± 1.0
Zeolite-NaY	7.1 ± 0.7	9.7 ± 1.0		6.8 ± 0.7	
Porous Silica	6.0 ± 0.6	12.8 ± 1.3	6.8 ± 0.7	< 0.8	< 0.1
Silica Aerogel	4 to 57				
$NaHCO_3$	5.0 ± 0.5	<0.1	< 0.2	28.0 ± 2.8	41.0 ± 4.1
Na_2CO_3	2.0 ± 0.2				

- It was not resolved whether the observed weight loss was due to desorption of undissociated $Fe(CO)_5$ or decomposed carbonyl.
- Comparison of columns 3 and 4 indicates that heating of the reacted particles had a small effect on the absorbed $Fe(CO)_5$ for zeolite particles, but a larger effect for porous silica particles. Hence, it is possible that most of the $Fe(CO)_5$ remaining in the unheated zeolite particles was no longer intact $Fe(CO)_5$ that could be liberated by heating, but rather was already decomposed.
- For porous silica, about half of the $Fe(CO)_5$ was decomposed or unavailable for liberation by heating.
- The Fe and Na mass fractions remaining in the zeolites were considerable and similar. If the Na could be liberated from the zeolite particles in the flame, they might provide flame inhibition even without added iron.

In order to determine whether any unreacted $Fe(CO)_5$ remained inside the particle after exposure to air, infrared (IR) spectroscopy analysis was performed. The reacted zeolite or porous silica particles were

crushed and then mixed with potassium bromide particles. This mix was then pressed to form a thin wafer and then tested in the IR spectrometer. The absence of significant absorption of the Fe-CO stretching bond (characteristic of $Fe(CO)_5$) indicated that there was little $Fe(CO)_5$ remaining in the solid support matrices.

The $Fe(CO)_5$-impregnated and reacted zeolite particles were also analyzed using the high-resolution transmission electron microscope (HRTEM). Images of zeolite-NaX particles after absorption of $Fe(CO)_5$ and exposure to air showed that a condensed phase substance formed on the exterior surface. For example, the left frame of Figure 3-43 shows an image of a zeolite particle after $Fe(CO)_5$ was absorbed and then the sample exposed to air. For comparison, the right frame shows an image of a pure zeolite particle. In the left frame, the zeolite-NaX particle is shown to have a diameter on the order of a micrometer, with pore sizes of the order of 1 nm, while nodules of condensed–phase material (perhaps Fe, FeO, or Fe_2O_3) have diameters of about 20 nm and are rather well dispersed on the support material. The formation of these condensed-phase nodules implies that $Fe(CO)_5$ may not be available from the matrix to provide gas phase Fe, which is required for efficient flame inhibition.

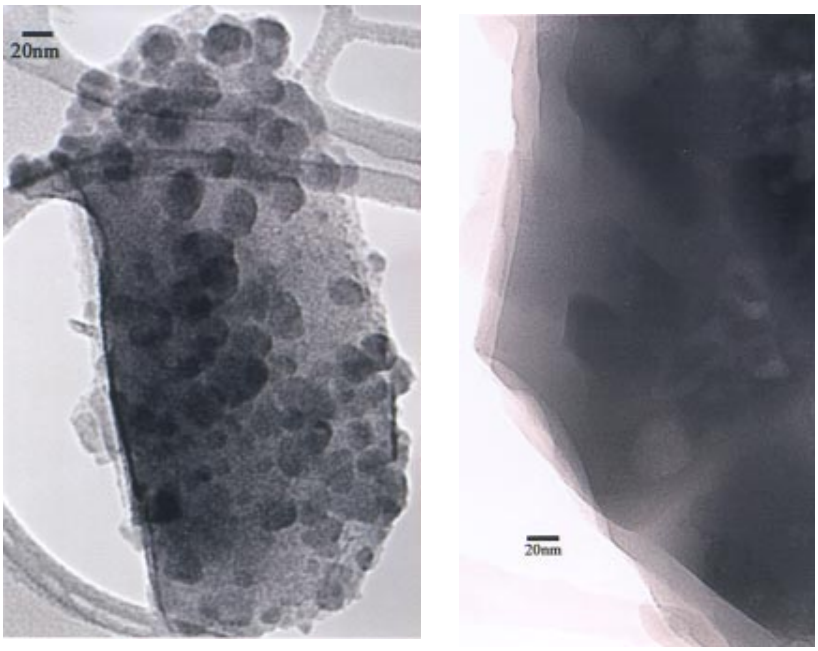

Figure 3-43. High Resolution Transmission Electron Micrograph Images of Zeolite-NaX Particles. Left: with condensed phase iron species on surface; right: without Fe_2O_3 clusters.

Methods of Quantifying Suppression Effects by Particulates

Test Burners

Two burner types were selected as test beds for the particles: a premixed Bunsen-type nozzle burner, and a gaseous counterflow diffusion flame burner, also with nozzle-generated flows. These flames were selected for several reasons:

- Both types, unlike co-flow diffusion flame burners (such as a cup burner), allowed unambiguous determination of the amount of agent that reaches the relevant high-temperature reaction region of the flame. This is difficult in cup burner flames, since the transport of agent or particles to the appropriate region of the cup burner is complex; moreover, stabilization (and therefore extinction) of cup burner flames is not presently well understood theoretically.
- Cup burner tests allowed flames at only one strain rate, whereas counterflow diffusion flames allowed tests at variable strain rates.
- The premixed flames mitigated the hazard from $Fe(CO)_5$-impregnated particles contaminating the laboratory space. Premixed flames involved much smaller quantities of gas and particles, and all of the reactants passed through a flame.
- Both counterflow diffusion flames and premixed flames directly provide a measure of the overall reaction rate in the flame, in a configuration which is easily interpreted or modeled. Peters[209] has shown, on a theoretical basis, that for the performance of a chemical catalytic inhibitor, the two burners should be correlated.

Particle Seeder

Chelliah and co-workers designed, built, and tested an effective particle seeding system for introduction of the $NaHCO_3$, silica, zeolite, or aerogel particles to both counterflow diffusion flames and premixed Bunsen-type flames. The design became the basis for particle experiments discussed in Chapter 4.

Because of the challenge in verifying the accuracy of previously reported data with $NaHCO_3$ particles,[210,211] considerable attention was devoted to the development of a particle seeder that could provide steady feed rates of particles of various diameters. For the small air flows involved (typically 0.1 L/s), the fluidized bed approach shown in Figure 3-44 gave satisfactory seeder performance for relatively small particles, i.e., less than 30 μm in diameter. This fluidized bed seeder consisted of a 19 mm diameter glass tube with two porous plugs at either end. The air flow to the seeder was controlled through a mass flow controller and split into two streams, which were connected to either end of the glass tube. The flow passing through the bottom, which controlled the fluidization level, was monitored through another flow controller. The fluidized particles and the air entering the fluidization tube (from the top and bottom) were extracted through a small tube located near the middle of the tube. By maintaining the total air flow to the fluidizer tube constant, the particle feed rate was steady, as verified by continuously monitored the light scattered from the particle stream (Figure 3-44). The detection system consisted of a laser diode (671 nm), a high speed silicon detector (Thor Labs DET1-SI) with a 3 cm focal length collection lens, a laser line filter at 671 nm (Edmund Scientific), and a strip chart recorder (Hewlett-Packard Model 7132) to monitor the detector output.

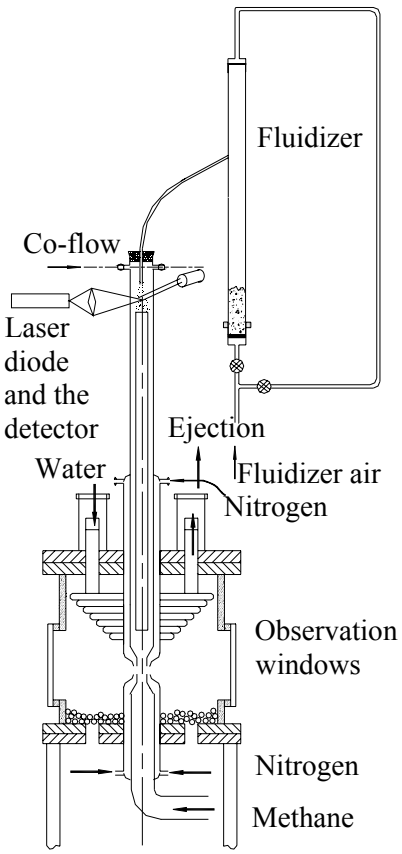

Figure 3-44. Schematic Diagram of Counterflow Diffusion Flame Burner with Provision for Addition of Particles to the Air Stream.

Flow Profile Measurement

For both burners, a laser Doppler velocimetry (LDV) system was used to establish the quality of the top hat velocity profile leaving the nozzle exit and to measure the local strain rate in the counterflow field. Because the enclosed counterflow burner permitted optical access from the two opposing sides, an on-axis forward scattering LDV configuration was selected. The LDV system consisted of an Argon Ion laser (Lexel Model 95) operating at 514.5 nm with a beam splitter and 300 mm focal length transmitting lens (DISA) to obtain two equal intensity beams forming a fringe pattern at the intersection of the focused beams. The probe volume was 0.151 mm wide and 1.51 mm long, with a fringe spacing of 2.57 μm. The collection optic system (DISA) gathered the forward scattered photons from the particles and imaged them on a photomultiplier tube (PMT). The PMT current was amplified (C-Cor Electronics Model 4375A Wideband Video Amplifier) and processed by a timer/counter (TSI Model 1990B) operated in the single burst mode using 8 cycles/burst. The filtered and amplified timer/counter signal was monitored by an oscilloscope (Tektronix Model 2212), and the digital output was interfaced to a personal computer using a digital input card (National Instruments DAQ pad 6510) and processed using data acquisition software (LabView). Measured frequencies were related to particle velocity using the known fringe spacing. To facilitate acquisition of velocity profiles in axial and radial direction of the counterflow field, both fringe generating and collecting optics were mounted on translation stages (Velmex Unislide Model MB2500), which had a minimum step size of 1 μm, with a reported accuracy of 5 μm in 100 mm. Figure 3-45 shows typical velocity profiles at the exit of the premixed burner nozzle for two different volume flows. For comparison, the calculated top-hat velocity profiles are also shown as dotted lines.

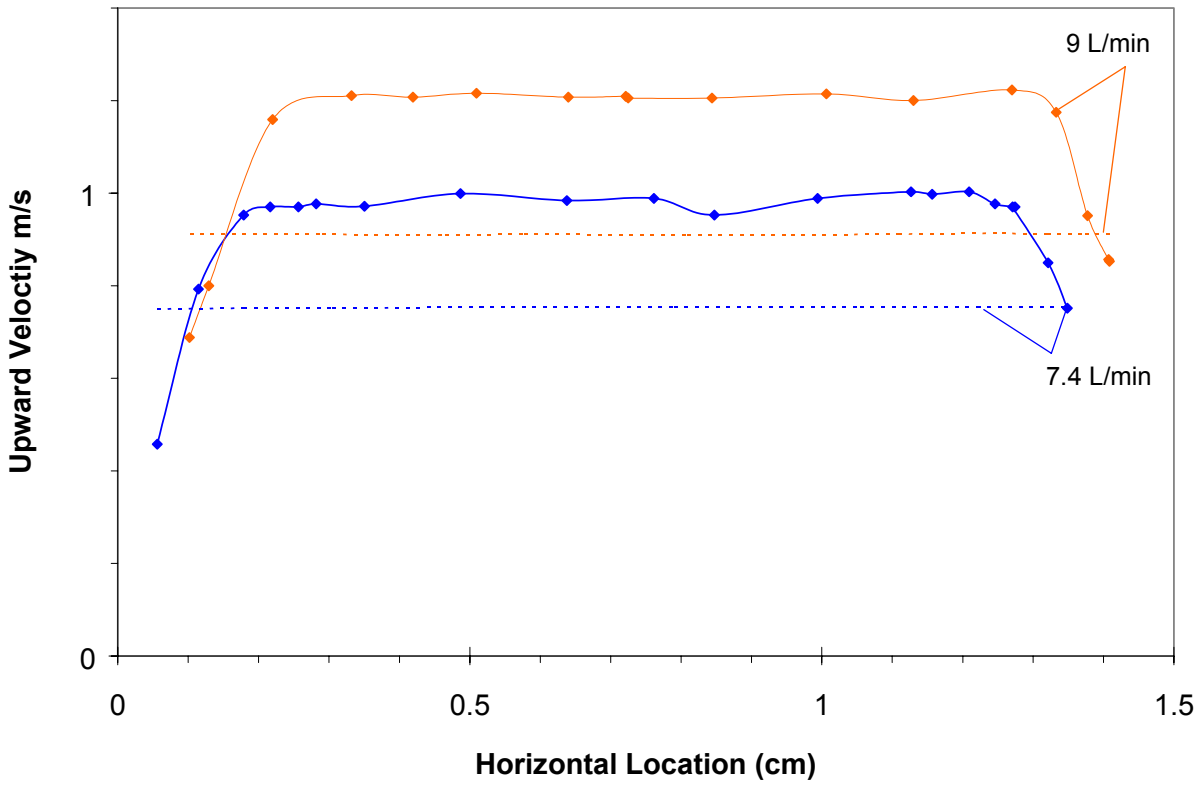

Figure 3-45. Calculated (dotted lines) and LDV-measured (points) Velocity Profiles at Exit of Premixed Burner Nozzle for Total Flows of 7.4 and 9 L/min.

Counterflow Diffusion Flames with Inert and $NaHCO_3$ Particles

Prior to testing agent-loaded particles, sodium bicarbonate and pure silica particles were used as the test cases for development of the seeding and burner systems.

Figure 3-44 shows the experimental setup of the counterflow burner. A steady, planar, non-premixed flame was established in the mixing layer of counterflowing methane and air streams. The fuel and air nozzles were made from Pyrex glass. The exit diameter of the inner tubes was 15 mm with a nozzle area contraction factor of 6.5, producing a nearly plug flow velocity profile at the nozzle exit. The co-annular nitrogen streams on both fuel and air sides helped maintain a stable planar flame disk. The cylindrical burner chamber included provision for dilution of the chamber with room air at the bottom (to minimize the occurrence of secondary flames), water cooling, and easy adjustment of the nozzle separation distance via o-ring sealed vacuum fittings (MDC). The typical separation distance between the two nozzles was 10 mm to 12 mm. The exhaust gases were evacuated using an air-driven mass flow ejector, with the chamber pressure monitored by a differential pressure gauge. The methane was BOC grade 4.0 with a purity of 99.99 %. The air was supplied by an oil-free compressor and dried by a series of desiccant beds. The flows of fuel and air were controlled using factory-calibrated mass flow meters (Teledyne Hastings-Raydist), with a reported accuracy of ± 1 %. Figure 3-46 shows an image of a typical flame disk established without and with $NaHCO_3$ particles.

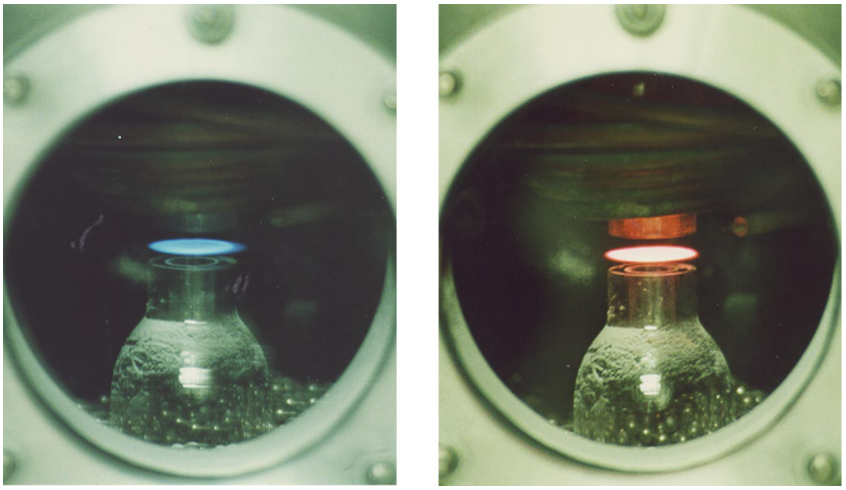

Figure 3-46. Methane-air Counterflow Diffusion Flames: Pure (left), and with $NaHCO_3$ Particles (right).

Experiments were conducted to test the system and to establish the effectiveness of particle size on non-premixed flame suppression. These results are shown in Figure 3-47 as the mass fraction of $NaHCO_3$ needed vs. flow strain rate at extinction, for particle sizes 10 μm to 20 μm, 20 μm to 30 μm, 30 μm to 40 μm, and 40 μm to 60 μm. For comparison, the effectiveness of 10 μm to 20 μm crystalline silica particles are also shown. It is clear that $NaHCO_3$ particles below 20 μm were significantly more effective in this flow field. As the $NaHCO_3$ particle size increased, the performance approached that of the inert silica particles.

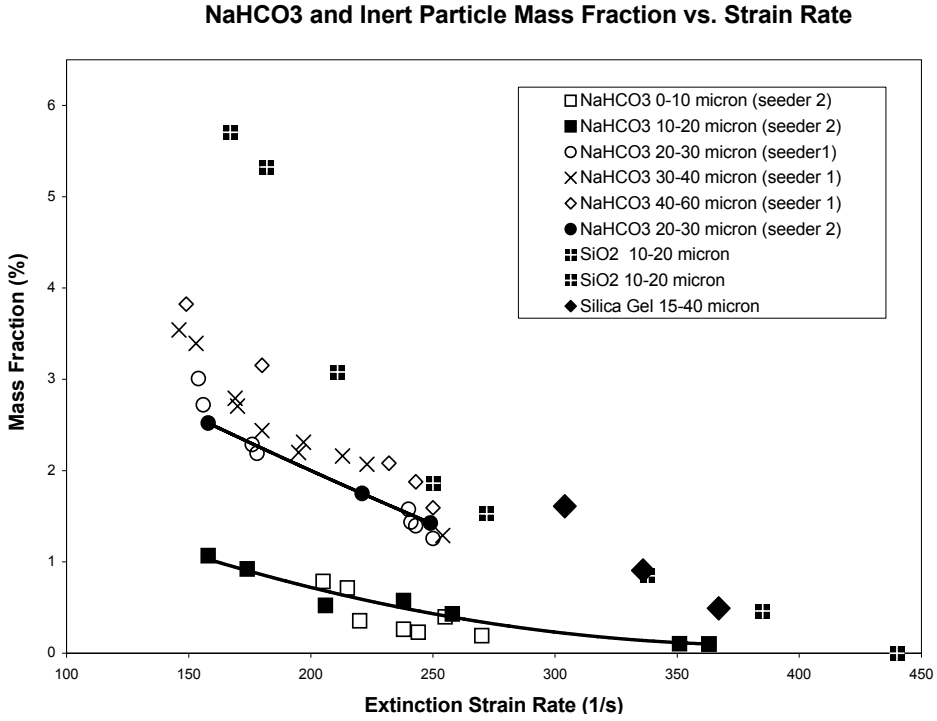

Figure 3-47. $NaHCO_3$ and Silica Mass Fraction vs. Methane-air Nonpremixed Extinction Strain Rate.

Figure 3-48 shows two photographs of the crossed laser beams from an LDV system penetrating a non-premixed counterflow methane–air flame seeded with 40 μm to 60 μm $NaHCO_3$ particles. In the upper image, the beams are above the flame, in the region between the flame and the incoming air stream (which is laden with particles), so that the particles have not yet reached the flame. Laser scattering from the particles is clearly visible. In the lower image, the beams are located below the flame and there is still obvious laser light scattering, indicating these large particles survive through the flame. This behavior results in the lower suppression effectiveness as illustrated in Figure 3-47. These results also indicate that even inert particles tend to reduce the flame extinction rate with increasing particle loading. Such effects can be related to the thermal effects associated with heating of these inert particles. (See Chapter 4.)

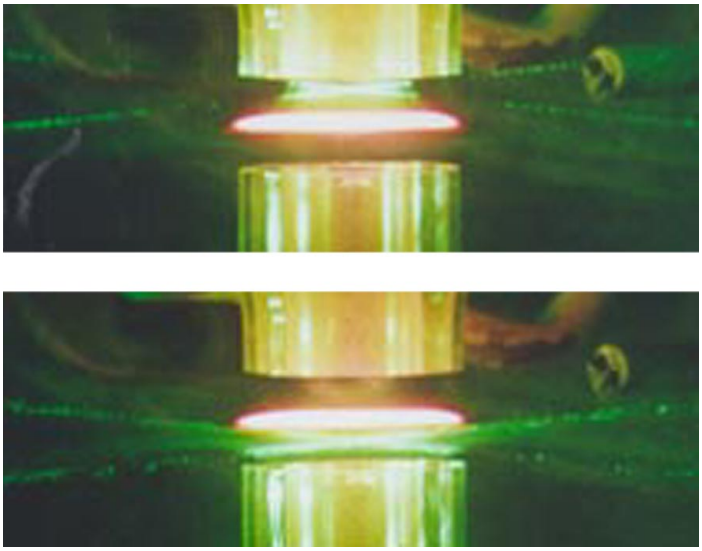

Figure 3-48 – Laser Scattering of $NaHCO_3$ Particles in a Counterflow Diffusion Flame of Methane and Air, Showing that the Particles Pass Through the Flame.

Parallel modeling efforts have shown that by selecting an appropriate value for the particle decomposition temperature, the experimental results shown in Figure 3-47 can be replicated. With a fixed particle decomposition temperature, the trends observed in Figure 3-47 for the variation in effectiveness due to particle size were then captured. The outcome of such modeling results was that the existence of a critical particle size which was effective in this flow field was directly related to the flow residence time, hence the heating of the particle and its decompositions rate, which would ultimately control the chemical effectiveness.

Premixed Flames with Inert and $NaHCO_3$ Particles

A Mache-Hebra nozzle burner (1.5 cm ± 0.05 cm diameter) produced a premixed Bunsen-type flame about 1.9 cm tall with a straight sided schlieren image that was captured by a CCD array camera connected through a USB port to a PC. Digital mass flow controllers held the equivalence ratio ϕ and the flame height constant while the mass flow of particles from the seeder was set at the desired value. The average burning velocity was determined from the reactant flows and the schlieren image using the flame angle method[187] from the measured velocity profile. The fuel gas was methane (BOC grade 4.0; 99.99 %), and the oxidizer stream consisted of laboratory air from an oil-free compressor which was dried by a series of desiccant beds. Air and fuel gas flows were set by PC-controlled mass flow controllers (Sierra, 860). Figure 3-49 shows this burner operating with methane-air, with and without $NaHCO_3$ particles added to the reactant flow.

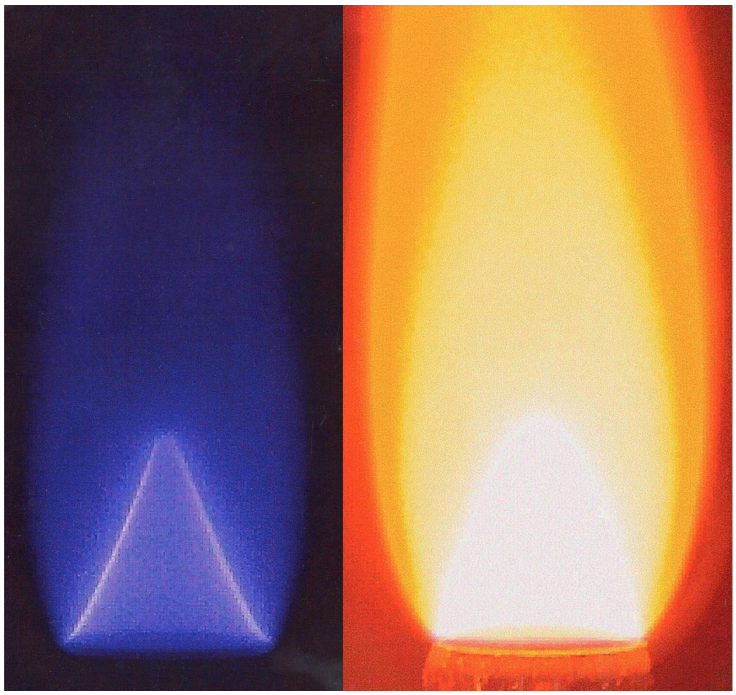

Figure 3-49. Premixed Methane-air Nozzle Burner Flames: Pure (left) and with $NaHCO_3$ Particles (right).

Using the LDV system, the burner exit velocity was characterized in the presence of silica, zeolite, and sodium bicarbonate particles (Figure 3-50). The results indicate that the inert silica particles and zeolite-NaX have a minor effect on the measured burning velocity, while $NaHCO_3$ has a noticeable effect.

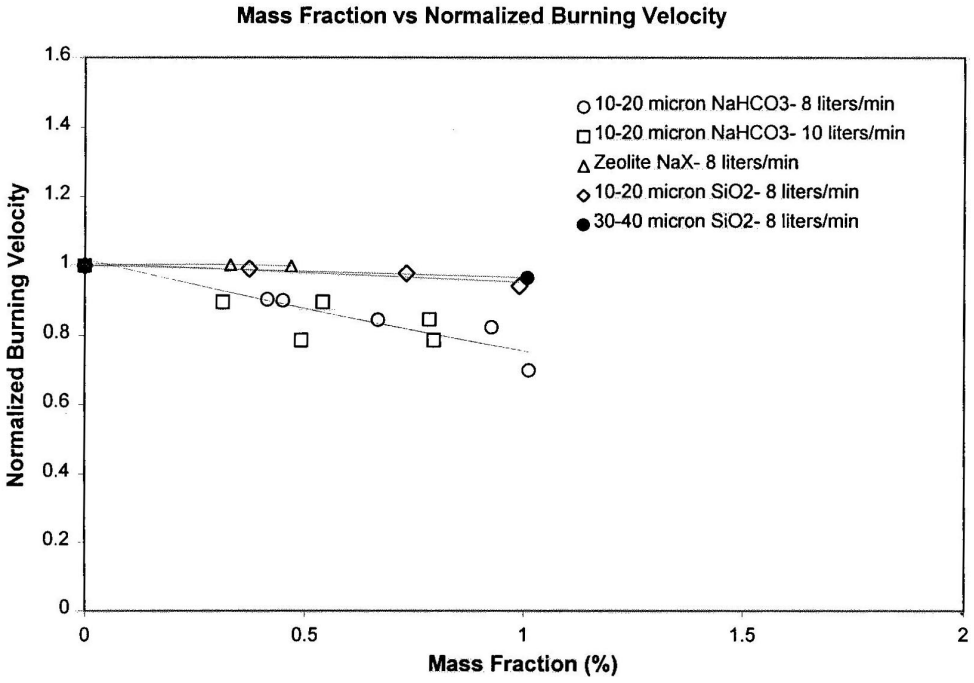

Figure 3-50. Comparison of Normalized Burning Velocities with Added Particles.

Comparison of the relative reduction of normalized, non-premixed flame extinction strain rates with normalized premixed burning velocities indicated significant differences. However, such comparisons should take into account the structural differences of the two flames. As shown by Peters[209] and employed by Chelliah et al.[212] for chlorinated hydrocarbon flames, the normalized burning rate is related the normalized extinction strain rate as $S_L/S_{L,0} = \sqrt{(a_{ext}/a_{ext,0})}$

Using this correlation, the comparison of the non-premixed and premixed flames inhibited with $NaHCO_3$ is shown in Figure 3-51. The disagreement between the two was somewhat greater than the uncertainty in each measurement; however, this disagreement was much less expected based on the significantly different structures of the premixed and diffusion flames. The results suggested that tests with either flame should be roughly comparable in demonstrating the effectiveness of chemically acting agents on the global reaction rate in methane-air flames. On the other hand, the data for inert particles in premixed and counterflow diffusion flames from Figure 3-47 and Figure 3-50, if plotted in Figure 3-51, would show a significant discrepancy. Most likely, these differences are related to the thermal effects associated with varying particle residence time in the two flows considered, and further analysis is required.

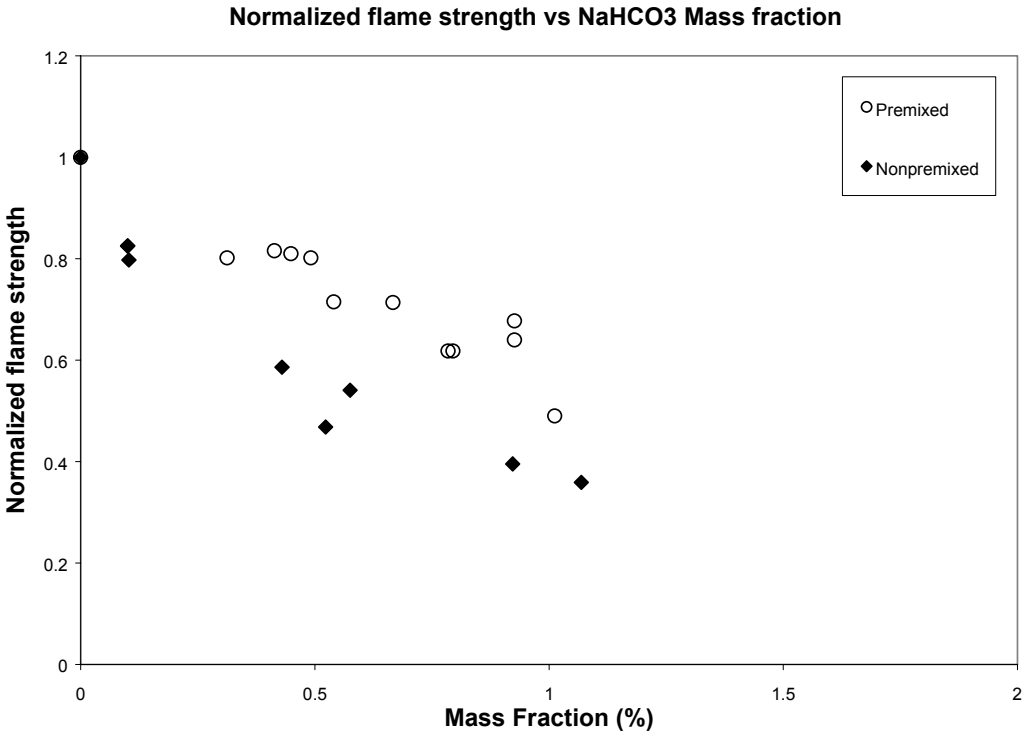

Figure 3-51. Normalized Flame Strength as a Function of Added $NaHCO_3$ Mass Fraction for Premixed and Counterflow Diffusion Flames.

In summary, this fluidized-bed seeding system described was effective for introducing particles smaller than 30 μm to the premixed and counterflow burners. The experimental techniques developed were amenable to testing the efficacy of particles with absorbed super-agents in these flames. The effectiveness of particles (which either decompose or release an absorbed agent) was expected to be dependent upon the residence time for this process.

Premixed Flames with Iodine

Due to the unexpected decomposition of $Fe(CO)_5$ within the solid support material and the potential hazard from desorption of this toxic compound, molecular iodine was used as a surrogate to assess the storage concept. The matrix material was selected to be silica gel, based on agent mass loading potential and the seeding properties of the particles in the flow.

- Absorption/desorption investigations indicated that an iodine mass fraction of about 24 % could be loaded into zeolite-NaX particles. However, the maximum particle seeding achievable with the present apparatus used in the premix flame configuration was about 0.5 % by mass (because of very small size, 2 μm). Thus, the total iodine mass loading of the air stream was about 0.12 %.
- About 6 % mass fraction of I_2 could be loaded into the milled and sized (10 μm to 20 μm size range) crystalline silica particles. Here, crystalline silica particles were considered because of their better fluidization and seeding characteristics. In the same premixed flame configuration, more than 2 % by mass of sized 10 μm to 20 μm crystalline silica particles could be introduced. The total iodine mass loading of the air stream was thus 0.12 %, similar to that for zeolite-NaX.
- Selection of the appropriate matrix material for the particles was based on An iodine mass loading of about 20 % was measured for porous silica gel particles (15 μm to 40 μm).[ii] Particle seeding of up to 6 % by mass was possible, for a theoretical iodine mass delivery of 1.2 %.

Figure 3-52 shows the normalized flame speed of a methane-air flame for increasing particle mass fraction, for pure silica gel and I_2-impregnated silica gel. Iodine-absorbed silica particles do not show any significant reduction in burning velocity compared to chemically inert silica particles.

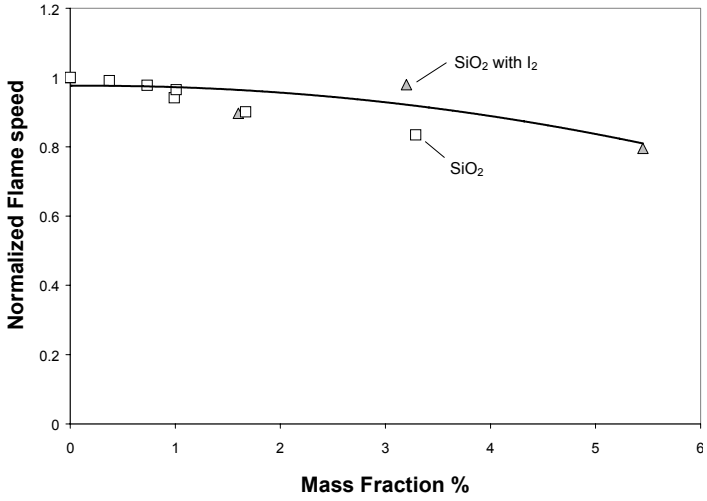

Figure 3-52. Normalized Flame Speed for a Methane-air Flame with Added Silica Gel Particles (14 to 40)μm, with and without I_2 Impregnated in the Particles.

[ii] For porous silica gel particles, TGA analyses of the absorption of iodine were performed on two samples: one tested immediately after the absorption process and the other after the particles had remained in the airflow of the fluidization seeder for several hours. The mass loss from the fresh particles was 19 %, while that from the "aged" particles was about 8 %. There was also a change in the particle color (to a lighter brown shade) after being in the seeder for several hours, a result consistent with the lower mass loss for the post-seeder particles.

This result was not surprising. Based on literature values of the burning velocity reduction of Br_2 in hydrocarbon flames,[186] an estimated I_2 mass loading of 10 % in the air stream would be required to reduce the burning velocity by a factor of two. Hence, even if all of the I_2 in the tested silica gel particles were liberated in the flame, the maximum expected burning velocity reduction would be about 5 % for a 6 % mass loading. In these experiments, such a difference in burning velocity would have been comparable to the experimental uncertainty. For lower iodine desorption rates, the difference between the I_2-laden and unladen particles would have been undetectable.

Nonetheless, this result was not discouraging. From Table 3-11, the mass loading of $Fe(CO)_5$ can be about half that of I_2. However, the flame inhibition effectiveness of $Fe(CO)_5$ is far higher than I_2. Thus, further experiments were conducted on alternative means of introducing iron atoms into the flames and on elucidating the potential synergism between super-effective metals and inert additives.

Complexes of Super-effective Metals

Super Agents and Complexing Ligands Considered

As a first step, the physical and chemical properties of complexes of potential super-effective metal agents were compiled and surveyed. The complexes involved main group metals or transition group metals with different ligands.

Table 3-11. Components of Metallic Complexes.

Ligands		Metals	
Organic	**Halide**	**Main Group Metals**	**Transition Group Metals**
acetonate (ac) acetylacetonate (acac) oxalate (ox) trifluoroacetylacetonate (TFacac) hexafluoroacetylacetonate (Hfacac) methoxide (OMe) ethoxide (OEt)	chloride (Cl) bromide (Br) iodide (I)	Group III - aluminum (Al) Group IV - tin (Sb), germanium (Ge), lead (Pb) Group V - antimony (Sb)	copper (Cu) titanium (Ti) chromium (Cr), molybdenum (Mo) manganese (Mn), nickel (Ni), cobalt (Co) iron (Fe)

For the metal-centered halides, it was found that the three most volatile compounds MX_4 were (in order of volatility): $TiX_4 < SnX_4 < GeX_4$. The bromides become volatile in the range 70 °C to 150 °C, while the chlorides were higher, in the range (180 °C to 240 °C). Germanium iodide was the iodide compound with the lowest boiling point, estimated near 350 °C.

For the organic-complexes, it was found that the order of volatility was generally

$$ox < ac < acac < OMe < OEt < TFacac < Hfacac.$$

Examples of this include $Cr(HFacac)_3$ and $Cr(ac)_3$, which sublime or decompose near 100 °C to 160 °C and 210 °C to 280 °C, respectively, and $Cu(HFacac)_2$, $Cu(TFacac)_2$, and $Cu(acac)_2$, which sublime or decompose near 130 °C to 180 °C, 180 °C to 210 °C, and 290 °C to 320 °C, respectively.

The relative volatility of complexes was dependent on the metal- or main-group-center atom. The order of volatility for compounds with different ligands varied, dependent upon the ligand. Consequently, a direct ordering was not exact. However, in general the volatility was

$$Al < Cu < Mo < Mn < Ni < Cr < Sn < Ti < Fe < Co < Sb < Pb < Ge$$

That is, aluminum and copper compounds were generally significantly less volatile than lead and germanium compounds.

The selection of a metal complex for initial study was based on the following:

- Known high flame inhibition effectiveness. This narrowed the field to Pb, Cr, and Fe.
- Low toxicity. Pb and Cr compounds are generally toxic in most states, while Fe compounds (other than the pentacarbonyl) are generally of low toxicity.
- The iron atom in the gas phase leads to the inhibiting iron-species intermediates, and that the main property required for the parent molecule is that it readily decomposes at flame temperatures to release iron atom.
- Ferrocene ($Fe(C_5H_5)_2$ (or Fec) was known to modify the sooting tendency of flames,[127,213-217] was added to materials as a flame retardant,[218] was an antiknock agent, and was used as a source of iron atoms for kinetic studies. It is also far less toxic than $Fe(CO)_5$.

Experimental Apparatus

Linteris and coworkers performed the first measurements of flame inhibition by ferrocene, and compared its performance with that of $Fe(CO)_5$ and CF_3Br in the same flames.[106] They numerically modeled Fec's flame inhibition using the iron-species mechanism developed for studies of $Fe(CO)_5$ flame inhibition. They also measured the performance of Fec in combination with other agents, including CO_2, and CF_3H.

The tests were performed in premixed flames of methane. Nonetheless, they are relevant to the suppression of practical fires. Babushok and Tsang [219] observed that for a wide variety of hydrocarbons, including methane, the burning velocity is most sensitive to the rates of the same reactions. Since these reactions are the ones most influenced by an inhibitor, the trends in inhibitor effectiveness are the same for most hydrocarbons. While burning velocity measurements are an important first step in assessing an inhibitor's effectiveness and testing mechanism performance, future research should test these highly-effective agents in flames more closely resembling actual fires.

The premixed flame burner was the same as that described in the previous section, modified to accommodate a new evaporator for ferrocene and heating of the gas lines and burner tube.[106] The fuel gas was methane (Matheson UHP, 99.9 %), and the oxidizer stream consisted of nitrogen (boil-off from liquid N_2) and oxygen (MG Industries, $H_2O < 50$ L/L, and total hydrocarbons < 5 L/L). The inhibitors used were Fec (Aldrich), $Fe(CO)_5$ (Aldrich), CF_3H (DuPont), CF_3Br (Great Lakes), N_2, and CO_2 (Airgas). The $Fe(CO)_5$ was added to N_2 carrier gas using a two-stage saturator in an ice bath. Because the vapor

pressure of Fec is much lower than that of iron pentacarbonyl, Fec addition at up to 650 μL/L required both higher bath temperature (79.1 °C held within 0.1 °C) and higher nitrogen carrier gas flows (up to 2800 cm^3/min) relative to $Fe(CO)_5$. Also, the solid state of Fec required an evaporator with larger surface areas for heat and mass transfer. The evaporator design, based upon that of Megaridis[213], had a (30 ± 5) cm^3 packed bed (to provide the bulk of the ferrocene), followed by 30 sublimation stages (to insure that the carrier gas was saturated with Fec at the bath temperature). Each sublimation stage consisted of a 5 mm layer of ferrocene on a 2.36 cm diameter 60 mesh stainless steel screen. A 4 mm gap separated each stage. The vapor pressure correlation of Pelino et al.[220] was used to determine the ferrocene fraction in the carrier gas. Temperature controllers maintained the transfer lines at (80 ± 3) °C and the burner tube at (80 ± 1) °C. For all flames, the equivalence ratio (in the absence of inhibitor) was 1.0, and agent mole fraction was calculated relative to the total reactant flow. The flows of fuel, oxidizer, Fec-N_2, and the blended agent (CO_2, or CF_3H) were mixed after the Fec evaporator. The inlet reactant stream temperature was (80 ± 1) °C, which corresponded to a calculated adiabatic flame temperature of 2260 K and 2391 K for uninhibited flames at $X_{O_2,ox}$=0.21 and 0.244.

Numerical modeling

The laboratory flames inhibited by Fec and Fec-CO_2 blends were numerically modeled as one-dimensional freely-propagating flames. Solutions were obtained using the Sandia flame code Premix,[203] and the CHEMKIN[204] and transport property[205] subroutines. Details of the calculations are provided elsewhere.[106] Little was known about the chemical kinetic behavior of ferrocene in flames. A rate constant existed for its thermal decomposition: $k = 2.188 \cdot 10^{16} \exp(-384 \text{ kJ/R}T)$ s^{-1},[221] but the activation energy is high, leading one to suspect that reactions with radicals may also be important. Thermodynamic data were available,[222,223] and the transport properties were estimates.[224,225] A reaction set for combustion of methane and larger hydrocarbon fragments was adopted from Sung et al.[226] The iron chemistry was from a mechanism developed for flame inhibition by $Fe(CO)_5$.[104] Overall, the kinetic model contained 105 species and 677 reactions. Calculations showed that addition of C_5H_5 at mole fractions up to 400 μL/L had negligible effect on the burning velocity, and that the major effect of Fec was from the iron chemistry. It should be emphasized that the reaction mechanism used for the present calculations should be considered only as a starting point. Numerous changes to both the rates and the reactions incorporated may be made once a variety of experimental and theoretical data are available for testing the mechanism.

Flame Inhibition by Ferrocene

Figure 3-53 shows the relative burning velocity reduction with addition of Fec (open symbols) or $Fe(CO)_5$ (closed symbols) to the present slightly pre-heated (80 °C) methane-air flames. (The uncertainties in the experimental data, described in detail previously,[227] were typically about ± 5 %.) The data are plotted as normalized burning velocity, which is the burning velocity of the inhibited flame divided by the value for the same flame in the absence of inhibitor. The uninhibited experimental burning velocities used for the normalizations were (53.7 ± 3) cm/s and (75.9 ± 6) cm/s for $X_{O_2,ox}$ = 0.21 and 0.244, respectively. For comparison, the calculations for uninhibited flames using GRI-MECH 1.2 yielded 55.5 cm/s and 72.6 cm/s. The effect of the two agents was essentially the same, with very strong initial inhibition followed by a loss of effectiveness above a few hundred μL/L of agent, as found previously for $Fe(CO)_5$ inhibition in flames with reactants at 21 °C.[96]

Figure 3-53 shows that for both Fec and $Fe(CO)_5$, the magnitude of the inhibition is strongly dependent upon the oxygen mole fraction in the oxidizer, with flames with lower mole fraction of O_2 showing more

rapid burning velocity reduction. As a result, blends of inert agents with iron-containing compounds may greatly increase the efficiency over that of the inert alone.

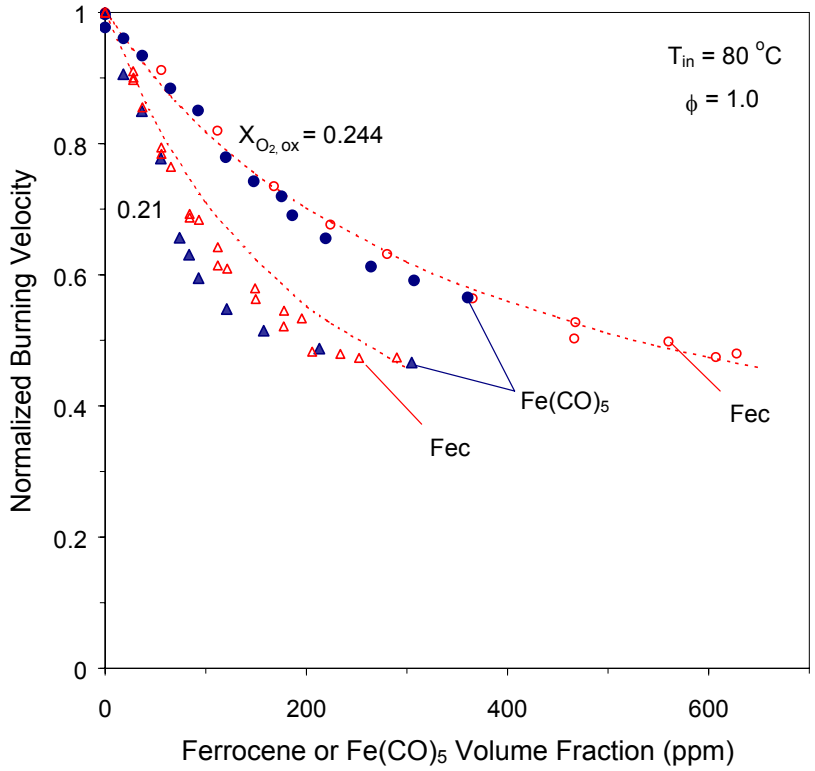

Figure 3-53. Normalized Burning Velocity of Premixed $CH_4/O_2/N_2$ Flames Inhibited by Ferrocene (open symbols) and $Fe(CO)_5$ (closed symbols) for $X_{O2,ox}$=0.21 and 0.244, Together with Modeling Predictions (dotted lines).

The modeling results for the ferrocene-inhibited flames are also shown in Figure 3-53. The calculations predicted the flame speed reduction caused by ferrocene reasonably well. The major difference between the ferrocene reaction scheme and that for $Fe(CO)_5$ was in the decomposition of the iron precursor. The mechanism included only the high activation energy thermal decomposition step for Fec consumption: $FeC_{10}H_{10}$ -> Fe + 2 C_5H_5, which had a peak reaction flux at 1800 K in the present flames. In contrast, iron pentacarbonyl decomposition had a peak reaction flux at about 900 K.

Figure 3-54 shows the normalized burning velocity for a methane-air flame with 400 μL/L of ferrocene as a function of the hypothetical activation energy E_a of the one-step decomposition reaction. In the temperature range of the stoichiometric methane-air flame of the figure, the predicted inhibition effect of Fec was independent of the overall activation energy of the decomposition of Fec for values of E_a less than about 400 kJ/mol. Hence, the decomposition rate of Fec used in the model (E_a = 384 kJ/mol) did not influence the predicted behavior. For other conditions, however, (for example non-preheated reactants and highly diluted flames) the decomposition of Fec may need to be modeled more accurately to provide agreement with experimental data.

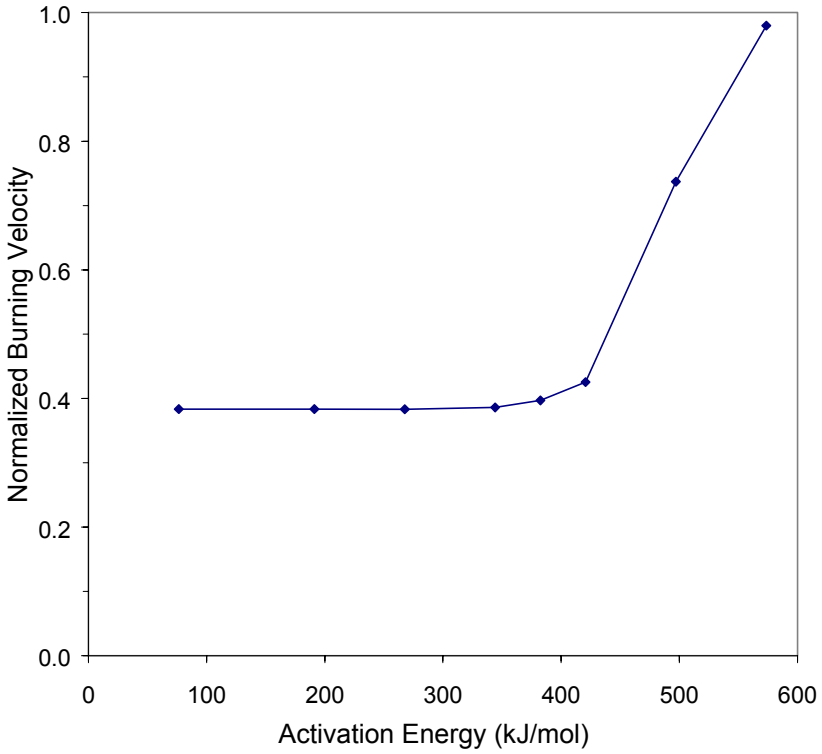

Figure 3-54. Normalized Burning Velocity of Stoichiometric CH_4-O_2-N_2 Flames at 400 µL/L of Ferrocene as a Function of the Activation Energy of the One-step Ferrocene Decomposition Reaction.

Since both the Fec and $Fe(CO)_5$ mechanisms used the same iron sub-mechanism, the mode of flame speed reduction in the model was the same. Decomposition of the ferrocene molecule released iron atom in the gas phase. Iron reacted with O_2 to form FeO_2, which reacted with O atom to form FeO. FeO is a long-lived intermediate, which together with $Fe(OH)_2$ and FeOH, entered into the catalytic cycle for H-atom recombination:

$$\begin{aligned} FeOH + H &\leftrightarrow FeO + H_2 \\ FeO + H_2O &\leftrightarrow Fe(OH)_2 \\ Fe(OH)_2 + H &\leftrightarrow FeOH + H_2O \\ \hline (\text{net: } H + H &\leftrightarrow H_2). \end{aligned}$$

The modeling results showed that the stronger burning velocity reduction for the cooler flames ($X_{O_2,ox}$ = 0.21) was due to their smaller radical pool. In these flames, a given amount of iron removed a larger *percentage* of the hydrogen radicals.

Ferrocene appears to be an alternative to the highly toxic iron pentacarbonyl for addition of gas phase iron to a flame. Unfortunately, its effectiveness also appeared to diminish as the mole fraction increased. For $Fe(CO)_5$, the loss of effectiveness was due to the formation of condensed-phase particulates in the reaction zone, and it was presumed that the same mechanism held for ferrocene.

Inhibition by Ferrocene and CO_2

It is desirable to take advantage of the strong initial flame speed reduction from iron species in the flame, while avoiding the loss of active species due to condensation. Since addition of nitrogen clearly increased the rate of burning velocity reduction at low mole fraction (note the results in Figure 3-53 for $X_{O_2,ox}$ = 0.21 and 0.244), it was logical to determine whether other thermally acting agents could be combined with Fec to mitigate the loss of effectiveness, and perhaps enhance the flame speed reduction at low Fec mole fraction. It was known, however, that addition of an inert, while reducing the burning velocity, also increases the residence time for particle formation in the flame, so that condensation would be increased. It was not known a priori if the net effect of combining thermal and iron-containing agents would reduce the overall reaction rate faster than the increase of the rate of active-species condensation.

Therefore, Linteris and coworkers conducted experiments to resolve this. Using the same apparatus, they added CO_2 to the methane-air-Fec system. Figure 3-55a and Figure 3-55b present the experimental data for tests at $X_{O_2,ox}$ = 0.21 and 0.244. Data are shown for pure CO_2 as well as for CO_2 -Fec blends corresponding to three values of the mole percentage of Fec in CO_2 (0 %, 0.25 %, and 1.5 % in Figure 3-55a, and 0 %, 0.4 %, and 1.5 % in Figure 3-55b).

For the pure compounds, addition of about 10 % of CO_2 (or 25 % N_2) reduced S_L by a factor of two at $X_{O_2,ox}$ = 0.21 or 0.244. Adding Fec to CO_2 produced a particularly effective agent. The equivalent of 0.35 % Fec in CO_2 reduced the required CO_2 for a 50 % reduction in the flame speed by about a factor of three at $X_{O_2,ox}$ = 0.21 and about a factor of two at $X_{O_2,ox}$ = 0.244. The combination of 1.5 % Fec reduced the required CO_2 by 10, making this blend about as effective as CF_3Br (for which addition of about 1 % halved the burning velocity). Nonetheless, the curvature in the ends of the data sets (particularly for 1.5 % Fec in CO_2) illustrates condensation was important. Although one might expect the slightly cooler, slower flames with added CO_2 to always show more condensation of iron species, the greater efficiency of the catalytic cycle in the diluted flames predominated for most of the conditions for the flame of Figure 3-55. Higher effectiveness of iron compounds in diluted flames has been observed previously for flames with $X_{O_2,ox}$ lowered below 0.21.[96]

The condensation behavior of the blends can be discerned from Figure 3-56a and Figure 3-56b, which present additional data for CO_2 and ferrocene in stoichiometric flames with $X_{O_2,ox}$ = 0.21 and 0.244, respectively. In Figure 3-55, CO_2 and ferrocene were added together in proportional amounts, whereas in Figure 3-56, CO_2 is first added at a constant volume fraction (0 %, 2 %, and 6 % in 7a; or 0 %, 4 %, and 12 % in 7b), and then the Fec is added. This approach allows a clearer delineation of the effects of each component of the blend. As the figures show, the curve with 0 % CO_2 (pure Fec) has a decreasing slope magnitude as X_{in} increases (due to increased condensation). For each of the other curves, the added CO_2 reduces the normalized burning velocity before the Fec is added, so that each curve starts at a value less than unity; addition of Fec further reduces the flame speed. Below an Fec volume fraction of about 70 L/L, the curves are all quite linear, showing that there no loss of effectiveness. But for curves extending beyond this amount of Fec, there is increasing curvature as X_{in} increases (due to condensation). Nonetheless, at low mole fractions, the inhibition by Fec is actually stronger for conditions of higher CO_2 mole fraction (note the larger magnitude of the slope for the 12 % CO_2 curve in Figure 3-56b). Hence, for some conditions, adding CO_2 makes Fec more effective. As discussed below, once the particles start to form, the deterioration of inhibition may be more rapid with added CO_2. These results imply that combinations of *non-condensing quantities* of several catalytic agents combined with a thermal agent can be particularly effective.

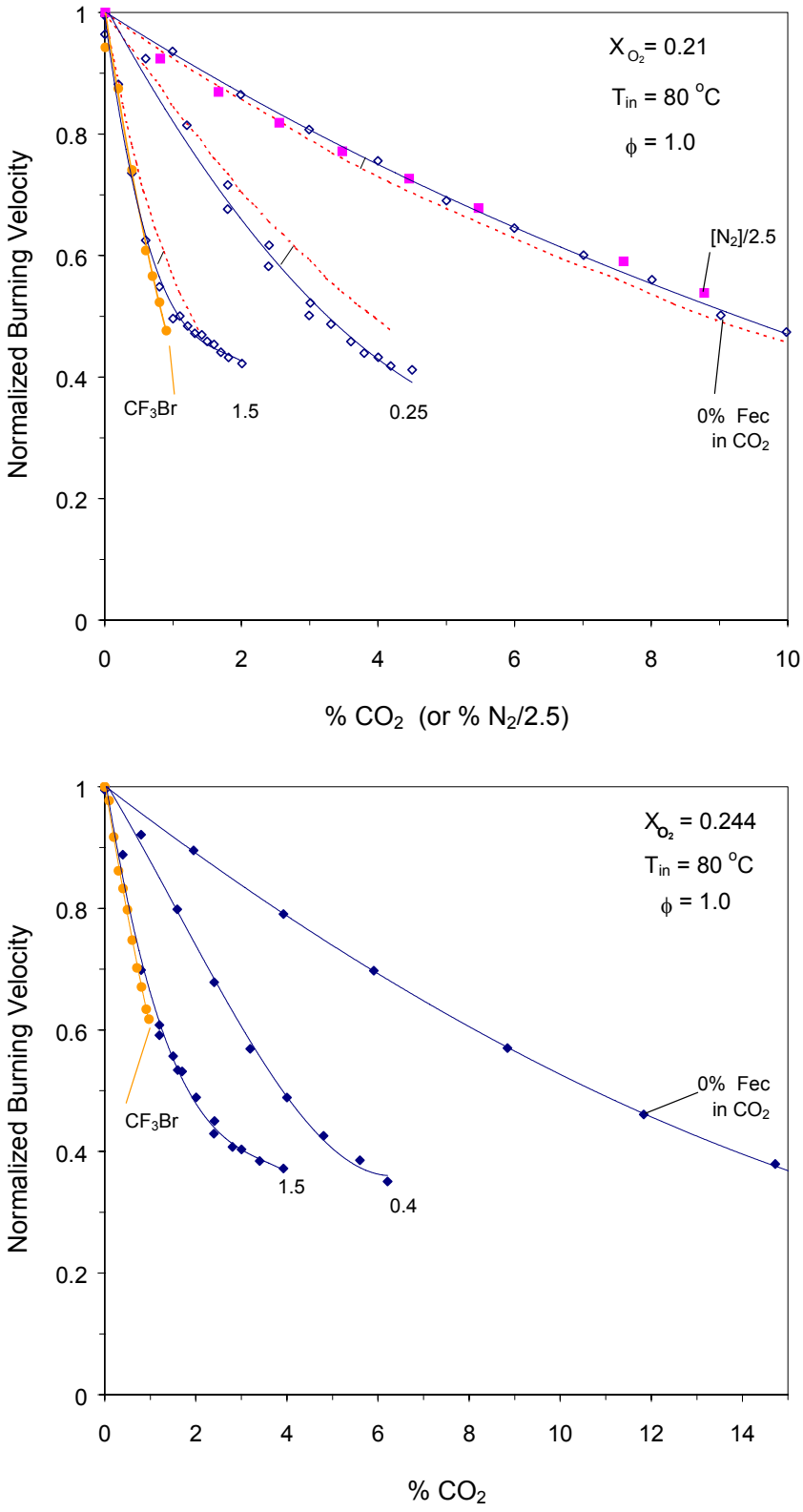

Figure 3-55. Normalized Burning Velocity of $CH_4/O_2/N_2$ Flames, a) $X_{O_2,ox}$ = 0.21, b) $X_{O_2,ox}$ = 0.244, Inhibited by CO_2, by CO_2–ferrocene Blends, and by CF_3Br. (The equivalent percentage of ferrocene in CO_2 (which is constant for each curve) is given. The solid lines are curve fits through the data, and the dotted lines, the calculated results. Data for nitrogen are included in the upper plot by dividing % N_2 by 2.5.)

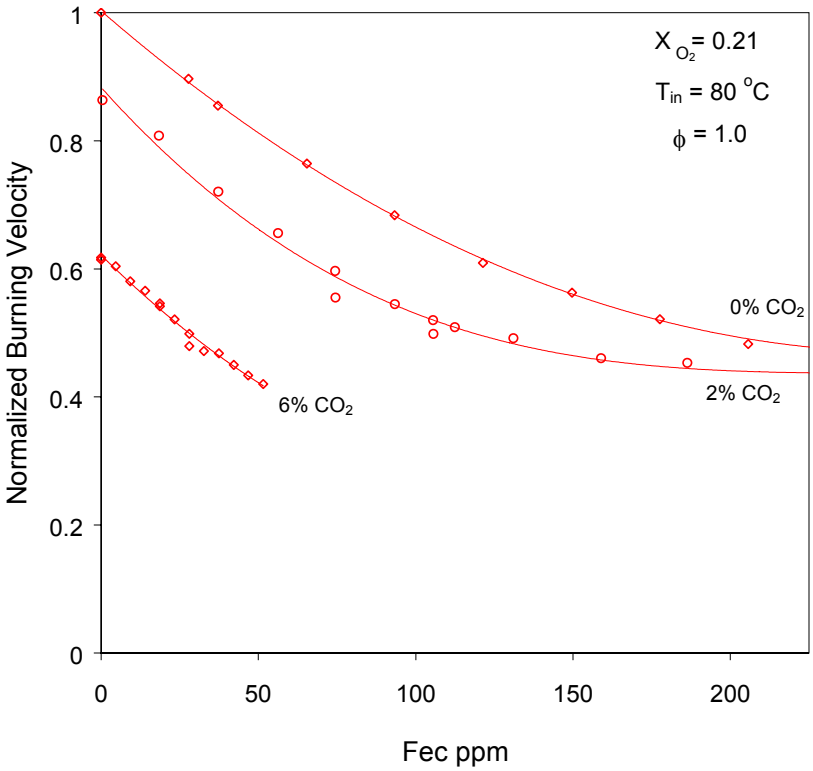

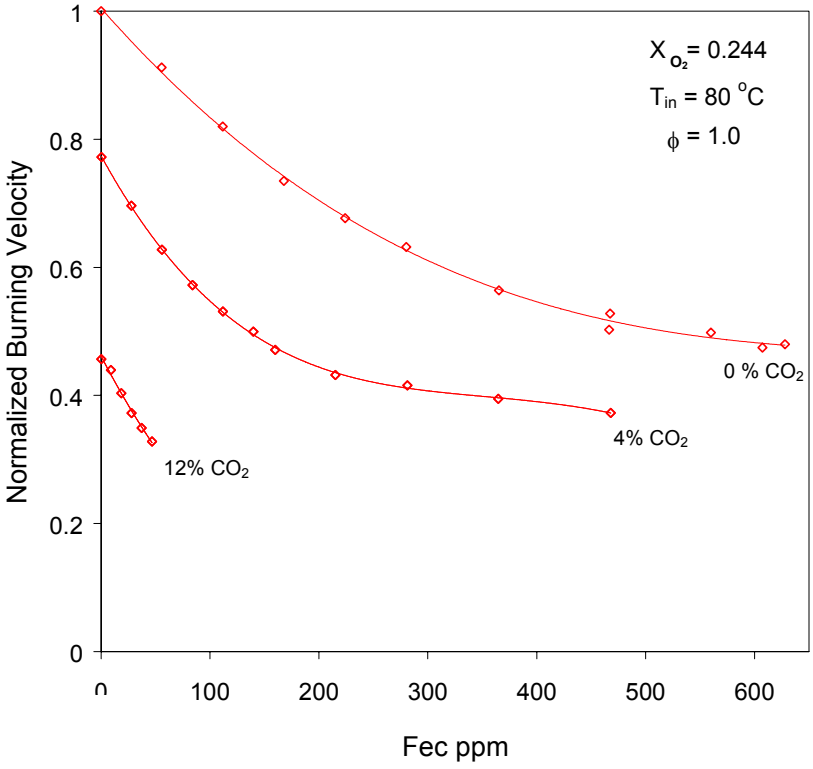

Figure 3-56. Normalized Burning Velocity of CH_4 / N_2 / O_2 Flames, a.) $X_{O_2,ox}$ = 0.21, b.) $X_{O_2,ox}$ = 0.244, with 0, 2, and 6, or 0, 6, and 12 Volume Percent of CO_2, Respectively, Added to the Reactant Stream, as a Function of Added Ferrocene. (The lines are curve fits to the experimental data.)

Inhibition by Ferrocene and CF_3H

Many compounds, both thermally and chemically acting, are candidates for blending with catalytic agents. Hydrofluorocarbons, which are easily stored at moderate pressure, were of interest since they were being used as halon replacements. These compounds had been found to reduce the burning velocity of premixed methane-air flames by reducing *peak* H-atom mole fractions by acting as a sink for H atoms through reactions forming HF, and by lowering the temperature of the flame. Since they had also been shown to reduce the *equilibrium* mole fractions of radicals in flames lower than expected based on temperature reduction alone,[58] they might show enhanced performance relative to CO_2 when combined with catalytic agents.

Figure 3-57 presents the burning velocity reduction caused by pure CF_3H addition to the above flames; a mole fraction of about 5 % was required to reduce S_L by two. Data are also presented for addition of 0.35 % Fec in CF_3H. Unlike ferrocene addition to CO_2, in which 0.35 % Fec in CO_2 reduced the amount of CO_2 required by a factor of about five, this amount of ferrocene in CF_3H reduced the amount of CF_3H required only by about one-third. This poor performance may have be due to reactions between iron species and fluorine, which would have reduced the gas phase mole fraction of the active iron-species intermediates, effectively poisoning the iron catalyst.[228]

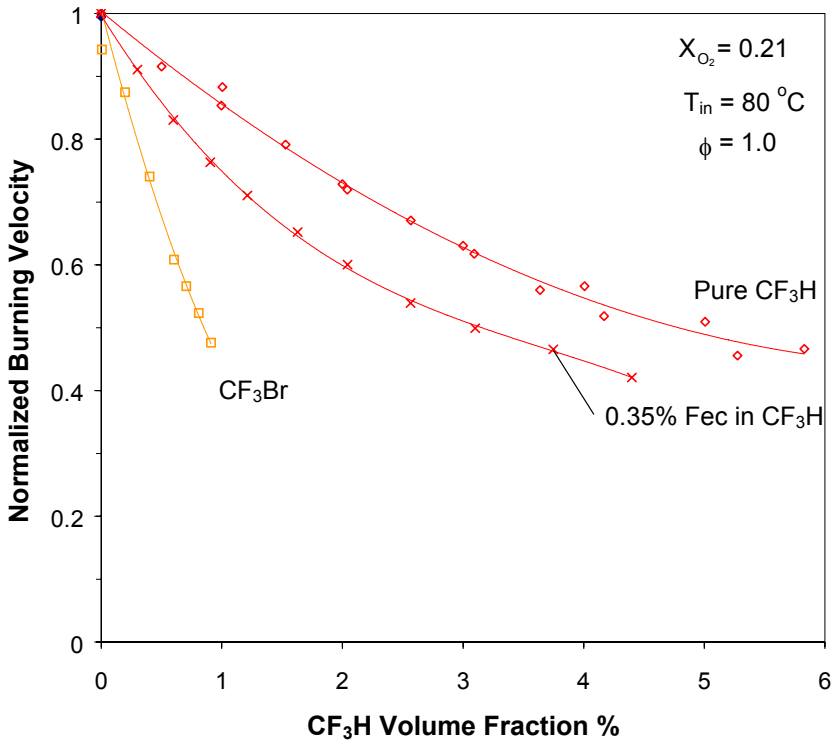

Figure 3-57. Normalized Burning Velocity of Premixed $CH_4/O_2/N_2$ Flames Inhibited by Pure CF_3H and by CF_3H with 0.35 % Ferrocene, Together with Data for CF_3Br. (Lines are curve fits to the data.)

Since there existed no experimental data on the rates of reactions of iron species with fluorine containing species in flames, the poisoning effect of fluorinated hydrocarbons on iron-catalyzed radical recombination reactions was assessed through equilibrium calculations for the combustion products. The species included in the calculations were those in the mechanisms for hydrocarbon oxidation, iron-inhibition, and fluorinated hydrocarbon-inhibition,[229] as well as the iron-fluorine species: FeF, FeF_2, FeF_3,

Fe_2F_4, Fe_2F_6.[197] Calculations were performed for the equilibrium products of a stoichiometric methane-air flame with 1 % to 4 % CF_3H containing 0.35 % Fec (the conditions of Figure 3-57). The results of the calculations, shown in Figure 3-58, indicated that FeF and FeF_2 were major product species when CF_3H was added. For 1 % to 4 % CF_3H, the amount of iron taken up by the sum of FeF and FeF_2 increased from 42 % to 84 %, making less iron available in the form of the active iron intermediate species Fe, FeO, FeOH, FeO_2, and $Fe(OH)_2$. The formation of fluorinated iron species with strong bonds clearly acted as a sink for iron in the flame, and reduced the mole fractions of active iron-containing species available to participate in the flame inhibition reactions. While the experiments and calculations were performed for CF_3H, the results are likely to be the similar for larger HFCs such as C_2HF_5 and C_3HF_7 since the decomposition of all of these proceeds largely through the CF_3, CF_2, and CFO intermediates.[55,57,58]

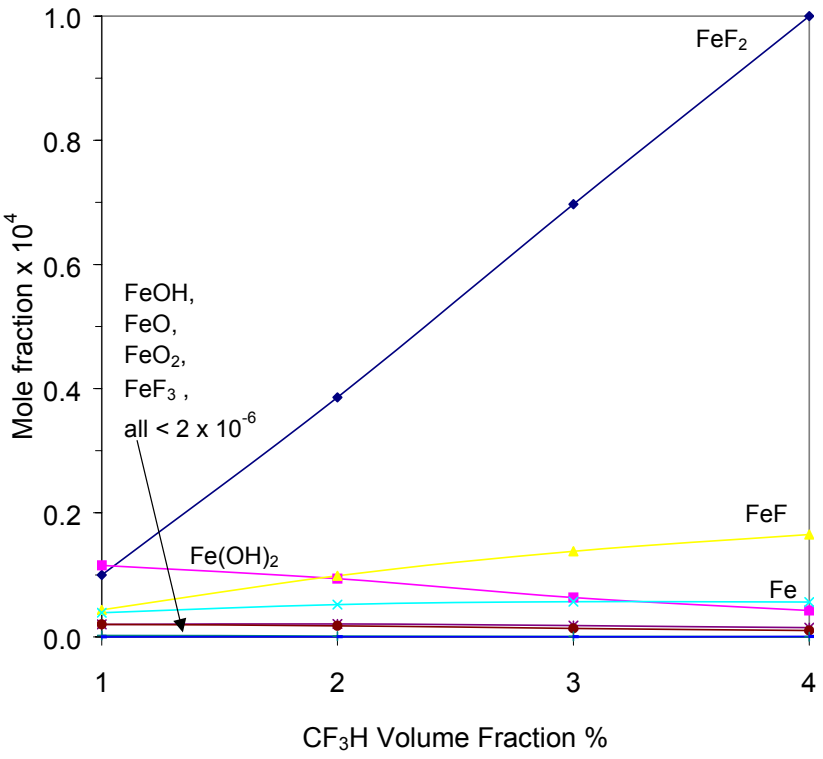

Figure 3-58. Equilibrium Mole Fraction of Active Inhibiting Species (Fe, FeO, FeOH, $Fe(OH)_2$) and Iron-fluorine Species with 1 % to 4 % CF_3H (containing 0.35 % Ferrocene) Added to a Stoichiometric Methane-air Reaction Mixture.

Comparison of Individual and Blended Performance

The behavior of the blends of agents was investigated by comparing the actual amount of flame speed reduction for the blend to the sum of the inhibition which would result from each agent individually. This approach is illustrated schematically in Figure 3-59. This uses the inhibition index $\Phi(X_{in})$ of Fristrom and Sawyer,[230] where $\Phi(X_{in})=\{\{(V_o-V(X_{in}))/V_o\}\{X_{O_2,ox}/X_{in}\}$ (and using the oxygen mole fraction in the oxidizer). The index $\Phi(X_{in})$ is seen to be the magnitude of the average slope of the normalized burning velocity curve (times $X_{O_2,ox}$) evaluated at the mole fraction of interest X_{in}. For a given blend, one can evaluate the amount of normalized burning velocity *reduction* that would have been caused by each individual component of the blend, e.g., components *a* and *b*. The predicted inhibition index is just a linear combination of the reduction from each component, or $X_a \cdot \Phi_{a+b}(X_a, X_b)|_{pred} = X_a \cdot \Phi_a(X_a)+X_a \cdot \Phi_b(X_b)$, in which *a* is the major component of the blend, (selected for defining $\Phi_{a+b}(X_a, X_b)$). The actual inhibition index $\Phi_{a+b}(X_a, X_b)|_{actual}$ was evaluated from the normalized flame speed of the blend (using X_a in its

definition). The ratio of $X_a \cdot \Phi_{a+b}(X_a, X_b)|_{actual}$ to $X_a \cdot \Phi_a(X_a) + X_a \cdot \Phi_b(X_b)$ provided a reasonable indicator of the performance of the blend relative to the individual components.

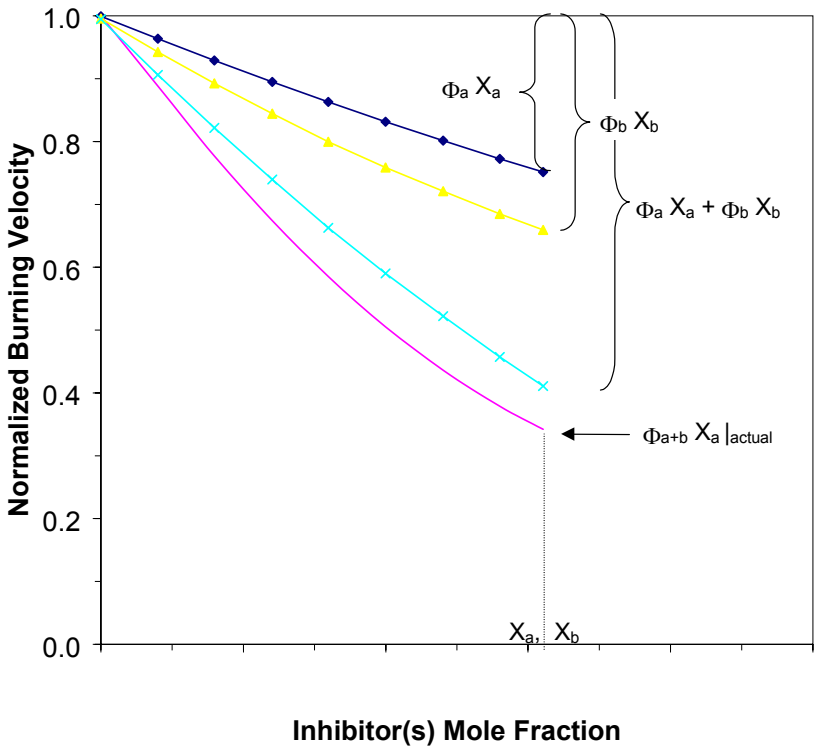

Figure 3-59. Linear Contribution of Burning Velocity from Each Component of a two-Component Blend of Inhibitors, Together with the Actual Reduction from the Blend.

As Figure 3-60 shows, a blend of CO_2 and N_2 (in the molar ratio of 1:2) provided a performance index of nearly 1.0 for N_2 added up to 12 % (i.e., containing 6 % CO_2). (The percent amount of the N_2/CO_2 mix plotted in Figure 3-60 was divided by two to allow plotting on the same scale.) In contrast, the poor performance of the Fec-CF_3H blend is clearly indicated by a decreasing performance index as X_{in} increases. For the CO_2/Fec blends, the combination worked slightly better than the individual components at low X_{in} of the blend, and slightly worse at higher X_{in} . The good performance at low X_{in} was due to the higher radical super-equilibrium which occurred with flame dilution, as observed previously for N_2 addition[96], and the degraded performance at higher X_{in} was due to the longer residence times for condensation which resulted from the lower flame speeds.[102] In Figure 3-60, the condition at which the curves for Fec/CO_2 crossover the unity ratio correspond roughly to the location on the curves in Figure 3-55, where the linear behavior has ended and the curvature begins.

Conclusions

The first data on flame inhibition by ferrocene showed that the efficiency of $Fe(CO)_5$ is not unique, and that there may be methods for overcoming its loss of performance.

- Ferrocene was as efficient as $Fe(CO)_5$ at reducing the burning velocity of premixed methane flames, but, like $Fe(CO)_5$, lost its effectiveness at a mole fraction above a few hundred µL/L. The experimental results were reasonably predicted by a gas phase iron inhibition mechanism. Thus,

similar results can be expected for any rapidly decomposing, iron-containing agent that releases atomic iron in the gas phase

- As with $Fe(CO)_5$, the magnitude of the inhibition by ferrocene had a strong dependence on the oxygen mole fraction. As a result, many combinations of CO_2 and Fec showed strong inhibition, mitigating the loss of effectiveness observed for pure Fec or $Fe(CO)_5$.
- These results suggest that an inert agent, together with multiple catalytic agents (to keep the absolute mole fraction of each below the saturation point) may prove to be highly effective for all conditions.
- In contrast to the results with CO_2, blends of CF_3H and Fec were not effective, implying that iron species and halogens may enter into undesired reactions which poison the catalytic cycles.

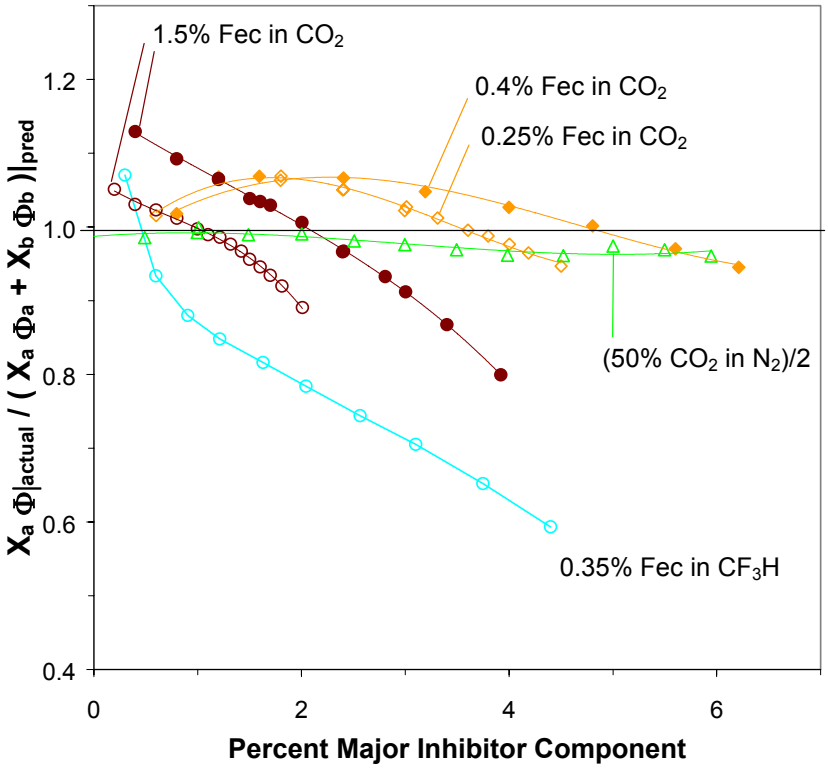

Figure 3-60. Ratio of the Actual Reduction in S_L from the Two-component Mix to the Predicted Reduction Based on Linear Combination of the Effect from Each Component. (Open and closed symbols are for $X_{O2,ox}$ = 0.21 and 0.244; lines are curve fits to the data. The percent CO_2/N_2 has been divided by two to fit on the figure.)

3.3.6 Potential for Loss of Effectiveness of Other Metals

There are multiple approaches for determining whether a metal will have a loss of effectiveness similar to that of iron:

- Obtain experimental data for flame systems in which the loss of effectiveness is evident. This requires that the inhibitor be added at volume fractions high enough to allow the loss of effectiveness. Many of the early studies with metal compounds did not provide data to high enough volume fractions to show the loss of effectiveness[34] or the inhibiting effect was not presented as a function of additive volume fraction (so the decreasing effectiveness was not illustrated).[92]

- Note a reported presence of particles in some flame system. Although the presence of particles depends upon the temperature of the flame, the concentration at which the metal moiety is added, and the residence time for particle formation, the observed presence of particles in one flame system is an indication that it may be important in other flame systems as well.
- Consider the local metal species volume fraction compared to the its local vapor pressure in the flame. A limitation of this method is that it relies upon knowledge of the metal species present in a flame system, the mechanism of inhibition, as well as the vapor pressure (or gas phase and condensed-phase thermodynamic data). Often, this information is incomplete. Further, the kinetic rates of the formation of more stable oxides of the metal must be known to assess the contribution of those compounds to condensed-phase particles (since often, the vapor pressure of these oxides is very low; e.g., Fe_2O_3).

Below, the available information related to the potential for condensation is presented for each metal species of interest.

Cr

Bulewicz and Padley[126] found particles in the post combustion region of premixed flat flames inhibited by chromium through visual observation and by detecting continuum radiation from them. They also observed saturation in both the inhibiting effect and in the concentration of gas phase Cr in the flame. In addition, solid deposits were observed on the burner in premixed flames inhibited by CrO_2Cl_2, indicating the potential for particle formation (similar deposits have been observed for premixed flames inhibited by Sn, and Mn [107] and for Fe.[103] Hence, the potential for condensation of Cr species exists and may be important in other flame systems. To further examine this potential, the vapor pressures of Cr, CrO, CrO_2, and CrO_3 above Cr_2O_3, under neutral and oxidizing conditions are shown in Figure 3-61.

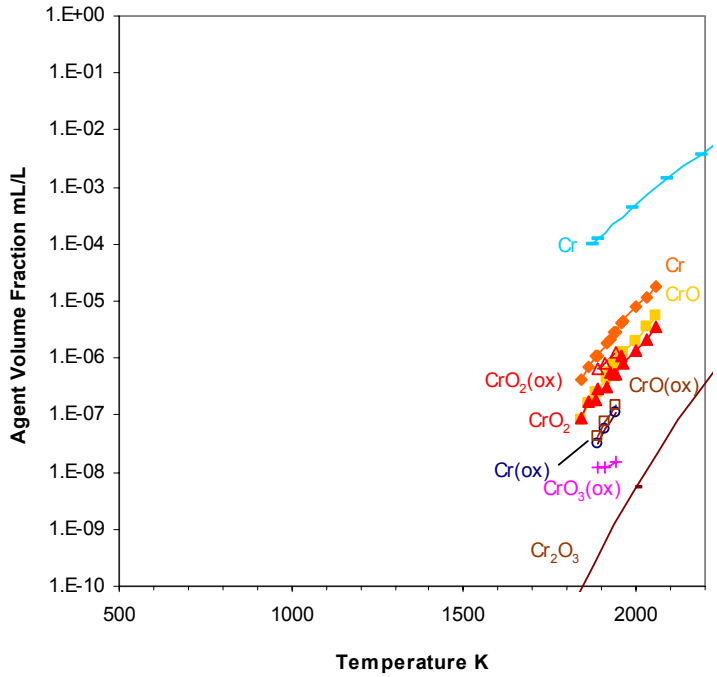

Figure 3-61. Volume Fraction of Cr-containing Species. Cr, CrO, CrO_2, and CrO_3 above Cr_2O_3 at 10.133 kPa under Neutral (closed symbols) and Oxidizing (open symbols). Conditions above Cr_2O_3 (reddish hues), and Cr above itself (blue). Data from References 197, 231, and 232

Note that since Cr_2O_3 is a particularly stable oxide, these vapor pressures will be lower than if the equilibrium included other, less stable condensed-phase oxides. For example, in Figure 3-61, the blue curve for Cr is for data for Cr vapor above Cr solid. Nonetheless, since it is not yet know for *any* metal inhibitor what the composition of the condensed phase oxide actually is, the potential for condensation of Cr species is illustrated. That is, many of the chromium oxides appear to have quite low vapor pressures.

Pb

The presence of PbO particles was detected in many engine knock studies,[94,95,99,109] and it was often argued that the strong inhibition of knock occurred from heterogeneous radical recombination on the particle surfaces. Although lead has been shown to be one of the more effective metal agents in flame screening studies,[34] the additive mole fraction (maximum 150 μL/L) was not increased high enough to show the loss of effectiveness that might occur. In the flash photolysis studies of Norrish et al.,[96] however, the TEL concentration was systematically increased, and a drop-off in the effectiveness was observed above a certain volume fraction. Hence, condensation is likely to limit lead effectiveness for at least some applications. It should also be noted, that the high effectiveness of Pb in premixed flames cannot be from particles since, as shown by Rumminger et al.,[102] the collision rate of radicals with solid particles is not high enough to account for the observed inhibition of premixed flames by super-effective agents such as iron or lead. The vapor pressure of Pb and PbO are shown as a function of temperature in Figure 3-62. The data for PbO_2 are too low to appear on this figure, and hence, condensation is clearly possible for Pb-inhibited flames if PbO_2 readily forms in the inhibition cycle, or if other higher oxides readily form.

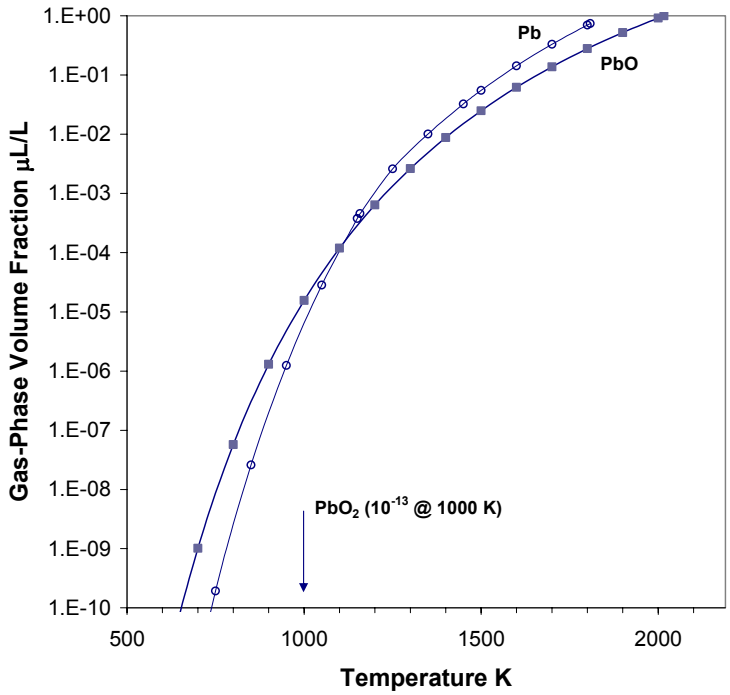

Figure 3-62. Pb Species Gas Phase Volume Fractions at Equilibrium over the Condensed Phase (at 101.3 kPa). (Vapor pressure of Pb and PbO from Reference 233, PbO2 from References 197 and 234.)

Mn

The effect of MMT on the flame speed of methane-air mixtures was measured by Linteris et al.,[107] as shown in Figure 3-63. The data clearly show a saturation effect, which was beyond that due to lowering of the radical concentrations. Additional tests in cup burner flames showed a much lower effectiveness than expected, as well as a rapid loss of effectiveness for MMT as its volume fraction was increased. (See Figure 3-23 inset.) The presence of solid particles was also observed visually, as were solid deposits on the burner. The vapor pressure of Mn, MnO, and MnO_2 are shown in Figure 3-64. Since the volume fraction necessary for flame inhibition exceeded 200 μL/L, the potential for condensation was apparent.

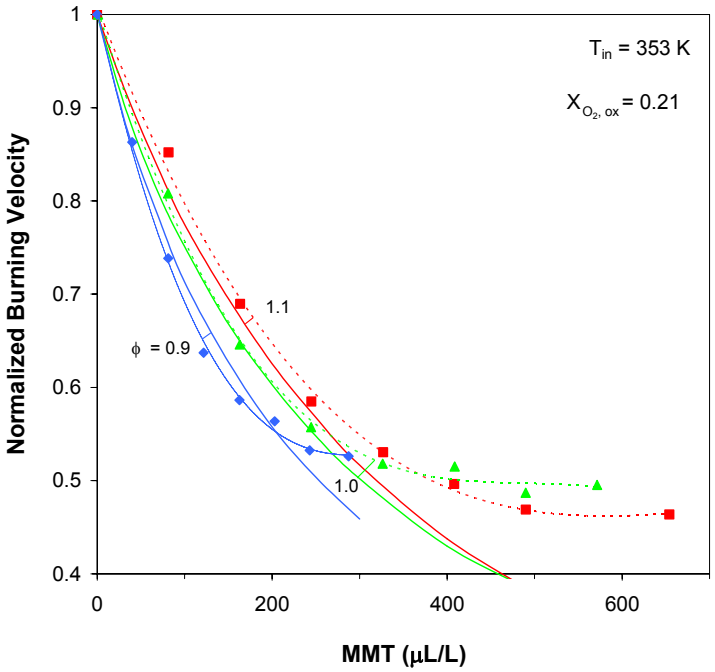

Figure 3-63. Normalized Burning Velocity of Premixed $CH_4/O_2/N_2$ Flames Inhibited by MMT with $X_{O2,ox}$ = 0.21 and ϕ = 0.9, 1.0, and 1.1. [107] (Dotted lines: curve fits to data; solid lines: numerical predictions.)

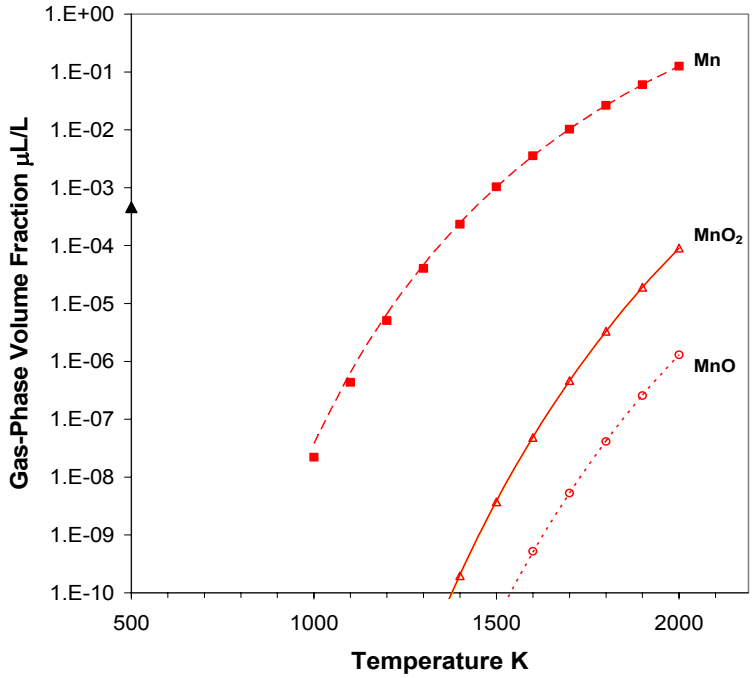

Figure 3-64. Mn Species Gas Phase Volume Fraction at Equilibrium over the Condensed-phase at 101.3 kPa. [107]

W

There are no published data concerning particle formation or loss of effectiveness of flames inhibited by tungsten compounds. A search for vapor pressure or thermodynamic data for tungsten oxides, hydrides, and hydroxides allowed generation of the results in Figure 3-65. As shown, WO_3 has a quite high vapor pressure at flame temperatures; on the other hand, the vapor pressures of WO_2 and W are low enough to allow particle formation. Depending upon the flame reactions of W-containing compounds and their rates, as well as the vapor pressures of other compounds which form in flames, condensation may or may not be important.

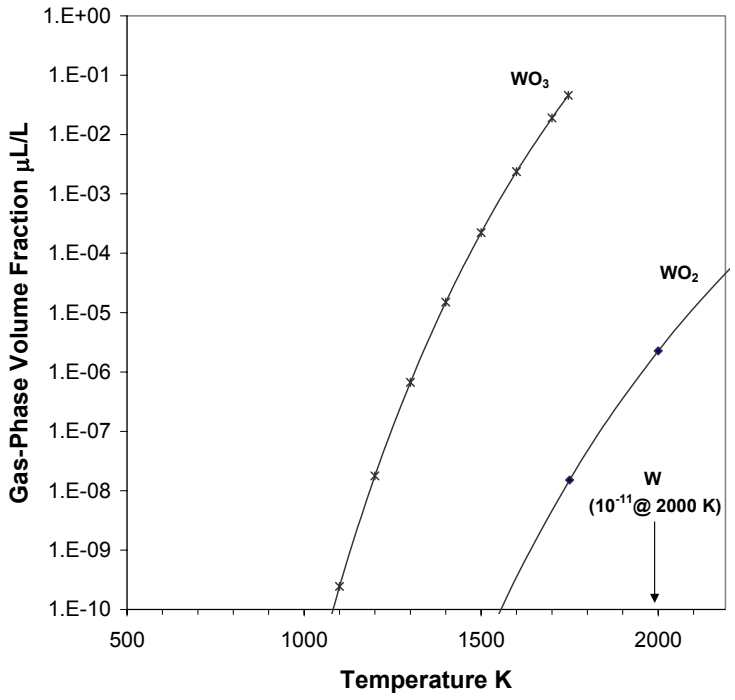

Figure 3-65. Tungsten-containing Species Gas Phase Volume Fraction at Equilibrium over the Condensed Phase at 101.3 kPa).[189,197,231]

Mo

There are likewise no published data concerning particle formation or loss of effectiveness for flames inhibited by Mo-containing species. The vapor pressures of Mo, MoO_2, and MoO_3 for flame conditions are shown in Figure 3-66. As for W compounds, the only species thought to participate in the catalytic cycle for which vapor pressure data are available (WO_3 and MoO_3) have quite high vapor pressures.

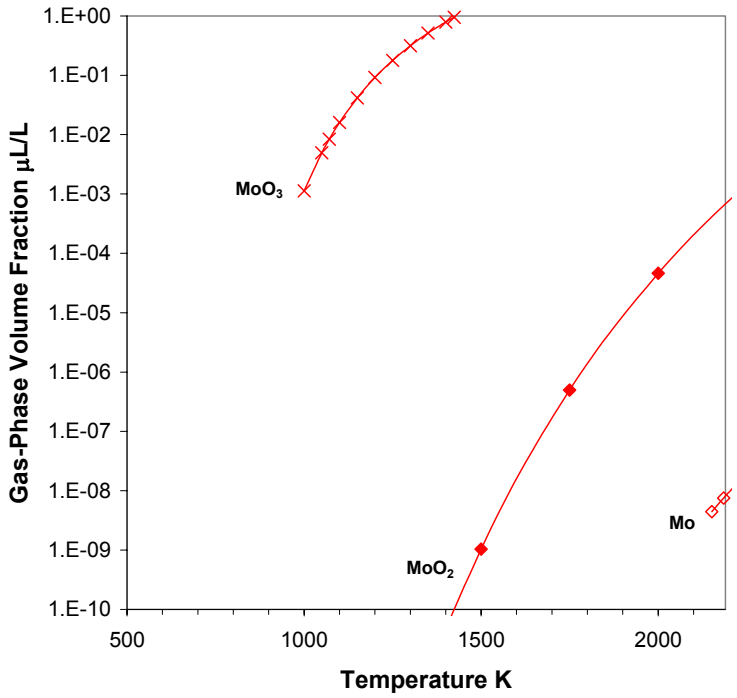

Figure 3-66. Mo-containing Species Gas Phase Volume Fraction at Equilibrium over the Condensed Phase at 101.3 kPa.[189,197,231]

Sn

The results for Sn are similar to that of Mn. At the volume fractions necessary for effective flame inhibition, a loss of effectiveness was observed in premixed flames, although not as dramatic as for Mn (Figure 3-67); particle deposits were observed on the burner. Cup burner tests showed much lower effectiveness than expected, as well as a further loss of effectiveness as the Sn volume fraction increased (Figure 3-23 inset), and solid particles were observed both in the flame and deposited on the burner. The vapor pressures of Sn, SnO, and SnO_2 are shown in Figure 3-68. Clearly, condensation is possible at the 3000 µL/L volume fraction needed for flame inhibition.

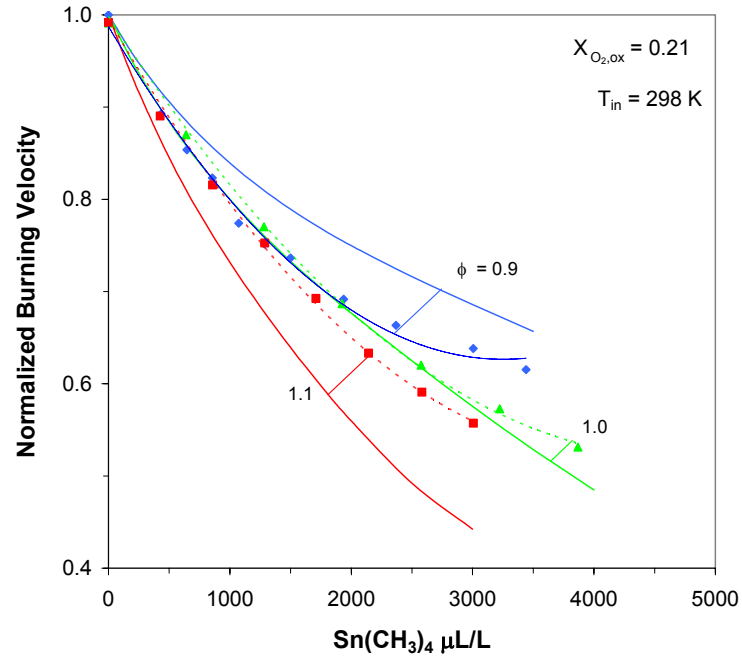

Figure 3-67. Normalized Burning Velocity of Premixed $CH_4/O_2/N_2$ Flames Inhibited by TMT with $X_{O_2,ox}$ = 0.21 and ϕ = 0.9, 1.0, and 1.1.[107] **(Dotted lines: curve fits to data; solid lines: numerical predictions.)**

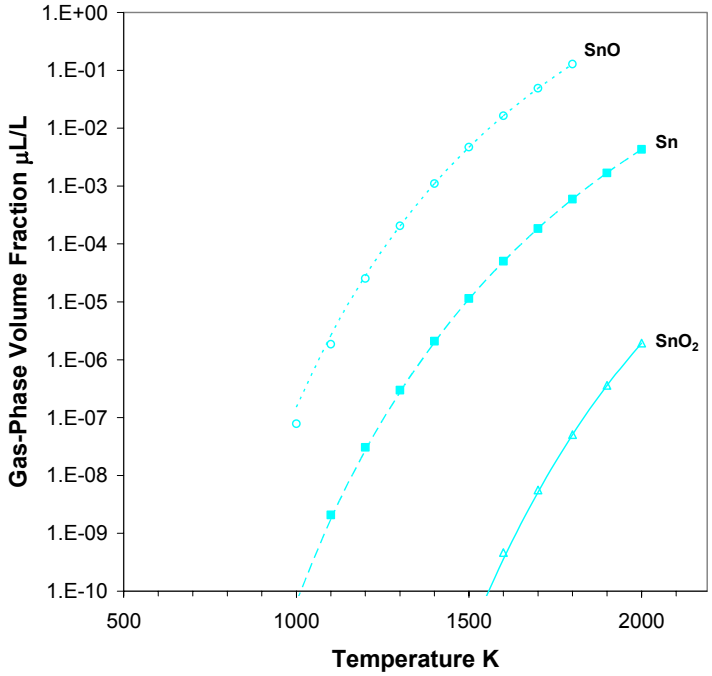

Figure 3-68. Sn-containing Species Gas Phase Volume Fractions at Equilibrium over the Condensed Phase at 101.3 kPa.[197]

Co

The data for Co effectiveness in various flame systems has not been measured as a function of Co concentration. Hence, a loss of effectiveness at higher concentrations has not been demonstrated. Likewise, particle formation in flames with added Co has also not been reported. The available vapor pressure data for Co oxides and hydroxides are shown below. Since CoO is an intermediate species in the proposed inhibition mechanism of Co in H_2-O_2-N_2 flames, and total Co loading in the flame is expected to be on the order of several thousand µL/L, condensation may occur. On the other hand, depending upon the relative rates of the inhibition reactions, the volume fraction of CoO may not build up too high, and hence it's propensity to condense could be lower than Figure 3-69 might lead one to believe.

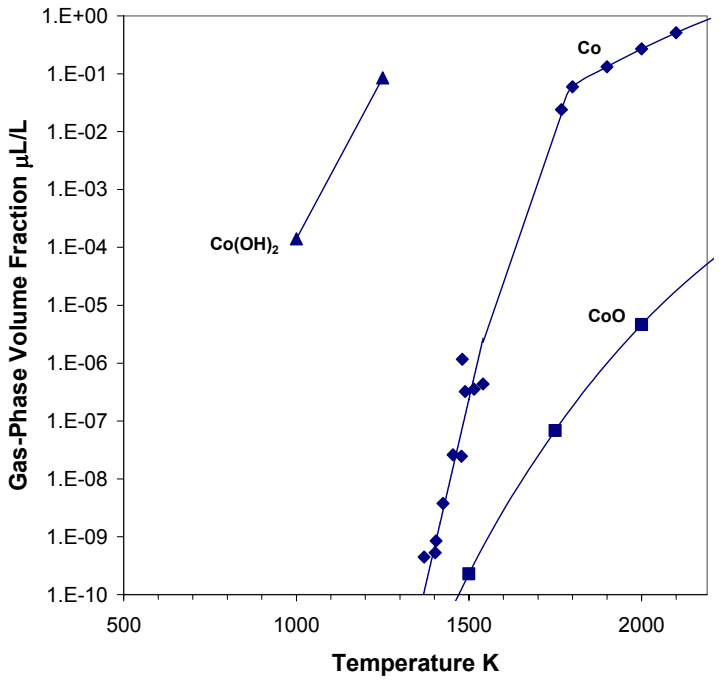

Figure 3-69 – Co-containing Species Gas Phase Volume Fraction at Equilibrium over the Condensed Phase at 101.3 kPa.[189,197,231]

Cu

As shown in Table 3-3, copper salts have been used in experiments on engine knock, ignition suppression, radical recombination above flat flames, as well as in flame screening tests. The compounds were added either as aqueous sprays or directly as particles. There has been no mention in the literature of observed particle formation after decomposition of the additive, or of any loss of effectiveness at higher mole fractions. Only one of these studies ran experiments over a range of additive mole fractions,[91] and in it, they attributed changes in the performance with additive mole fraction to heating effects of the particles (not condensation of active species or saturation of the radical recombination cycle). Hence, it was difficult to assess from previous work if condensation were possible for copper-based inhibitors. To assess the condensation potential, Figure 3-70 assembles the available vapor pressure data for copper compounds which may exist in flames. Although data are not available for other possible hydrides, oxides and hydroxides (e.g., CuH, CuOH) CuO and Cu_2O have quite high vapor pressures, and that of Cu is also relatively high at flame temperatures.

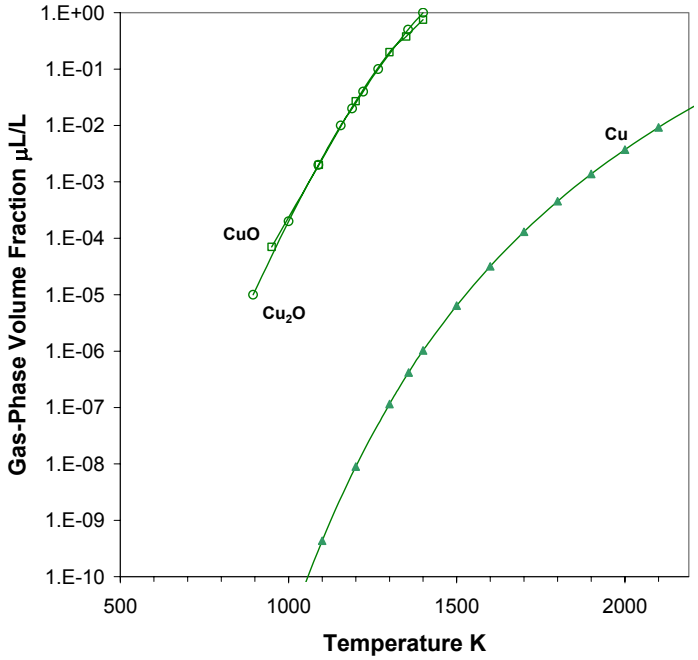

Figure 3-70. Cu-containing Species Gas Phase Volume Fractions at Equilibrium over the Condensed Phase at 101.3 kPa.[233,234]

Sb

Although the only flame data for antimony inhibition[34] did not go to high enough concentrations to show loss of effectiveness, antimony may form condensed-phase particles in flames. In studies of polymers with added Sb_2O_3 and halogen, Fenimore and Martin[134] showed that the fire retardant effect increases linearly with Sb_2O_3 at low mass fractions of Sb_2O_3, but saturates at some value, above which further addition of Sb_2O_3 is ineffective. Hence, the fire retardancy effect of antimony shows a strong saturation, much like that for iron, manganese, and tin in cup burner flames.[180] To illustrate this, the data in Figure 3-23 (CO_2 required for extinction with metal species added) are re-plotted below in Figure 3-71 in terms of the limiting oxygen index (based on N_2). The top of the figure shows the limiting oxygen index for polyethylene/halogen blends as a function of the volume fraction of the metallic inhibitor in the gas phase. The curves for Sb_2O_3 were calculated based on data available in Fenimore and Martin.[136] The effectiveness of the antimony/halogen system saturated at Sb_2O_3 volume fractions near 400 µL/L (based

on Sb). On the bottom of the figure, curves for Fe, Mn, and Sn added to the air stream of heptane-air cup burner flames are also shown.[180] Although those experiments were conducted with CO_2 added as the diluent, the data were converted to an equivalent LOI with nitrogen diluent by correcting for the difference in heat capacity between N_2 and CO_2.

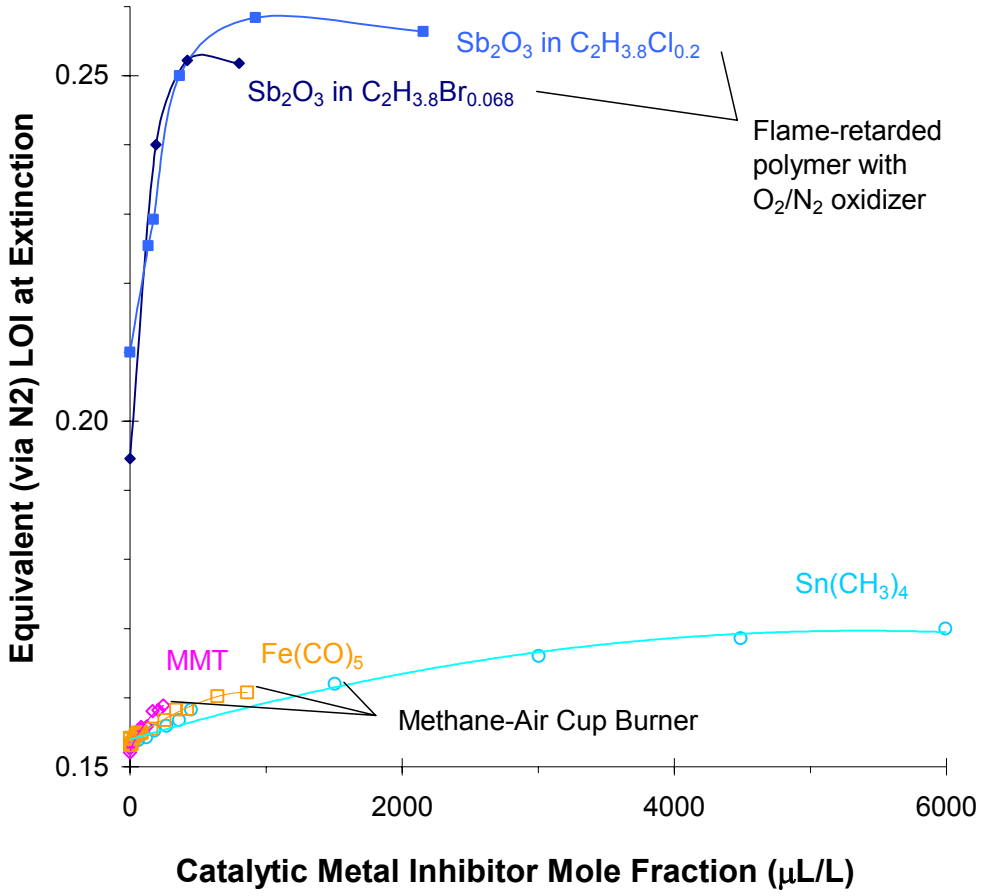

Figure 3-71. Equivalent N_2/O_2 Limiting Oxygen Index for Extinction of Polyethylene (PE)-halogen- Sb_2O_3 Blends[136] and Methane-air Cup Burner Flames with MMT, $Fe(CO)_5$, and $Sn(CH_3)_4$.

Although the influence of Fe, Mn, and Sn on the LOI when added to the air stream of methane-air cup burner flames was much weaker than that of Sb_2O_3 in halogenated polyethylene, a similar saturation behavior was observed. It would be of value to understand why saturation occurs in the antimony-halogen system, since it has not been explained in the literature.

3.3.7 Flame Inhibition and Loss-of-effectiveness Summary

The current state of understanding of the inhibition of flames by metal compounds is summarized in Table 3-12.

Table 3-12. Current State of Knowledge Relevant to Inhibition Potential of Metals, and Loss of Effectiveness due to Condensation. ▓: high, ▒ : medium, ░: low, -none.

	Inhibition Information						Condensation Information			
Element	Inhibition Potential		Gas phase Species Identified		Kinetic Mechanism State of Development	Demonstrated Loss-of-Effectiveness		Experimental Evidence of Particles		Experimental Vapor Pressure Data
Cr	▓		░		░	▓		▓		▒
Pb	▓		▒		▒			▓		▒
Fe	▓		▓		▒	▓		▓		▒
Mn	▓		▓		▒	▓		▒		▒
Ni	▒									
W	▒				▒					▒
Mo	▒				▒					▒
Cu	▒		▒							▒
Te	▒									
Tl	▒									
Bi	▒									
U	▒									
Zn	▒									
La	▒									
Th	▒									
Se	▒									
Sn	▒		▓		▒	▓		▒		▒
Ti	▒							▒		
Co	▒		▓							▒
Ge	▒									
Sb	▒		▒		▒	▒				
P	▓		▓		▓	▒		▒		

The inhibition potential is summarized in terms of the known inhibition behavior, the detection of metal-containing species in flames, and the state of development of a kinetic description of the inhibition. The knowledge of the potential for loss of effectiveness is characterized in terms of the demonstrated loss of effectiveness in flame systems, the presence of particles, and the availability of vapor pressure data for the condensed-phase metal-containing species. In the "Inhibition Potential" column, the *quality* of the information is rated as high, medium, low, and none, not the inhibition ability itself. Even for elements such as iron, which has been the most extensively studied, there were fragmented data on the gas phase species in flames, the gas phase kinetic mechanism had many estimated rate constants and the dominant inhibition cycles were assumed, and vapor pressure data for some of the important intermediates were not available. As the table illustrates, most of the information needed to accurately predict both the inhibition potential as well as the potential for loss-of-effectiveness were incomplete.

The last row in the column shows the state of information relevant to flame inhibition by phosphorus compounds. Due largely to NGP research, the state of understanding of the inhibition potential, the active species for flame inhibition, and the kinetics of the inhibition cycles are fairly well known. However, there is not nearly as complete an understanding of the potential for loss of effectiveness due to condensation of intermediate species formed in a flame. The only data which indicate, indirectly, a potential for condensation are the cup burner extinguishment data from researchers at New Mexico Engineering Research Institute,[235] in which the volume fraction for extinguishment is high relative to other flame systems. In a section below, the NGP work to understand the gas phase flame inhibition mechanism of phosphorus compounds is described in detail.

Approaches for Ascertaining the Potential of Metal-containing Compounds

Actually calculating the condensation potential of metal inhibitors in flames is quite challenging. To do this in a *quantitative* way requires knowledge of the species present in the flame, the inhibition mechanism with its associated rate constants, the vapor pressures of the metal species, the condensation, agglomeration, and re-evaporation rates for the particles, and the actual species present in the particles. This is far from being achieved even for iron, the most highly studied metal.

An alternative way to assess the potential for condensation of metal inhibitors in flame systems may be simple screening experiments with cup burners. In order to determine both the variation with concentration, as well as the potential benefit of using the metal compounds with inert agents, tests need to be conducted with the added metal compound and a secondary inert agent added together. In such a test, described above and in the literature[86,110,236] the amount of a diluent (e.g., CO_2, or N_2) added to the air stream necessary to cause blow-off of the cup burner flame is determined, both with and without the metal agent added at increasing concentration in the oxidizer stream. Since, to some extent, the flames resemble the low-strain conditions of fires, there is expected to be much higher correlation between the behavior in this system and in actual suppressed fires. By adding the metal compounds in the form of organometallic agents (rather than metal salts), the complicating effects of particle evaporation and decomposition are avoided.

A more empirical approach to evaluating metal-containing compounds would be to add them to a solid propellant-based extinguisher. There is inert gas in the effluent, as well as fragmented metal-containing species, so that by proper application to an appropriate fire, the utility of the metal additive could be

assessed at a larger scale. The challenge would be to find a configuration which has the proper sensitivity to the inert gas flow so that the effects of the additive could be quantified.

Approaches for Overcoming Condensation

There may exist approaches for overcoming the loss of effectiveness of metal compounds due to condensation of metal oxides. For example, halogens could be used to attack the metal oxide and provide metal-halogen species in the gas phase. As described by Hastie and co-workers,[140] the halogen in the antimony-halogen fire retardant system acts to release the antimony from the condensed phase through a series of halogenation steps involving successive oxychloride phases.[139] Bromine has been used in the past to etch off the lead oxide deposits on engine valves, and halogens are used to remove the oxide coating from the incandescent filament in quartz-halogen light bulbs. It is clear that halogens can release metals from solid oxides, and it may be possible to use this property to re-introduce the metals from the condensed oxide into the gas phase where they can again inhibit the flame. Finally, the use of carboxylic acids as extenders of antiknock agents[100] (through the formation of metal salts which can persist in the gas phase) leads naturally to the question of whether such an approach would work for metal-based fire suppressants as well.

3.3.8 Conclusions

Extensive analysis of published data and new data obtained from experiments and calculations has enabled new understanding of the flame-inhibiting mechanisms of metal-containing compounds and their potential as successors to halon 1301.

- There are several metal atoms whose compounds have shown very high effectiveness at reducing the rates of the chemical reactions that propagate flames. These are iron, manganese, chromium, antimony, lead, and tin. NGP research has also uncovered additional metals whose compounds are likely to be effective at low concentrations, but which had not been suggested in previous reviews of metal flame inhibition. These are tungsten, molybdenum, and cobalt.
- Most of the metals discussed above have the potential to lose their effectiveness at concentrations below those needed to extinguish flames, due to condensation of the active species. Were this condensation to occur in practical fires, compounds of these metals would likely not demonstrate fire suppression capabilities commensurate with their high flame velocity inhibition efficiency that was observed when added at low concentration to laboratory premixed flames. On the other hand, for the metals W, Mo, Co, and Cu, there is no direct evidence of the potential for loss of effectiveness, and the vapor pressures of the suggested flame-quenching species (for which data are available) are reasonably high. In general, prediction of the potential loss of effectiveness is beyond the current state of the art. Empirical testing in a cup burner or a solid propellant fire extinguisher (Chapter 9) is needed.

3.4 PHOSPHORUS

3.4.1 Introduction

Reasons for Interest

Phosphorus-containing compounds (PCCs) are known to be effective at reducing flammability, with some ambiguity as to whether their effectiveness in these applications can be attributed to gas phase reactions involving phosphorus. The use of various PCCs as fire retardant additives to plastics[237,238] has increased dramatically[239] in recent years, with the 1998 estimated U.S. market for organophosphorus fire retardants at 80 million lb.[240] In this application, the relative importance of gas phase chemistry and solid-phase effects such as char promotion has been debated, with recent work suggesting comparable importance for the two mechanisms, depending on the specific PCC chemistry.[238,241-244] Monoammonium phosphate has been used for many years as a dry chemical fire-extinguishing agent,[245] and has also been found to be very effective in preventing dust explosions.[246,247] Since it is applied as a powder, it is possible that physical properties may contribute substantially to its effectiveness. (See Chapter 4.) Finally, phosphorus is often applied in combination with halogens, making it difficult to assess the contribution of the phosphorus. For example, a mixture of trialkyl phosphates and CF_3Br for fire-fighting applications has been patented.[248] Phosphorus and halogens often appear in the same molecule as well: a recent evaluation of phosphorus compounds as halon replacements focused on fluorinated phosphazenes and phosphines, showing good flame suppression properties for these compounds in cup burner and streaming tests.[249,250]

The NGP was thus interested in developing further understanding of how PCCs affect flames, with the intent of using this knowledge to identify and screen candidate chemicals as successors to halon 1301. Such foreknowledge was necessary because of potential obstacles to their use as flame suppressants:

- Many, if not all, of these compounds, have low vapor pressures at ambient temperature.[251] (See Chapter 7.)
- Some PCCs have a significant heating value due to alkyl and alkoxy groups attached to the phosphorus atom.
- There are diverse bonding states of the phosphorus atom and a variety of ligand groups within the realm of PCCs. The import of these to flame suppression effectiveness was uncertain.
- PCCs range in their toxicity from non-toxic, essential food constituents and FDA approved additives to some of the most toxic compounds (chemical warfare agents) known.[249,252]

Chemical Effects

Well-characterized investigations of the flame inhibition properties of PCCs have been sparse, and in some cases ambiguous or contradictory.

- Korobeinichev et al. investigated the flame structure of low-pressure, premixed stoichiometric $H_2/O_2/Ar$ flames with the non-halogenated PCC additives trimethyl phosphate (TMP)[253] and dimethyl methylphosphonate (DMMP).[254] They compared oxygen profiles in flames with and without the PCC additive, interpreting more rapid oxygen consumption as flame promotion and less rapid oxygen consumption as flame inhibition. Both DMMP and TMP acted as inhibitors in

the low-temperature zone near the burner surface and as promoters in the higher-temperature region downstream.

- Fenimore and Jones[255] found that TMP addition produced *no* change in the oxygen consumption rate in a low-pressure, rich, H_2/O_2/Ar flame. In a more dilute, rich flame at atmospheric pressure, they observed a reduction in the oxygen consumption rate with increasing TMP loading.
- A more comprehensive study was conducted by Hastie et al.[256] with TMP, triphenylphosphine oxide and $POCl_3$ additives in premixed and non-premixed atmospheric-pressure propane, methane, and hydrogen flames. PCC effects were evaluated from measurements of H radical concentrations and burning velocities. Inhibition was observed for rich and lean flames with temperatures up to 2350 K. At higher temperatures, flame promotion was observed. Inhibition in premixed flames has been observed in terms of reduced laminar flame speeds for several halogenated PCC additives and one non-halogenated PCC additive, TMP.[34]

A more complete literature review of the influence of PCCs on flames can be found in References 79 and 257.

The emerging premise for flame suppression by PCCs was as follows. Phosphorus-containing radicals, such as HOPO and $HOPO_2$ (formed from PCCs during combustion[253,254]) catalyze the recombination of the important combustion radicals, H and OH, slowing the overall reaction rate and thus inhibiting the flame.[256] Since it is the phosphorus-containing radicals that participate in the recombination mechanism, and not the parent PCC, the form of the parent compound is relatively unimportant.[19] If supporting evidence were found for this hypothesis, then further studies of flame inhibition by PCCs could investigate alternative forms of the parent compounds that might be less toxic and more amenable for delivery to the flame.

Several mechanisms for catalytic cycles resulting in $H + OH \rightarrow H_2O$ and $H + H \rightarrow H_2$, have been suggested.[140,256,258-260] Partial validation of the radical recombination hypothesis was provided by flow reactor experiments showing that the addition of PH_3 (phosphine) to H_2-O_2 combustion product gases increased H+OH recombination rates following laser photolysis.[260] Flame experiments have also shown that the presence of PCCs affects radical levels. The addition of small quantities of the $POCl_3$, a halogenated PCC, produced lower OH levels in non-premixed methane and ethene flames than did other halogenated compounds not containing phosphorus.[47] The addition of TMP lowered H levels in premixed low-pressure $H_2/O_2/N_2$ flames under rich, dilute conditions, and raised H levels under stoichiometric, less dilute conditions.[256]

Transport Effects

A key factor affecting suppression is the amount of the additive reaching the non-premixed flame,[261] and several studies [36,45,51,103] of both fuel-side and oxidant-side doping of various fuel/inert vs. oxygen/inert flames have found dramatic changes in additive effectiveness with these changing conditions. When hydrocarbons are burned in air, the stoichiometric contour, where the flame is assumed to be, is situated on the oxidant side of the stagnation plane. Fuel-side additives must diffuse across the stagnation plane to reach the flame, while air-side additives are convected through the flame. The result is that fuel-side additive mole fractions at the flame are substantially reduced from their fuel-stream values, while oxidizer-side additive mole fractions are only slightly reduced from their oxidizer-stream values. The

extent of this additive loading reduction at the flame location varies with the stoichiometric mixture fraction (Z_{st}), defined as the mass fraction of material originating from the fuel stream at the location where the concentrations of reactants are in stoichiometric proportions. For hydrocarbon/air flames, Z_{st} is typically < 0.1. Considerably different values of Z_{st} can be achieved by varying the compositions of the fuel and oxidant streams, either via dilution or enrichment. For Z_{st}>0.5, the flame is on the fuel side of the stagnation plane, and additive loading reduction at the flame is more severe for oxidant-side additives than for fuel-side additives.

In several experimental studies of flame extinction by CF_3Br, the effect of additive loading reduction at the flame location has been quantified, assuming unity Lewis number. Results have been mixed. For methane/air opposed-jet diffusion flames, Trees et al.[261] found that CF_3Br was roughly twice as effective as an air-side additive than as a fuel-side additive, when the quantity of additive at the stoichiometric contour is compared for equal extinction strain rates. Work by Masri[45], on the other hand, found that oxidizer-side and fuel-side addition of CF_3Br had very similar effectiveness in extinguishing turbulent natural-gas/air piloted jet flames, when corrected for additive concentrations at the flame location. Niioka et al.[36] reported comparable effectiveness for fuel-side and oxidizer-side addition in extinguishing various ethene/nitrogen vs. oxygen/nitrogen opposed-jet diffusion flames, including one with Z_{st} >0.5. Close examination of the Niioka data showed that the fuel-side addition was generally less effective than oxidizer-side addition.

Temperature Effects

Extinction studies under a variety of flame conditions found a significant temperature dependence for DMMP effectiveness, with higher effectiveness being observed at lower stoichiometric adiabatic flame temperatures.[120] The existence of a temperature dependence for phosphorus-based flame inhibition was first suggested by Hastie and Bonnell in 1980,[256] but since then there has been little investigation of this behavior. There is one computational study on premixed flame speeds,[257] but aside from Reference 79, there has been no experimental work in which flame temperature has been systematically varied.

The influence of flame temperature on inhibition effectiveness is an important consideration in evaluating the feasibility of new phosphorus-based flame suppressants, and has direct bearing on how to maximize their effectiveness in practical applications. The indicated trend implied that a mixture of inert and phosphorus-based suppressants could interact synergistically as the inert component cooled the flame, thus increasing the efficiency of the chemically active component. This would lower the needed quantity of the chemically active component, thus reducing system weight and decreasing environmental concerns and possible health impacts. A similar temperature dependence has been demonstrated for CF_3Br, including the observation of synergistic interaction with the inert suppressants N_2, CO_2 and H_2O.[14,262] Increased effectiveness at lower flame temperatures has also been observed for the iron-based suppressant $Fe(CO)_5$. [103]

3.4.2 Inhibition of Non-premixed Flames by Phosphorus-containing Compounds

Fisher and co-workers[79] examined the inhibiting effects of two PCCs: dimethyl methylphosphonate (DMMP) [CAS #756-79-6, $P(=O)(CH_3)(OCH_3)_2$], and trimethyl phosphate (TMP) [CAS #512-56-1, $P(=O)(OCH_3)_3$], along with other additives for comparison, on a non-premixed methane-air diffusion flame. Their results have led to greater understanding of how a phosphorus-containing fire suppressant

would act to quench flames and developed some guidance for the selection of candidate PCCs for this purpose. Their research:

- Established a novel and sound protocol for conducting such experiments.
- Measured the effectiveness of the two PCCs relative to other, reference suppressants and to each other.
- Determined how the flame inhibition effectiveness of the two additives changed as a function of the agent loading and the adiabatic flame temperature, using the reduction in [OH] as a marker.

Experimental

Apparatus and Materials

The opposed-jet burner is shown schematically in Figure 3-72.

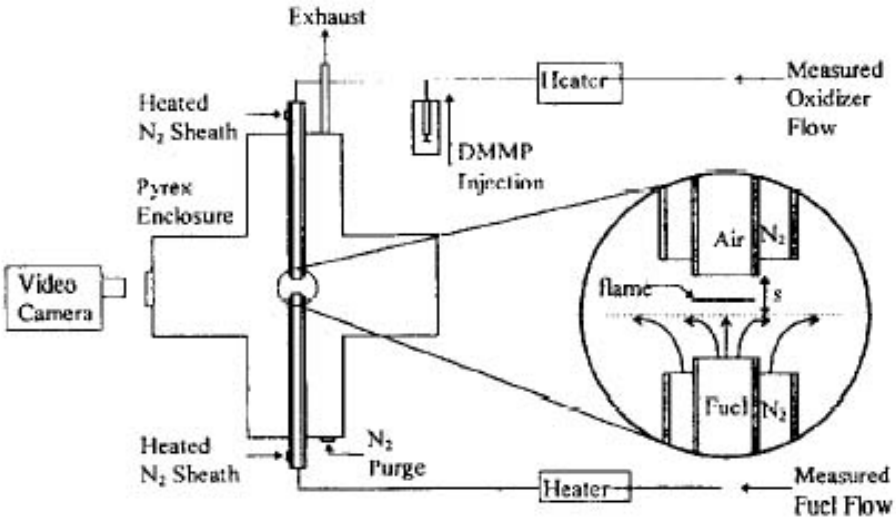

Figure 3-72. Schematic of Opposed-jet Burner.

The burner was constructed from straight, open glass tubes 30 cm long with an ID of 0.98 cm, and a separation distance of 0.95 cm between opposing nozzles. Annular sheath flows of nitrogen were provided through 2.22 cm ID glass tubes. The sheath tube exits were offset by approximately 1 cm, upstream of the reactant tube exits, to minimize the impact of the sheath flow on the development of the reactant flows. A flat flame was produced when the oxidant and fuel stream velocities were such that the flame was situated in the central portion of the space between the burner nozzles. The entire burner was isolated in a glass enclosure for control of exhaust gases. This enclosure was purged with nitrogen and maintained slightly below atmospheric pressure.

The burner was aligned vertically with the lower tube used as the fuel source and the upper tube as the oxidizer source. The results of a few experiments conducted with the reverse orientation to study the effect of buoyancy showed no significant change in extinction strain rate.

The extreme sensitivity of the extinction strain rate to the mass fraction of oxygen in the oxidizer stream necessitated very precise metering of reactant flows in order to achieve repeatable results. Precision mass

flow controllers, supplied by MKS Industries, were used to measure reactant flows. Even so, to minimize variability, measurements comparing doped and undoped flames were conducted by first evaluating the undoped extinction strain and then adding the dopant to one reactant stream without otherwise altering the composition of either stream.

Most of the extinction measurements were conducted using premixed oxygen and nitrogen (21 % ± 0.2% oxygen by volume) or Ultra Zero Grade air (21 % ± 2% oxygen by volume, total hydrocarbon content < 0.1 μL/L) as the oxidizer and methane (99 % pure) as the fuel. All gases were supplied by MG industries. For the extinction measurements with flame and stagnation plane coincident, oxygen (99.994 % pure) was mixed with nitrogen (99.998 % pure) in measured proportions to form the oxidizer stream, and the methane fuel was diluted with nitrogen (99.998 % pure).

The chemically active flame inhibitors, DMMP and TMP, were obtained from Aldrich Chemical Company (each 97 % pure). They were liquids at room temperature with low vapor pressures (less than 100 Pa at ambient temperature). In order to maintain sufficient concentrations of the PCC in the vapor phase, the reactant lines were heated to approximately 100 °C with electrical heating tapes. Wall temperatures on the outside surface of the heated lines were measured with adhesive thermocouples. The temperature of the reactant streams 10 cm upstream from the exit of the nozzles was maintained at 100 ºC ± 1 °C via active control of the sheath flow temperature. These final reactant temperatures were measured by sheathed thermocouples in direct contact with the gas flow. The liquid PCC dopant was added to the reactant streams via a syringe pump that provided a constant volume flow. The gas flow at the injection site was preheated to approximately 130 °C for a rapid vaporization of the incoming liquid dopant. The liquid density, syringe size, and motor speed fixed the mass flows of the dopants. Previous pyrolysis experiments with DMMP and TMP [263,264] have shown that thermal decomposition is negligible below 1000 K; thus the preheating of the reactant streams should have had no effect on their chemical composition.

Measurements

The enclosure had a glass window on one end, approximately 25 cm from the centerline of the flow. A video camera, located a few centimeters from this window, was used to measure flame position. Flame position was measured relative to the oxidizer nozzle exit plane using the separation gap between the nozzles for reference.

OH concentration measurements were made using pointwise LIF. Figure 3-73 shows a schematic of the experimental set up. Profile measurements were made by traversing the laser beam and collection optics simultaneously across the flame in 100 μm steps. The translation stages used had a resolution of 10 μm. Excitation of the $P_1(9)$ transition of the $A \leftarrow X$ (1,0) band near 286 nm was made using a frequency-doubled Quanta Ray PDL 2 pulsed dye laser, nominal linewidth of 0.2 cm^{-1}, with rhodamine 590 dye. This transition was selected due to the weak temperature dependence of the rotational ground state population in the temperature region of interest (< 10 % variation for 1400 K < T < 2500 K), which helps maintain a strong LIF signal across the entire OH profile. The dye laser was pumped with a 6 ns to 7 ns pulse at 532 nm provided by a frequency-doubled Spectra Physics DCR 2A Nd:YAG laser operating at 10 Hz.

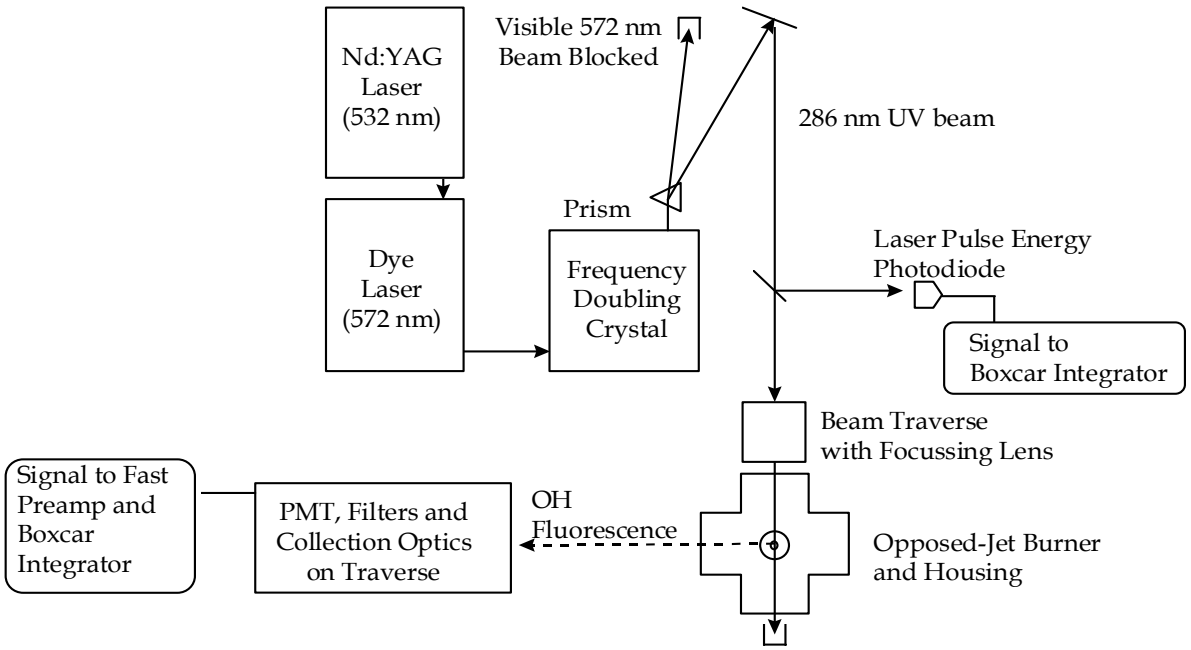

Figure 3-73. Schematic of LIF Apparatus.

Detection of OH fluorescence was performed at 90° to the laser beam axis using an RCA 8850 photomultiplier tube and color glass filters (Schott WG305 and UG11) which transmit light in the 305 nm to 371 nm range. The photomultiplier signal was amplified by a SRS240 Fast Preamplifier (Stanford Research Systems). The filter combination used blocks elastically scattered laser light (and near-elastic resonant fluorescence) while passing fluorescence emission from the (1,1) band (312-326 nm) and emission from the overlapping (0,0) band (306-320 nm) which can occur following collisionally driven Vibrational Energy Transfer (VET) from the $\nu' = 1$ to the $\nu' = 0$ states. At atmospheric pressure, VET rates can be significant[265,266] with more than a third of the total measured fluorescence originating from the (0,0) band when using excitation/detection schemes similar to this.[267] Fluorescence trapping of emission from the (1,1) band was negligible due to the small population of the electronic ground state with $\nu'' = 1$ over the temperature range under consideration. Some trapping occurred for fluorescence emission originating from the (0,0) band, but the effect was small due to the short path length through the flame (less than 1 cm) and is not expected to influence the measurements.[268,269] PAH fluorescence[268] was expected to be negligible because the moderately strained laminar flames under investigation were virtually soot-free. This was confirmed by measurements taken with the dye laser tuned off resonance. The combination of the focused (f = 30cm quartz focusing lens) UV laser beam and slits in the detection optics give a probe volume of less than 100 μm in diameter and 1.5 mm in length. The opposed-jet burner flame was locally planar near the centerline with the long axis of the probe volume aligned in the plane of the flame surface. Laser pulse energy was monitored using a UV-sensitive photodiode. Both the LIF and laser energy signals were integrated on a shot-by-shot basis using an SRS 250 Boxcar Integrator and Averager (Stanford Research Systems), and recorded on a personal computer using a GW Instruments data acquisition card. Operation within the linear LIF regime was ensured by checking the linearity of LIF signal strengths with pulse energy for all measured data points.[270]

To avoid errors associated with wavelength drift of the dye laser and the resulting changes in the spectral overlap of the laser and molecular absorption line shapes, the output wavelength of the dye laser was

scanned across the $P_1(9)$ transition at each measurement location using a stepper motor to adjust the grating in the dye laser cavity. 100 measurements of OH fluorescence and laser pulse energy were acquired at each half-step of the motor (corresponding to a wavelength change of approximately 0.0012 nm), and the half-step motor position with the maximum average ratio of fluorescence signal to laser pulse energy was taken to be the absorption line center for the transition. LIF data for that half-step motor position were used for the subsequent evaluation of OH concentration. The repeatability of this procedure was found to be within ± 5 % of the mean observed ratio. The average ratio of OH fluorescence signal to laser pulse energy was found by fitting the 100 measurements to a straight line using linear regression analysis. The statistical uncertainty (one standard deviation) in the fitted slopes was less than ± 3 %. Additional uncertainty in these slopes arose from statistical uncertainty in the measurement of the zero level in the presence of electrical noise from the Nd:YAG laser. Statistical scatter in the zero measurement (± one standard deviation) corresponded to an uncertainty of ± 3 % to 5 % of the peak slope for all data points in the profile. In addition to shot noise and electrical noise, the statistical uncertainty in the measurements reflected fluctuations in flame location. For these aerodynamically stabilized flames, perturbations in the reactant flow can cause small, momentary flame displacements. The 100 shot LIF averaging process largely compensated for these oscillations. The total uncertainty for each measured data point in a given profile due to random errors was found by summing the contribution of the uncertainties described above (assuming statistical independence) and is estimated to be less than ± 10 % of the peak value in the profile.

In order to quantify the fluorescence measurements, corrections for collisional quenching and the fraction of the OH population that is in the pumped rotational level must be made. However, the overall effect of these corrections on the profile shape is small, as is expected for our excitation/detection scheme in non-premixed atmospheric-pressure flames.[271-273] Equation 3-3 relates the fluorescence signal to the concentration of OH assuming low laser energy (i.e. negligible saturation of the excited transition):

$$F = CBIfN\Phi \tag{3-3}$$

Here F is the total fluorescence signal; C is a constant that incorporates geometric factors such as collection solid angle and probe volume as well as detector efficiencies and gain characteristics of the integrators, amplifiers etc.; B is the Einstein coefficient for stimulated absorption; I is the spectral overlap integral between the laser intensity and the molecular absorption line shape, temporally integrated over the duration of the laser pulse; N is the total OH population, and f is the fraction of the population that is present in the ground state rotational level excited by the laser; and Φ is the fluorescence quantum yield, which depends on the local quenching and VET rates.

Species and temperature profiles from the undoped-flame calculations were used to estimate the required corrections to the linear LIF data for both doped and undoped flames. The fraction of the ground state population in the pumped rotational level is determined using the local gas temperature given by the calculations and assuming rotational thermal equilibrium (Boltzmann distribution), as implemented in the spectral simulation software LIFBASE.[274]

The total fluorescence yield, Φ, was estimated using:[267]

$$\Phi = \frac{A_1 + \frac{V_{10}}{Q_0} A_0}{Q_1 + V_{10}} \tag{3-4}$$

where A_1 and A_0 are the spontaneous emission rates for the $\nu' = 1$ and $\nu' = 0$ vibrational levels, respectively. Equation 3-4 has been simplified by assuming equal transmission and detection efficiencies of the collection optics and PMT for both the (1,1) and (0,0) bands. Q_1 and Q_0 are the total quenching rates for the $\nu' = 1$ and $\nu' = 0$ levels, and V_{10} is the total VET rate from $\nu' = 1$ to $\nu' = 0$. The influence of VET rates on the fluorescence quantum yield is primarily due to the higher spontaneous emission rate of the $\nu' = 0$ state ($A_1/A_0 \approx 0.575$) [275]. The quenching and VET rates were evaluated using Equation 3-5.[267,276]

$$Q,V = \left(P/k_b T\right) \sum_i \chi_i \langle v \rangle_{i-OH} \sigma_i^{Q,V}(T) \tag{3-5}$$

where P is pressure; T is temperature; k_b is Boltzmann's constant; χ_i is the mole fraction of OH collision partner species i; $\langle v \rangle_{i\text{-}OH}$ is the mean relative collision velocity of species i and OH given by $\langle v \rangle_{i\text{-}OH} = (8k_bT/\pi\mu_{i\text{-}OH})^{1/2}$, where $\mu_{i\text{-}OH}$ is the reduced mass of species i and OH; and $\sigma_i^{Q,V}(T)$ is the value of the quenching or VET (superscript Q or V respectively) cross section for collisions with species i, averaged over all rotational levels in a given vibrational level, assuming rotational thermal equilibrium.

Substitution of Equation 3-5 into Equation 3-4 followed by some algebraic manipulation yielded:[267]

$$\Phi = \frac{A_0}{Q_0} \left[\frac{\left(\frac{A_1}{A_0}\right)\left(\frac{\langle \sigma^Q \rangle_0}{\langle \sigma^Q \rangle_1}\right) + \frac{\langle \sigma^V \rangle_{10}}{\langle \sigma^Q \rangle_0}}{1 + \frac{\langle \sigma^V \rangle_{10}}{\langle \sigma^Q \rangle_0}} \right] \tag{3-6}$$

where $\langle \sigma^Q \rangle_1$, $\langle \sigma^Q \rangle_0$ and $\langle \sigma^V \rangle_{10}$ represent the sum over all collision partners of the thermally averaged cross sections for quenching from $\nu' = 1$, quenching from $\nu' = 0$, and VET from $\nu' = 1$ to $\nu' = 0$, respectively. Quenching cross-section measurements for the $\nu' = 1$ and the $\nu' = 0$ state indicated similar values.[265,275] The ratio of averaged VET cross sections to the averaged quenching cross sections was assumed to be independent of position in the flame (e.g., $\langle \sigma^V \rangle_{10}/\langle \sigma^Q \rangle_0 \approx$ constant). As a result, the quantity in square brackets in Equation 3-6 became a constant, and the fluorescence yield was simply inversely proportional to the quenching rate for the $\nu' = 0$ state. The error in the assumption $\langle \sigma^V \rangle_{10}/\langle \sigma^Q \rangle_0 \approx$ constant was less than 5 %. Values for the quenching rate cross-sections used in this work were taken from temperature-dependent quenching cross-section data compiled by Tamura et al.[277] from the extensive measurements that have been made for the $\nu' = 0$ state of OH.

The calculated quenching rate varied by 15 % across the OH containing regions in N_2-O_2 flames. This variation was moderated by the presence of a large concentration of N_2 which has a relatively small

gradient in the flame zone. For flames where Ar (a highly inefficient quencher) fully replaced N_2, the variation was substantially higher at 30 %.

The same quenching environment was assumed for flames both with and without DMMP loading. The maximum phosphorus loading was only 715 μ/L. Since the mole fractions of phosphorus-containing species were small in this case, it was expected that they would not contribute significantly to quenching of OH. Changes in major species profiles due to the presence of DMMP were not expected to be large enough to significantly change the overall quenching environment. Changes in flame temperature due to the addition of these small loadings of DMMP were also found to be negligible (< 10 K).

After correcting for the fluorescence yield and the Boltzmann fraction of the pumped rotational level, the corrected LIF profile was directly proportional to OH concentration. An estimate of the scaling constant relating the corrected LIF measurements to absolute OH concentrations was made by matching the peak of the measured profile from the undoped flame to the peak OH concentration predicted by the flame calculations. This matching did not affect observations of PCC effects on OH, which were all presented normalized to the undoped flame measurements. For profiles measured in flames doped with phosphorus-containing additives, the scaling constant was determined from undoped profiles taken on the same day with the same instrument settings. Because the same constant was used for both doped and undoped flames, quantitative comparisons could be made between the two cases. Determination of the magnitude of the scaling constant was performed by minimizing the mean-square-error between calculated and measured profiles (via a least squares technique). For this minimization, only data points above 50 % of the measured peak value were considered. Minimization of error was performed via adjustment of the scaling constant and a position offset (i.e., the offset between the measured flame center, as indicated by the translation stage micrometers, and the computational flame center). Determination of this scaling constant calibrated the constant C from Equation 3-3, assumed to be constant for a given set of instrument settings. This scaling procedure affected only the magnitude and position of the observed fluorescence profile and not the shape or width.

Determination of Extinction Strain Rates

The flame strength can be characterized by the strain rate at extinction,[278,279] and here, the effectiveness of additives as flame inhibitors was determined by measuring the dependence of extinction strain rate on additive loading. The inverse of the strain rate is one of several related measures of the characteristic diffusion time of the flame.[280] The strain rate at extinction was approximated using the following expression involving global flame parameters:[76]

$$a_q = \frac{2V_O}{L}\left(1+\frac{V_F\sqrt{\rho_F}}{V_O\sqrt{\rho_O}}\right) \tag{3-7}$$

where L refers to the separation distance between the nozzles, V is the average stream velocity at extinction, ρ is the stream density and the subscripts O and F refer to oxygen and fuel respectively. This expression is equal to the velocity gradient on the oxidant side of the stagnation plane under certain restrictive conditions: reactions, diffusion, and viscous effects must be confined to a narrow region around the stagnation plane, and plug flow boundary conditions must be imposed at the nozzles. Under less restrictive conditions, this expression has been determined experimentally to be nearly proportional to the local oxidant-side velocity gradient: Recent measurements performed in an open-tube burner with

geometry very similar to our own have found a nearly proportional relationship between the a_q of Equation 3-7 and the maximum local velocity gradient on the oxidant side of the flame, as measured by laser-Doppler velocimetry.[281] The same proportionality was found to hold for methane/air and propane/air flames, with and without flame-inhibiting additives in the air stream. Thus, Equation 3-7 can be used to determine relative changes in extinction strain rates obtained on the same apparatus. In particular, the ratio of doped to undoped a_q measured using Equation 3-7 should be equal to the same ratio of local oxidant-side velocity gradients. The validity of this approach was borne out by the good agreement between the current data and those of other researchers for inert additives.

In determining extinction conditions for use in calculating a_q, Fisher and co-workers developed a novel method for approaching extinction, motivated by a need to minimize transient effects of dopant loading. Commonly, extinction studies with opposed-jet burners adjusted the strain rate by varying both the oxidizer and fuel streams simultaneously so that the flame position remained constant,[63] or so that a momentum balance between the two streams was maintained.[80] This required varying the mass flows of both reactant streams, and resulted in changing concentrations of the inhibiting agent when the agent was delivered via a constant-mass-flow syringe pump. The resulting transients in the adsorption/desorption of the agent on walls made it difficult to predict the concentration of agent at the exit plane of the doped reactant stream at extinction.

The new method circumvented the difficulties associated with dopant loading transients. The concentration of dopant in the relevant reactant stream (fuel or oxidizer) was fixed by maintaining constant flows of all the constituents of the doped reactant stream. After waiting a sufficient time for equilibrium conditions to be established, extinction was approached by varying only the flow of the undoped stream. One consequence of using this method is that the position of both stagnation plane and flame varied during the extinction experiment. This was found to have only a minor influence on the measured extinction strain except when the flame or stagnation plane was very close to one of the nozzles.

To validate this method, experiments were performed over a large range of methane and air flows, achieving extinction with the flame in a variety of positions. Figure 3-74 shows the resulting global extinction strain rates (a_q) as a function of the observed flame position.

The extinction strain of the undoped flame varied only ± 2 % (from a mean value of 359 s^{-1}) for flame positions between 0 mm and 7mm. This region of consistent global extinction strain rates was denoted as the *acceptable* region. For experiments in which extinction occurred with the flame outside the acceptable region, large deviations in a_q occur.

Also shown in Figure 3-74 are sets of data from experiments conducted with a 300 μL/L doping of DMMP and 50,000 μL/L doping of N_2, both in the oxidizer stream. (The limited number of data points in the DMMP series was a result of the coarsely quantized mass flows of dopant available from the syringe pump.) Because of the inhibitory effect of the DMMP or N_2 additive, these data sets had markedly lower mean global extinction strain rates than the data for the undoped flames. However, both data sets showed the same systematic trends with flame position, and both had only small variations in extinction strain over the acceptable region.

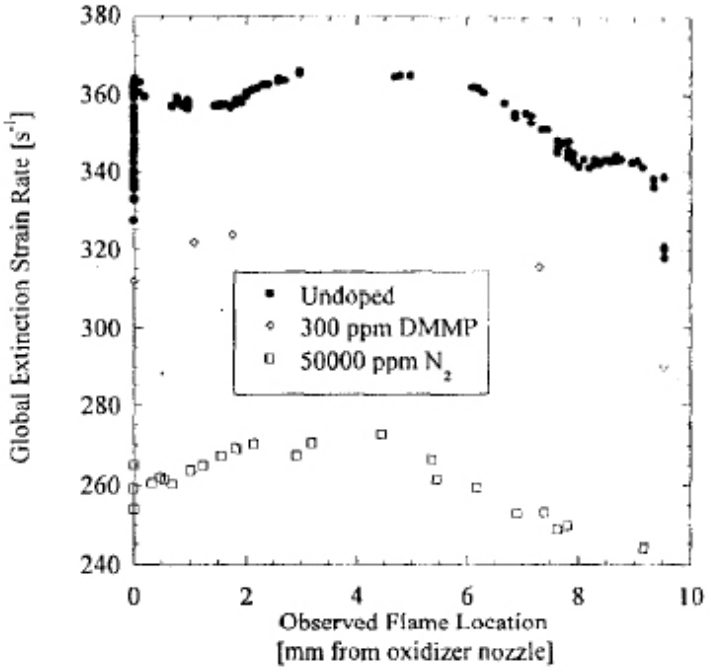

Figure 3-74. Variation of Global Extinction Strain, a_q, with Observed Flame Position at Extinction.

The existence of the same acceptable region for a range of flame extinction strain rates validated this method for approaching extinction. Within this region, the results should be within experimental uncertainty of those obtained using more conventional methods that maintain a nearly constant flame position. The nearly constant extinction strain rates over the central region were consistent with the previous computational findings of Nishioka et al.[282]

The asymmetrical dependence of extinction strain rate on flame position was due to the offsetting of the flame to the oxidant side of the stagnation plane, which was conveniently characterized using the stoichiometric mixture fraction, Z_{st}. The stoichiometric mixture fraction, Z_{st}, is the fraction of the material present at the stoichiometric contour that originated in the fuel stream. Z_{st} was evaluated from reactant compositions in the nozzles and the stoichiometry of the overall combustion reaction, using Equation 3-8:

$$Z_{st} = \frac{Y_{O,-\infty}}{\left(\left(\frac{MW_O \nu_O}{MW_F \nu_F}\right) Y_{F,+\infty} + Y_{O,-\infty}\right)} \tag{3-8}$$

where Y is mass fraction, MW is molecular weight, ν is the stoichiometric coefficient for complete combustion, the subscripts O and F refer to oxygen and fuel, respectively, and the subscripts ±∞ refer to conditions at the fuel and oxidizer nozzles. The undiluted flame used for the first series of experiments in Figure 3-74 had $Z_{st} = 0.054$. Other researchers have found that, near extinction, this corresponds to a displacement of the flame of approximately 1 mm to the oxidizer side of the stagnation plane.[67,283]

The importance of this displacement was investigated by measurements in which the flame and the stagnation plane were coincident. By varying the dilution of the fuel and oxidizer streams it is possible to move the location of the stoichiometric contour (the presumed flame location), relative to the stagnation

plane. For reactants of equal diffusivities, setting $Z_{st} = 0.50$ placed the flame at the stagnation plane. Since Z_{st} depended on two independent variables, Y_F and Y_O, fixing Z_{st} left one degree of freedom on reactant concentrations. Unique conditions for the $Z_{st} = 0.50$ tests were established by choosing the mass fraction of oxygen to give approximately the same undoped global extinction strain rate as was obtained for the undiluted flame. Results from these conditions, $Z_{st} = 0.50$ with $Y_O = 0.387$ and $Y_F = 0.097$, are shown in Figure 3-75. During these experiments, in which the oxidizer stream was mixed from separate O_2 and N_2 bottles, it was found that the global extinction strain rate was very sensitive to the concentration of O_2, consistent with experimental results from Puri and Seshadri for diluted methane-air flames.[80] This sensitivity contributed to the greater scatter in the $Z_{st} = 0.50$ tests than in the $Z_{st} = 0.054$ tests, which were conducted with premixed air. Nonetheless, the global extinction strain rate varied less than 3 % of the mean value of 336 s^{-1} for flame locations between 0 and 9mm. Within experimental scatter, results with $Z_{st} = 0.5$ were symmetrical about the center of the region between the two burners.

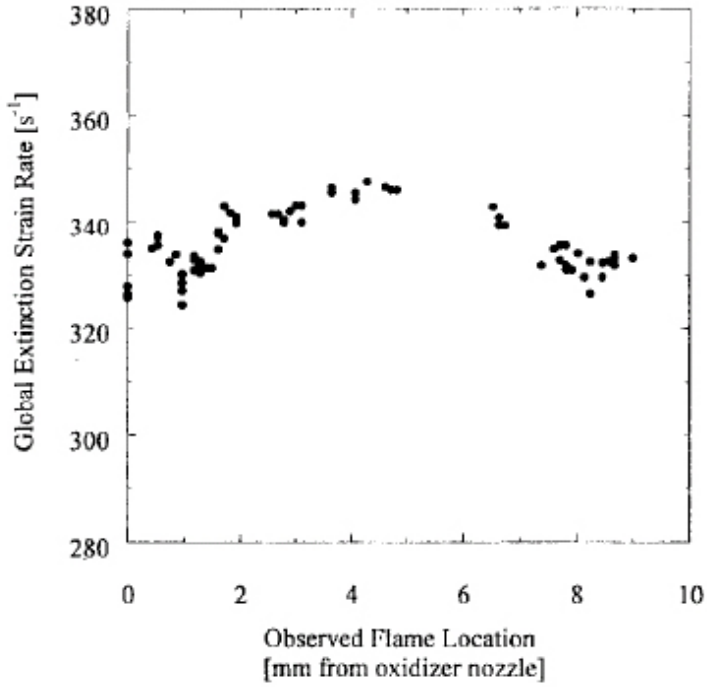

Figure 3-75. Variation of Global Extinction Strain, a_q, with Observed Flame Position at Extinction for Non-premixed CH_4/N_2-O_2/N_2 Flames, with $Z_{st} = 0.50$.

Although the acceptable region of Figure 3-74 is defined in terms of the observed flame position, in practice it is not necessary to determine the experimental observation of flame location at extinction for all measurements. Rather, a parameter S is introduced which can be calculated from the reactant stream properties at the nozzles. S approximates the distance from the oxidizer nozzle to the stagnation plane and is given by the expression in Equation 3-9, again derived by Seshadri and Williams for plug flow boundary conditions:[76]

$$S = L \Big/ \left(1 + \frac{V_F \sqrt{\rho_F}}{V_O \sqrt{\rho_O}} \right). \tag{3-9}$$

Figure 3-76 shows a plot of observed flame location for both $Z_{st} = 0.50$ and $Z_{st} = 0.054$ against the parameter S. The observed flame location did not vary linearly with the predicted location of the stagnation plane, but instead followed a sigmoidal curve, being much more sensitive to flow variations

when it was near the middle of the separation gap. The data presented in Figure 3-76 show flame positions for only high strain cases (275 s^{-1} to 360 s^{-1}). It was found that, in general, the steepness of the sigmoidal curve increased with increasing strain rates. For purposes of conducting experiments with the new method, it sufficed to observe that the flame location, for each condition, was a well-correlated one-to-one function of this parameter S. Therefore, one can map the experimentally determined acceptable region in terms of S, and direct observation of flame position became unnecessary. For Z_{st} = 0.0544, this region is 3.50 mm < S < 5.25 mm. All extinction results reported below were for flames inside this acceptable region.

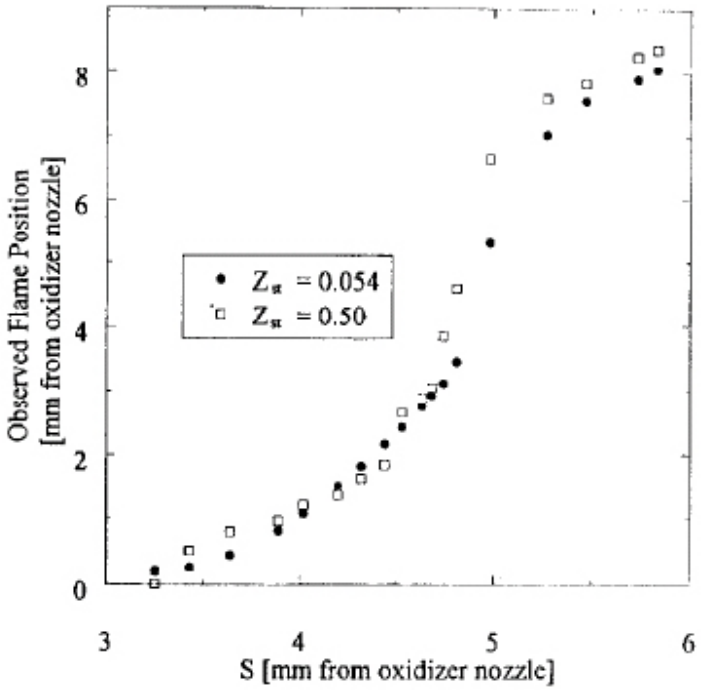

Figure 3-76. Observed Flame Positions as a Function of Predicted Distance to the Stagnation Plane for Non-premixed Flames of CH_4-air (Z_{st} = 0.054), and CH_4/N_2-O_2/N_2 Flames, (Z_{st} = 0.50) Near Extinction.

Flame Extinction Results

Initial tests were conducted with undoped reactant streams at ambient temperature to compare results with those of other researchers. For undiluted methane burning in air, the measured global extinction strain rate was 296 s^{-1}. When the reactant streams were preheated to 100 °C, the measured value for a_q increased to 360 s^{-1}. Extinction measurements on undoped flames using the same oxidizer source were consistent to within ± 5 s^{-1}. Variation in a_q up to 80 s^{-1} was observed with different bottles of high purity compressed air, and was attributed to slightly different mass fractions of oxygen. All the results for doped flames were normalized to undoped experiments using the same oxidizer source.

The unheated global extinction strain value was comparable to the value found by Puri and Seshadri[80] of 280 s^{-1} and to the value of 255 s^{-1} computed from flows at extinction reported by Papas et al.[63] using Equation 3-7. All three numbers fell within the range of variation attributed to differences in composition of high purity air batches. This agreement was surprisingly good in light of the significantly different boundary conditions and aspect ratio of the burner used by Puri and Seshadri. Agreement with literature values of local extinction strain rate was not as good; measurements and calculations ranged from 340 s^{-1} to 400 s^{-1} [63,67,78] and from 354 s^{-1} to 544 s^{-1} [67], respectively. We attribute the discrepancy of our measurements with these values to our use of the global strain expression under conditions where it is not

strictly valid. Comparable differences between global and local strain rates have been observed by other researchers.[63]

Further validation experiments were conducted with nitrogen as a chemically inert flame-inhibiting additive. Normalized extinction strain rates for nitrogen addition to the air side of a methane/air flame are shown in Figure 3-77.

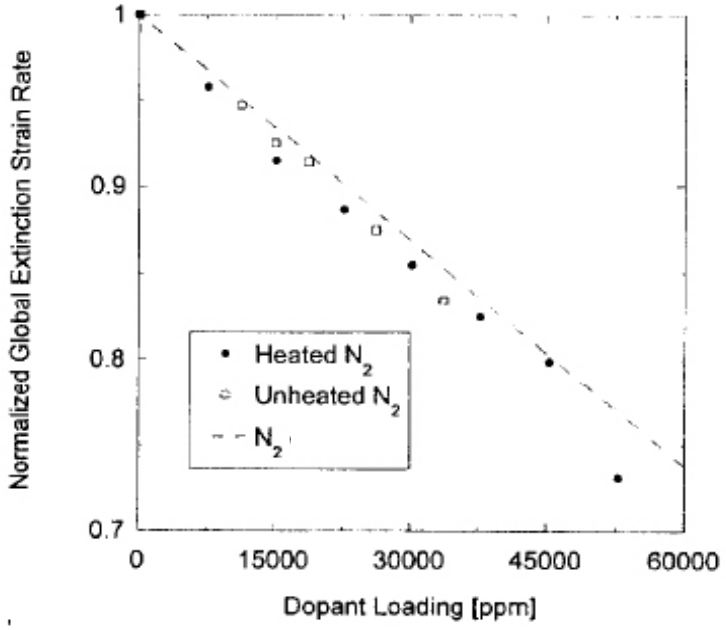

Figure 3-77. Inhibition of Non-premixed Methane-air Flames, Based on Reduction in the Global Extinction Strain Rate by Oxidizer-side Addition of Nitrogen, with and without Preheated Reactants.

Each data point represents the average of at least three measurements, and is normalized by the extinction strain rate for a pure methane/air flame. The extinction strain rate dropped linearly with increasing loading of this additive. The results were independent of whether or not the reactants are preheated to 100 °C, consistent with the findings of Trees et al.[284] The nitrogen dilution data can be compared to room-temperature data of Puri and Seshadri,[80] also shown in Figure 3-77. Agreement is good, with least-mean-square slopes agreeing within 7 %. However, it should be noted that the diluted flame experiments of Puri and Seshadri were conducted at a fixed value of Z_{st} = 0.0544. This required some nitrogen addition to the fuel flow. Here, nitrogen was added only to the oxidizer stream. Previous experiments by Fisher and co-workers[285] indicated that correcting for the effect of this fuel-side addition would lower the present measured extinction strain rates by about 3 %, resulting in an overall discrepancy of 10 % with the Puri and Seshadri data.

Figure 3-78 shows the results for PCC addition to the air stream of methane-air flames. Again, points represent averages of at least three measurements, and were normalized by the undoped extinction strain. For DMMP addition, the global extinction strain rate decreases linearly with additive mole fraction. Experiments indicated that at a volume fraction of 1500 μL/L, a_q was reduced by 35 % of the undoped value. Detectable inhibition (≈3 % reduction in a_q) was found at loadings as low as 100 μL/L. For volume fractions below 100 μL/L, preheating of reactants was not necessary to prevent condensation of DMMP. This allowed for ambient temperature testing of low DMMP loadings which demonstrated inhibition effectiveness similar to that found in the preheated experiments. Figure 3-78 also shows the results from TMP-doped flames. TMP exhibited similar inhibitory properties to DMMP over the common range of loadings. This was consistent with the hypothesis[19] that it is phosphorus radicals

formed in the flame that are important and not the parent compound. Consistent flame inhibition was observed, with no sign of the flame promotion noted by others.[63,254] A possible explanation is that the relatively low peak temperatures typical of highly strained methane vs. air flames[67] were below the 2230 K transition between inhibition and promotion observed by Hastie and Bonnell.[256]

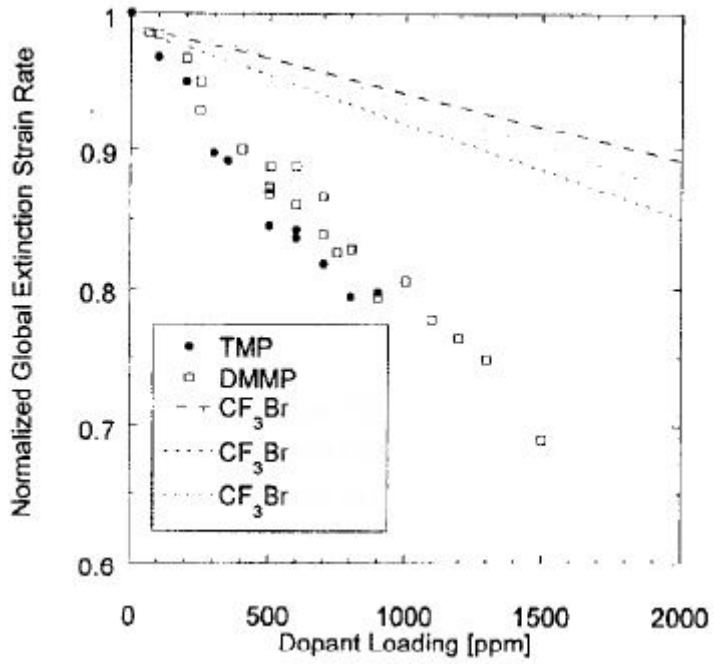

Figure 3-78. Inhibition of Non-premixed Methane-air flames, Based on Reduction in the Global Extinction Strain Rate, by Oxidizer-side Addition of trimethyl phosphate (TMP), and dimethyl methylphosphonate (DMMP). Also shown are reported literature values for inhibition by CF_3Br.

Also shown in Figure 3-78 are published flame inhibition data for CF_3Br.[16,45,261] The flame inhibition efficiencies of DMMP and TMP are two to four times better, on a molar or mass basis, than those reported for CF_3Br. Comparisons of these PCCs with $Fe(CO)_5$, one of the most effective flame inhibitors known, show that $Fe(CO)_5$ is a stronger inhibitor at low loadings: inhibition at 200 μL/L[103] is comparable to the PCC's effectiveness at 1500 μL/L. However, $Fe(CO)_5$'s effect as an inhibitor plateaus for mole fractions between 200 μL/L and 500 μL/L, the highest gas phase concentration achievable with ambient temperature reactants.[103] The PCCs' inhibition performance can also be compared to the N_2 data presented in Figure 3-77. DMMP and TMP are approximately 40 times more effective than N_2 on a molar basis, ≈10 times as effective on a mass basis. It is important to note that the range of extinction strain rates achieved in these PCC experiments represents only the upper portion of the range of local strain rates encountered in a realistic, turbulent, fire.[21] Extending the experimental range to much lower strains would require a different method of introducing the PCC.

Fisher and co-workers also performed an experiment to determine whether the hydrocarbon content of the PCCs contributed significantly to the inhibition effectiveness. In certain chemical systems, such as carbon monoxide-air combustion, trace amounts of hydrocarbons had been observed to inhibit combustion.[286,287] It is thought that the inhibition occurred because the hydrocarbon acted as a radical sink. Hastie et al.[140,256] attributed 8 % of TMP's inhibition effectiveness in hydrogen flames to this effect. In order to determine whether radical scavenging by the methyl groups, found in the PCCs under investigation, may be responsible in part for the PCCs' inhibition observed here, tests were conducted with isooctane as the dopant. Isooctane has a similar structure to the PCCs, but lacks the central phosphorus atom. It is expected that any contribution from methyl groups to flame inhibition by the

PCCs would be observed during the isooctane tests. However, these tests showed a 4 % increase in the global extinction strain at a loading of 400 μL/L, indicating that the effect of the hydrocarbon was to promote the flame, not to inhibit it. This result provided further support for the hypothesis that the phosphorus atom was crucial to the flame inhibition effects measured in this study.

Effects of Stoichiometric Mixture Fraction

Experiments

Fisher and co-workers[120] investigated how the effectiveness of the two additives changed as a function of the adiabatic flame temperature, T_{ad}, and the stoichiometric mixture fraction, Z_{st}. DMMP is mainly chemically active; argon is inert.

Suppressant effectiveness was defined as the change in extinction strain rate when the additive was introduced, normalized by the undoped extinction strain rate, a_{qo}. [79,288]For low loadings, the effectiveness should vary linearly with dopant loading. T_{ad} and Z_{st} were changed by varying the dilution level of the fuel and oxidizer streams.

For tests of chemically suppressed flames, a constant loading of 500 μL/L of DMMP was added to one of the reactant streams. Argon additive testing was conducted with a loading of 25000 μL/L. The disparity between DMMP and argon concentrations was required because of the stronger suppression effect of DMMP. Experiments were performed for stoichiometric mixture fractions ranging from 0.055 to 0.7. Adiabatic flame temperatures for the various values of Z_{st} and overall dilution of the flames were evaluated for the undoped case using the STANJAN code.[9]

To accurately estimate the quantity of dopant at the flame surface, numerical calculations using the OPPDIF code[211] were made with plug flow velocity boundary conditions, multicomponent diffusion but no thermal diffusion, and detailed chemistry (excluding phosphorus compounds), using the GRI mechanism[289] with nitrogen chemistry omitted. The mole fraction of dopant was evaluated at the maximum temperature in the reaction zone, taken to represent the flame location. The estimated diffusivity of DMMP was based on the interaction potentials of similar molecular weight compounds. The numerical calculations were required because this diffusivity was significantly different from the rest of the reactant stream components, making the effect of preferential diffusion important.[261]

In these transport calculations for estimating relevant dopant loadings, the chemically reactive compound DMMP was treated as inert because complete chemical kinetic and transport data were not available for it or its combustion products. This treatment gave a reasonable estimate of the quantity of phosphorus present in all chemical forms.

Two types of experiments were performed. The first varied Z_{st} from 0.055 to 0.7. At each Z_{st}, a_{qo} was matched to 350 s^{-1} ± 10 s^{-1}, by trial-and-error variation of the dilution of both reactants with nitrogen. This process entailed changing the overall dilution, a parameter which is independent of Z_{st}. Due to the high sensitivity of a_{qo} to reactant composition, this narrow range in allowed a_{qo} resulted in an even narrower range of allowed reactant compositions at a given Z_{st}. Experimentally determining those allowed compositions accurately became difficult at high Z_{st}, where the low methane flows resulted in a higher percentage uncertainty in their values.

As Z_{st} was increased with fixed a_{qo}, T_{ad} declined steadily, as seen in Figure 3-79. Calculations by Grudno et al.[280] for a fixed T_{ad}, were qualitatively consistent with this result, finding that a_{qo} increased monotonically as Z_{st} was increased from 0.055 to 0.4. This variation in a_{qo} and T_{ad} with Z_{st} was attributed to the changing relationship between the strain rate and the appropriate time scale for diffusion of reactants. While the strain rate is always considered to be a good measure of that time scale, the relationship between the two depends on Z_{st}.[168,280,290,291] The error bars in Figure 3-79 represent standard deviations of the measurements. The large error at high Z_{st} represent the methane flow uncertainty described above.

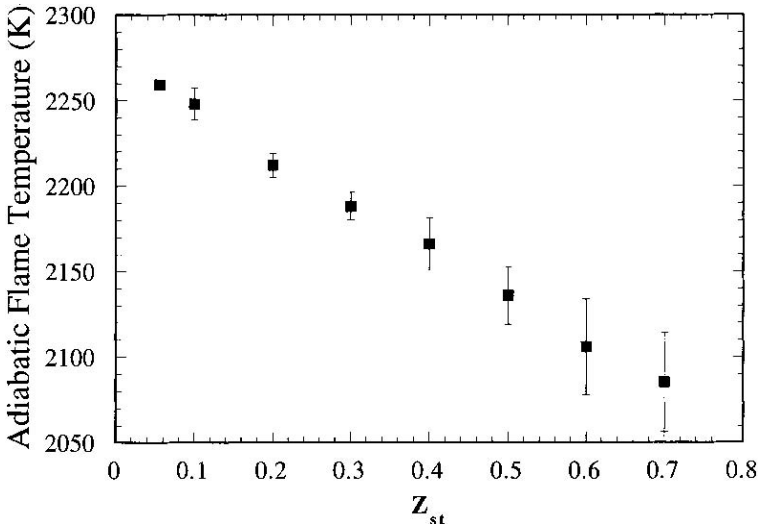

Figure 3-79. Adiabatic Flame Temperature vs. Stoichiometric Mixture Fraction for a Methane-nitrogen-oxygen-nitrogen Flame with the Extinction Strain Rate Held Constant at 350 ±10 s^{-1}.

It was expected that the inert dopant's effectiveness would depend solely on the quantity of dopant present at the flame. Previous experiments had demonstrated that, for a range of loadings greater than that considered here, the effectiveness of the inert suppressant nitrogen increased linearly with dopant loading, at fixed Z_{st}.[79,80,280] Because flame temperature is reduced by the addition of dopant, this implies temperature invariance of suppression effectiveness over that loading range.

The second type of test varied only the adiabatic flame temperature at a fixed Z_{st}. This was accomplished in two ways: changing the overall dilution of the flame at a fixed Z_{st}, and manipulating the temperature of the reactant streams. These experiments were intended to isolate the temperature dependence of the suppression from other effects.

Results of Tests with Argon

Results from the first series of tests are shown in Figure 3-80. The effectiveness of the argon, both oxidizer and fuel side addition, is illustrated. Each data point represents the average of four extinction measurements. The error bars on the figures represent the standard deviation of the observed values, which in this case is larger than the systematic error due to the method of approaching extinction. As expected, effectiveness with oxidant-side doping decreases as the flame moves towards the fuel side (increasing Z_{st}). The converse is true with fuel-side doping. Argon has a diffusivity similar to that of the reactants; thus, the quantity present at the stoichiometric contour, which determines its effectiveness, will vary linearly with Z_{st}.

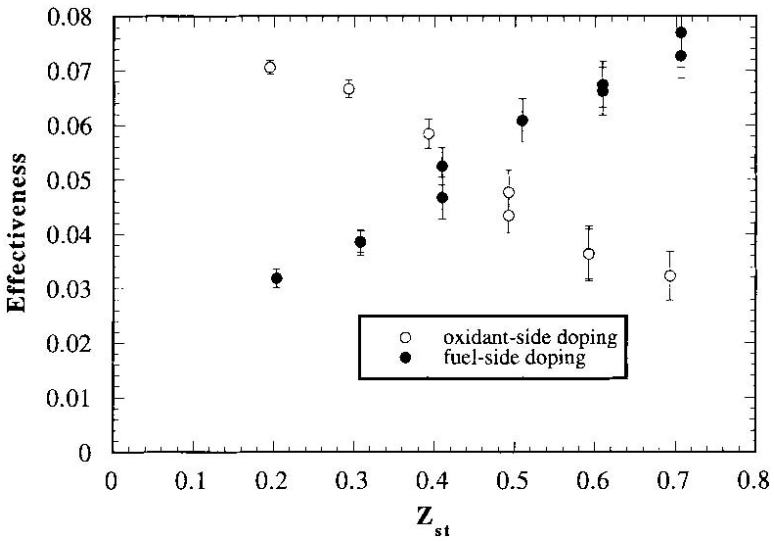

Figure 3-80. Flame Suppression Effectiveness of 25,000 µL/L Argon as an Oxidant-side or Fuel-side Additive vs. Stoichiometric Mixture Fraction.

Figure 3-81 depicts the argon effectiveness results. The uncertainty in the calculated mole fraction of dopant at the flame was dominated by the uncertainty in the experimental flow of the dopant, which was ± 10 %, as determined by the manufacturer's stated repeatability of the mass flow controller. The smooth trends in the data indicated a significantly better repeatability. The effectiveness curves show no trend with Z_{st}, indicating that the concomitant changes in T_{ad} and flame structure, collectively, had no significant influence on the argon effectiveness. Other tests, described below, further demonstrated that the argon effectiveness was independent of T_{ad}. In addition, Figure 3-81 shows no significant difference, in view of the experimental uncertainty, between the effectiveness of argon with oxidizer- or fuel-side addition, except perhaps at the lowest value of Z_{st}.

To further clarify the influence of temperature on this system, a series of tests were performed for a fixed Z_{st} = 0.055. T_{ad} was manipulated by varying the reactant stream temperature from 22 °C to 112 °C (±1 °C). This resulted in a range of T_{ad} from 2237 K to 2283 K. There was a significant influence on the overall flame strength, as seen in the variation of a_{qo} from 254 s^{-1} to 375 s^{-1}. However, the effectiveness for argon at different temperatures varied less than 4 % and showed no trend with T_{ad}. These results confirmed that argon's effectiveness displayed no dependence on temperature, as well as none on Z_{st}.

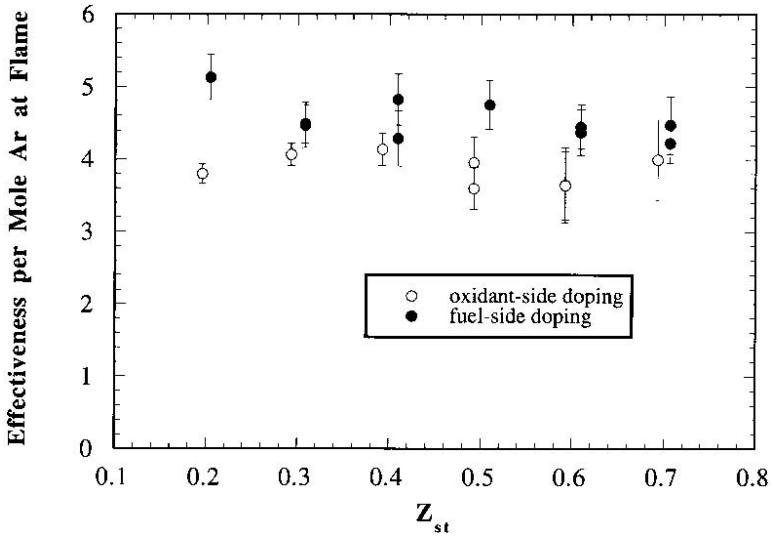

Figure 3-81. Normalized Flame Suppression Effectiveness of Argon-doped Flames vs. Stoichiometric Mixture Fraction at Fixed a_{qo}.

Results of Tests with DMMP

Figure 3-82 shows the results of extinction measurements performed with DMMP for Z_{st} between 0.055 and 0.7. The observed effectiveness variation with Z_{st} was somewhat more complicated than for the inert tests, although it still followed the same general trend. Each data point in Figure 3-82 represents the average of 8 extinction measurements, with error bars representing the standard deviation of the measured values. Differences between individual data points at a given Z_{st} showed that tests repeated at identical conditions yielded slightly different results. This variation was limited largely by the repeatability of the dopant injection system. The dopant effectiveness may also have been influenced by small changes in flame temperature resulting from lack of repeatability of the reactant stream compositions. The resulting overall experimental scatter was significantly higher than in the inert tests. The systematic uncertainty due to the method of approaching extinction became significant for the oxidizer-side addition tests due to the high observed effectiveness. The result was an estimated overprediction between 3 % and 15 % of DMMP effectiveness for this range of conditions due to this systematic uncertainty. The effect was small for the fuel-side addition data.

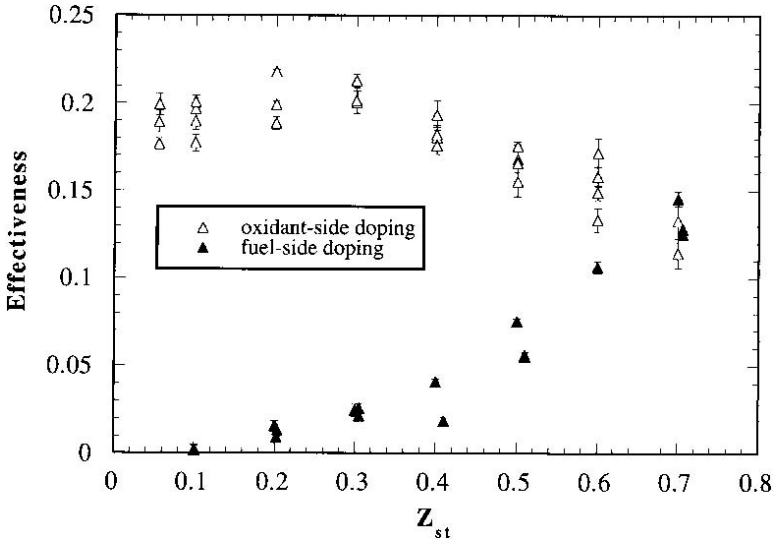

Figure 3-82. Flame Suppression Effectiveness of 500 µL/L DMMP as an Oxidant-side or Fuel-side Additive vs. Stoichiometric Mixture Fraction.

The normalized effectiveness results for DMMP, seen in Figure 3-83, have some notable features. Firstly, for a given mole fraction, the DMMP effectiveness is roughly 100 times that of argon, indicating strong chemical suppression by DMMP. Secondly, the curves for oxidizer- and fuel-side addition are offset significantly with respect to one another. This increased oxidizer-side effectiveness has also been observed for the chemically active agent, CF_3Br.[261] The oxidizer-side curve in Figure 3-83 displays an effectiveness roughly triple that of the fuel-side curve. The slight systematic overprediction of the oxidizer-side addition effectiveness, described above, would reduce the magnitude of this disparity, but would not reconcile the difference in these curves. It is possible that since the chemically active suppressant operated by interfering with the radical chemistry rather than as a heat sink within the flame, that the maximum flame temperature contour may not have been the most relevant location for evaluating the mole fraction of dopant. Rather, the appropriate normalization depended on the quantities present in the regions of the flame where the most important radical chemistry occurred. Since key radical reaction rates peaked on the oxidizer side of the flame, a more appropriate normalization might have involved mole fractions at some location to the oxidizer side of the maximum temperature contour. Such an assessment was performed using mole fractions at the point of the maximum reaction rate for the chain branching reaction $O_2 + H \rightarrow OH + O$. Because the concentration gradients of oxidizer- and fuel-side

dopants had opposite directions, this shift in location toward the oxidizer side brought the two curves closer together. However, oxidant-side doping remained more effective.

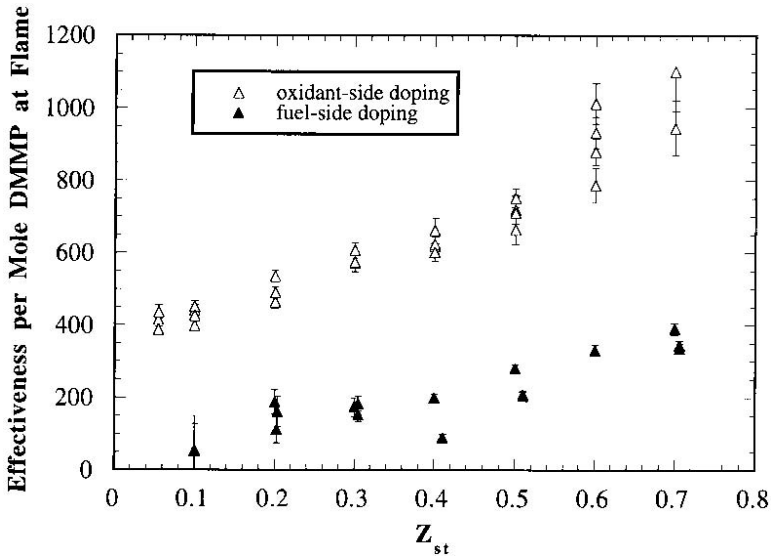

Figure 3-83. Normalized Flame Suppression Effectiveness of DMMP-doped Flames vs. Stoichiometric Mixture Fraction at Fixed a_{qo}.

The disparity between oxidizer- and fuel-side addition may also be associated with the types and quantities of radicals and products that are formed from the parent molecule as it approaches the flame from different directions and their relevance to the suppression action.[45] Assuming that the important suppression action takes place on the oxidizer side of the flame, then additives to the fuel stream must travel through the flame to reach this point. This may have a significant effect on what phosphorus-containing species are present in the region of important radical chemistry for different modes of addition, i.e., oxidizer- or fuel-side doping.

A third feature of Figure 3-83 is that for both the oxidizer- and fuel-side tests, the normalized effectiveness' increases with Z_{st}. The existence of this slope implies that the suppressant effectiveness varied with either temperature, structure of the flame, or both. Studies in a variety of premixed flames had indicated that at high temperatures (above 2350 K),[254,256] DMMP can become a flame promoter. Thus, presumably, the suppression effectiveness of DMMP should decrease with increasing flame temperature. Figure 3-83 is consistent with this expectation, showing decreasing suppressant effectiveness with increasing adiabatic flame temperature (lower Z_{st} values). However, it is possible that changes in flame structure, which occur at different Z_{st} values, may also have influenced suppressant effectiveness.

Further tests were conducted to clarify this temperature dependence. Due to condensation of the dopant below 80 °C, control of the reactant temperatures to vary T_{ad} over a significant range was not possible. Instead, the overall dilution of the flame, at a fixed value of Z_{st} = 0.5, was used to vary T_{ad}. In this experiment, the mass fraction of oxygen in the oxidizer stream ranged from 0.39 to 0.44, resulting in a T_{ad} ranging from 2132 K to 2261 K and an a_{qo} range of 294 s^{-1} to 572 s^{-1}. Unfortunately, the variation in reactant stream compositions increased the susceptibility of the results to the sensitivity to random uncertainties in relative flows, producing considerable scatter. The results from this experiment are shown in Figure 3-84, along with the data for oxidizer-side addition at fixed a_{qo}, but varying Z_{st} values; all are plotted against T_{ad}. Although the large experimental scatter makes it difficult to draw quantitative conclusions, there is a clear trend of decreasing effectiveness with increasing T_{ad}, comparable to that seen

in the constant a_{qo} data. However, these results did not conclusively eliminate the possibility of flame structure and the detailed chemistry of dopant action influencing dopant effectiveness.

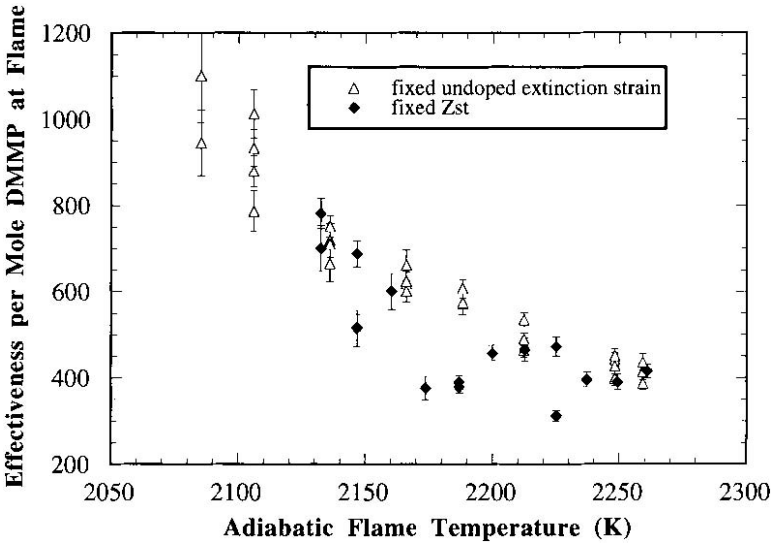

Figure 3-84. Normalized effectiveness of DMMP-doped Flames as a Function of Adiabatic Flame Temperature. The symbol Δ represents changing Z_{st} from 0.1 - 0.7, fixed aqo = 350 ±10 s^{-1}, while ◆ represents a fixed Z_{st} = 0.5, changing a_{qo} from 294 s^{-1} to 572 s^{-1} by varying mass fraction of oxygen. Error bars represent standard deviation of data for each set of data runs.

Effect of Flame Temperature

Experiments and Calculations

The temperatures of laboratory flames and the flames from real fires can differ significantly. Fisher and co-workers[119] conducted experiments in the same burner used above to quantify the temperature dependence for flame inhibition by DMMP and to gain further insight into the inhibition mechanism. The indicator of inhibition was the degree of decrease in the OH concentration ([OH]) profiles, as measured using LIF. Only a limited number of measurements of [OH] in the counterflow configuration have been reported.[271,292-294] A few studies have utilized LIF to observe changes in [OH] in flames doped with halogenated suppressants [156, 51,61] work with flames doped with phosphorus-containing agents is far more limited.[294,295]

Here, a series of four non-premixed, atmospheric-pressure flames of methane-O_2/N_2/Ar mixtures were studied (Table 3-13).

Table 3-13. Flame Conditions.

Flame #	Oxidizer Composition	$T_{adiabatic}$ [K]	$T_{calculated\ peak}$ [K]	DMMP [μL/L]	V_O [cm/s]	V_F [cm/s]
1	21 % O_2 – 79 % N_2	2261	1967	0 to 572	71	96
2	21 % O_2 – 53 % N_2 – 26 % Ar	2353	2080	0 to 715	71	101
3	21 % O_2 – 26 % N_2 – 53 % Ar	2450	2189	0 to 715	71	106
4	21 % O_2 – 79 % Ar	2547	2286	0 to 715	71	110

Flame temperature was varied by changing the proportions of N_2 and Ar in the oxidizer side diluent, while maintaining 21 % (by volume) O_2 and thus a constant stoichiometric mixture fraction of 0.055. The

experimental results were compared to predictions from numerical calculations using a kinetic mechanism[294] for DMMP decomposition and phosphorus-containing radical chemistry. The key reactions in the mechanism responsible for the observed inhibition of OH were identified.

Calculations of the undoped flames were made using the OPPDIF code version 8.5 from the CHEMKIN III Suite.[296] The full GRI-MECH 3.0 mechanism, including nitrogen chemistry, (53 species, 325 reactions)[206] was employed. Mixture-averaged diffusion velocities were used, and thermal diffusion was neglected. Opposed-jet burners are typically modeled as having either potential flow (linear axial velocity gradient) or plug flow (zero axial velocity gradient) boundary conditions, although measurements indicate that the actual velocity field lies somewhere between the two approximations.[67] Calculations were performed for several different boundary conditions. The boundary conditions of potential flow with centerline axial velocities of twice the measured volume averaged velocities for the fuel and oxidizer streams were selected for use in this study, because the resulting OH profiles most closely agreed with the observed profiles. The factor of two for the centerline velocities was appropriate because the flow in the straight-tube reactant nozzles (L/D > 30) was expected to be close to Poiseuille flow, in which the centerline velocity is twice the volume average. Temperature profiles predicted by 1D calculations have been found by other researchers to be in good agreement with measurements made in opposed-jet burners under a variety of conditions using spontaneous Raman scattering in CH_4 /O_2/N_2[297] and H_2/air[292] flames, thin SiC filament pyrometry in CH_4/O_2/N_2 flames,[298] and CARS in propane/air flames.[299]

Calculations with Phosphorus Kinetics

To investigate the cause of the OH concentration changes observed in the LIF experiments, a set of flame calculations was performed using a proposed mechanism for DMMP decomposition and phosphorus-radical chemistry.[294] This mechanism was based on (1) the kinetic data used for the analysis of the influence of PH_3 on radical recombination rates in the combustion products of a hydrogen flame[258,259] and (2) on kinetic models used for describing DMMP and TMP destruction in a low pressure hydrogen flame.[300,301] Reactions of phosphorus-containing species with radicals and intermediate species of hydrocarbon combustion were included.[294] Reactions were added to the scheme to complete destruction pathways for some species. The used version of this phosphorus mechanism included 27 species and 166 reactions. Thermochemical data compiled by Babushok[302] for phosphorus-containing species were mostly taken from References 197, 303, 304, and 304 {Gurvich & Glushkov 1998 #2420}. Methane-O_2 chemistry was modeled using GRI Mech 3.0 with nitrogen chemistry removed (36 species, 219 reactions retained). The phosphorus mechanism predicted reductions in extinction stain rates for non-premixed methane-air flames due to the presence of DMMP that were in agreement with experimental results from MacDonald et al.[79] An earlier version of the mechanism had also been used to predict the effect of DMMP on premixed flame speeds.[257]

Calculations were performed for all four flames using the combined mechanisms (phosphorus and GRI Mech), both with and without the addition of 572 μL/L of DMMP. Calculations with the combined mechanisms required a higher degree of mesh refinement (both GRAD and CURV parameters for OPPDIF script = 0.1, yielding 250-300 grid points) than the GRI Mech calculations in order to produce [OH] profiles for the doped flames that were independent of grid size. Figure 3-85 illustrates the major species profiles from these calculations for flames 1 and 4 without dopant addition.

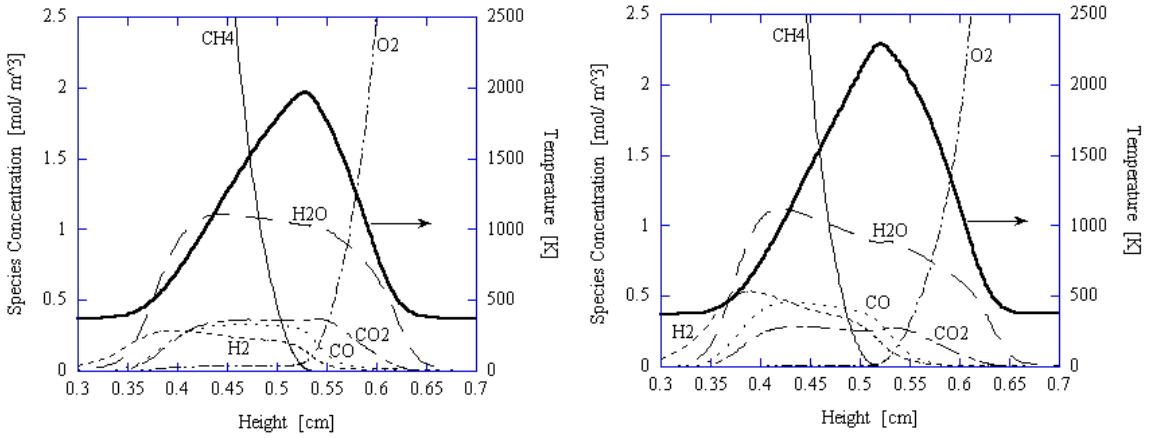

Figure 3-85. Calculated Major Species and Temperature Profiles for Flame 1 (left) and Flame 4 (right), both undoped.

Measurements

Figure 3-86 shows a comparison between measured and calculated [OH] profiles for flames 1 and 4, the coolest and hottest conditions respectively. Multiple profiles, all undoped, are shown to illustrate the repeatability of these measurements.

The agreement between measured and calculated profiles was quite good. The intermediate cases of flames 2 and 3 were in similar agreement between measured and computed profiles. Agreement in peak [OH] was expected since calculated profiles were used to estimate peak concentrations in the measurements for each flame. There was also good agreement in the profile shape, which was not affected by the matching procedure, including the degree of asymmetry, and width (FWHM). The peak concentration, as determined by the calculations, increased by 66 % from 0.041 mol/m^3 for flame 1 to 0.069 mol/m^3 for flame 4, which had a stoichiometric adiabatic flame temperature that was 286 K hotter than flame 1. The peak temperatures (Table 3-13), for these moderately strained flames were approximately 300 K cooler than the stoichiometric adiabatic flame temperatures, although the difference in calculated peak temperatures for flames 1 and 4 (319 K) were comparable to the change in the stoichiometric adiabatic flame temperature (286 K).

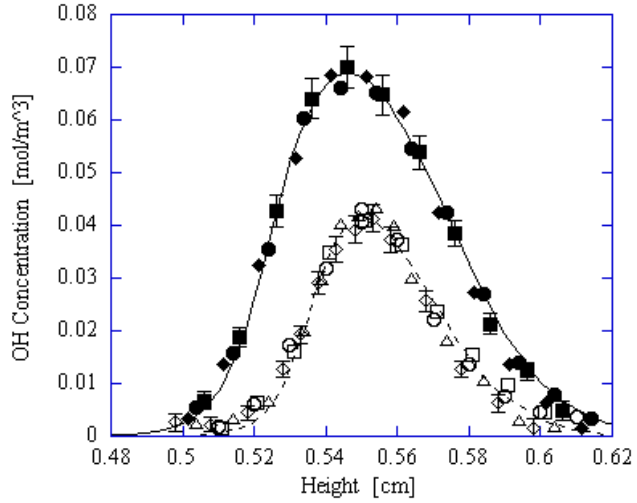

Figure 3-86. Calculated and Measured OH Concentration Profiles for Flames 1 and 4. Flame 1: dashed line – computations; open symbols - four measured profiles. Flame 4: solid line - computations; filled symbols - three measured profiles. Error bars represent statistical uncertainty in the measured values.

Figure 3-87 illustrates the variation in computed and measured OH profile widths (FWHM) with adiabatic flame temperature. All flame conditions are undoped. Both the calculated and measured OH profile widths are observed to increase by approximately 40 %, from 0.4 mm to 0.55mm, across the range of temperatures investigated. Good agreement between calculated and measured profile widths is observed for all undoped flames.

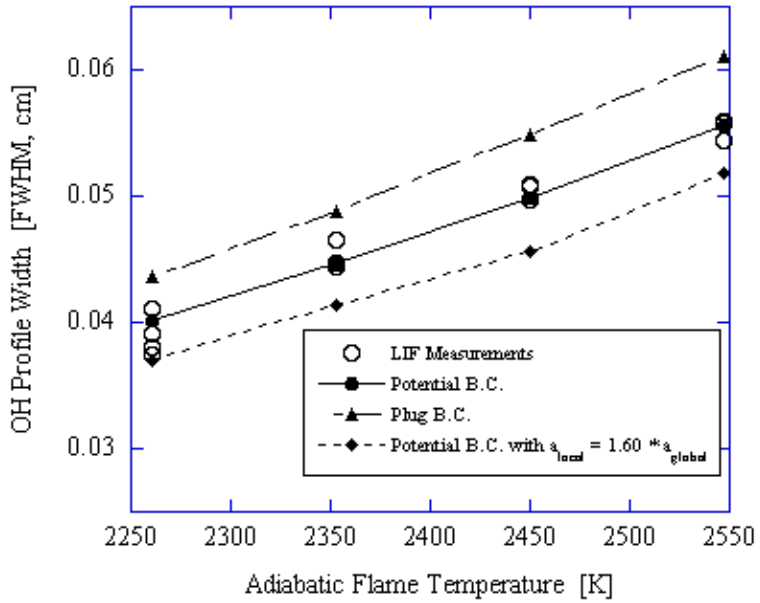

Figure 3-87. [OH] Profile Widths (FWHM). Open circles: measured values for all undoped flames. Lines with filled symbols: computational values for three different velocity boundary conditions (B.C.). Filled circles: potential flow B.C. with velocities of twice the volume average (Poiseuille flow). Filled triangles: plug flow B.C. with velocities equal to the volume average. Filled diamonds: potential flow B.C. with local strain rate equal to 1.60 times the global strain rate given by Equation 3-7.

The velocity boundary conditions in the calculations had a noticeable effect on the calculated width of the [OH] profile. In order to investigate the influence of these boundary conditions, two additional sets of calculations were performed, one for plug flow boundary conditions with the measured volume averaged velocities and the other for potential flow while matching the maximum local strain rate to 480 s^{-1}, or 1.60 times the global strain rate (Equation 3-1) (which required increasing the centerline velocity for the calculations to 2.8 times the volume averaged value). The higher strain case was motivated by measurements of axial velocity profiles made using Laser-Doppler Velocimetry in a similar burner configuration.[281] These measurements indicated a substantially higher local strain rate (axial velocity gradient on the oxidizer side, evaluated just upstream of the heat release region) of approximately 1.60 times the global strain rate. The original calculations, with boundary conditions of potential flow and velocities of twice the volume average, gave a computed velocity profile with a peak local strain rate of approximately 1.18 times the global strain rate or 355 s^{-1}. The calculated [OH] profile widths for the two additional sets of boundary conditions are also shown in Figure 3-87. Both additional sets of boundary conditions predicted similar variation in profile width with flame temperature. However, the plug flow boundary condition overestimated the profile widths by 10 % to 15 %, and the higher strain rate case underestimated the widths by 5 % to 8 %. Finite spatial resolution in the measurements (100 μm) limited the accuracy with which the experimental width could be determined. Heat and radical losses to the burner as well as radiation, which were ignored in these calculations, also contributed to the discrepancy between measured and calculated profiles. However, these physical loss mechanisms were significant in these well isolated, non-sooting flames. Uncertainties associated with the chemical

mechanism used influenced the computed profile width and also affected the level of agreement between computed and measured profile widths.

The good agreement between the measured profiles and the calculations made with potential flow boundary conditions with centerline velocities of twice the volume average supported the selection of this boundary condition for use in the quenching and Boltzmann fraction corrections to the LIF data. Because of the relatively small impact of the temperature and quenching correction, the choice of the appropriate boundary conditions did not substantially influence the conclusions below about the influence of phosphorus additives on [OH]. Using profiles calculated with either of the alternate boundary conditions to correct the LIF data changed the observed reductions in total [OH] by less than 1 %, well within the uncertainty of the measurements.

Figure 3-88 illustrates the effect of 572 µL/L of DMMP on OH concentrations in flame 1. With this loading, flame 1 is close to extinction.

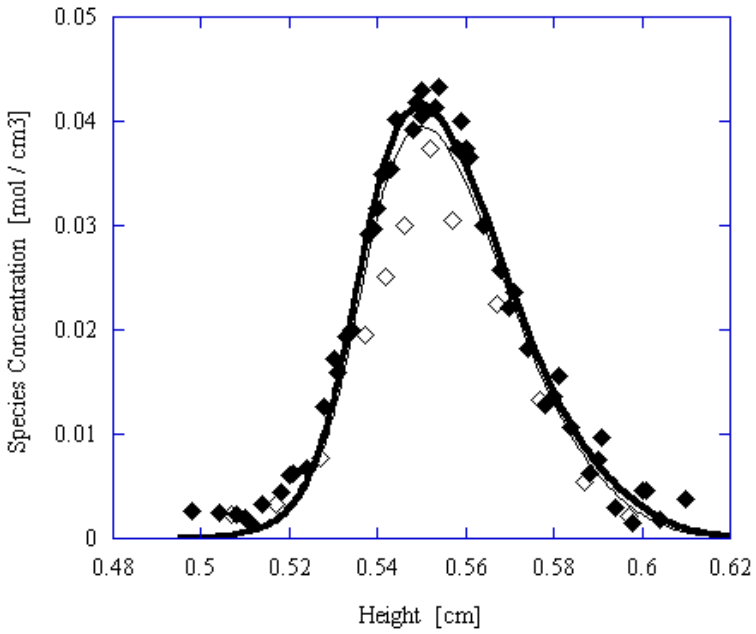

Figure 3-88. Effect of 572 µL/L of DMMP on [OH] in Flame 1. Filled symbols: undoped profiles. Open symbols: doped profile. Thick line: computational prediction for the undoped profile. Thin line: doped profile. Phosphorus kinetic mechanism from Wainner et al.[294]

A substantial reduction, approximately 20 %, in OH concentration was observed. The doped profile was smaller in magnitude, but the width was not significantly affected. In order to determine changes in the total flame OH concentration, the profiles were numerically integrated, using a simple trapezoidal rule approximation, across the width of the flame, and then the integrals from the doped and undoped flames were compared. The integration technique was particularly useful for quantifying changes in the higher temperature flames, where the [OH] profile was less affected by the phosphorus-containing additive. There was a 23 % ± 3 % reduction in total OH (by this definition) for the data shown in Figure 3-88. The uncertainty resulted from the estimated statistical uncertainty of the individual data points from the profile, and was closely comparable to the repeatability of the measurement.

OH concentration profiles were measured for all four flames with DMMP loadings up to 715 µL/L, with the exception of flame 1. A loading of 715 µL/L of DMMP in flame 1 caused extinction at the global strain rate used in this study. Therefore, the maximum loading used for that flame was 572 µL/L, the next

highest loading readily achieved experimentally. Figure 3-89 illustrates the ratio of doped to undoped total [OH] for the four flames as a function of loading. Raw data for profiles for all conditions studied in this work can be found in the appendix of Reference 305. Within experimental uncertainty, total [OH] decreased linearly with DMMP addition over this range of loadings. Results from the calculations performed with the phosphorus kinetic mechanism, discussed below, for a range of DMMP loadings from 0 μL/L to 720 μL/L, confirmed the linear variation in the [OH] reduction with loading. The linear trends were consistent with extinction measurements on non-premixed methane-air flames which indicated a linear variation in DMMP effectiveness, defined in terms of reduction in the global extinction strain rate, for loadings up to 1500 μ L/L.[79] Linear variation in effectiveness with loading was observed with most flame suppressants at low loadings. Linear regression fits to the data for each flame are also shown in Figure 3-89. The most striking observation from Figure 3-89 is the increase in inhibition effectiveness with decreasing flame temperature. The highest temperature case, flame 4, shows less than 5 % reduction in total [OH] at the maximum loading of 715 μL/L, compared to 23 % reduction in flame 1 for only 572 μL/L.

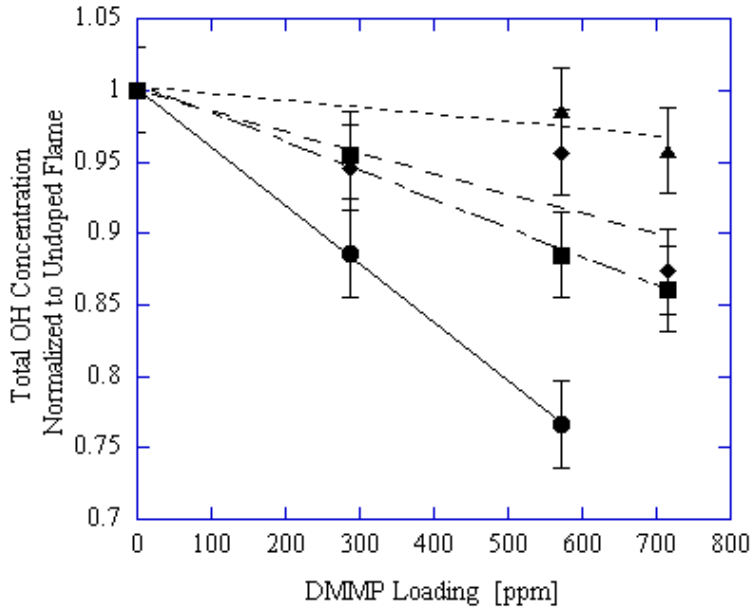

Figure 3-89. Effect of DMMP Loading for All Flames. Lines are linear regression fits to data. Flame 1: solid line and circles. Flame 2: dot-dash line and squares. Flame 3: dashed line and diamonds. Flame 4: dotted line and triangles. Error bars represent uncertainty in measurements.

Extinction measurements for the flames were not successful because the high extinction strain rates for flames 2 through 4 required dramatically higher flow velocities that were well into the turbulent flow regime. However, an earlier study had investigated the effect of DMMP on global extinction strain rate for a variety of different flame conditions with different stoichiometric mixture fractions and stoichiometric adiabatic flame temperatures.[120] Effectiveness in terms of extinction strain rates for that work was defined as the fractional reduction in global extinction strain rate divided by the mole fraction of phosphorus in the flame:

$$Effectiveness_q \equiv \frac{\left(a_{q,0} - a_q\right)}{a_{q,0}} \frac{1}{\chi_P} \tag{3-10}$$

The subscript q indicates that the measurement was made at extinction conditions, and the subscript 0 denotes the value for the undoped flame. Flame calculations were used to estimate the mole fraction of

phosphorus at the flame surface, χ_p, taken to be the maximum temperature contour. There was a similar trend of decreasing effectiveness with increasing temperature. The stoichiometric adiabatic flame temperature in that study was varied in two ways. The first was by changing the stoichiometric mixture fraction from 0.05 to 0.7 while maintaining a fixed undoped global extinction strain rate. The second was by decreasing the overall dilution of the flame while maintaining a stoichiometric mixture fraction of 0.5. The range in adiabatic flame temperatures from that work (2130 K to 2260 K) was substantially lower than that investigated here. Comparing the temperature dependence from the previous investigation to that of the current work requires a measure of effectiveness, analogous to the one used in the previous study, in terms of [OH] reduction as the fractional reduction in total [OH] concentration:

$$Effectiveness_{OH} \equiv \frac{\left(TotalOH_0 - TotalOH\right)}{TotalOH_0} \frac{1}{\chi_P} \tag{3-11}$$

Again, the subscript 0 denotes the measured value for the undoped flame. The flame calculations made with the combined GRI Mech and phosphorus mechanisms were used to determine χ_p, the total mole fraction of phosphorus (sum of mole fractions of all phosphorus-containing species) predicted at the flame surface, taken to be the maximum temperature contour. Because the stoichiometric mixture fraction was fixed for all flames, changes in χ_p were negligible. The use of this parameter did not affect the observed trends and was introduced solely to provide a definition for effectiveness that is analogous to that used in Reference 120 to facilitate a comparison to previous extinction studies. This effectiveness definition is essentially a measure of the slope of the linear trends indicated in Figure 3-89.

Figure 3-90 shows a comparison of this effectiveness based on OH with the one based on the extinction measurements from the previous study. The trends observed in the two data sets are in good qualitative agreement, given that different measures of effectiveness were used. When comparing the two data sets, it should also be noted that for a given stoichiometric adiabatic flame temperature, measurements performed at extinction conditions, such as those from Reference 120, had a peak flame temperature that was cooler than that seen in the LIF measurements, which were performed at a fixed global strain rate of 300 s^{-1}, below the value required to extinguish the flame. The effectiveness data in Figure 3-90 show a substantial decrease in DMMP effectiveness with increasing temperature. The unambiguous trends in the LIF data confirmed the hypothesis of Hastie and Bonnell[256] of decreasing inhibition with increasing flame temperature, with nearly a 90 % decrease in effectiveness for a 300 K increase in temperature.

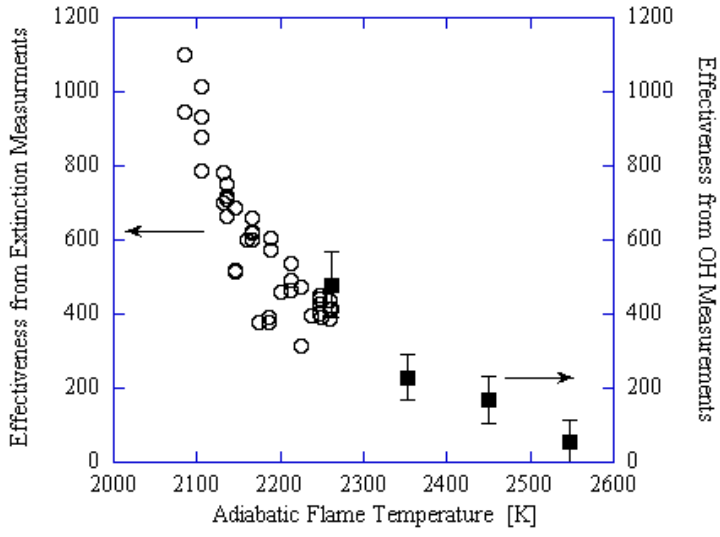

Figure 3-90. Temperature Dependence of Effectiveness. Open circles: effectiveness data from Reference 9 defined in terms of reduction of global extinction strain. Filled squares: effectiveness data from the current work defined in terms of reduction in OH concentration. Error bars represent uncertainty in the measurements.

Calculations with Phosphorus Kinetics:

The combined mechanism of phosphorus kinetics by Wainner et al.[294] and CH_4-O_2 kinetics from GRI Mech[206] was used to calculate species and temperature profiles for all four flames with and without the addition of 572 µL/L of DMMP. The predicted temperature profiles showed no significant effect from the addition of DMMP (< 10 K change in peak temperature). However, significant changes were observed in OH, H and O profiles. Figure 3-91 illustrates the doped and undoped profiles of OH, H, and O for flame 1. Relative to the undoped profile, the OH profile for the doped flame was lower in magnitude. The change was similar to that observed in the measured data, but not as large. A comparison of computational predictions to measured data is shown in Figure 3-88. The reduction in H and O atom concentrations seen in Figure 3-91 was significantly greater than the reduction for OH, indicating a larger effect of phosphorus chemistry on the concentrations of those species.

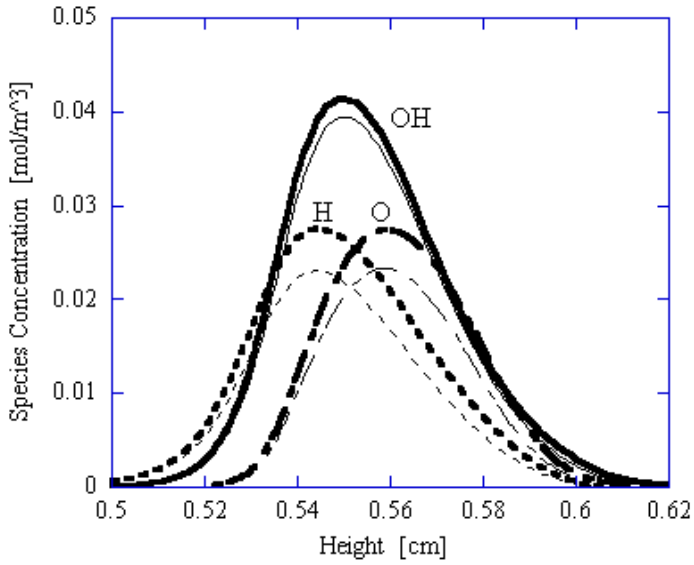

Figure 3-91. Effect of 572 µL/L of DMMP on Calculated OH, H, and O Concentration Profiles in Flame 1 ($CH_4/O_2/N_2$). Dark lines are undoped profiles and thin lines are with DMMP addition.

After performing the spatial integration of the computed profile across the flame, as described above, the change in total OH between the doped and undoped cases was evaluated. Figure 3-92 shows a plot of effectiveness, as defined in terms [OH] reduction (3-11), as a function of the stoichiometric adiabatic flame temperature for both the experiments and the computations. The computational and experimental results in Figure 3-92 showed the same trend of decreasing effectiveness with increasing temperature, although the temperature dependence of the computational results was weaker. The magnitude of effectiveness from the flame calculations agreed well with LIF data from the highest temperature case, flame 4, but the calculations underpredict effectiveness for flames 1 through 3. In these calculations the magnitude of the reduction in OH (i.e., total $OH_{undoped}$ - total OH_{doped}) was nearly constant for all flames. For these flame calculations, changes in the effectiveness (which was a fractional measure of the reduction of total OH) with temperature were due mainly to the increases in the total $OH_{undoped}$, which was larger by a factor of 2.25 for flame 4 ($CH_4/O_2/Ar$) compared to flame 1 ($CH_4/O_2/N_2$) in the calculations. This estimate of the increase of total OH for the undoped flames was not sufficient to explain the variation in effectiveness observed in the LIF measurements (reduced by a factor of 10 in flame 4 compared to flame 1).

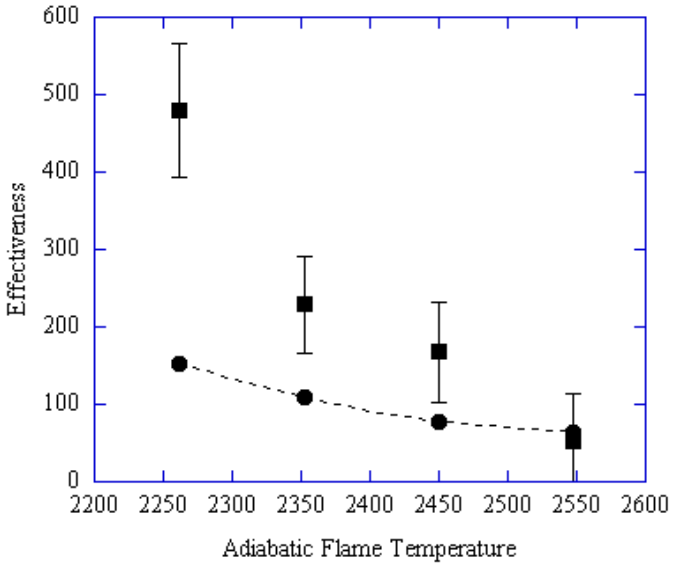

Figure 3-92. Temperature Dependence of Effectiveness Defined as in Terms of Reduction in total [OH]. Filled circles with the dashed line: computational predictions. Filled squares: measured data. Error bars represent uncertainty in the measurements.

The processes responsible for the observed reductions in [OH] were determined by analysis of individual reaction rates from the phosphorus mechanism. Since the experimental and computational results both showed a reduction in [OH] with the addition of DMMP, it was expected that the reactions involving phosphorus removed OH from the flame. In fact, for all four flames, the sum of the chemical production rates for OH over all reactions involving phosphorus in the mechanism was positive across most of the [OH] profile, indicating that these reactions directly produced OH rather than destroyed it. Thus, the drop in [OH] upon introduction of phosphorus kinetic sub-mechanism must have occurred indirectly, through an effect on rates of reactions not involving phosphorus-containing species. Poor efficiency for direct recombination of OH by reactions involving suppressant species has been observed previously for iron-based[104] and halogen-based[55,57] suppressants. The net production rates for flame radicals OH, H, and O by all reactions involving phosphorus in flames 1 and 4 are shown in Figure 3-93. It is clear from these figures that the action of the phosphorus-containing species was similar in both flames. The regions of radical production/destruction in flame 4 were somewhat wider, in keeping with the wider flame (see Figure 3-87), but the peak magnitudes of the production rates for H, O, and OH were 5 % to 10 % lower.

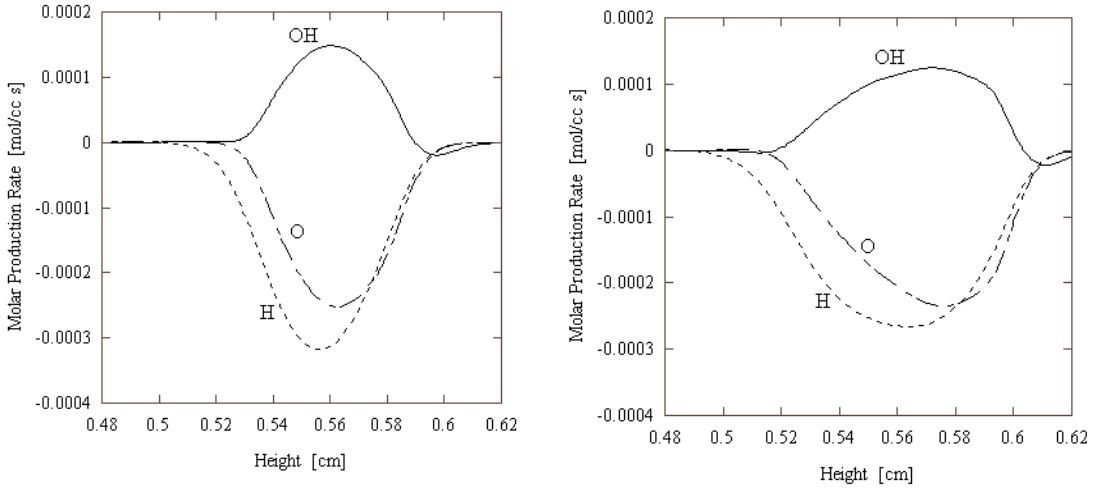

Figure 3-93. OH, H, and O Production Rates in Flame 1 (left) and Flame 4 (right), Summed over All Reactions Involving Phosphorus.

The cause of the observed reduction in OH was the fast removal of H and O atoms by the reactions involving phosphorus. Smyth et al.[306] have studied the interrelationships of H, O, and OH concentrations in non-premixed methane-air flames and found that while these species were generally not in equilibrium, their respective populations were still interdependent on one another through a variety of fast radical shuffle reactions. Because of this interdependence, the reductions in H and O atom levels created by the reactions involving phosphorus, observed in Figure 3-91 for flame 1, caused the radical shuffle reactions not involving phosphorus to respond by reducing OH.

Figure 3-94 illustrates the shift in OH production rates by the GRI sub-mechanism (sum of OH production rates over reactions not involving P) due to the addition of 572 μL/L of DMMP to flame 1.

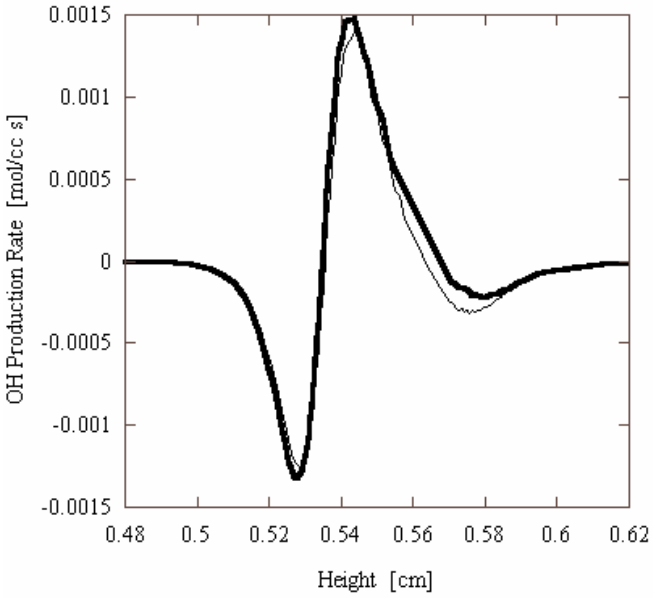

Figure 3-94. Total OH Production Rates in Flame 1 by Reactions Not Involving Phosphorus. Dark line: Undoped Rate. Thin line: Rate with the Addition of 572 μL/L of DMMP.

The OH production in the doped flame was generally lower than that in the undoped case, particularly on the oxidizer side of the flame. Three individual reactions that were primarily responsible for the shift seen in Figure 3-94 were identified by comparing the shift in doped and undoped reaction rates for all reactions not involving phosphorus. Two of these reactions, R3-8 and R3-9, underwent a substantial decrease in OH production for the doped flame. R3-8 is one of the important chain branching reactions:

$$O + H_2 \leftrightarrow OH + H \qquad \text{(R3-8)}$$

$$H + HO_2 \leftrightarrow OH + OH. \qquad \text{(R3-9)}$$

The third reaction that underwent significant changes due to addition of phosphorus is R3-10:

$$OH + H_2 \leftrightarrow H_2O + H. \qquad \text{(R3-10)}$$

This reaction has been identified by Twarowski[258,259,303] as playing an important role in increased recombination rates $OH + H \rightarrow H_2O$ due to the presence of phosphorus containing compounds. In the current non-premixed flames, the overall effect of R3-10 in the presence of phosphorus addition was not clear, as the reaction had regions of increased OH production as well as regions of decreased OH production across the flame width.

Figure 3-95 shows the contribution of individual reactions involving phosphorus to OH production rates and compares them to the changes in the reaction rates of R3-8 R1 and R3-9 R2 (doped rate minus undoped rate) that occurred when DMMP was added to the flame 1.

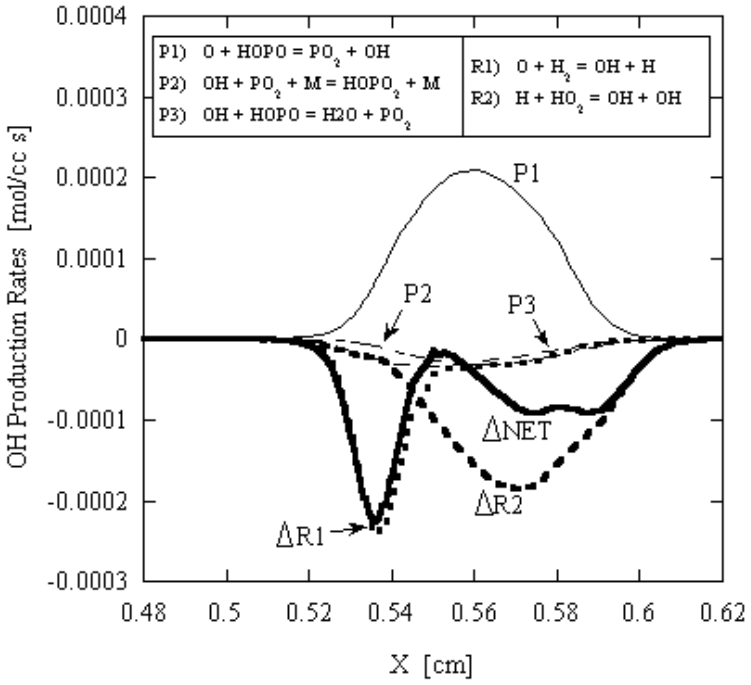

Figure 3-95. Influence of the Addition of 572 µL/L of DMMP on OH Production Rates in Flame 1. Rates of OH production by reactions involving phosphorus P1 - P3 and changes (ΔR3-8 and Δ R3-9) in OH production (doped rate - undoped rate) for non-phosphorus containing reactions R3-8 and R3-9. The net effect (ΔNET) of these reactions is shown in bold.

OH production by reactions involving phosphorus was dominated by R3-11 :

$$O + HOPO \leftrightarrow OH + PO_2. \quad \text{(R3-11)}$$

There were two phosphorus containing reactions that consumed OH, but the rates were small (15 % to 30 %) relative to 3-11:

$$OH + PO_2 + M \leftrightarrow HOPO_2 + M \quad \text{(R3-12)}$$

$$OH + HOPO \leftrightarrow H_2O + PO_2. \quad \text{(R3-13)}$$

Figure 3-95 also shows the net change in OH production for all reactions in that figure (R3-11, R3-12, R3-13, R3-8 and R3-9). The net rate curve shows overall destruction of OH, indicating that the shift towards decreased production by R3-8 and R3-9 was more than sufficient to balance the direct production of OH by R3-11.

Removal of H and O atoms by reactions involving phosphorus clearly played an important role in the observed inhibition. Calculation results showed that removal of H atoms by reactions involving phosphorus was done primarily by:

$$H + PO_2 + M \leftrightarrow HOPO + M \quad \text{(R3-14)}$$

and to a lesser extent by:

$$H + HOPO_2 \leftrightarrow H2O + PO_2 \quad \text{(R3-15)}$$

$$H + HOPO \leftrightarrow H2 + PO_2 \quad \text{(R3-16)}$$

Figure 3-96 shows the contribution of R3-14 to the total H destruction rate by all reactions involving phosphorus.

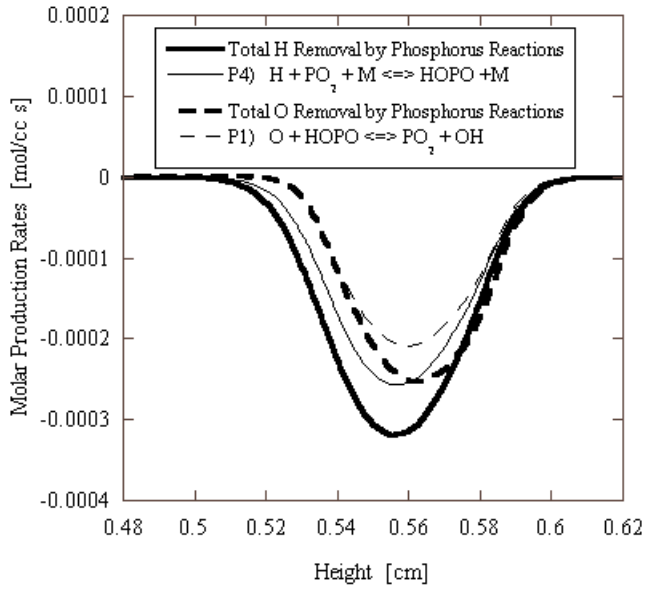

Figure 3-96. H and O Production Rates by All Reactions Involving Phosphorus (solid lines) and by Individual Reactions (dashed lines) in Flame 1.

Removal of O atoms by reactions involving phosphorus was done primarily by the OH-producing reaction R3-11. The contribution of R3-11 to O removal was also shown in Figure 3-95. Significant uncertainties remained for the rate coefficients of several of the key reactions involving phosphorus species that have been identified here (R3-11, R3-12 and R3-14).[302] Suggestions that the rate coefficients for the recombination reactions R3-12 and R3-14 might need to be increased by a factor of 2 or more [302] could help reconcile the observed differences in magnitude of effectiveness between the measurements and the computational predictions.

3.4.3 Effects of Dimethyl Methylphosphonate on Premixed Methane Flames

Introduction

Fire suppression science would benefit from a reliable detailed chemical kinetic mechanism for combustion of organophosphorus compounds. Two mechanisms have recently been proposed for organophosphorus combustion[294,307,307] but they have been validated against only limited experimental data.

Most previous DMMP combustion experiments yielding species data have involved low pressure hydrogen/ oxygen/argon flames. Korobeinichev et al. [254,308] and Werner and Cool[300] both used molecular beam mass spectrometry to study the structure of premixed stoichiometric H_2/O_2/Ar flat flames doped with DMMP, between 50 kPa and 100 kPa. They were able to measure DMMP and various stable and unstable products and intermediates. Temperature was measured by thermocouple. DMMP loading was between 1000 μL/L and 11,000 μL/L. Both sets of investigators observed substantial increases in post-flame temperature (approximately 300 K) with the addition of DMMP. Species measurements differed in some respects: certain intermediates observed by each group were not seen by the other. Each group proposed destruction mechanisms for DMMP that formed a basis for further mechanism development.

Aside from species profiles, Korobeinichev et al. also inferred changes in adiabatic flame speed by observing how maximum flame temperature varied with DMMP loading. They found that adding under 5000 μL/L of DMMP increased the flame speed, and above this concentration, the opposite held in low-pressure H_2/O_2/Ar flames. More recently, Korobeinichev et al.[309] performed experiments in a premixed CH_4/O_2/Ar flame at 10 kPa with a different organophosphorus compound, TMP. In contrast to their experiments with TMP[310,311] and DMMP[254,308] in hydrogen flames, these experiments showed an inhibitory effect on the flame.

Flame inhibition and suppression effects of DMMP and other organophosphorus compounds have been observed in non-premixed opposed-jet hydrocarbon flames, both through extinction measurements[79,120] and through measurements of flame radical levels.[119] They have also been seen in premixed flames by measuring the heat loss from the flame to a Bunsen burner.[312] Flame suppression effectiveness decreased as temperature increased,[119,120] and appeared to be greatest under near stoichiometric conditions.[312] There has been some agreement on the likely mechanism of flame inhibition by DMMP: phosphorus-containing radicals that are produced from DMMP at flame temperatures participate in catalytic cycles resulting in the recombination of standard flame radicals such as H and OH.[258,260,294,303]

Nogueira and Fisher[313] tested these mechanisms against experimental data under flame conditions that were realistic for flame suppression: a $CH_4/O_2/N_2$/Ar premixed flame doped with DMMP at near ambient pressure. Only stable species not containing phosphorus were measured. The impact of phosphorus on the flame was studied by comparing the undoped with doped profiles of the observed species.

Experimental

Apparatus

Experiments were conducted using a brass flat-flame burner resembling the one used by Korobeinichev et al.[254,308-311,314,315] In the burner, the premixed reactants entered a plenum from the bottom of the burner, flowed upward through a bed of 3 mm diameter glass beads, and then passed through an array of hexagonally spaced 0.58 mm diameter holes with center-to-center spacing of 0.95 mm in the upper surface of the burner. The use of a perforated plate, rather than a sintered metal plug, made it possible to clean phosphorus-containing products from the burner. The diameter of the flow region was 53.4 mm, and the thickness of the brass plate was 6.35 mm. Surrounding the plenum was an annular passage through which cooling water flowed. A centrifugal pump and resistance heater kept the cooling water, at 91°C, flowing at a rate slightly above 0.3 mL/min through a closed circuit including the water channel of the burner, a rotameter, and an annulus surrounding the reactants gas flow line.

Gas samples and temperature measurements at different heights were obtained by moving the burner relative to stationary probes. The burner was mounted on a motorized linear motion feedthrough, which was controlled by a programmable stepping motor. This device allowed vertical movement with steps of 0.008 mm over a range of 100 mm. The repeatability of returning to a position was about 0.08 mm. The burner and the traverse were sealed within a vertical 146 mm ID stainless steel cylinder that served as a vacuum chamber.

Gaseous reactants (CH_4, O_2, N_2, and Ar) were metered with calibrated mass flow controllers and meters. Upstream of the location where the nitrogen mixed with the other gases, liquid DMMP was introduced via a syringe pump (model A with 25 ml Hamilton Syringe; Razel, Stanford, CT). Downstream of the

injection point, a chamber with a residence time of 12 s smoothed out fluctuations in the DMMP loading. The electrical heating and cooling water jacket maintained all reactant streams containing DMMP above 85 °C, high enough to avoid DMMP condensation.

The vacuum chamber pressure was measured at the exhaust line downstream of the vacuum chamber by a capacitance pressure gauge (model PDR-C-1C; MKS, Andover, MA), calibrated using a "U" mercury manometer. For safety reasons, the chamber was maintained at a pressure slightly below ambient and a dry ice/acetone (200 K) cold trap removed PCCs and water from the exhaust stream.

Sampling

Sampling for species and temperature measurements made use of a stationary quartz microprobe. The probe was 200 mm long and constructed of 6.0 mm OD, 3.8 mm ID quartz tubing, tapering to an orifice. Repeatability tests involved probes of different diameters. The specific probe orifice diameters, measured before each experiment, are listed in Table 3-14. Downstream of the orifice was a 20 mm long vertically oriented section diverging with an angle of 11º. In the following 25 mm, the probe underwent a smooth 90º bend to a horizontal orientation, allowing it to be mounted in a sampling port in the side of the vacuum chamber.

The gases flowed through the probe, lengths of perfluoroalkoxy tubing, a gas cell, and a needle valve, and into a vacuum pump. The pressure downstream of the probe was kept under 20 kPa to guarantee choked flow at the probe's orifice. A 50 SFM bubble meter (SGE International PTY LTD, Australia) was used to measure the volumetric flow through the probe. The bubble meter was located downstream of the small vacuum pump, where the flow pressure and temperature were close to room conditions. Depending upon the gas temperature and orifice size, between 15 min and 45 min was needed to fill the FTIR cell with the gas sample.

Table 3-14. Probe Orifice Diameters (μm) Used in Specific Experiments.

DMMP	Fuel-rich Flames	Near-stoichiometric Flames
Doped	61, 66	60, 65
Undoped	56, 67	59, 64

Species Measurements

Fuel and product gases were measured with a Mattson RS-1 FTIR spectrometer, operating in the wavelength range from 500 cm^{-1} to 4000 cm^{-1} with a resolution of 1 cm^{-1} and signal gain of 4. The sample gases flowed continuously through an 884 mL multi-pass White cell (Infrared Analysis, Madison, WI) with gold-coated mirrors, zinc selenide windows, and a path length of approximately 5.4 m. The cell was maintained near 15 kPa during data acquisition, and was purged and conditioned with gas flow between samples. The scanning time for the FTIR to obtain a sample spectrum was 7.2 min.

Compound concentrations were quantified using an interactive subtraction technique that compared sample spectra to calibration spectra with known species concentrations. Spectral regions were chosen to minimize overlap, but in some cases interfering species had to be subtracted from the spectrum before quantification. Table 3-15 lists spectral regions and sensitivities.

Table 3-15. FTIR Detection Limits and Wavenumber Ranges.

Species	Wavenumber Range Used for Quantification (cm^{-1})	Detection limit (µL/L)[a]
CH_4	3176–3133	400
CH_2O	2920–2870	100[b]
CH_3OH	1060–1010	10
CO	2220–2030	1350
CO_2	715–670	1200
C_2H_6	3000–2950	70[b]
C_2H_4	960–905	60
C_2H_2	740–710	10

[a] Lower detection limit could be achieved with a different choice of spectral region for many species.
[b] Quantified after subtraction of CH4 and CH3OH.

Radicals could not be measured with this technique because their lifetimes were too short to persist through the sampling system. Although spectral features associated with DMMP and some of its phosphorus-containing products were observed, their levels were not repeatable. Previous research with extractive FTIR of organic phosphates and phosphonates and their pyrolysis products[263,316,317] suggested that the bulk of the lower-vapor-pressure products were lost by deposition on the surfaces upstream of the FTIR cell. DMMP itself should have reached the gas cell, but at these low flows, transients associated with wall adsorption and desorption resulted in a prohibitively long conditioning time requirement for reliable measurements. Reactions of DMMP and other species in the probe also posed problems in obtaining quantitative species profiles. O_2, N_2, and H_2 are not detectable via IR absorption.

Probe effects

The choking at the probe orifice was experimentally verified by measuring flows of post-flame gases through the probe while varying the back pressure in the sampling system. The flow did not vary as long as the back pressure was below 25 kPa, confirming that flow was choked under sampling conditions.

Literature correlations[318] indicated that the location from which gases were sampled should be approximately 3 orifice diameters, or 0.18 mm, upstream of the probe tip location. However, this was largely irrelevant to the comparison between calculated and experimental profiles, as the calculated profiles were based on temperatures measured using a choked-probe technique that entailed the same location error, as described below. Within 10 orifice diameters, or 0.6 mm, of the burner surface, surface/probe interactions led to sampling of gas from both *downstream* and upstream of the probe.[319] This effect was seen in the overrepresentation of products and under representation of methane in samples taken near the burner surface.

Experiments with varying back pressure and with different probe designs were performed to assess the extent of reactions inside the probe.[320] In these experiments, dependence of species concentrations on the gas residence time in the hot region of the probe was seen as evidence for probe reactions. For undoped flames, the main distortion introduced by the probe was in the post-flame zone, where some conversion of CO to CO_2 was seen. In the flame zone, C_2H_2 was the only species affected by a factor of two reduction in residence time: its concentration dropped by a factor of two. For the preheat and flame zones of doped flames, there was evidence of very significant probe reaction involving CH_2O. All other species changed

concentrations by less than a factor of 1.5 when the probe residence time was lowered by a factor of two (flame zone) or three (preheat zone). Many species concentrations were unchanged, and only CH_3OH changed by more than a factor of 1.3. Under the same conditions, CH_2O concentrations dropped by factors of 4 and 11, respectively, in the flame and preheat zones when residence time was reduced. DMMP conversion to CH_2O by probe reactions was significant in the pre-heat zone. Although CH_2O measurements in this region were not representative of flame concentrations, they were used as an indicator of the presence of DMMP.

Temperature Measurements

Temperatures in the flame zone were measured using the choked probe technique described by Kaiser et al.[319,321] In this method, measured flows through the choked probe were compared to those obtained under reference conditions with known upstream temperature. Approximating the flow as one-dimensional and inviscid, the ratio of unknown to reference temperature was obtained. Two different reference conditions were used: (1) room conditions, and (2) post-flame conditions, where the temperature was measured with a platinum/platinum-rhodium thermocouple and corrected for radiative losses. Calculations based on the two different reference conditions yielded temperatures that differed by less than 4 %. Approximations to fluid properties were estimated to introduce errors between 1% and 2%, depending on the location in the flame.[320]

Materials

The reactants, bought from MG industries, were: CH_4 (99.99 %), O_2 (99.994 %), N_2 (99.998 %), and argon (99.998 %). DMMP (97 %) was bought from Aldrich Chemical Co. and used as is. Calibration curves to quantify the FTIR results used the following gases, bought from MG Industries: CO (99.5 %), CO_2 (99.99 %), C_2H_2 (99.6 %), C_2H_4 (99.9 %), and C_2H_6 (99.0 %). Certified methanol (99.9 %) was bought from Fisher Scientific for methanol calibration. A solution of formaldehyde (37 %) with methyl alcohol (14 %) and water (47 %) was bought from Mallinckrodt Baker for formaldehyde calibration.

Operating Conditions

Table 3-16 shows the operating conditions used in the current work. Four flames in all were studied: fuel-rich doped and undoped, and near-stoichiometric doped and undoped. Doping refers to the addition of a small quantity of DMMP. As can be seen from the table, reactant flows were chosen to match or nearly match several parameters: the reactants' cold flow velocity, the loading of DMMP for the doped cases, the ratio of inerts (N_2 and Ar) to O_2, and the adiabatic flame temperature. In addition, the chamber was at the same pressure and essentially the same inlet gas temperature for all measurements. Within these constraints, conditions were chosen by trial and error to provide a significantly lifted, yet non-cellular flame when DMMP was present.

Table 3-16. Operating Conditions.

	Fuel-rich Flames	Near-stoichiometric Flames
Equivalence ratio	1.13	0.95
Flows (L/min): CH_4	1.61	1.37
O_2	2.84	2.88
N_2	12.48	10.80
Ar	0	1.94
DMMP	9.18E-3 (doped) or 0 (undoped)	9.18E-3 (doped) or 0 (undoped)
Ratio of Ar/N_2 to O_2	4.39	4.42
Cold flow velocity (cm/s)	12.6	12.6
Mole fraction DMMP in doped cases (L/L)	540	540
Adiabatic flame temperature (K)	2093	2139
Pressure (kPa)	0.92	0.92
Inlet gas temperature (K)	376	373

Computational Method

Premixed flame calculations were performed using the CHEMKIN suite of programs.[296] The steady laminar flame calculations used detailed chemical kinetics with mixture-averaged species diffusivities. Thermal diffusion was neglected. Temperature profiles were specified as their measured values.

Two chemical kinetic mechanisms for DMMP combustion were used, referred to in this work as the Babushok[294] and Glaude[307] mechanisms. The mechanisms had in common the mechanism for destruction for small phosphorus compounds developed by Twarowski[258,260,303] but they differed somewhat in the paths for DMMP conversion into the small phosphorus-containing species. The Babushok mechanism had 32 species and 199 elementary reactions. Many Arrhenius parameters came from Werner and Cool's work. In the Werner-Cool mechanism, there some were estimates by the authors, and some heats of formation and activation energies were evaluated by BAC-MP4 calculation. The Werner-Cool mechanism for DMMP destruction was validated with relative species profile measurements from a low-pressure H_2/O_2/Ar premixed flame at 66 kPa,[300] and the Babushok mechanism was validated with data from opposed flow propane/air flames at 85 kPa.[294] Glaude's mechanism for DMMP combustion had 43 species and 537 elementary reactions. It too was based on the work of Twarowski, Melius, Werner and Cool, but included new initial reactions for DMMP destruction. It was validated against Korobeinichev's low pressure premixed flame results.[254,308,310,311] Korobeinichev and coworkers[314] had also proposed an updated kinetic mechanism using the mechanisms of Twarowski and Werner and Cool as their starting point. This mechanism was not evaluated in the present work.

Each of the DMMP combustion mechanisms was combined with the GRI 3.0 methane combustion mechanism,[206,206] from which nitrogen chemistry had been removed. Nogueira and Fisher[320] describe a series of calculations for which GRI 3.0 results were compared to those of a different methane combustion mechanism.[322] GRI 3.0 was selected because it was more successful in reproducing the experimental results for undoped flames, especially for methanol profiles.

Results and Discussion

Temperature profiles

Figure 3-97 shows the temperature profiles obtained with and without DMMP doping. Measurements included duplicate data points taken on different days to ascertain repeatability. Choked flow measurements were processed using room conditions as a reference. Post-flame temperatures measured by thermocouple are presented for comparison. In all cases, the lowest measured temperature was about 250 K higher than that of the reactant stream. This was likely a result of the probe/burner interaction near the burner surface, resulting in sampling from both upstream and downstream of the probe orifice.

Both profiles had the same trend. Near the burner surface, doped and undoped temperatures were nearly the same, with doped slightly higher than undoped. The doped temperature increased less rapidly than the undoped one in the early part of the flame, and then increased more rapidly to achieve approximately the same post-flame value as the undoped case.

The shift of DMMP-doped flames away from the burner surface, seen in Figure 3-97, was interpreted by considering the heat transfer interaction between the flame and the burner surface. As there was a negligible change in cold velocity with doping, the change in position indicated that less heat transfer was required to stabilize the doped flame at a given velocity than was required for the corresponding undoped flame. This difference implied that the adiabatic flame speed of the doped mixture was lower than that of the undoped one, or that the overall reaction rate was slowed by the addition of DMMP. This conclusion was consistent with observations of flame suppression effects of organophosphorus compounds in non-premixed methane flames.[79,119,120] In the absence of a change in adiabatic flame temperature with doping, the flame shift away from the burner should have lead to lower heat loss and thus a higher post-flame temperature in the doped case. Under these conditions, thermocouple measurements suggested that this was a small effect. Temperatures measured by the choked-orifice method were similar for doped and undoped cases at the highest sampling location, but the undoped flame was actually slightly hotter. However, the shape of the curves suggests that the final post-flame temperature had not been reached for some profiles at that location, leading to uncertainty in the final temperatures.

The shift away from the burner, or broadening of the reaction zone, was consistent with the results of Korobeinichev et al. for TMP in a $CH_4/O_2/Ar$ flame at 10 kPa.[309] The lack of significant effect of the additive on final temperature, however, was different from Korobeinichev's observations, which indicated that doped final temperatures exceed the corresponding undoped ones by about 200 K. Korobeinichev et al. attributed this higher temperature to the lower heat loss and more complete combustion in the doped case. As observed by Korobeinichev,[309] organophosphorus additives had a distinctly different effect on lower-pressure hydrogen flames, narrowing the reaction zone and raising the final temperature by 350 K to 450 K.[254,300,310] This change from promotion to inhibition behavior was predicted by low pressure flame speed calculations performed by Korobeinichev and coworkers,[309] who offered a qualitative explanation for it based on the effect of radical termination reactions on the heat release rate. Korobeinichev and co-workers[309] observed that the inhibitory behavior of organophosphorus compounds increased with pressure, and was greater in methane than in hydrogen flames. The current experiments, performed at still higher pressures, confirmed this trend.

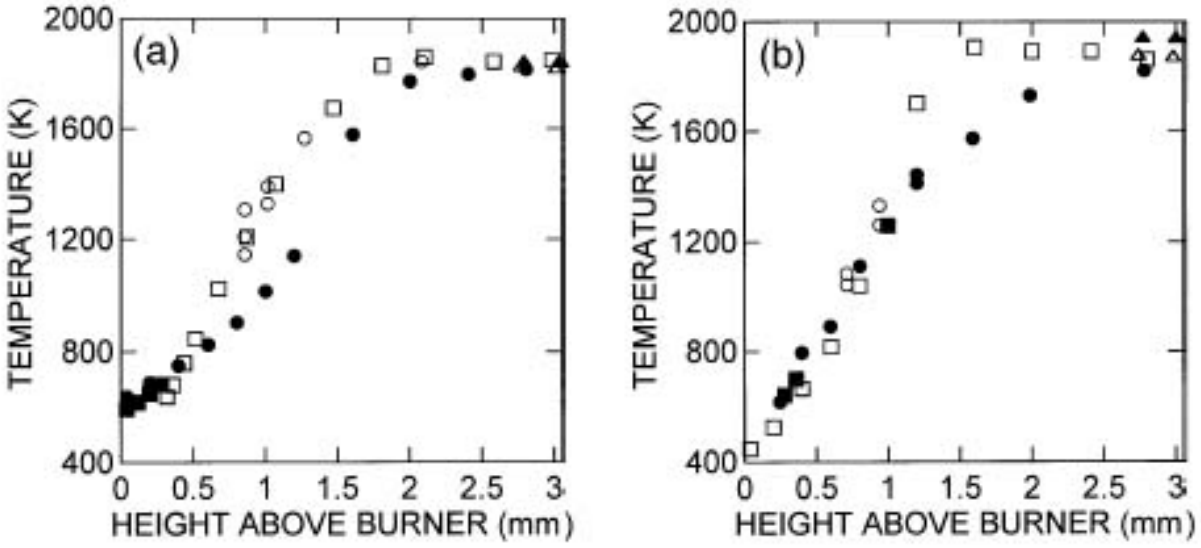

Figure 3-97. Temperature Profiles Measured in (a) Rich and (b) Near-stoichiometric Flames. Filled symbols: doped flames. Open symbols: undoped flames. Squares: data from larger probe. Circles: data from smaller probe. Triangles were taken with thermocouples.

Comparison of Doped and Undoped Profiles

Figure 3-98 through Figure 3-105 are profiles for the eight measured species. Each profile shows undoped and doped experimental results (symbols), along with computational results (lines). In each figure, the dashed line is the undoped calculation using the GRI 3.0 mechanism, while the dotted and solid lines are the doped calculations with Glaude and Babushok mechanisms, respectively. Each profile includes some data points acquired on a different day, with a different probe orifice diameter, as indicated in the figure captions.

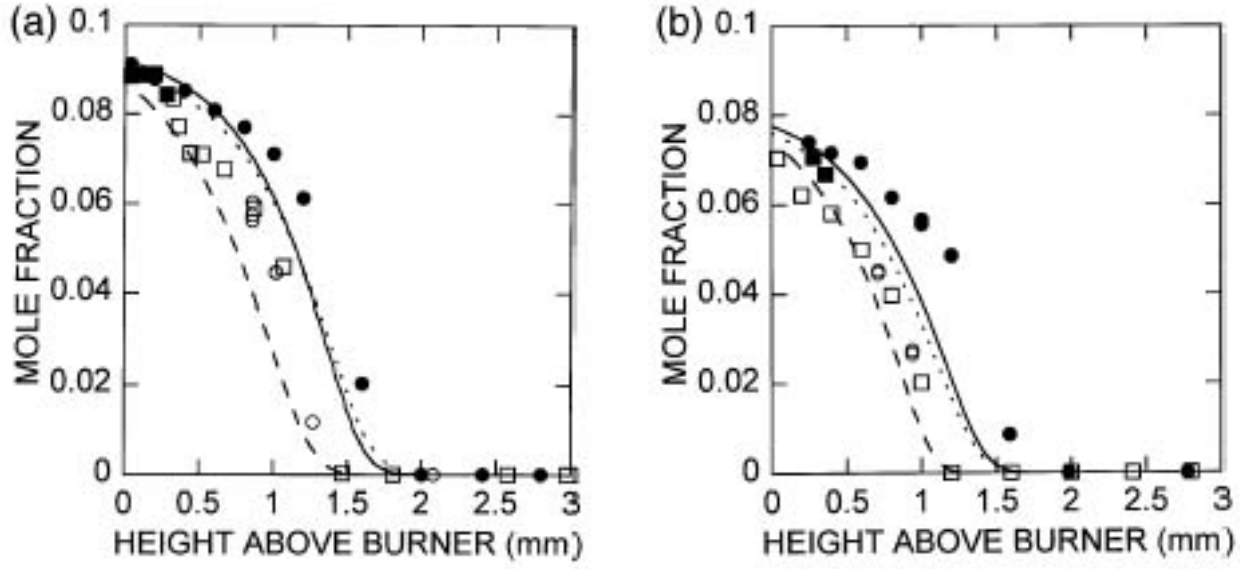

Figure 3-98. CH_4 in Doped and Undoped (a) Rich and (b) Near-stoichiometric Flames, with GRI (undoped) and Babushok and Glaude (doped) Predictions.

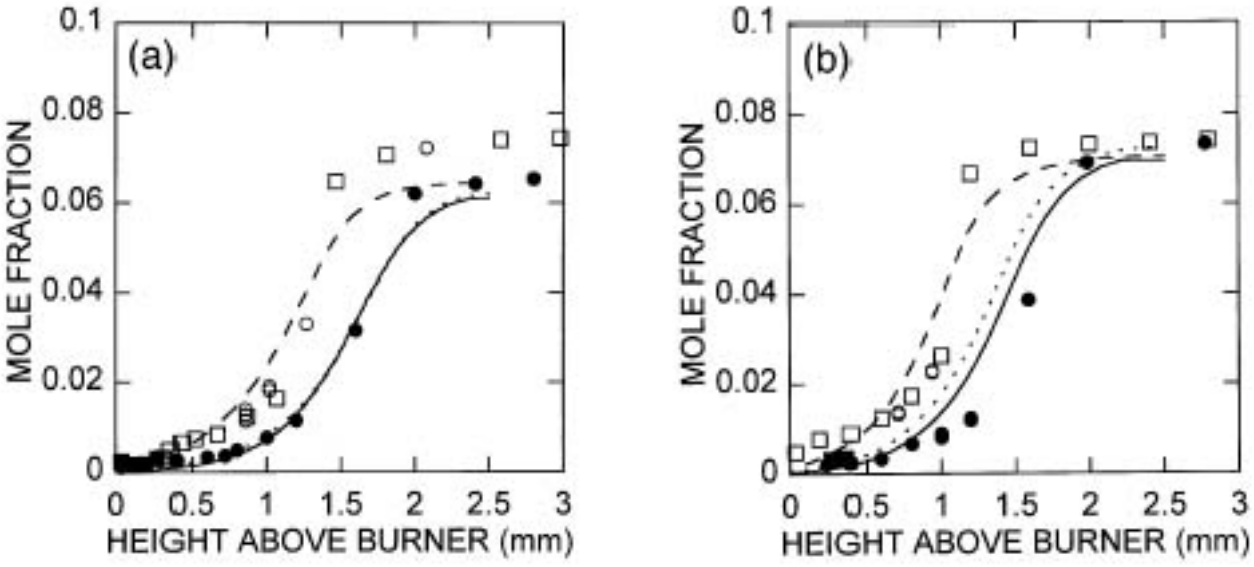

Figure 3-99. CO_2 in Doped and Undoped (a) Rich and (b) Near-stoichiometric Flames, with GRI (undoped) and Babushok and Glaude (doped) Predictions.

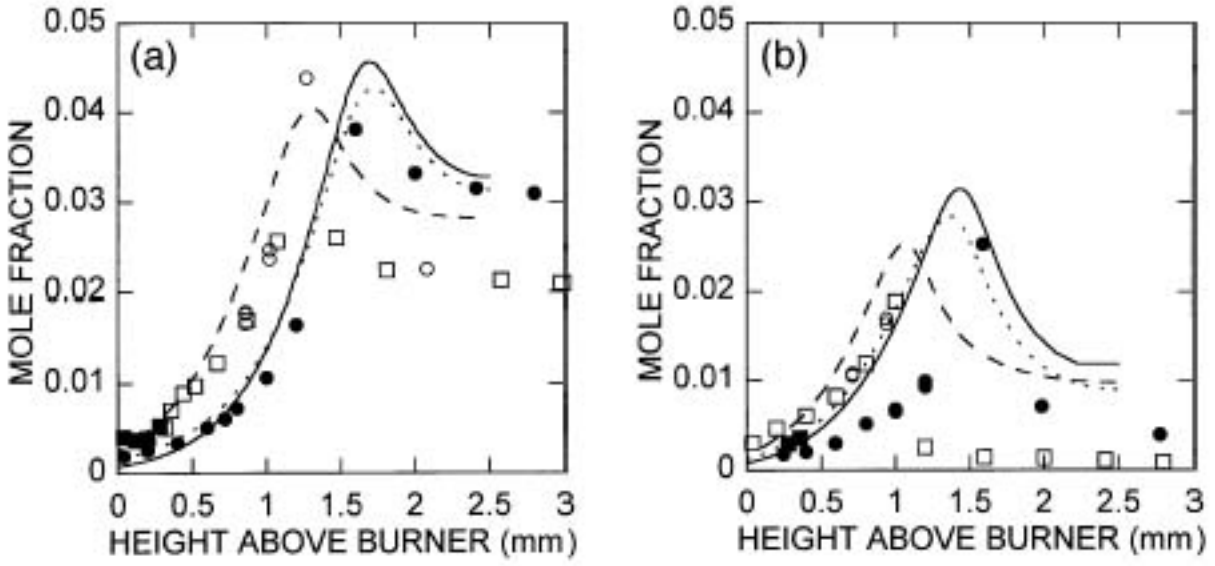

Figure 3-100. CO in Doped and Undoped (a) Rich and (b) Near-stoichiometric Flames, with GRI (undoped) and Babushok and Glaude (doped) Predictions.

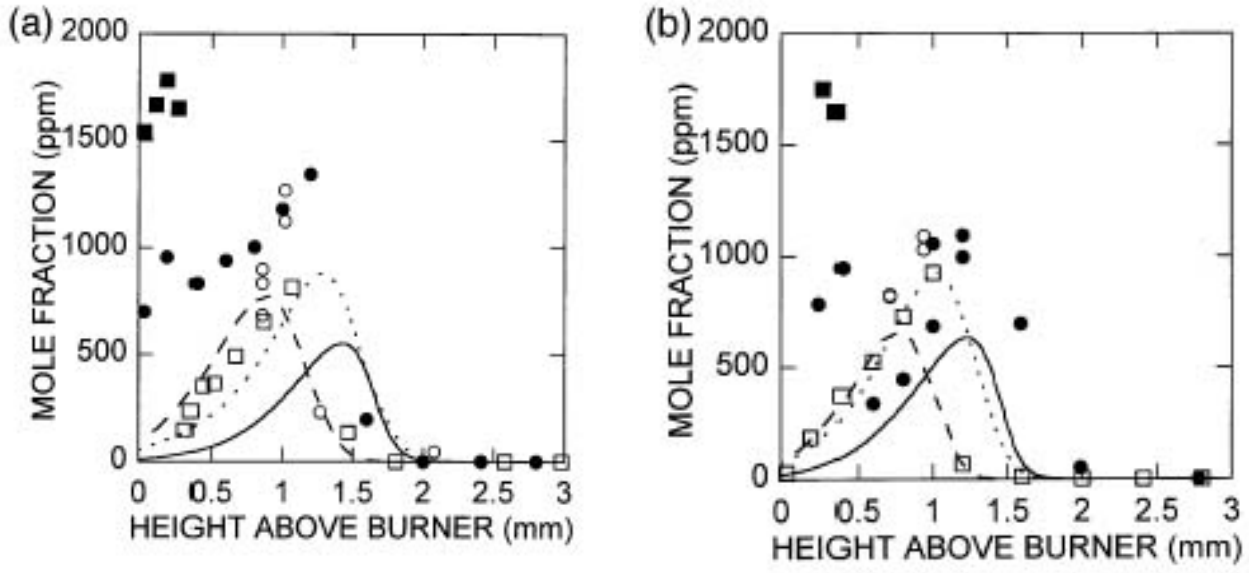

Figure 3-101. CH_2O in Doped and Undoped (a) Rich and (b) Near-stoichiometric Flames, with GRI (undoped) and Babushok and Glaude (doped) Predictions.

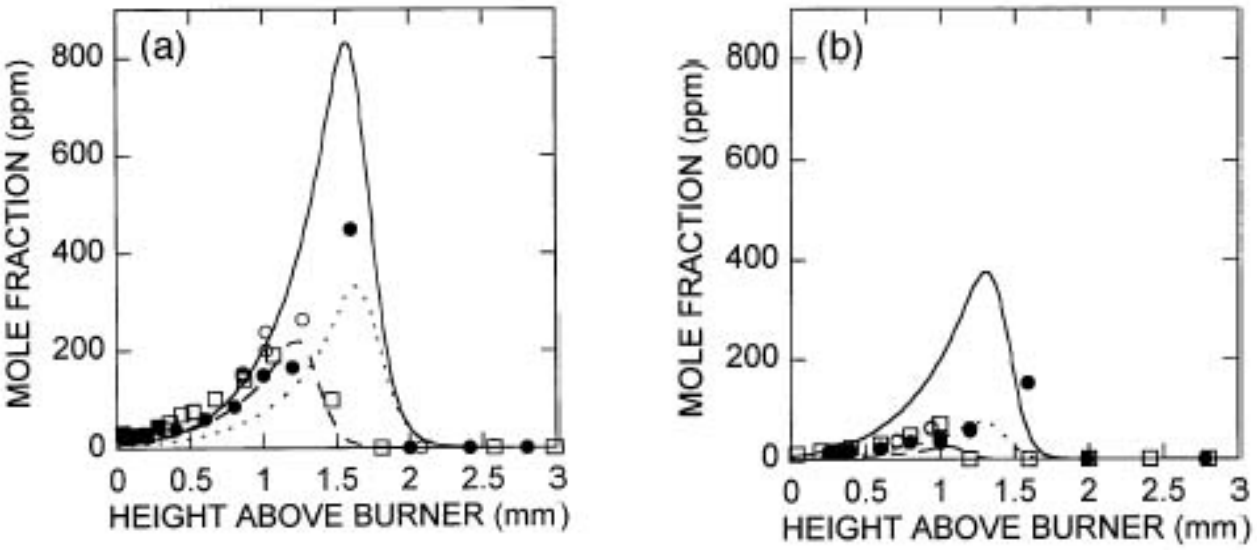

Figure 3-102. C_2H_2 in Doped and Undoped (a) Rich and (b) Near-stoichiometric Flames, with GRI (undoped) and Babushok and Glaude (doped) Predictions.

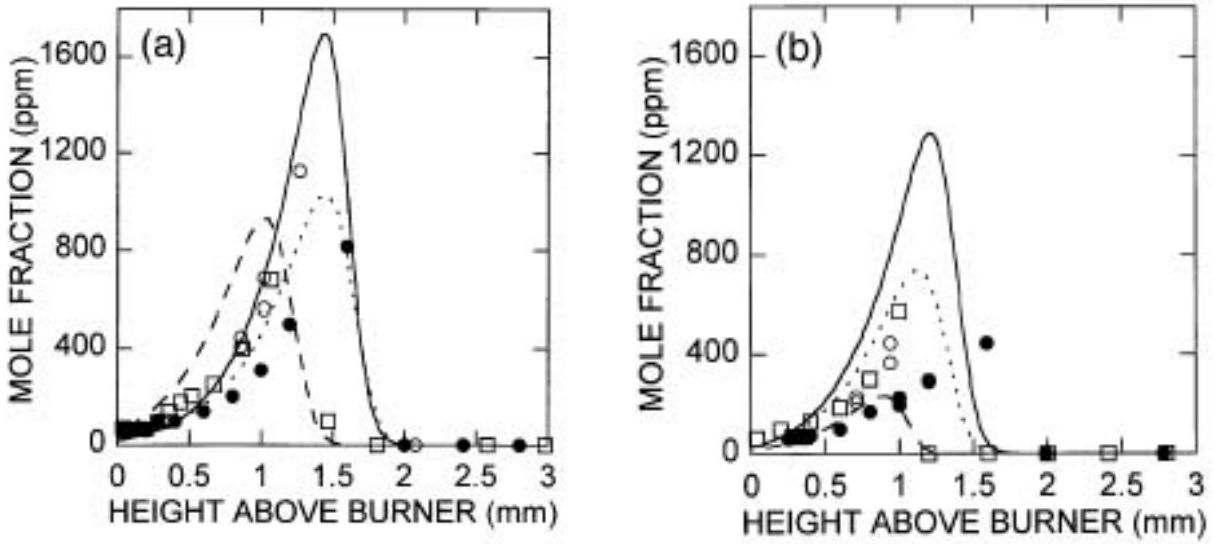

Figure 3-103. C_2H_4 in Doped and Undoped (a) Rich and (b) Near-stoichiometric Flames, with GRI (undoped) and Babushok and Glaude (doped) Predictions.

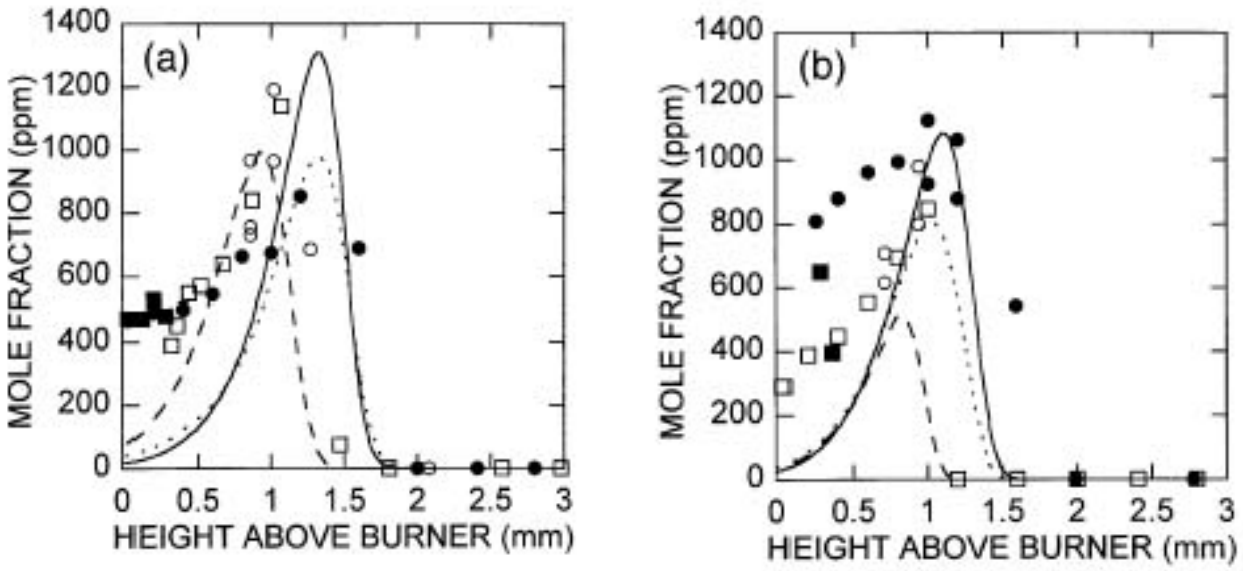

Figure 3-104. C_2H_6 in Doped and Undoped (a) Rich and (b) Near-stoichiometric Flames, with GRI (undoped) and Babushok and Glaude (doped) Predictions.

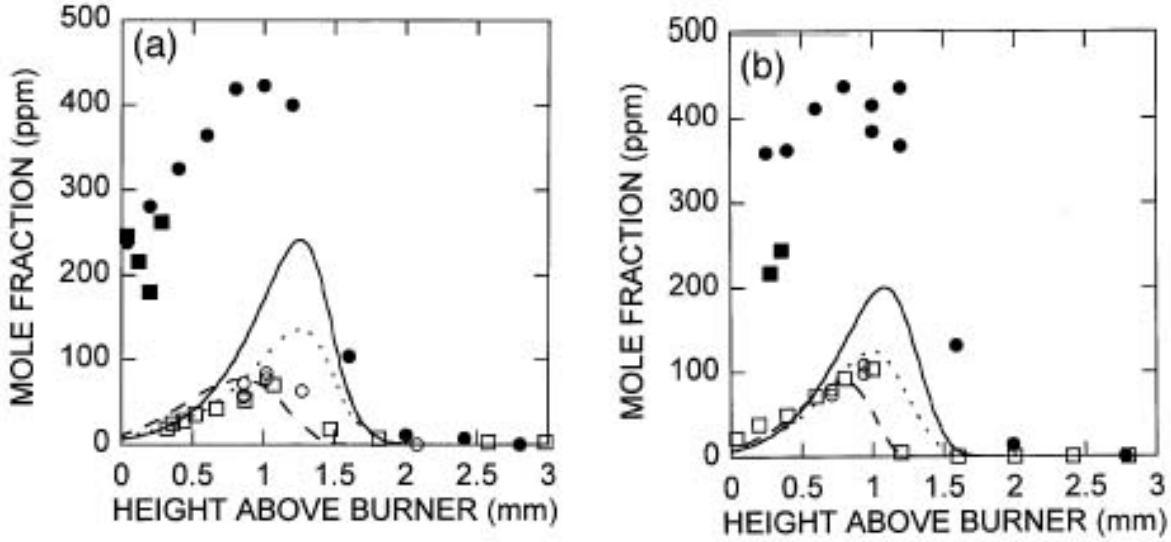

Figure 3-105. CH_3OH in Doped and Undoped (a) Rich and (b) Near-stoichiometric Flames, with GRI (undoped) and Babushok and Glaude (doped) Predictions.

Doping the flame shifted all species profiles downstream, similar to the behavior of the temperature as described above. The magnitude of this shift was best evaluated from the monotonic CH_4 or CO_2 profiles, as the axial spacing of sampling locations was too large to allow reliable comparisons of peak locations for intermediate species. These profiles were fitted to a scaled Weibull cdf form to reduce the impact of noise. Defining the shift as the change in position in the curve fit where half the initial methane was consumed, the experimental values were 0.33 and 0.49 mm for the rich and near-stoichiometric flames, respectively. Similarly, using the location where CO_2 reached half its maximum value, the experimental shifts were 0.34 and 0.53 mm, respectively. Thus, DMMP consistently had a larger effect on flame location for the near-stoichiometric than for the rich flame under these conditions, and defining flame position in terms of fuel or product profiles yielded similar shifts.

The sampling technique produced artifacts in some profiles, most notably CH_2O. For this species, two peaks can be seen in each of the experimental doped profiles, while the undoped experimental profiles and all the computational profiles show single peaks. The earlier doped peak occurs 0.25 mm from the burner for both equivalence ratios, and was likely due to probe reactions. The location of the first peak close to the burner surface suggested that the upstream peak came directly from DMMP destruction, but the low temperatures (700 K) and presumed low radical levels there implied that destruction of significant quantities of DMMP in the free stream was very unlikely.[264] The magnitude of this peak increased strongly with probe residence time, as shown in the back pressure experiments described in the previous section. The current data set showed further evidence of this dependence: The highest values of CH_2O in Figure 3-101 were repeat data points measured using slightly smaller probe orifice diameters than the other data points. The points taken with the smaller probe orifice (and corresponding longer residence time in the probe with choked flow) had much higher CH_2O levels than the points taken with the larger probe orifice. Although it was a sampling artifact, this upstream CH_2O peak provided information about the DMMP profile. The drop in CH_2O levels at 0.25 mm above the burner indicated that DMMP levels in the gas stream entering the probe began to drop at this location.

For most intermediates, there was no clear change in peak height due to doping. The measured peak height changed with doping by about a factor of two for C_2H_2, about a factor of 1.5 for CO and for the second peak of CH_2O, and by smaller amounts for C_2H_2 and C_2H_6. In each of these cases, a narrow peak along with limited spatial resolution made it hard to determine whether the true height had been sampled.

CH_3OH levels, on the other hand, showed a dramatic change in peak height with doping, increasing by factors of seven and four for the rich and near-stoichiometric cases, respectively. The broad peak shape (see Figure 3-105 greatly reduced uncertainty due to limited spatial resolution of sampling. Accounting for probe reactions would have increased the difference between doped and undoped profiles, as can be seen from the doped data points taken with smaller probe orifice size (longer residence time). Werner and Cool[300] did not measure methanol and formaldehyde because the energy needed for their ionization was above the capability of their apparatus. Korobeinichev and co-workers[254,308,310] did not report profiles for these species.

Comparison between Experimental and Computational Profiles

Figure 3-98 through Figure 3-105 also show how successful the two chemical kinetic mechanisms for phosphorus[313] combustion (Babushok and Glaude) were at duplicating experimental data in doped flames. (The first experimental CH_2O peak was excluded from the comparison below as it was considered a sampling artifact.) Using the GRI-MECH predictions of undoped species profiles as a benchmark, the

phosphorus mechanisms were as successful as the GRI mechanism. All mechanisms successfully predict the direction of change in peak height when the equivalence ratio changed from rich to near-stoichiometric for CH_2O, CO, C_2H_2, and C_2H_4, and all mechanisms failed for C_2H_6. For CH_2OH, GRI failed while the Babushok and Glaude mechanisms succeeded. None of the mechanisms succeeded in predicting the ranking of peak heights in a particular doped or undoped flame.

More quantitatively, in predicting peak heights, the Glaude mechanism for doped flames was roughly equally successful to the GRI mechanism for undoped flames. Glaude's fractional differences in peak height between experiment and calculation were smaller than or about the same magnitude as the corresponding GRI values for all species except CH_3OH. Babushok's mechanism was less successful, producing larger fractional differences than GRI for all cases except C_2H_6 in the near-stoichiometric flame and CO in both flames. In the case of over-predictions, these discrepancies must be viewed with some caution because true peaks may not be sampled experimentally. Another explanation for some differences was probe reactions, which produced changes of 30 % or so in most species concentrations in the flame zone. The discrepancies between experiment and calculations with the Babushok mechanism clearly exceeded errors due to probe reactions (i.e., exceeded the observed sensitivity to probe residence time) only for C_2H_2, C_2H_4, and CH_3OH.

Methanol computational results showed large discrepancies with experiment for both phosphorus combustion mechanisms. Qualitatively, the mechanisms succeeded in predicting that the doped CH_3OH peak was higher than the undoped peak. However, they predicted the peak to be too narrow and located too far downstream, and they substantially underpredicted its height. Babushok and Glaude mechanisms predicted that the CH_3OH peak height increased, respectively, by factors of 1.4 to 1.8 and 2.2 to 3.2 over the undoped calculated values. The experimental increase was by factors of 4 (near-stoichiometric) and 7 (rich). This difference indicated an area in which improvements to both mechanisms are needed. The early location of the start of the doped CH_3OH peaks suggested that CH_3OH was an important intermediate in the early decomposition process for DMMP.

Both phosphorus mechanisms agree with experiments in predicting that doping produced a downstream shift of species profiles. The magnitude of the shift was similar for the two mechanisms, an expected result, as calculations with both mechanisms made use of the same specified experimental temperature profiles. The two calculations predicted almost identical shifts in the rich case for all species. In the near-stoichiometric flame, the shift was somewhat larger for Babushok than for Glaude, especially for CH_2O. With the measures of shift size based on the position where CH_4 concentration was half of the initial concentration as described in the previous section, Glaude and Babushok gave almost identical shifts for the rich case, while Babushok's shift was 30 % larger in the near-stoichiometric flame. In comparison to experimental shifts, calculations were about 20 % too large in the rich flame, and about 45 % too small in the near-stoichiometric flame. Both mechanisms failed to predict that the shift in the near-stoichiometric flame was greater than the one in the rich flame. The magnitudes of the shifts were predicted slightly better by Babushok than by Glaude.

It is important to note that in the current work Glaude's and Babushok's phosphorus mechanisms were combined with the same methane combustion mechanism (GRI 3.0). It is possible that either mechanism would make more successful predictions when used with the methane combustion mechanism with which it was developed.

3.4.4 Summary: Phosphorus-containing Compounds in Flames

A novel method for performing repeatable extinction measurements was developed to maintain constant loadings of phosphorus-containing compounds (PCCs) in the oxidizer stream using syringe pump delivery. This method requires that the locations of the flame and stagnation plane relative to the nozzles change during an extinction measurement. The global extinction strain rate was invariant (within ± 2 %) over a broad range of flame locations for methane-air non-premixed flames. Findings using these flames and this technique included:

- Extinction measurement and OH reduction were equivalent markers of agent effectiveness.
- Phosphorus-containing compounds can be 40 times more effective than nitrogen and 2 to 4 times more effective than CF_3Br at quenching non-premixed hydrocarbon flames.
- DMMP and TMP were roughly equivalent in suppression efficiency, independent of the differences in their ligands.
- DMMP was more effective when added to the air side – as in fire suppression.
- The effectiveness of DMMP has a strong temperature dependence, with lower effectiveness at higher adiabatic flame temperatures.
    - These very high temperatures were well above those in ordinary hydrocarbon fires.
    - A mixture of inert and phosphorus-based suppressants could interact synergistically as the physical agent cools the flame, thus increasing the efficiency of the chemically active component.
- Current computational models adequately (but somewhat under-) predicted the effect of DMMP on flame extinguishment. This may have been due to the significant uncertainties in several of the reaction rate coefficients in the phosphorus mechanism.
    - The direct role of the phosphorus-containing species in the flame was the fast removal of H and O atoms, leading indirectly to a decrease in OH.
    - Inhibition was due to the phosphorus-containing radicals, PO_2, HOPO, and $HOPO_2$, formed after the decomposition of the parent compound.
    - PCC flame inhibition does not depend on the form of the parent compound, provided that the parent breaks down in the flame. Thus, a broad class of potential PCC fire suppressants should exist, from which an alternative to halons with minimal health and environmental impact may be selected.

Additional experiments with methane-nitrogen-oxygen-argon premixed flames showed:

- DMMP addition caused a downstream shift of temperature profiles and all species profiles except CH_3OH. This shift was a consequence of the flame inhibition properties. The magnitude of the shift was over 50 % greater for a near-stoichiometric flame than for a rich flame.
- Flame calculations again were reasonably successful in predicting the effects of DMMP on the flame.

3.5 COMPARATIVE FLAME INHIBITION MECHANISMS OF CANDIDATE MOIETIES

3.5.1 Introduction

A goal of NGP research was to develop a unified understanding of flame inhibition and extinguishment, so that basic principles could then be used to interpret data from a wide range of inhibitors, as well as a wide range of fire scales. The following sections present work to that end. Since the mechanisms of chemically acting fire suppressants were widely believed to involve recombination of free radicals in the flame, radical concentrations measurements were made for flames with addition of various inhibitors, including CF_3Br. Since CF_3Br was often used as the benchmark for comparison of new agents, an analytical study was undertaken to determine if its mechanism is representative of chemically acting inhibitors in general, or a special case. Further work sought to correlate the effectiveness of agents with the bond strength of the active intermediates. Finally, an idealized inhibitor was used to investigate the properties of the flames themselves which lead to the most effective inhibition.

3.5.2 Spectroscopic Studies of Inhibited Opposed Flow Propane/Air Flames

Introduction

Skaggs and co-workers[93] applied optical diagnostics and chemical modeling to a propane-air, opposed flow, non-premixed flame to investigate the similarities and differences among the characteristics of flames inhibited and extinguished by a diversity of additives:

- N_2 represented purely physical influence on flame inhibition since it has no chemical inhibition capability.
- HFC-227ea (C_3F_7H) and HFC-236 ($C_3F_6H_2$). Hydrofluorocarbons, although they typically increase the heat release rate in the flame, also remove H atoms from the reaction zone and reduce the overall reaction rate.[323]
- $Fe(CO)_5$ is a highly efficient flame inhibitor. It is chemically active and representative of a class of metal-containing compounds.
- DMMP ($CH_3P(O)(OCH_3)_2$) and PN (cyclo-$P_3N_3F_6$) are also efficient chemically active inhibitors, representative of phosphorus-containing compounds.
- Halon 1301 (CF_3Br) is both an efficient halogenated fire suppressant and the reference agent for the NGP.

Experimental

The flame imaging experiments were conducted using the arrangement presented in Figure 3-106**.** All flames were at atmospheric pressure and consisted of 7.0 L/min synthetic air (79 % N_2 + 21 % O_2) flowing from the lower duct, and 5.6 L/min of propane flowing from the upper duct. The oxidizer and fuel ducts were separated by a distance of 1.2 cm, and the duct diameters were each 2.54 cm. The inhibitors were added to the oxidizer flow in gaseous form at room temperature with the exception of $Fe(CO)_5$, which was cooled to 11°C and DMMP which was heated to 70°C. Based on the flow conditions

and duct separation, the luminous flame zone was located on the oxidizer side of the stagnation plane, and the global strain rate was calculated to be 72.5 sec^{-1}.[76] The burner apparatus was located inside a stainless steel hood to contain any toxic fumes that were exhausted from the burner.

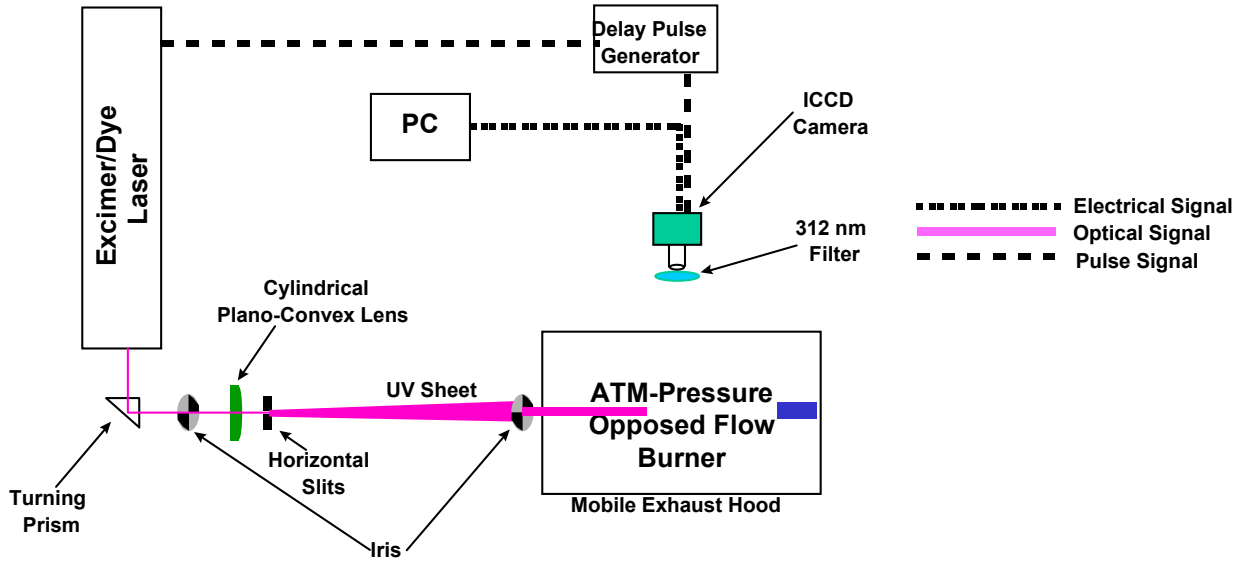

Figure 3-106. Schematic Diagram of the Experimental Apparatus.

Previous studies of non-premixed propane/air flames had experimentally determined global extinction strain rates of 489 s^{-1}.[324] A decrease in the extinction strain rate was used as an indicator of an inhibitor's efficiency.

Planar laser induced fluorescence (PLIF) and laser induced fluorescence (LIF) were used to measure the H atom, O atom, and OH radical species concentrations as flame extinction was approached. These measurements complemented the extinction strain rate by illustrating an inhibitor's influence on the radical concentration profiles in the flame zone which indicated if the flame's radical chemistry was being perturbed by agent addition.

PLIF images were measured using a Lambda Physik excimer/dye laser system. This system consisted of a Lambda Physik Compex 102 XeCl excimer laser, a Scanmate 2 dye laser (Coumarin 153) and a Second Harmonic Generator (SHG). The fundamental output of the dye laser (560 nm wavelength) was frequency doubled in the SHG unit with a BBO crystal to approximately 281 nm. The UV laser radiation was tuned to the peak of the $R_2(9.5)$ transition at 281.8 nm ((1,0) $A^2\Sigma^+ \leftarrow X^2\Pi$).[158-160] The UV light output of the SHG unit entered an optical train where the beam is turned 90°, apertured by a sub mm iris, projected through a cylindrical plano-convex lens to form the UV beam into a vertical sheet. To create a uniform sheet width, the sheet was apertured with 0.5 mm vertical slits as it was projected toward the center of the burner. The UV sheet was apertured just before the burner to produce a vertically uniform intensity that was 1.2 cm in height, allowing passage through the entire burner flow field. The OH fluorescence passed through a band pass filter centered at 312 nm with a 11 nm bandwidth and was detected with a Princeton Instruments ICCD camera (Model 120) coupled with a Nikon UV lens located at 90° with respect to the UV sheet. The ICCD camera, which had an active area of 384 x 576 pixels, had a field of view with this optical arrangement of approximately 33 cm^2 and each image recorded was acquired with 25 total

accumulations on the camera. With this arrangement, the entire relative OH concentration profile was obtained.

Laser induced fluorescence excitation spectra were measured in the flame using the same excimer/dye laser system. This arrangement has been utilized before for similar measurements.[157] The UV laser radiation was scanned from 281.5 nm to 282 nm.[158-160] Low laser energies were used, and the laser was operated in the linear regime. The UV light output of the SHG unit was focused to the center of the burner 30 cm focal length fused silica lens and had a vertical and horizontal beam waist of 0.4 and 0.5 mm, respectively. Fluorescence was collected at 90º to the direction of the excitation laser beam, focused through an 0.5 mm iris to define the collection volume, passed through a band pass filter centered at 312 nm with an 11 nm bandwidth, and detected by a photomultiplier tube (PMT) (Phillips Model XP2018B).

Before inhibitor addition, the uninhibited flame was profiled using LIF between the fuel and oxidizer ducts to obtain a profile of the uninhibited temperature values. To expedite measurements upon addition of an inhibitor, the burner was translated about ± 1 mm around the OH maximum, and excitation spectra were collected. Each excitation spectrum was fit using a non-linear least squares algorithm to obtain the OH rotational temperature for the spectral measurement.[160]

Results

Figure 3-107 presents two representative, two-dimensional images of OH fluorescence for an uninhibited propane-air flame and for a propane-air flame to which CF_3Br was added (1.5 % by volume).

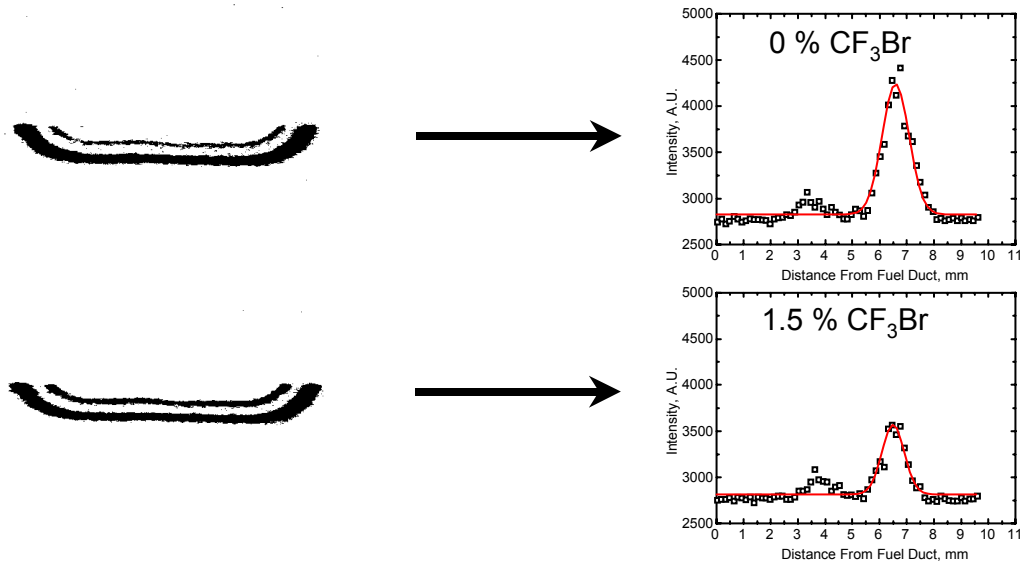

Figure 3-107. Representative PLIF Images and the Corresponding OH Intensity Profiles from an Opposed Flow Propane-air Flame Seeded with 0 % (by volume) CF_3Br and 1.5 % (by volume) CF_3Br. The fuel and air ducts are at the top and bottom of each PLIF image.

Both images, which were uncorrected for laser energy fluctuations and local quenching rates, illustrated the presence of two luminous zones as the UV sheet passed through the flame. The lower, thicker zone

was the fluorescence from the OH transition while the upper, thinner zone was the broadband fluorescence due to derivative fuel species such as polycyclic aromatic hydrocarbons. To construct a spatially resolved OH LIF profile from an OH PLIF image, as shown on the right hand side of Figure 3-107, the pixel intensity corresponding to a given height between the fuel and oxidizer ducts (spatial resolution approximately 0.149 mm/pixel) was summed and averaged over a 1 mm horizontal width. The two-dimensional images and LIF profiles illustrated that addition of CF_3Br to the propane flame caused a decrease in the OH fluorescence signal while the broadband fluorescence increased just slightly. Similar results had been observed previously for CF_3Br addition to hydrocarbon diffusion flames.[51,156]

Table 3-17 lists the measured inhibitor concentrations in the air stream at extinction and their estimated uncertainties.

Table 3-17. Inhibitor Concentrations (% by volume) and Uncertainty (± % by volume) at Flame Extinction.

	Inhibitor						
	N_2	**CF_3Br**	**HFC-236**	**HFC-227ea**	**PN**	**DMMP**	**$Fe(CO)_5$**
Extinction Concentration	23.1	2.3	6.1	5.3	2.7	0.3	0.2
Estimated Uncertainty	8.20	0.93	1.29	1.08	1.00	0.04	0.03

- The extinction concentration for CF_3Br was similar to cup burner values, 2.90 %[325], but slightly lower than values obtained in a co-flowing propane-air flame and a co-flowing propane-air cup burner, 4.1 % and 4.3 %, respectively.[21,51]
- HFC-227ea and HFC-236 had extinction concentrations that were above double that for CF_3Br, consistent with cup burner values of 6.3 % and 6.6 %, respectively.[325]
- For the phosphorus compounds, PN had an extinction concentration similar to CF_3Br, while DMMP's value was seven to eight times lower than CF_3Br. Previous studies by MacDonald et al.[79,120] had shown DMMP to be two to four times more effective than CF_3Br. However, Fisher et al.[324] reported that for an opposed flow propane-air flame with DMMP added to the air stream, a 25 % decrease in the normalized extinction strain rate corresponded to a DMMP concentration ≈ 1200 μL/L. Linear extrapolation of the cited Fisher et al. data[324] to the strain rate used for the opposed flow, propane-air flame studied here gave a DMMP concentration of 4080 μL/L to 6500 μL/L or 0.4 % to 0.65 % by volume. The DMMP concentration obtained from the extrapolated strain rate data supported the DMMP extinction concentration determined in this study. For PN, cup burner experiments had found an extinction concentration of 1.08 % by volume.[249] The results reported here for PN and DMMP were of concern for several reasons. First, the obtained value for PN was higher, while the DMMP value was lower than other cited experiments. Second, it was assumed prior to these experiments, that if a given compound contained a phosphorus atom, then regardless of its chemical structure, similar extinction concentrations would be observed. A possible explanation for the contrasting behavior between the two phosphorus agents is that the resonant P-N ring structure of PN could be very stable and thus less efficient at delivering phosphorus to the flame.[326]

Figure 3-108 contains the results of the analyzed OH profile areas vs. each agent's concentration as the flames were stepped towards extinction. The reported OH profile areas were averaged over three or more

separate inhibitor extinction experiments, where the data for each experiment were normalized to the [OH] profile area measured in the uninhibited flame acquired prior to each inhibitor extinction experiment to account for changes in burner and camera conditions. The data indicated that there were both physical and chemical modes of inhibition being observed for the agents studied. That is, N_2 which is chemically inert, had the least impact on [OH] with respect to the other agents studied. For the concentration range plotted in Figure 3-108**,** the flame was not even extinguished by N_2. Similar results were observed for the two fluorinated propanes which showed initially small declines in [OH], but more rapid decreases just before extinction. Addition of the other inhibitors showed precipitous decreases in the measured [OH] values up to the extinction concentrations where the data decreased more gradually, as highlighted for DMMP and $Fe(CO)_5$ with the inserted graph in Figure 3-108.

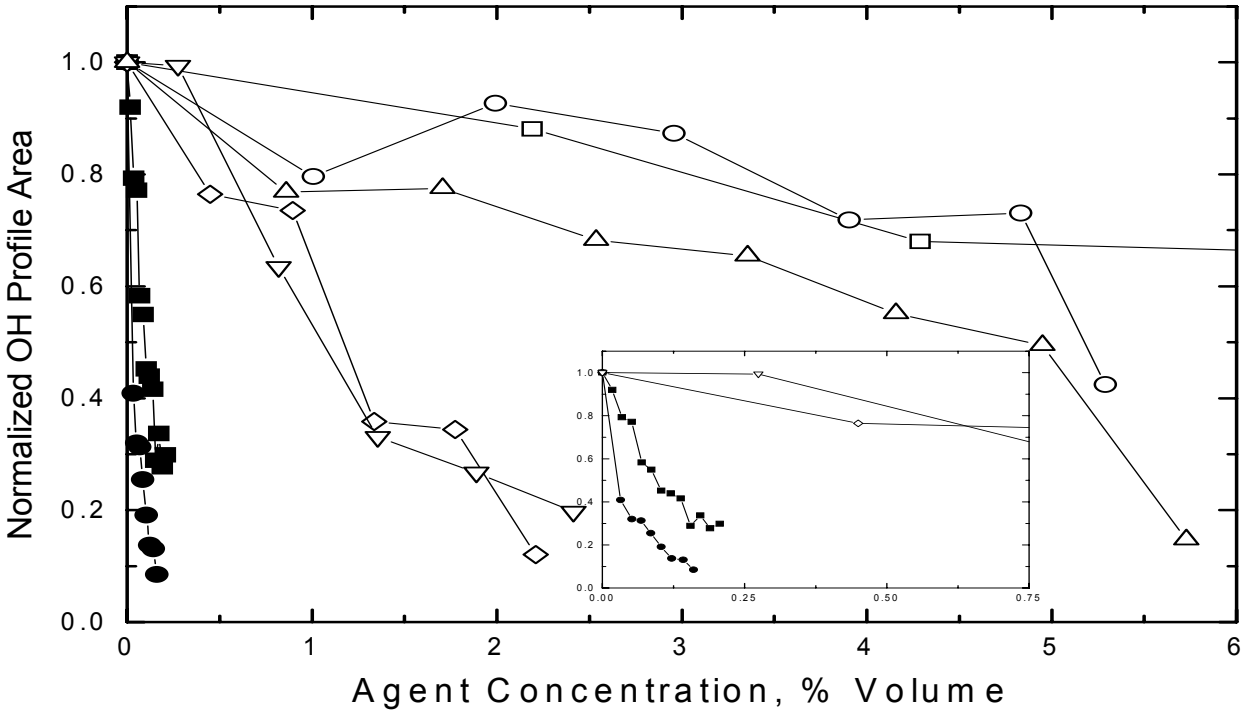

Figure 3-108. Normalized OH LIF Profile Areas vs. Inhibitor Agent Delivery Concentrations. □: N2, O: HFC-227ea, Δ: HFC-236, ▽ : PN, ◊: CF3Br, ■: DMMP, and ●: Fe(CO)5. Insert: Expanded data for PN, CF3Br, DMMP, and Fe(CO)5 Concentrations up to 0.75 % by Volume.

The addition of an inhibitor can change the position and width of the flame's reaction zone. Previous studies had shown[168-170,172,173] that a decrease in the flame's reaction zone width indicated increased localized strain, which can cause local quenching or flame extinction.[171] For the analysis of reaction zone modifications and relative OH concentrations, each OH intensity profile was fit to a Gaussian function. The area under the Gaussian profile curve provided a general indicator of the entire OH population for a given flame condition. The width of the flame's reaction zone was characterized by the width of a radical profile.[173] The width of the flame's reaction zone was defined here as the distance of one half of the maximum intensity of the Gaussian OH profile which was similar to previous studies[170] that estimated the width of a laminar flame reaction zone using one half of the maximum value of a temperature profile.

Table 3-18 lists the measured flame widths determined from the relative OH concentration profiles for each flame situation studied. For the inhibited flames, the widths were measured at 50 % of each agent's determined extinction concentration. The uncertainty in the reported widths due to measurement variance was 11 %.

Table 3-18. Measured OH Profile Widths (FWHM, mm) for the Uninhibited Flame and Inhibited Flames at 50 % of the Inhibitor Extinction Concentrations.

Agent	OH Profile Width, mm
Uninhibited	1.30
N_2	1.24
FE-36	1.31
FM-200	1.26
CF_3Br	0.96
PN	0.96
DMMP	1.04
$Fe(CO)_5$	0.83

The Table 3-18 width values indicated that the widths for N_2, FE-36, and FM-200 were not significantly different from the uninhibited flame. By contrast, CF_3Br, PN, DMMP, and $Fe(CO)_5$ exhibited width changes that were at least 20 % of the uninhibited width value. The OH width trends suggested that inhibitor agents with more physical inhibition capabilities exhibited less effect on the flame structure than inhibitors with enhanced chemical inhibiting capabilities.

Similar trends were expected for the peak flame temperatures. Figure 3-109 presents a plot of peak LIF measured flame temperatures vs. agent delivery concentrations for each inhibited flame. The peak flame temperature for the uninhibited flame was between 2125 K and 2200 K. The obtained temperature values for N_2 and FM-200 were not statistically different from those measured in the uninhibited flame with an estimated uncertainty of ± 300 K. For CF_3Br and PN, temperature differences with respect to the uninhibited flame were not observed until near extinction concentrations were added. Previous studies of an atmospheric pressure, axisymmetric propane/air flame inhibited by addition of CF_3Br to the oxidizer flow, found only small temperature differences in comparison with the uninhibited flame.[36,51] By contrast, Masri et al.[156] reported for a non-premixed atmospheric pressure CH_4-air flame, that higher temperatures existed in the reaction zone of a CF_3Br inhibited flame than in the reaction zone of an uninhibited flame near extinction. With mixed results from previous investigations and the large degree of uncertainty in these measurements, the only creditable temperature values are those close to extinction. For $Fe(CO)_5$ and DMMP, temperature decreases with respect to the uninhibited flame were not observed until proximal extinction concentrations were reached as well. On a concentration basis, $Fe(CO)_5$ and DMMP had decreased flame temperatures, $T \approx 1700$ K, at agent concentrations lower than the other agents studied. For $Fe(CO)_5$, small decreases in flame temperatures had been observed by Brabson et al.[327] in studies of low-pressure premixed flames inhibited by $Fe(CO)_5$.

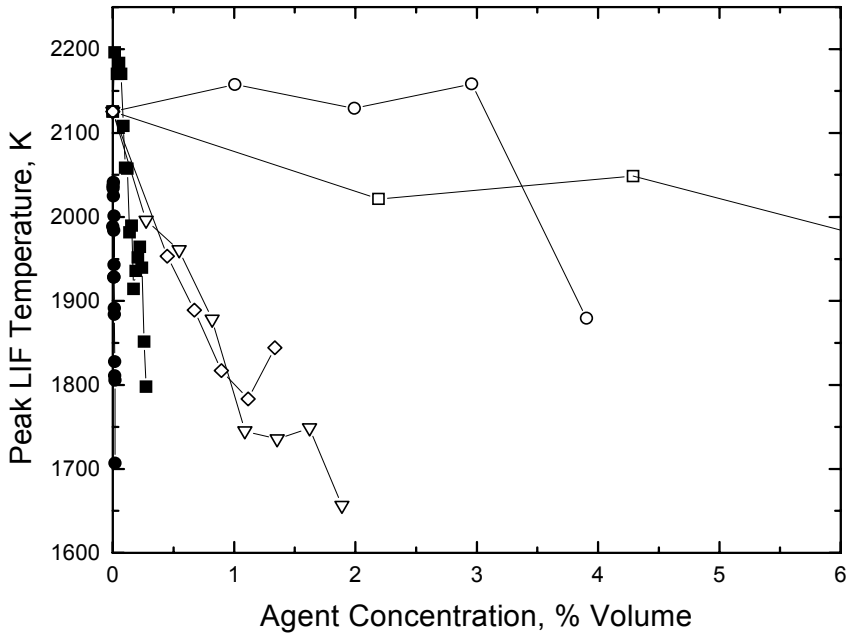

Figure 3-109. Peak LIF Measured Temperatures (K) vs. Inhibitor Delivery Concentrations. Data Legend: □: N_2, O: HFC-227ea, Δ: HFC-236, ▽: PN, ◊: CF_3Br, ■: DMMP, and ●: $Fe(CO)_5$.

Numerical Modeling

Numerical modeling of a stoichiometric, premixed, propane-air flame inhibited by DMMP, $Fe(CO)_5$, CF_3Br, and N_2 flame was carried out using the CHEMKIN suit of programs.[204] For the simulations, a kinetic model for propane combustion developed by Marinov et.al.[328-330] was slightly modified and combined with a C1-C2 hydrocarbon kinetic model[52] that had been employed in earlier inhibition studies. For routine calculations, a simplified model was used to decrease computational time. The kinetic mechanism for phosphorus containing species was based on the model suggested for the analysis of the influence of PH_3 products on the recombination of hydroxyl and hydrogen atoms in a hydrogen flame.[331] and kinetic models[254,300,301] developed to simulate destruction of DMMP and TMP in low pressure hydrogen flames. Additional reactions were added to the phosphorus mechanism to complete the reaction pathways for the consumption of some of the P-containing species. For the modeling of $Fe(CO)_5$ and CF_3Br inhibition, previously developed mechanisms for these two species[42,104] were added to the hydrocarbon model.

Computations of the propane flame inhibited by DMMP demonstrated that the consumption of DMMP led via a sequence of reactions to the formation of CH_3PO_2. Reactions of CH_3PO_2 with H and OH created HOPO and $HOPO_2$. At this stage, reactions of HOPO, $HOPO_2$, and PO_2 with chain carriers formed the following two inhibition cycles:

$$\begin{aligned} H + PO_2 + M &= HOPO + M \\ OH + HOPO &= H_2O + PO_2 \\ H + HOPO &= H_2 + PO_2 \\ O + HOPO &= PO_2 + OH \end{aligned} \qquad \text{(R3-17)}$$

$$\begin{aligned} OH + PO_2 + M &= HOPO_2 + M \\ H + HOPO_2 &= H_2O + PO_2 \end{aligned} \qquad \text{(R3-18)}$$

These inhibition cycles represent the catalytic scavenging cycles that accelerate radical recombination in combustion products containing phosphorus compounds.[260] It is well known that the addition of an inhibitor decreases the burning velocity for premixed flames. Numerical results for burning velocity decreases of 20 % to 30 % using the original rate constants given by Twarowski,[259] indicated that DMMP decreased the flame's burning velocity by a factor of 1.5 to 2 relative to CF_3Br in a methane-air flame. Sensitivity analysis revealed that the burning velocity was receptive to changes in the rate constants for the reactions of PO_2 radical: $H + PO_2 + M = HOPO + M$ and $OH + PO_2 + M = HOPO_2 + M$. Reasonable adjustment of rate constants led to agreement with experimental data.

Phosphorus compounds have a wide range of thermal stability. Activation energies of decomposition reactions are in the range 15 kcal/mol to 90 kcal/mol. The influence of the decomposition rate was studied using global kinetics for the decomposition to PO_2 to HOPO species by varying the overall activation energy for the decomposition reaction. Calculations showed that for the compounds with global activation energies less than 50 kcal/mol, the burning velocity was not affected by the stability of the phosphorus compounds.

Suppression calculations were carried out with increasing additive loadings until suppression concentration levels were achieved (burning velocity ≤ 5 cm/s [332]). The calculations were conducted for a gas phase model without taking into account possible condensation processes. Calculation results, Figure 3-110, show that DMMP had less effect in reducing the burning velocity in comparison with $Fe(CO)_5$, but relative to CF_3Br both were more effective. For increases in the concentration of $Fe(CO)_5$ and DMMP, both agents exhibited increasing saturation effects. Typically, two types of saturation have been discussed in the literature: (1) saturation of chemical influence,[52] and (2) saturation due to condensation processes.[104]

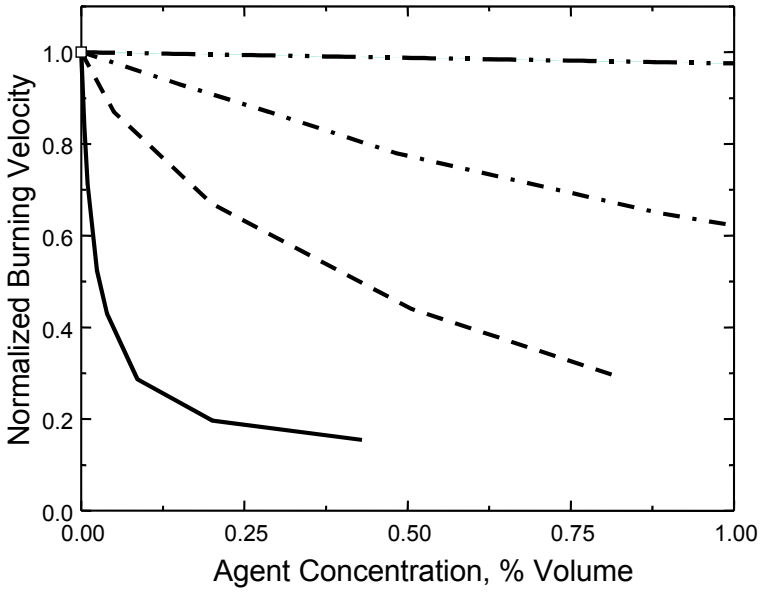

Figure 3-110. Calculated Burning Velocities vs. Delivered Inhibitor Concentration for a Numerical, Stoichiometric, Premixed, Propane-air Flame. Dashed line: DMMP data. Solid line: $Fe(CO)_5$ data. Dashed dot dashed line: CF_3Br data. Near-horizontal Dashed Dot Dot Dashed Line: N_2 data trend.

Both processes resulted in a decrease in inhibitor efficiency with increased inhibitor concentration. For example, to decrease the burning velocity to 10cm/s required a DMMP loading of approximately 0.9 %, but an additional 1.2 % of DMMP was needed to decrease the burning velocity to the extinction level of 5 cm/s. Such a strong saturation effect led to a substantial increase in extinction concentrations and a decrease in inhibitor efficiency relative to CF_3Br. The calculated extinction concentrations, in units of % volume, for the numerical propane/air flame were: DMMP: 2.1; CF_3Br: ≈ 3.5; $Fe(CO)_5$: 0.4 to 0.5; and N_2: ≈ 40. The modeling results supported DMMP and $Fe(CO)_5$ exhibiting superior inhibition capabilities relative to CF3Br.

Finally, comparison of the normalized OH concentrations dependency on inhibitor concentrations demonstrated a correlation between experimental and calculated OH concentrations. Figure 3-111 illustrates that two different propane flames inhibited by the same agents had normalized OH concentrations that tracked more or less with one another. At the experimental OH extinction level, i.e., 0.3 to 0.1, both data sets (experimental/computational) had similar normalized OH reductions.

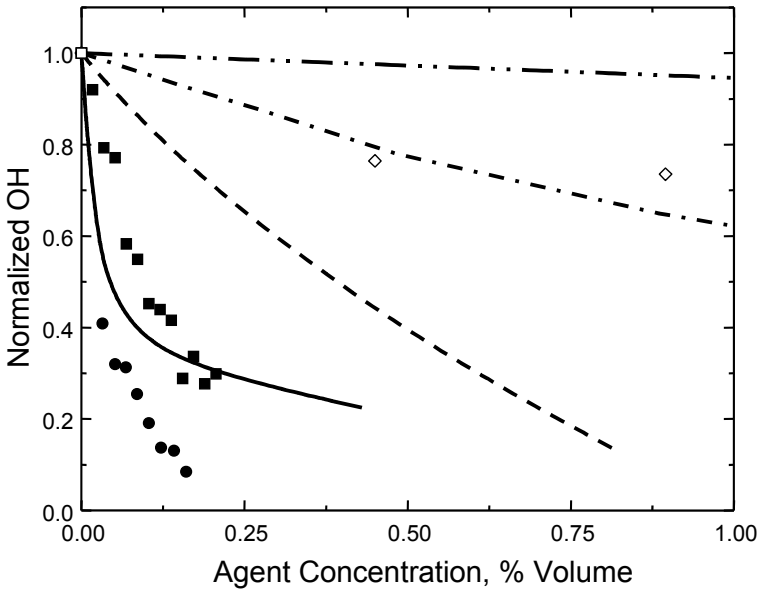

Figure 3-111. Normalized OH Concentrations vs. Delivered Inhibitor Concentrations. Data legend: experimental (●) and numerical (solid line) $Fe(CO)_5$ data; experimental (■) and numerical (dashed line) DMMP data; experimental (◇) and numerical (dash-dot line) CF_3Br data; dashed dot dot dashed line, N_2 data trend.

Conclusions

The experimental results presented here showed for the first time changes in [OH] profiles as extinction was approached in a series of inhibited, atmospheric pressure, non-premixed, propane/air flames. There was a good relationship between the narrowing and peak intensity of [OH] profiles in these flames with the degree of chemical activity of added inhibitors. N_2, HFC-236, and HFC-227ea, with little chemical activity, showed no peak narrowing relative to the uninhibited flame. By contrast, CF_3Br, PN, DMMP and $Fe(CO)_5$ demonstrated chemical inhibition capabilities and significant decreases in the [OH] peak width.

Contrary to prior hypothesis, there was a difference among PCCs in their flame extinguishment concentrations, on a per-phosphorus atom basis. PN, with the phosphorus atoms in its resonance-stabilized ring structure, was less efficient than DMMP.

3.5.3 CF_3Br and Other Suppressants: Differences in Effects on Flame Structure

Introduction

With some exception, the working hypothesis of the NGP was that significant catalytic scavenging of flame-propagating free radicals was necessary to match or exceed the efficiency of halon 1301. A logical issue was the extent to which the knowledge of the flame inhibition mechanism of CF_3Br, itself a catalytic scavenger, was applicable to identifying alternative suppressants. Was CF_3Br "typical" of efficient fire suppressants in general? Would all promising replacements for CF_3Br show similar behavior? Was commonality of properties with CF_3Br a useful guide in the search for alternatives?

To this end, Williams and co-workers[26] performed modeling studies of premixed flames containing substances representative of different classes of inhibitors, including inert gases, fluorocarbons, and catalytic scavengers of flame radicals. While suppression of nonpremixed flames is the typical scenario in fire extinguishment, the behavior of suppression agents in premixed flames is important in mitigating deflagrations and protecting against re-ignition. Furthermore a large body of suppression data in different types of flames compiled by Babushok and Tsang[333] had shown that for many agents, extinction of nonpremixed flames correlated with reduction of burning velocity in premixed flames.

Williams and co-workers compared the effects on burning velocity and flame structure of CF_3Br with those of the catalytic inhibitor NaOH, the non-catalytic hydrofluorocarbons CF_3CHFCF_3 (HFC-227ea) and CF_3CH_2F (HFC-134a), and the inert agents N_2 and CF_4. (CF_4 undergoes little decomposition in the reaction zone of most flames,[61] and is thus predominantly a physical agent). For exploratory purposes, they also considered an idealized, constrained version of $Fe(CO)_5$ inhibition which includes only the much less effective iron catalytic cycles for O-atom recombination.

Computational Methodology

The PREMIX code [203] was used to compute burning velocities and flame structures of atmospheric pressure, stoichiometric methane-air flames with and without suppressants. A domain of 85 cm was used in the calculations, extending 25 cm from the reaction zone on the cold boundary and 60 cm from the reaction zone on the hot boundary. The mesh extension and refinement were such that the spacing between the outermost grid points on each boundary was 1 cm, to minimize any temperature or species gradients at the boundaries. Multicomponent transport formulations, as well as the Soret effect for the species H and H_2, were used for all calculations. Refinement tolerances of 0.1 for the normalized species gradient (GRAD keyword) and 0.2 for the normalized second derivative (CURV keyword) were used for all calculations. The final meshes typically contained 90 to 125 grid points, depending on the number of additional species introduced by the inhibitor chemistry.

Comparison of the PREMIX results with thermal equilibrium calculations for several inhibited and uninhibited flames showed that, at the final grid point, temperatures were within 5 K and that radical concentrations of H, OH, and O were within a few percent of their equilibrium values. Thus, the radical equilibrium values and adiabatic temperatures were assumed to be those calculated at the hot boundary. All flames were stoichiometric, with the inhibitors listed above added in various concentrations. For the hydrocarbon chemistry, the GRIMech 2.11 [334] (excluding nitrogen chemistry) was used as the chemical

kinetic mechanism. For the uninhibited, stoichiometric methane air flame, a predicted burning velocity of 39.5 cm/s ± 0.2 cm/s was obtained.

The fluorocarbon chemistry was based on the mechanism developed by Westmoreland et al., as refined in previous studies performed at the Naval Research Laboratory [61,335] The bromine chemistry used in the modeling of CF_3Br was that developed by Noto et al. [175] The kinetic mechanism for NaOH was based on that of Zamansky et al.,[335] while that for $Fe(CO)_5$ was described by Rumminger and Linteris.[118] NaOH must vaporize before being able to participate in the flame chemistry, but the PREMIX code had no provision for inclusion of condensed phase species. To simulate the evaporation effect, the sodium hydroxide was therefore assumed to initially consist of the gas phase dimer $Na_2O_2H_2$, which was required to dissociate (ΔH_f = 42 kcal/mol) before inhibition chemistry could proceed. N_2 and CF_4 were assumed inert: no nitrogen or fluorine chemistry was included in the respective calculations.

Inhibition Parameter

The effectiveness of an inhibitor at reducing burning velocity in a fuel/oxidizer mixture may be placed on a quantitative basis in terms of the inhibition parameter, Φ, proposed by Rosser et al.[33] and modified by Noto et al.:[175]

$$\Phi = \ln(U_0/U_i)\,(X_{O_2}/X_i) \tag{3-12}$$

where U_0 and U_i are the burning velocities of the uninhibited and inhibited flames, respectively, and X_{O2} and X_i are the reactant mole fractions of oxygen and inhibitor. In Reference 175, the burning velocity of a given fuel/air mixture was found to exhibit an exponential dependence on concentrations of several inert and fluorocarbon inhibitors, including CF_3Br. A constant value of Φ with inhibitor concentration indicated that the exponential behavior found in Reference 175 held.

Catalytic radical scavengers necessarily manifest saturation effects, because catalysis cannot reduce concentrations of flame radicals below the thermal equilibrium level at the local flame temperature. The existence of a similarity transform, obtained by solving Equation 3-12 for U_i [175], which caused the flame speed reduction curves for CF_3Br and non-catalytic agents to coincide, was thus somewhat unexpected.

Changes in burning velocity, adiabatic flame temperature, radical super-equilibrium, and Φ are plotted as a function of $(NaOH)_2$ concentration in Figure 3-112 and CF_3Br concentration in Figure 3-113. The error bars for Φ were determined by propagating a change of 0.2 cm/s in the inhibited flame speed (the estimated computational uncertainty for the mesh refinement tolerances used) to determine the change in Φ in Equation 3-12. The points at low inhibitor concentrations had high uncertainties in Φ due to the small reductions in burning velocities. The radical super-equilibrium was defined as the ratio of the peak concentrations of the radical to its concentration at thermal equilibrium at the adiabatic flame temperature. The value for this ratio is always unity or greater; a value greater than unity means the radical exists in super-equilibrium concentration somewhere in the flame.

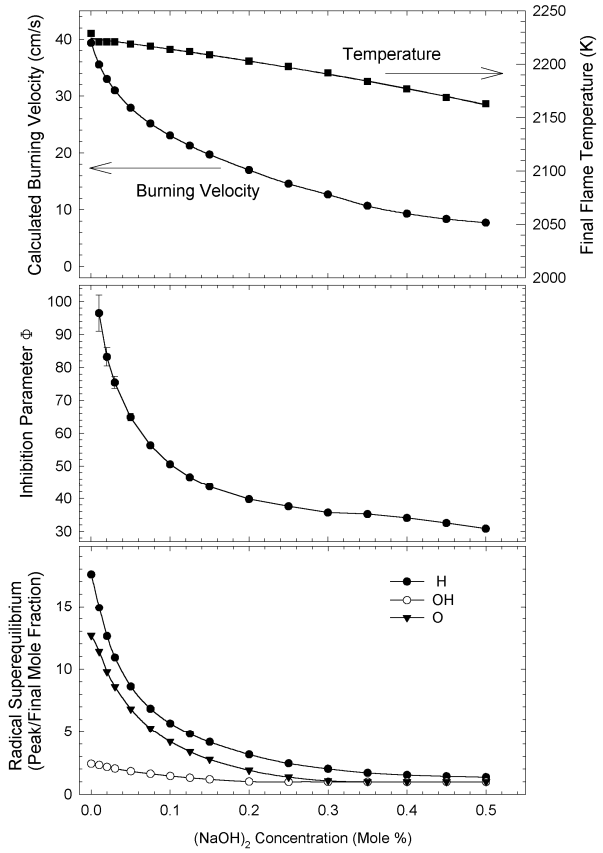

Figure 3-112. Burning Velocity, Final Flame Temperature, Inhibition Parameter, and Superequilibrium Concentrations of Flame Radicals Computed for Atmospheric Pressure Stoichiometric Methane-air Mixtures Inhibited by NaOH.

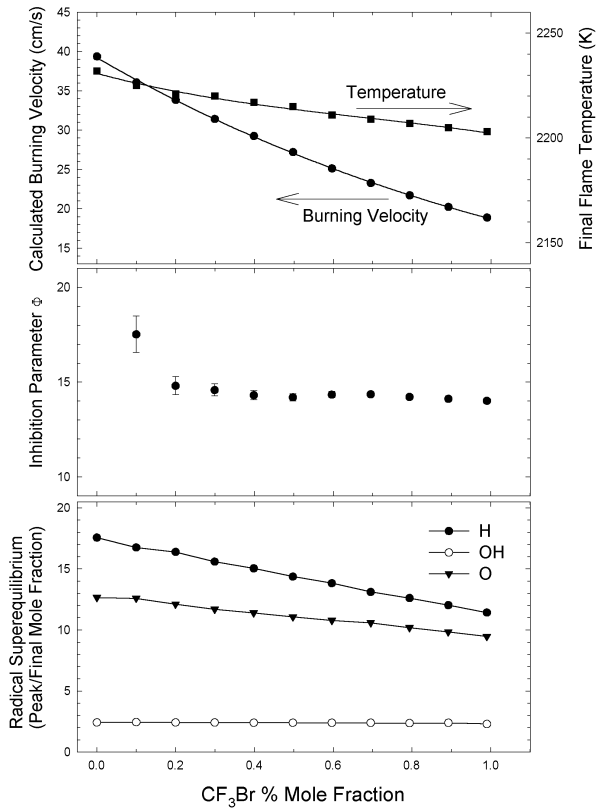

Figure 3-113. Burning Velocity, Final Flame Temperature, Inhibition Parameter, and Superequilibrium Concentrations of Flame Radicals Computed for Atmospheric Pressure Stoichiometric Methane-air Mixtures Inhibited by CF_3Br.

The behavior of the inhibition parameter in Figure 3-112 was different from that in Figure 3-113. For sodium, the inhibition parameter was not constant as a function of inhibitor concentration, but varied by more than a factor of three over the range of sodium concentrations considered here. The similarity relationship identified in Reference 336 did not hold for sodium. For CF_3Br, by contrast, the inhibition parameter was nearly constant as a function of inhibitor concentration. For comparison, the inhibition parameter of N_2, up to a 50 % reduction in burning velocity maintained an almost constant value of 0.5 (data not shown). The results for CF_3Br agreed with the findings of Noto et al.[336] although the modifications to the fluorocarbon kinetics yielded better agreement with the experimental value of 14.0 for the inhibition parameter, compared to the value of 11.1 reported in Reference.[336] The value of approximately 100 for the inhibition parameter of $(NaOH)_2$ per sodium atom at low concentrations is comparable to measured values for various sodium compounds ranging from 114 to 200.[336]

Radical Super-equilibrium

In Figure 3-112, the radical super-equilibrium was drastically reduced with increasing NaOH. For inert agents, by contrast, the radical super-equilibrium was increased as the flame is inhibited. When the flame speed was reduced by 40 % by the addition of N_2, for example, the H atom super-equilibrium increased from 17 to 70. Although peak radical concentrations decreased as an inert agent was added, the reduction in flame temperature reduced the equilibrium concentrations proportionately more.

For inhibition by CF_3Br (Figure 3-113), the degree of radical super-equilibrium was also reduced with increasing agent concentration, although not as dramatically as for sodium. CF_3Br reduced the H atom super-equilibrium by only 30 % for a 50 % reduction in burning velocity; NaOH reduced the H atom super-equilibrium by nearly 80 % at a 50 % burning velocity reduction. This finding supported the conclusion of Saso et al.[337] that saturation was a minor effect in the suppression effectiveness of CF_3Br/inert mixtures. Saturation was not as pronounced for CF_3Br inhibition because the peak radical concentrations remained far from equilibrium for substantial reductions in burning velocity.

Another factor contributing to the lack of a saturation behavior for CF_3Br was that the bromine catalytic cycle involved the sequence of reactions[332]

$$Br + Br + M \Rightarrow Br_2 + M \qquad \text{(R3-19)}$$

$$H + Br_2 \Rightarrow HBr + Br \qquad \text{(R3-20)}$$

as an important pathway in regeneration of HBr. The direct reaction

$$H + Br + M \Rightarrow HBr + M \qquad \text{(R3-21)}$$

has slow kinetics. This has two consequences: the second order dependence of reaction R3-19 on the bromine concentration compensates for the saturation effect with increasing CF_3Br concentration. Also, a high concentration of bromine is required for this reaction to be significant, leading to a much smaller inhibition parameter for bromine than for iron and sodium,[333] whose scavenging cycles are not thought to depend on second order kinetics.

Synergism Between Catalytic and Physical Agents

Several experimental and modeling studies had observed that the effectiveness of CF_3Br [91,337] as well as other chemical agents[14,106] could be enhanced by the addition of a physical agent. Saso et al. [337] attributed synergism in mixtures of CF_3Br and inert inhibitors to a temperature effect on the inhibition effectiveness of CF_3Br, rather than a saturation phenomenon. Over a range of adiabatic flame temperatures, Saso et al. found CF_3Br to have virtually identical inhibition parameters at loadings of 0.5 % and 1 % (by volume) in methane/oxygen/inert mixtures, indicating the absence of significant saturation effects.

To extend the computational investigation of synergy to other combinations of agents, inhibition by iron was modeled in combination with nitrogen. For this modeling, iron was considered to participate in a three step mechanism involving only O + O recombination. This pathway was identified by Rumminger and Linteris[118] but was usually secondary in importance to an H + H recombination pathway. This model was not intended as an accurate description of iron's combustion chemistry, but rather to consider whether synergism occurred in the absence of a temperature dependence on the inhibition kinetics.

Of the three reactions making up the O + O catalytic cycle of iron:

$$Fe + O_2 + M \Rightarrow FeO_2 + M \qquad \text{(R3-22)}$$

$$FeO_2 + O \Rightarrow FeO + O_2 \qquad \text{(R3-23)}$$

$$FeO + O \Rightarrow Fe + O_2 \qquad \text{(R3-24)}$$

R3-23 and R3-24 were assumed to have rate coefficients independent of temperature. The reaction R3-22 had a slight increase in rate with increasing temperature, but the product of the rate coefficient and the number density of third body colliders varied by less than 10 % over the temperature range from 1400K and 2500K.

The iron + nitrogen combination exhibited synergy, as seen in Figure 3-114, which plots burning velocity, flame temperature, and differential inhibition parameter of the O + O cycle of 500 μL/L FeO_2 as a function of nitrogen addition.

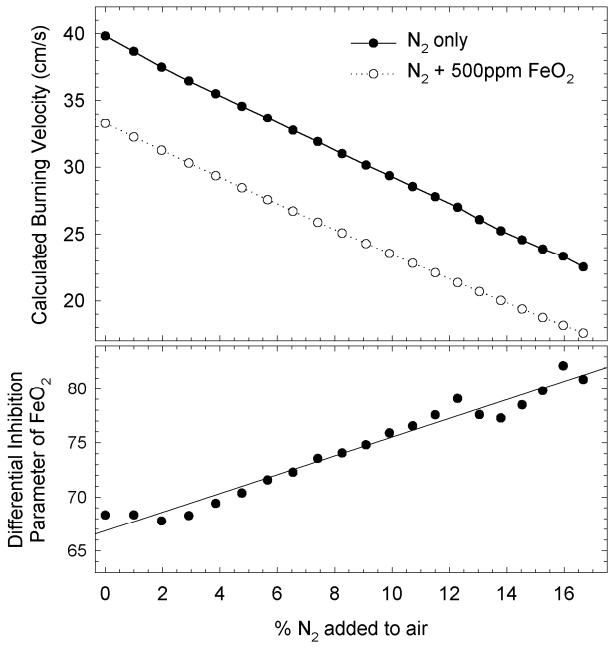

Figure 3-114. Burning Velocity and Differential Inhibition Parameter computed for Atmospheric Pressure Stoichiometric Methane-air Mixtures Inhibited by N_2 and FeO_2 in Combination.

The differential inhibition parameter for inhibitor B in the presence of inhibitor A is

$$\Phi = \ln(U_A/U_{A+B})\ (X_{O2}/X_B) \qquad (3\text{-}13)$$

where U_A and U_{A+B} are the burning velocities in the flames inhibited by inhibitor A alone and A and B in combination, respectively. The differential inhibition parameter of 500 μL/L FeO_2 increased by about 23 % as the flame temperature was lowered by nitrogen addition from 2230 K to 2010 K. Saso et al.[337] found that the inhibition parameter of CF_3Br increased by some 45 % at loadings of both 0.5 volume % and 1.0 % volume % over the same range of final flame temperatures.

While the findings of synergism agreed qualitatively between CF_3Br/inert and Fe/inert mixtures, the final flame temperature influenced the inhibition parameter of CF_3Br twice as much as that of the O + O recombination cycle of iron, due to the lack of explicit temperature dependence of the Fe kinetic cycle. Thus, these results showed that synergism in catalytic/inert mixtures did not require temperature dependence of the inhibition cycle, although this could influence its magnitude.

Correlation of Burning Velocities with Changes in Flame Structure

Padley and Sugden[338] observed in studies of H_2-O_2-N_2 flames that the burning velocity correlated with the partial pressure of atomic hydrogen in the reaction zone. More recently, this correlation had been observed to hold also for hydrogen flames inhibited by CF_3Br. [339] Figure 3-115 plots the peak H atom concentration against burning velocity for a variety of inhibited methane/air flames. For methane flames inhibited by N_2, CF_4, and CF_3Br, there was a nearly identical linear relationship between the peak H atom mole fraction and burning velocity, as with the hydrogen flames.

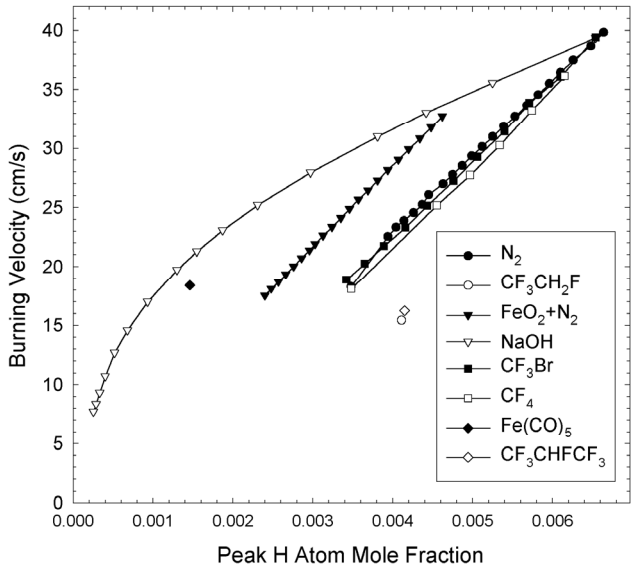

Figure 3-115. Relationship between Burning Velocity and Peak Concentration of Atomic Hydrogen for Methane-air Flames Inhibited by Various Compounds.

Examination of the effect of other inhibitors, however, demonstrated that this correlation was not a general one. The fluorocarbon agents CF_3CHFCF_3 and CF_3CH_2F both reduced burning velocity more

than would be expected based on the peak H atom concentrations. Inhibition by sodium or iron produced the opposite effect. Noteworthy in the sodium data was the curvature which coincided with the onset of saturation. The coincidence of the CF_3Br data points with those of the inert agents appears to have been accidental. The calculations for the fluorocarbons and catalytic agents lay on opposite sides of those of the inert agents, and CF_3Br was in some sense a combination of the two.

An alternate correlation between burning velocity and flame structure was based on the proportionality between the burning velocity and the square root of the overall reaction rate.[337] In modeling the burning velocity of a large number of inhibited flames, the burning velocity correlated in almost all cases with the product of the peak H atom mole fraction and a global activation energy:

$$S_L^2 = A^2 X_H \exp(-E_a/kT_f) \; . \qquad (3\text{-}14)$$

where S_L is the laminar burning velocity, X_H the peak mole fraction of atomic hydrogen, and T_f the final flame temperature. The fitted parameters A and Ea, obtained by considering the flame inhibited by nitrogen, were A=7940 cm/s, E_a=103 kJ/mol. The same empirical correlation held for inhibition by other inert gases, by iron and sodium, by nitrogen and iron in combination (Table 3-19), and by artificially increasing the H + OH recombination rate. For catalytic agents which did not significantly change the final flame temperature, the burning velocity correlated with the square root of the H atom peak mole fraction, but not with those of atomic oxygen or OH radicals. The effect of catalytic agents on reducing burning velocity proceeded through reduction of the atomic hydrogen concentration, whether or not the scavenging cycle directly involved H atom recombination (as in the O + O cycle of iron).

Table 3-19. Comparison of Calculated Burning Velocities.

Flame Condition	$T_{adiabatic}$	X_{Hmax} x 10^3	S_{premix}	S_{eqn}	$\Delta S_{premix}/\Delta S_{eqn}$ [a]
CH_4-air (uninhibited)	2234	6.64	39.8	39.8	---
+9.09 % N_2	2121	5.12	30.2	30.2	1.00
+16.67 % N_2	2015	3.94	22.6	22.7	1.01
+8.26 % CF_4 (inert)	1968	3.50	18.4	19.9	1.07
+200 μL/L $Fe(CO)_5$	2223	1.46	18.4	18.6	1.01
+1.0 % CF_3Br	2203	3.42	18.9	27.6	1.71
+0.5 % HBr	2221	5.36	30.3	35.2	2.08
+3.8 % CF_3CH_2F	2031	4.11	15.5	23.9	1.54
+2.9 % CF_3CHFCF_3	2161	3.86	16.3	26.1	1.73
+0.05 % $(NaOH)_2$	2219	2.97	28.0	26.2	0.87
+0.40 % $(NaOH)_2$	2177	0.33	9.4	8.3	0.97
Increase H+OH+M rate x 100	2234	1.35	19.8	18.0	0.92

[a] $39.6\text{-}S_{premix})/(39.6\text{-}S_{eqn})$

Table 3-19 compares the burning velocities estimated using Equation 3-14 to the calculated values for a variety of flame inhibitors. In 6 of the 11 cases, the reduction in burning velocity relative to the uninhibited flame, predicted by Equation 3-14 was within 13 % of the result of the PREMIX calculation. However, the correlation stated in Equation 3-14 greatly underpredicted flame speed reduction by the fluorocarbons CF_3CH_2F and C_3HF_7, as well as CF_3Br and HBr. Flame structure modeling indicated that

the breakdown of this relationship involving the peak H atom concentration was a consequence of these agents reducing the H atom concentration mostly in the early part of the flame, prior to the peak concentration, as discussed below.

Changes in Flame Structure Due to Different Agents

Insight into why the correlation between burning velocity, H atom concentration, and temperature did not hold for either fluorocarbons or bromine-containing compounds was gained from examination of these compounds' effects on flame structure. In Figure 3-116, the mole fraction of atomic hydrogen is plotted against the local temperature for flames inhibited by a variety of agents. All the inhibited flames had burning velocities approximately 50 % that of the uninhibited flame, whose structure is also plotted for comparison. For all these flames, the temperature monotonically increased with position passing from reactants to products.

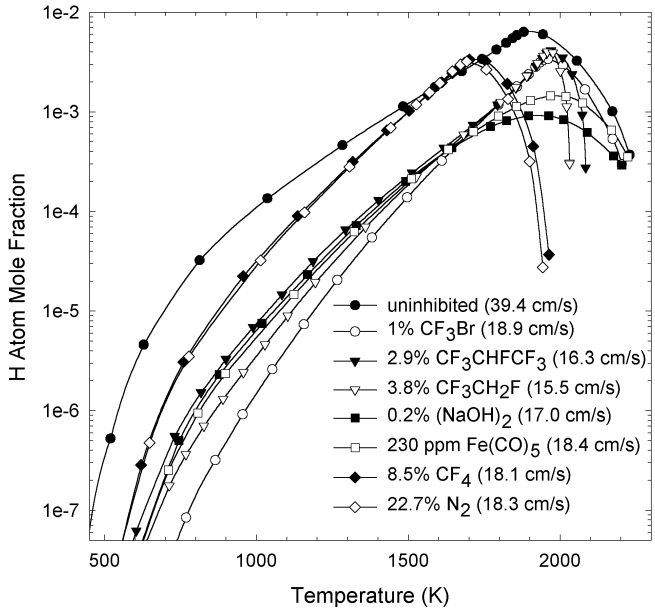

Figure 3-116. Mole Fraction of Atomic Hydrogen as a Function of Local Flame Temperature for an Uninhibited and Uninhibited Atmospheric Pressure Methane-air Flame.

The relationship between H atom mole fraction and local temperature shown in Figure 3-116 was characteristic of each type of agent except for CF_3Br. The physical agents reduced the final flame temperature, but the H atom mole fraction at a given isotherm (above approximately 1300 K) was changed very little from its value in the uninhibited flame. Both iron and sodium reduced the H atom mole fraction by a relatively constant factor throughout the reaction zone. The fluorocarbons reduced the H atom mole fraction early in the flame (in the region below about 1200 K) but had relatively little impact on the peak concentration. This diminished effectiveness at the location of maximum hydrogen atom concentration also occurred for CF_3Br; in this respect CF_3Br bore more resemblance to nonbrominated fluorocarbons than it did to other catalytic agents such as iron and sodium. Since Babushok et al. [167] found that iron approached the performance of an "ideal" catalytic inhibitor, the different effect of CF_3Br on flame structure from that of iron and sodium indicated a departure from ideality, in particular it only scavenged radicals significantly in low temperature regions of the flame. All the flames inhibited by chemically active suppressants showed nearly equal reductions in H atom mole fraction at 1700 K. In the flames inhibited by inert agents, the H atom concentration at this isotherm was essentially the same as in the uninhibited flame. Therefore, the H atom mole fraction at 1700 K (or any other fixed temperature)

cannot be used as a predictor of burning velocity which is applicable to all inhibited flames. Given the different influences of the suppressants on flame structure, it seemed unlikely that an empirical relationship between flame speed and some other quantity can be found which applies to all suppressed flames.

The depletion of radical species early in the flame had a marked influence on the burning velocity. It is for this reason that fluorocarbons and bromine compounds are better inhibitors than the changes in temperature and peak H atom concentrations predicted. This observation suggested that agents which deplete radicals in high temperature regions but not early in the flame were likely to be less effective inhibitors than would otherwise be expected. This may be the case for condensed-phase agents which must vaporize before inhibition can begin.

Conclusions

In several respects, CF_3Br is not representative of catalytic fire suppressants in general. Several features of its kinetics, including the strong temperature dependence of the catalytic suppression cycle and the preferential reduction of atomic hydrogen concentrations in low temperature regions of the flame, were not shared by other catalytic suppressants. In these regards, sodium and iron exhibited behavior much more typical of this class of suppressants. For these reasons, caution is required in using specific kinetic properties observed for CF_3Br as a basis for identifying other efficient fire suppressants.

3.5.4 Influence of Bond Energies on Catalytic Flame Inhibition

Introduction

The suppression effectiveness of CF_3Br and related compounds is primarily due to the chemical activity of bromine,[13,332,340] which participates in a catalytic cycle and reduces concentrations of the free radicals involved in flame propagation. As documented earlier in this Chapter, several chemical elements besides bromine have been shown to exhibit catalytic radical scavenging in flames, sometimes much stronger than that of bromine,[333] although practical issues have limited their implementation. Among the halogens, iodine is a good catalytic scavenger.[20,167] Among non-halogens, good suppression efficiency has been demonstrated for alkali metals,[341] phosphorus,[79] and several transition metals including iron,[104] lead,[92] chromium,[126] and manganese.[107] The elements comprising this list vary greatly in their chemical properties, while other elements in the same groups of the periodic table (e.g., nitrogen, fluorine) do not cause efficient catalytic suppression of flames.

Finding a common basis for efficient chemical suppressants, whose results can be extrapolated to other elements with combustion chemistry which has not yet been thoroughly explored, was of importance to the NGP. Previous work had pointed to the binding energy of a suppressant (or one of its decomposition products) to one or more flame radicals as an important parameter.[42,342] This approach has been used previously to explain, for instance, the greater suppression effectiveness of bromine compared to chlorine.[42] Under the NGP, Fleming and co-workers[343] broadened the scope of the previous work by focusing on a common thermodynamic basis for catalytic suppression by different families of elements, and different types of catalytic cycles. The rationale for revisiting the effect of bond energies at the present time was threefold:

- Computational tools had become available to model the effect of thermodynamics directly, rather than resorting to simplifying approximations such as zone modeling of flame structure[342] or partial equilibrium assumptions of species concentrations.[42]
- The NGP objective was to assess the fire suppression potential of elements that had not yet been extensively investigated, rather than to explain the behavior of elements whose properties were already (empirically) known. By contrast, the work which elucidated the suppression kinetics of bromine was performed after halons were identified and implemented as fire suppressants.
- A great deal of additional chemical kinetic data had become available, including provisional suppression mechanisms for a number of non-halogen-containing species.

Simplified but representative catalytic cycles for known inhibitors (bromine, sodium, iron) were used in conjunction with detailed kinetic modeling of the hydrocarbon flame structure.

General Features of Catalytic Scavenging Cycles

In most flames, the peak concentrations of the radicals H, O, and OH are much higher than the thermal equilibrium concentrations at the adiabatic flame temperature. This is a consequence of the kinetic rates of the chain branching reactions, for example

$$H + O_2 \Rightarrow OH + O \quad \text{(R3-25)}$$

$$O + H_2 \Rightarrow OH + H, \quad \text{(R3-26)}$$

exceeding the rates of chain termination reactions such as

$$OH + H + M \Rightarrow H_2O + M \quad \text{(R3-27)}$$

$$O + O + M \Rightarrow O_2 + M \quad \text{(R3-28)}$$

$$H + H + M \Rightarrow H_2 + M, \quad \text{(R3-29)}$$

which require a third body for stabilization of the product.[344] Chemical fire suppressants generally participate in a catalytic cycle whose net effect is equivalent to one of the recombination reactions.

For a substance to scavenge flame radicals, there must exist some species X derived from the inhibitor which can bond to H, O, or OH. The species XR, where R is one of the flame radicals, must react with another flame radical R' to form X and RR', where RR' is usually a stable molecule such as H_2, H_2O, or O_2. Possible scavenging reactions include. [345]

$$XH + H \Rightarrow X + H_2 \quad \text{(R3-30)}$$

$$XH + OH \Rightarrow X + H_2O \quad \text{(R3-31)}$$

$$XOH + H \Rightarrow X + H_2O \quad \text{(R3-32)}$$

$$XO + O \Rightarrow X + O_2 \quad \text{(R3-33)}$$

To complete the cycle, X must then be converted back to XR through one or more steps. For significant inhibition to occur, the kinetic rate of the scavenging cycle must exceed that of the equivalent direct recombination reaction.

Inhibition by bromine occurs primarily through (R3-30) and to a lesser extent (R3-31),[346] while alkali metals operate primarily through (R3-32).[347] Reaction (R3-33) is likely to occur for metallic elements.[118] Some elements, including iron[118] and phosphorus,[258] are thought to participate in more than one cycle.

Computational Methodology

The computer code PREMIX[203] was used to model freely propagating atmospheric pressure premixed flames. The baseline condition consisted of stoichiometric methane/air, with an initial reactant temperature of 298.2 K. Tolerances for mesh refinements in PREMIX were set as follows: GRAD = 0.10, CURV = 0.20, up to a maximum of 150 grid points. Multicomponent viscosities and thermal diffusion (Soret effect) were used. The computational domain extended 25 cm from the flame into the reactants gases, and 60 cm into the exhaust gases. The domain was extended in such a way that on both boundaries, the second last grid point was 1 cm from the boundary.

The reaction set given in GRI-MECH 2.11[289] (without nitrogen chemistry) was used for modeling the uninhibited flames. Calculations were carried out using bromine, sodium, and iron as examples of chemical inhibitors. Kinetics of chemical inhibition for these elements were added to the hydrocarbon mechanism as described below.

Kinetic Mechanisms of Specific Inhibitors

The inhibition cycle of bromine is believed to proceed by H atom scavenging.[42,342] The reaction

$$HBr + H \Rightarrow Br + H_2 \qquad \text{(R3-34)}$$

is thought to be the primary scavenging reaction, with the reaction with OH

$$HBr + OH \Rightarrow Br + H_2O \qquad \text{(R3-35)}$$

also contributing. The conversion of Br to HBr involves several pathways. The direct recombination

$$H + Br + M \Rightarrow HBr + M \qquad \text{(R3-36)}$$

has rather slow kinetics and is typically not the predominant pathway. Atomic bromine can abstract hydrogen atoms from such species as HO_2, HCO and CH_2O; these play an important role in most flames.

Two simplified kinetic mechanisms describing inhibition by bromine were constructed and are listed in Table 3-20. Both mechanisms included Br and HBr as the only bromine-containing species. For these calculations, HBr was chosen as the bromine-containing reactant. In the first mechanism, HBr was assumed to react only with atomic hydrogen to form Br, which was converted back to HBr by a direct recombination with H, as well as abstraction of H from HO_2, HCO, and CH_2O. The second mechanism was identical, except that HBr was allowed to react only with OH, rather than H.

Table 3-20. Kinetic Mechanisms for Suppressants ($k = AT^b exp(-E_a/kT)$).

Reaction	A (cm^3/mol-s)	b	E_a (kcal/mol)	Source
Mechanism for Na (H + OH cycle only)				
$(NaOH)_2 + M = NaOH + NaOH + M$ [a]	3.0E14	0.0	48	
$NaOH + H = Na + H_2O$	1.0E13	0.0	1.97	
$Na + OH + M = NaOH + M$ [a]	1.8E21	-1.0	0	
Mechanism for Br (reactions in common for all cycles)				
$H + Br + M = HBr + M$ [a]	1.92E21	-1.86	0	348
$Br + CH_2O = HBr + HCO$	1.02E13	0.0	1.59	349
$Br + HO_2 = HBr + O_2$	8.43E12	0.0	1.17	349
$Br + HCO = HBr + CO$	1.69E14	0.0	0	350
Addition for Br (H + H cycle):				
$HBr + H = H_2 + Br$	6.25E13	0.0	2.40	348
Addition for Br (H + OH cycle):				
$HBr + OH = H_2O + Br$	6.62E12	0.0	0	351
Mechanism for Fe (O + O cycle):				
$Fe + O_2 + M = FeO_2 + M$ [a]	1.57E18	0.0	4.05	352
$FeO_2 + O = FeO + O_2$	1.73E13	0.0	0.0	a
$FeO + O = Fe + O_2$	1.73E13	0.0	0.0	b

[a] No reaction rate reported; assumed equal to the rate in the next row.
[b] Based on reverse reaction of Reference 353.

For iron-containing compounds, Rumminger and Linteris[118] identified catalysis of H atom recombination as the most important scavenging cycle in hydrocarbon flames. In addition, they found that an O atom recombination cycle could be significant in moist CO flames. The three-step cycle is shown in the last three rows of Table 3-20. This mechanism was not intended as an accurate depiction of the overall inhibition chemistry of iron, only the contribution of the O + O scavenging cycle (which is small for hydrocarbon fuels). Analogous O + O cycles may exist for other transition metal elements as well.

For sodium and other alkali metals, Jensen and Jones[347] propose the primarily cycle:

$$X + OH + M => XOH + M \quad \text{(R3-37)}$$

$$XOH + H => X + H_2O. \quad \text{(R3-38)}$$

The simplified mechanism for sodium consisted of (R3-37) and (R3-38), together with a reaction converting the NaOH dimer (specified as the reactant) to the monomer to simulate an evaporation step.[26] Comparisons of thermal equilibrium calculations with NaOH(s) and $(NaOH)_2$ as reactants indicate that the very minor reduction in the adiabatic flame temperature caused by the addition of NaOH dimer was about 70 % that of adding an equal amount of solid NaOH.

Using the simplified mechanism, the predicted flame speed of a stoichiometric methane/air mixture inhibited by 0.1 % mole fraction of $(NaOH)_2$ was 25.0 cm/s, compared to 23.1 cm/s using a more comprehensive mechanism[26] adapted from Zamansky et al.,[335] and 39.4 cm/s for the uninhibited flame.

This result confirmed that the OH + H cycle identified by Jensen and Jones was indeed the most important for suppression of near stoichiometric hydrocarbon flames.

Influence of Bond Energies on Suppression Cycles

For an efficient scavenging cycle to exist, the bond energy between the scavenging atom or radical X and a flame radical R must satisfy certain conditions. If it is too high, the scavenging reaction (R3-30) to (R3-33) would be endothermic. This is the case for fluorine, which binds irreversibly to hydrogen and thus cannot sustain a catalytic cycle. On the other hand, if the bond were too weak, the equilibrium between XR and X + R would be so far toward dissociation that there would be insufficient XR to participate in the scavenging reactions. Stated another way, the rates of the reverse reactions must be small compared to those of the forward reactions, since any catalytic recombination cycle would become a catalytic chain branching cycle if it ran backwards.

These considerations indicated that there would be a limited range of bond energies for which an efficient scavenging cycle could exist. Putting these qualitative arguments on a quantitative basis by computational investigation of the effect of hypothetical changes in bond energies on suppression efficiencies allowed the determination of the bond energies compatible with efficient suppression. Suppression depends on kinetic as well as thermodynamic factors, so appropriate bond energies by themselves do not guarantee good suppression properties. The elements chosen as examples, however, were known to have good suppression properties, so they possess kinetics favorable to scavenging.

Bromine was used as the example element for Reactions (R3-30) and (R3-31), sodium for (R3-32), and iron for (R3-33). During the combustion process, each of these elements can have multiple binding partners and thus could have several bond energies hypothetically relevant to combustion. In order to simplify the situation so that sensitivity to bond energy can be determined in a relatively straightforward way, it was assumed that only one catalytic cycle involving one type of bond existed for each element.

For each set of calculations, the thermodynamic functions for the species XR were not altered, but the heat of formation of the species X at 298 K was varied, while keeping the heat capacity and entropy unchanged. This had the effect of changing the dissociation energy of X-R. In the kinetic mechanisms, the chemical reactions for the scavenging cycle were written in the exothermic direction, and the Arrhenius parameters of the forward reaction were unchanged. All reactions were assumed to be reversible, however, so changing the heat of formation altered the activation energy of the reverse reaction, even without any explicit changes to the kinetic parameters.

In the PREMIX code, the facility existed for determining the sensitivity of the solution vector, including the flame speed eigenvalue, to changes in the heats of formation of species (HSEN keyword). This was distinct from sensitivities with respect to changes in the kinetic rates (ASEN keyword) which have been more commonly reported in modeling studies. Sensitivity analysis, however, only provided the first derivative of the flame structure with respect to thermodynamic or kinetic quantities. The dependence of suppression efficiency on heats of formation is non-monotonic. A small sensitivity coefficient for the enthalpy of a particular species on the flame speed may mean that the species in question is unimportant to suppression, or it could mean that its enthalpy is very close to the optimal value, leading to a vanishing first derivative.

Bromine: H + H and H + OH Recombination

For this series of calculations HBr was chosen as the bromine-containing reactant. The kinetic mechanism was chosen to model the effect of a single catalytic mechanism, with Br and HBr as the only bromine species. Two sets of calculations were performed, the difference being whether HBr was assumed to react with H or with OH. Figure 3-117 shows the predicted flame velocity of a stoichiometric methane/air mixture inhibited by 0.5 volume % of HBr. The catalytic cycle was found to be most efficient for H-Br bond energies (which were artificially varied in the calculations) between 65 kcal/mole and 90 kcal/mole.

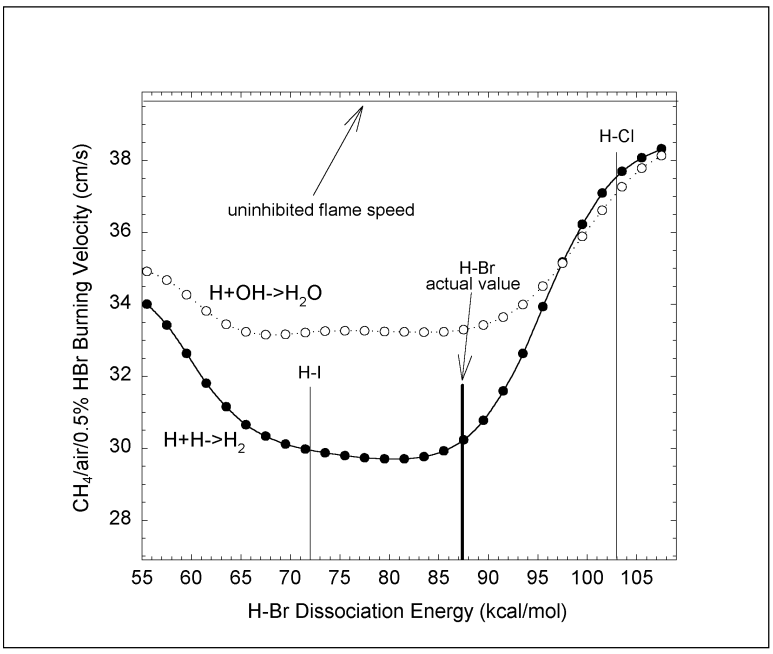

Figure 3-117. Calculated Flame Velocity as a Function of Hypothetical Variation of the H-Br Bond Energy for Premixed Methane-air Flames Inhibited by 0.5 % HBr Using the H + H and H + OH Scavenging Cycles of Table 3-20. The accepted values for the bond energies of H-Br, H-Cl, and H-I are indicated by vertical lines.

The accepted value of the H-Br bond energy lies near the upper limit of the range, which permits an optimally efficient catalytic cycle (Figure 3-117). The bond energy of H-I is near the lower limit of the optimal range, while the H-Cl bond is too strong for good suppression. The bond energy of H-F (135 kcal/mole) is so high that the molecule is completely inert in this environment. Although the kinetics of the analogous reactions are somewhat different for the other halogens, the bond energy factor by itself led to the correct prediction that the measured suppression effect of iodine was nearly equal that of bromine[20], while chlorine had a much smaller effect.[354]

Sodium: OH + H Recombination

The effect of hypothetical variation of the Na-OH bond energy is illustrated in Figure 3-118. There was a more pronounced falloff in suppression efficiency with bond energy than for either of the bromine scavenging cycles. The Na-OH bond energy was close to the optimal value for good suppression, as were the bond energies for all the other alkali metals except lithium. Experimental studies have found that potassium is a considerably more efficient flame suppressant than sodium.[333] In view of the similarity of the thermodynamic properties, this difference may be due to differences in kinetic rates between the two elements, particularly for the recombination step (R3-37).

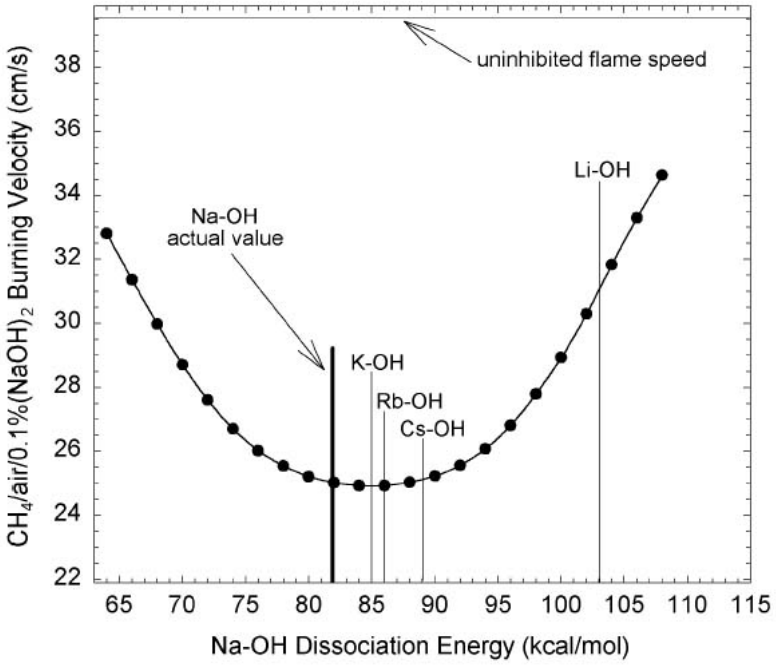

Figure 3-118. Calculated Flame Velocity as a Function of Hypothetical Variation of the Na-OH Bond Energy for Premixed Methane-air Flames Inhibited by 0.1 % $(NaOH)_2$ using the H + OH scavenging cycle of Table 3-20. The accepted values of X-OH bond energies for the alkali metals are indicated by vertical lines.

Iron: O + O Recombination

The three step O + O catalytic cycle modeled for iron had two relevant bond energies, Fe-O and OFe-O, which differed by about 3 kcal/mole. The bond energies were varied in the calculation by keeping the standard state enthalpy of FeO fixed, while varying those of Fe and FeO_2 in opposite directions from their "normal" values. For FeO_2, the "normal" standard state enthalpy used was not the actual value, but was chosen such that the bond energy of OFe-O was equal to that of Fe-O, 99 kcal/mole.

In the calculation, FeO_2 was chosen as the reactant. For most iron-containing compounds such as $Fe(CO)_5$, the parent agent was quickly converted to Fe,[104] which then combined with oxygen through R3-22, making the original identity of the iron compound unimportant. Because of iron's high suppression efficiency, a smaller concentration of suppressant was used (500 μL/L) than for the calculations with sodium or bromine.

Results of the calculations are shown in Figure 3-119. The accepted bond energies of both Fe-O (99 kcal/mol) and OFe-O (96 kcal/mol) are close to the optimal value for efficiency of the catalytic cycle.

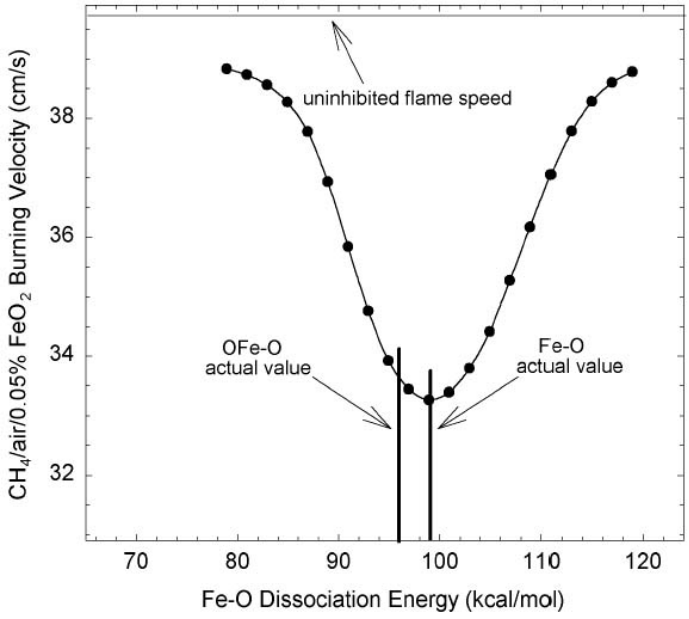

Figure 3-119. Calculated Flame Velocity as a Function of Hypothetically Variation of Fe-O Bond Energy for Premixed Methane-air Flames Inhibited by 500 µL/L FeO_2 Using the Three-step O + O Scavenging Cycle of Table 3-20. The accepted values of the Fe-O and OFe-O bond energies are indicated by vertical lines.

Discussion

These calculations indicated that for an efficient scavenging cycle, the bond energy between a catalytic scavenger and a flame radical must lie in the range of 70 kcal/mol to 100 kcal/mol, the optimal value varying somewhat for different net recombination reactions. This range of values was consistent with the expectation that the bond must be strong enough to be thermodynamically stable at flame temperatures, but not so strong as to prevent regeneration of the active scavenging radical. Table 3-21 shows that the more efficient a scavenging cycle (in terms of the inhibition parameter[175]), the more sensitive it is to changes in bond dissociation energies.

Table 3-21. Efficiencies and Sensitivities to Bond Energies of Catalytic Cycles.

Element	Net Cycle	Inhibition Parameter[175]	ΔD(kcal/mol)[a]	D_{max}(kcal/mol)[b]	$\Delta D/D_{max}$
Br (0.5%)	H + OH	6.9	39	77	0.51
Br (0.5%)	H + H	11.5	33	77	0.43
Na (0.2%)	H + OH	46	29	85	0.34
Fe (0.05%)	O + O	66	14	99	0.14

[a] Range of bond energies for which the suppression index is at least 75 % of its maximum value.
[b] Bond energy at which the maximum value of the suppression index is achieved.

Other factors also play a role in suppression efficiency, although less definitive than does the bond energy. In most catalytic cycles, there is likely to be at least one recombination step, e.g., Na + OH = > NaOH, Fe + O2 = > FeO_2. In many cases, the recombination reaction may be the rate limiting step in the catalytic cycle. This recombination step must have a faster rate than the direct radical-radical recombination for the catalyst to cause inhibition. In general, the recombination complex is more likely to be stabilized by third body colliders if it is polyatomic, rather than diatomic. Also, if the recombination reaction involves a stable, rather than a radical flame species, it is likely to proceed faster due to the higher reactant concentrations. This is the case for the Fe + O_2 recombination step.

Many transition metals whose compounds showed good suppression properties exhibit more than one stable valence. This did not appear to be a fundamental requirement for efficient suppression, since alkali metals only exhibit one valence yet are efficient suppressants. The existence of multiple valences greatly increases the number of possible species, increasing the likelihood that an efficient catalytic cycle may occur. Multiple valences may also facilitate recombination reactions. If the reactant and product of a recombination reaction corresponded to two stable valences of the inhibitor element, then the kinetics of the reaction might be more favorable.

3.5.5 Temperature Regions of Optimal Chemical Inhibition of Premixed Flames

Introduction

Unwanted fires vary considerably in the spatial distributions and peak values of their temperatures. Hence, understanding the temperature sensitivity of chemical inhibition can aid in the search for halon alternatives. Premixed flames [4,39,150,332,346,355] are a useful medium to resolve any temperature effects. These flames have commonly been divided into various zones or regions, and prior to the NGP there was some knowledge of the flame chemistry in these zones.[356-359]

Analysis of the region of a flame most sensitive to chemical or thermal inhibition has been an active area of flame inhibition research for many years.[4,26,38,39,41-43,150,230,304,346,360] Several investigations have indicated that the important region of action for halogenated agents is the low-temperature region of the flame.[360] It was deemed worthwhile to examine this claim and determine if it applied either to CF_3Br or to other chemicals.

Numerical simulations of flame inhibition chemistry using complex kinetics and *model* inhibitors would allow simulations of inhibitors which had not yet been identified or synthesized. Linteris and co-workers perturbed the reaction rates of selected chemical reactions in a region that was defined by temperature, species concentration, time, and space.[361] Using model inhibitors introduced at concentrations below those typically used to suppress fires, they calculated the magnitude of the burning velocity reduction for two types of perturbations: impulsive or stepwise. The perturbations were induced by addition of CF_3Br, addition of a perfect inhibitor, variation of the rate of chain branching, or variation of the heat release rate from CO oxidation.

Numerical Technique

Perturbation Mechanics

The reacting system was perturbed by modifying selected reaction rates in a region or regions, also called bands. In some cases, reactions were turned "on" in the band, and in others, they were turned "off" in the band. In this study, a band was defined by a temperature range. The perturbations were designed to limit the chemical action of an inhibitor in one or more of these bands. A perturbation could affect a single reaction (e.g., $H+O_2 \leftrightarrow OH+O$), a class of reactions (e.g., CO_2 formation reactions), or a portion of a chemical mechanism (e.g., reactions involving Br-containing species).

A perturbation factor, B_i, was defined for the selected group of reactions as, e.g.:

$$B_i = 1 \qquad T < T_b$$
$$0 < B_i < 1 \qquad T_b \leq T \leq (T_b + \Delta)$$
$$B_i = 1 \qquad T > (T_b + \Delta)$$

where T is the gas temperature, T_b is the temperature at the low edge of the band, and Δ is the width of the band. Figure 3-120a illustrates the band shape for this example. The reaction rates of the selected reactions were multiplied by B_i, and the rest of the reactions were not directly disturbed (i.e., B_i=1). To study different types of perturbations, the band depth (the magnitude of B_i), width (Δ), and shape (the variation of B_i with T) were varied.

For the study of flame inhibition, the pertinent reactions were turned off outside the band (B_i=0) and turned on inside the band (B_i=1), as illustrated in Figure 3-120b. For modeling of activation or deactivation of an inhibitor, a forward-facing or backward-facing step function was used; the inhibition reactions were turned off (or on) below a certain temperature and turned on (or off) above that temperature, as shown in Figure 3-120c and d.

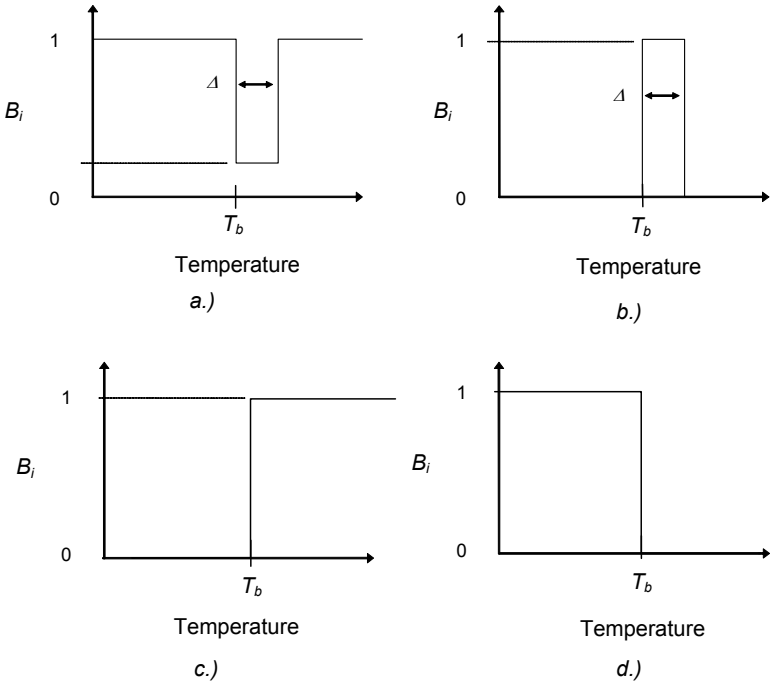

Figure 3-120. Shapes of the Reaction Rate Profile B_i Used to Describe: a) Perturbation of Chain Branching and Heat Release Rates, b) Addition of Perfect Inhibitor or CF_3Br, c) Rapid Inhibitor Activation, and d) Rapid Inhibitor Deactivation.

The band was smoothed at the edges to avoid numerical convergence problems caused by infinite gradients. The smoothing function was $B_i = a - b\ \mathrm{erf}(-c\ T^* + d)$, where $T^* = (T - T_b) / \Delta$ at the low temperature edge and $T^* = (T_b + \Delta - T) / \Delta$ at the high temperature edge. The constants a, b, c, and d were selected such that the width of the smoothed portion of the band was approximately $0.1 \cdot \Delta$ at each end.

Flame Modeling Approach

The Sandia flame code Premix[203], with the kinetic[204] and transport[205] subroutines, was used to simulate the freely-propagating premixed flame. The CHEMKIN subroutine CKRAT was modified to accommodate the chemical behavior of the model inhibitors. Part of the post-processing was performed using a graphical postprocessor.[362] For all calculations, the initial reactant temperature was 300 K and the pressure was 0.10133 MPa. The "GRAD" parameter was set to 0.15, and "CURV" was set to 0.35 for all of the calculations except those involving CF_3Br, where higher values of GRAD (0.35) and CURV (0.55) were used to reduce the calculation time. The former values of GRAD and CURV yielded 90 to 125 active grid points in the calculation, and the latter, 65 grid points. As discussed in Reference 57, the calculated burning velocity was estimated to be reduced about 6 % relative to a calculation with a (computationally more intensive) infinite number of grid points.

The kinetic and thermodynamic data of GRI-MECH 1.2[334] (32 species and 177 chemical reactions) served as a basis for describing the methane combustion, except when the inhibitor was CF_3Br. In that case, the mechanism of Babushok et al.[52] described the C_1/C_2 hydrocarbon chemistry and the halogen chemistry (70 species and 595 reactions). Reference 52 also provided experimental verification of the CF_3Br mechanism.

The perfect inhibitor model[167] represented an upper limit to the catalytic action of an inhibitor. The model assumed that the inhibitor-containing species In and InX (in which X is a flame radical H, O, or OH), reacted with radicals at gas-kinetic rates. All reactions were bimolecular, with an activation energy and temperature exponent of 0, and a pre-exponential factor of 1×10^{14} cm^3/mol-s; the transport properties of Ar were used for the species In and InX. The perfect inhibitor species were present at low concentrations, so their contribution to the energy balance was small. Also, since the reactions for these species were listed as forward and reverse rates, the choice of thermodynamic properties for these species did not affect their reaction rates. The perfect inhibitor reactions[167] were combined with those of GRI-MECH 1.2. Since the perfect inhibitor mechanism was a theoretical construct, it could not be experimentally verified. However, it had been compared with the experimental results for inhibition by the very powerful flame inhibitor $Fe(CO)_5$, and found to give burning velocity reductions reasonably close to that agent.[167]

A stoichiometric, freely-propagating premixed CH_4-air flame was perturbed in temperature bands of $\Delta = 300$ K. The following four types of perturbation were used:

- Reduction of the rate of chain branching by $H+O_2 \leftrightarrow OH+O$ (referred to as "$H+O_2$" below), because it provided a majority of the chain branching at high temperature.
- Reduction of the rate of heat release by $CO+OH \leftrightarrow CO_2+H$ (referred to as "CO+OH" below), because of its importance in determination of the final flame temperature.
- Catalytic scavenging of radicals (O, OH, and H) by a perfect inhibitor,[167] to investigate the maximum inhibition effect.
- Inhibition by CF_3Br, because it was a benchmark in flame inhibition studies.

The band width of 300 K was selected after conducting extensive numerical experiments with different band widths ranging from 50 K to 2000 K. The results consistently showed that the location of maximum inhibition was independent of the width of the band. The minimum burning velocity decreased as the

band became wider, but the band-center temperature of minimum burning velocity remained nearly constant for the perturbation considered. The choice of a 300 K bandwidth was made as a compromise between having too little effect (a 100 K band only decreased burning velocity by 15 %) and being too wide to provide insight into the inhibition mechanisms. Selected input parameters and calculated results are listed in Table 3-22.

Table 3-22. Input Parameters and Calculated Temperatures and Flame Speeds.

Perturbation	ϕ	B_i Inside Band	B_i Outside Band	Inhibitor Volume Fraction	T_{max} (K)	$S_{L,0}$ [a] (cm/s)	$S_{L,all}$ [b] (cm/s)	$S_{L,min}$ [c] (cm/s)	T_c for $S_{L,min}$ (K)
$H+O_2$	0.7	0.45	1.0	n.a.	1850	20.7	n.c.	15.5	1550
$H+O_2$	1.0	0.45	1.0	n.a.	2235	41.2	n.c.	31.0	1800
$H+O_2$	1.3	0.45	1.0	n.a.	2056	25.2	n.c.	18.0	1850
CO+OH	1.0	0.1	1.0	n.a.	2235	41.2	n.c.	29.1	1850
Perfect	0.7	1.0	0.0	$2.0\cdot10^{-5}$	1850	20.7	13.8	16.2	1650
Perfect	1.0	1.0	0.0	$4.0\cdot10^{-5}$	2235	41.2	27	30.9	1950
Perfect	1.3	1.0	0.0	$2.6\cdot10^{-5}$	2056	25.2	16.8	18.3	2000
CF_3Br	1.0	1.0	10^{-4}	0.00755	2235	41.2 [d]	26.4	29.2	1750

[a] Flame speed of the unperturbed or uninhibited flame.

[b] Flame speed with perturbation throughout flame.

[c] Minimum flame speed with perturbation in a bandwidth of 300 K.

[d] The flame speed is 39.0 cm/s when the halogen chemistry is turned off throughout the flame because of the physical effects of CF_3Br.

n.a. = not applicable.

n.c. = not calculated.

For $H+O_2$ and CO+OH, the smoothing function constants are a=0.55, b=0.45, c=60, d=57.

For the perfect inhibitor, the smoothing function constants are a=0.5, b=0.5, c=60, d=57.

For the $H+O_2$ and CO+OH perturbation, the reaction of interest was unaffected outside the band ($B_i = 1$) and damped inside the band ($B_i = 0.45$ for $H+O_2$, $B_i = 0.1$ for CO+OH). Thus, the reduction in heat release for the CO+OH reaction was achieved through a reduction in the rate of this reaction within the band. For the perfect inhibitor, reactions involving the perfect inhibitor were turned off outside the band ($B_i = 0$), and turned on inside the band (B_i=1). The volume fraction of the perfect inhibitor in the unburned gas was $4.0\cdot10^{-5}$, which resulted in a flame speed (S_L) of 27 cm/s when the inhibitor was active throughout the flame. (For comparison, S_L=41 cm/s for the uninhibited flame.)

For inhibition by CF_3Br, the reactant stream consisted of a stoichiometric mixture of methane and air a volume fraction of added CF_3Br of 0.0755, resulting in a one-third reduction in flame speed (to 26.4 cm/s) when the inhibitor was active throughout the flame. Ideally, when simulating the model inhibitors, the reactions involving Br- and F-containing species would be turned on ($B_i = 1$) in the band and turned off outside the band ($B_i = 0$). Because of convergence problems compounded by the size of the mechanism, a very small value of B_i ($= 10^{-4}$) for the halogen chemistry was used outside the band.

Results and Discussion

Figure 3-121 shows the response of the flame to each of the four perturbations**.** The calculated volume fractions of OH, H, and O (right axis) are shown for an uninhibited stoichiometric methane-air flame. The minimum flame speed occurred at a band-center temperature (T_c) of 1750 K for CF_3Br, 1800 K for $H+O_2$, 1850 K for CO+OH, and 1950 K for the perfect inhibitor. Using reaction flux analyses, it was possible to *infer* that the burning velocity of the flames would be most strongly perturbed at these temperatures: for $H+O_2$ and CO+OH, these temperatures correspond to the maximum reaction rate of the affected reaction (as shown in Figure 3-122). Similarly, for the perfect inhibitor, the temperature is near the temperature corresponding to the peak volume fractions of O, H, and OH (as shown in Figure 3-121). In this figure,

- "CF_3Br baseline" refers to the flame speed when the halogen chemistry is damped by 10^{-4}.
- The band width Δ is 300 K, so the band extends 150 K below and above the temperature shown on the x-axis.
- The kinks in some of the curves in Figure 3-121, as well as in Figure 3-123 and Figure 3-125, were caused by a somewhat coarse progression of calculated band-center temperatures, and would not be present for a finer series of calculations.
- The reduction in flame speed for $H+O_2$ and CO+OH can only be compared qualitatively to results for the perfect inhibitor and CF_3Br, because of the different value of B_i in the bands.

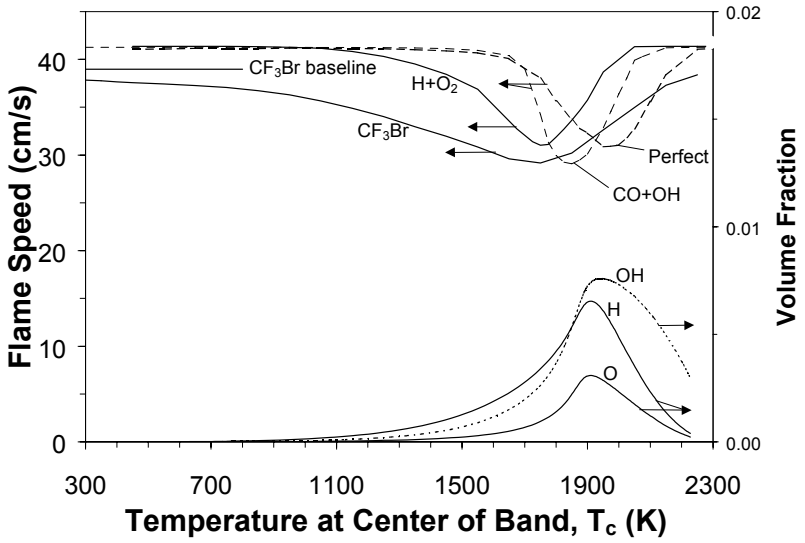

Figure 3-121. Variation of Flame Speed for Four Types of Perturbation. The calculated volume fraction of OH, H, and O (right axis) is shown for an uninhibited stoichiometric methane-air flame.

The difference in location of peak effectiveness of CF_3Br vs. the perfect inhibitor was caused by the shift of the partial equilibrium of the scavenging reactions. For CF_3Br at higher temperature, the equilibrium for the inhibition reaction $H+HBr \leftrightarrow H_2+Br$ shifted to the left,[41] reducing the effectiveness.

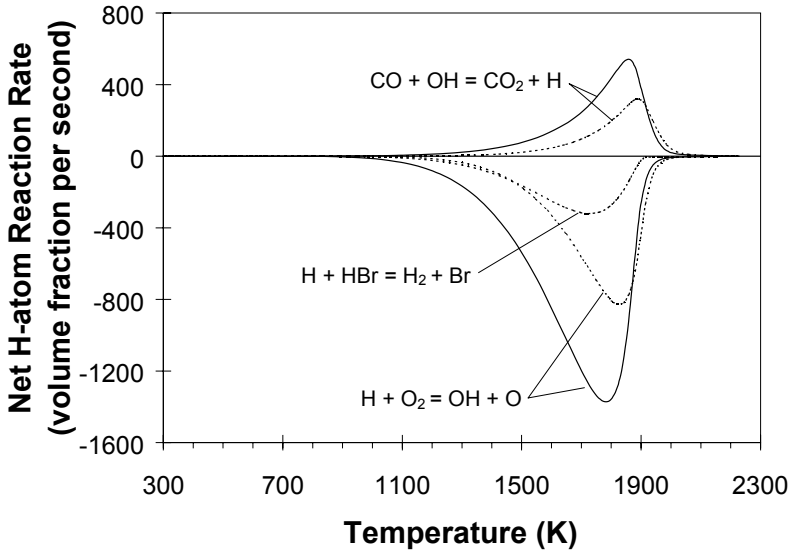

Figure 3-122. Net H-atom Reaction Rate for Three Important Reactions in Stoichiometric Methane-air Flames. Solid lines: uninhibited flame; dashed lines: CF_3Br-inhibited flame (agent volume fraction of 0.00755).

These results show that, although some of the inhibition effect of HBr and CF_3Br occurred upstream of the locations of the maximum rates for the chain branching and heat release reactions, the most sensitive temperature region (1600 K to 1900 K) was higher than had been found in prior work. In studies of inhibition of premixed flames by CH_3Br, CF_3Br and HBr, it had been argued that the primary inhibition occurred upstream of the main reaction zone. Wilson[4] and Wilson et al.[39] investigated inhibition of low pressure (5.1 kPa) methane-oxygen flames inhibited by CH_3Br and HBr. Based on flame structure measurements and calculations, they suggested that inhibition occurred through reduction of radical generation in the "pre-ignition" part of the flame. In a numerical modeling study, Westbrook[332] argued that HBr had its maximum effect in a temperature range between about 1000 K and 1400 K, where the reaction of H atom with HBr competed with its reaction with CH_4 or O_2. Williams and Fleming [26] also described CF_3Br as reducing H-atom concentrations significantly in the lower temperature regions of the flame (< 1200 K); nonetheless, their data showed that the largest absolute reduction in the H-atom volume fraction occurred near 1700 K. Casias and McKinnon[346] also contended that reactions in the low temperature region were of highest importance for inhibition by CF_3Br, although the conditions of their calculated flames (ethylene-air with 1 % CF_3Br) were somewhat different.

Figure 3-123 shows the effect of chain branching perturbation (Δ = 300 K) on normalized flame speed for three equivalence ratios: lean (ϕ = 0.7), stoichiometric (ϕ = 1.0), and rich (ϕ = 1.3). Table 3-22 lists calculated maximum temperatures and flame speeds for uninhibited flames at each equivalence ratio. The normalized flame speed was defined as the ratio of the flame speed of a band-inhibited flame to the flame speed of the corresponding uninhibited flame. The temperature of minimum flame speed of the different flames followed the relative position peak of the H-atom volume fraction (Figure 3-124a). The temperature range of maximum influence varied with ϕ, however, because the final temperature of the flame changed with ϕ (Table 3-22).

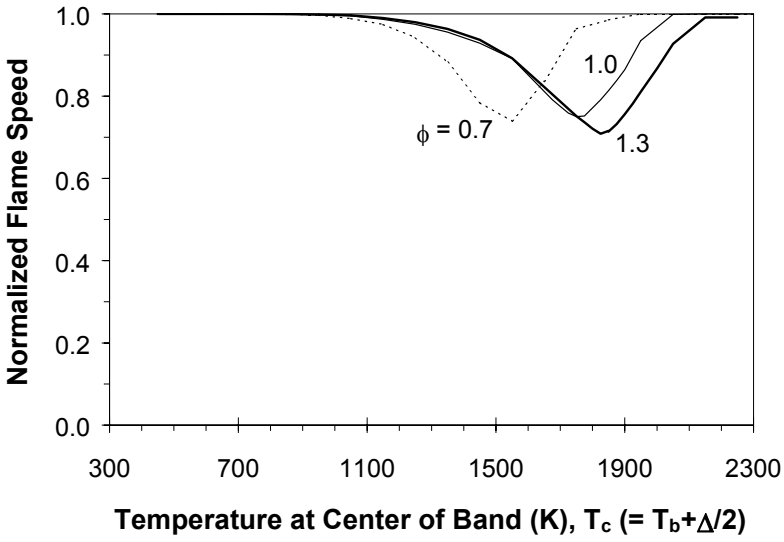

Figure 3-123 Effect of damping the rate of the $H+O_2$ reaction on normalized flame speed for ϕ=0.7, 1.0, and 1.3.

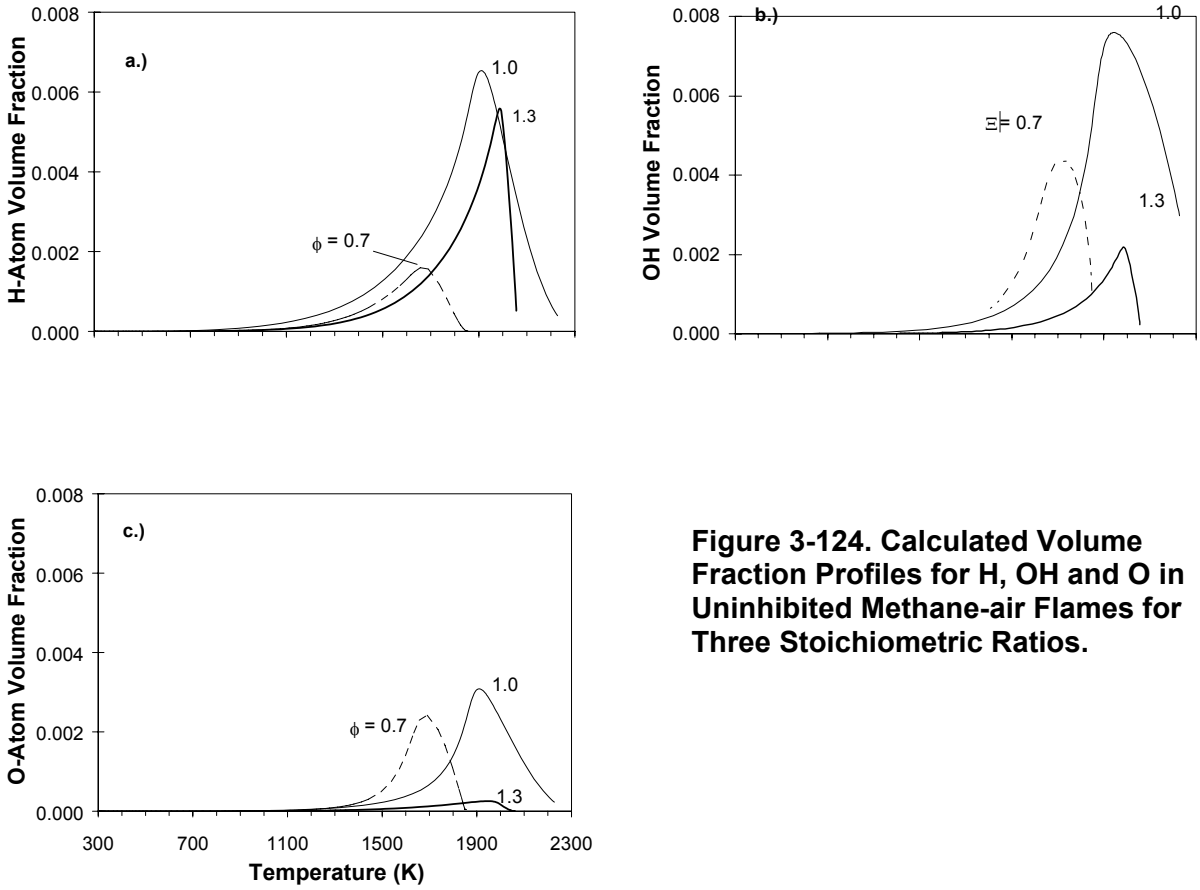

Figure 3-124. Calculated Volume Fraction Profiles for H, OH and O in Uninhibited Methane-air Flames for Three Stoichiometric Ratios.

The flame speeds for stoichiometric, rich, and lean flames inhibited by the perfect inhibitor are shown in Figure 3-125. The initial volume fraction of perfect inhibitor used for the calculations was the amount needed for a one-third reduction of flame speed (with the inhibiting reactions active throughout the flame) from the uninhibited condition (see Table 3-22). For band inhibition at the three values of ϕ, the perfect inhibitor showed flame speed reductions qualitatively similar to the results for $H+O_2$ suppression (as indicated in Table 3-22): the temperature range for maximum effect was lowest for the lean flame, and was higher for stoichiometric and rich flames, which were nearly the same. The ordering followed that of the peak radical volume fractions that are shown in Figure 3-124a-c. The calculations generally demonstrated that inhibition in only a small portion of the flame was responsible for most of the inhibitory effect. For example, as shown in Figure 3-125, when the inhibiting reactions in the lean flame were turned on between 1500 K and 1800 K (T_c = 1650 K), the reduction in flame speed was 65 % as much as when the inhibiting reactions occurred over the entire flame domain. The equivalent results for stoichiometric and rich flames were 72 % and 82 %.

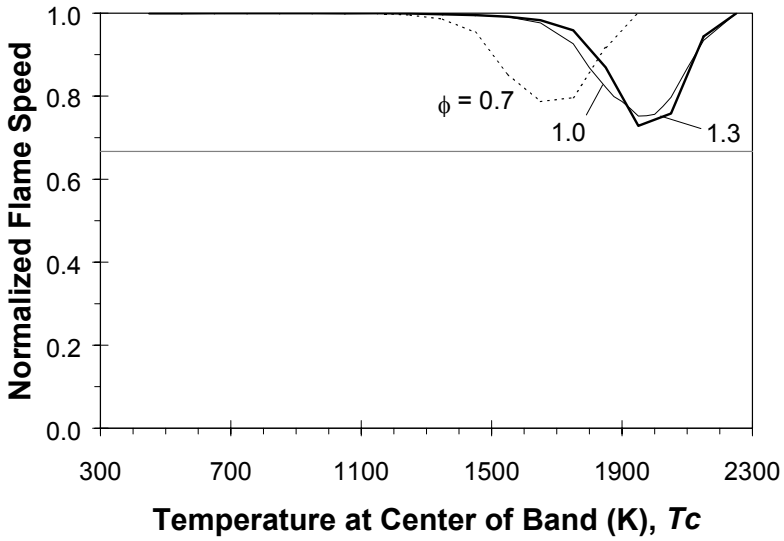

Figure 3-125. Effect of the Location of Perfect Inhibition on Normalized Flame Speed for ϕ=0.7, 1.0, and 1.3. The horizontal line marks the normalized flame speed when the flames are inhibited throughout the flame.

A general result of the calculations for the perfect inhibitor was that perturbation near the region of high radical volume fraction had the strongest effect on flame speed. In other words, removing H atoms from the high temperature region before they could diffuse upstream had the strongest effect on flame speed because inhibition reactions are faster in regions of high radical volume fraction and high temperature. The results for CF_3Br however, showed that the shift of the partial equilibrium at high temperature for certain reactions could influence the region of maximum influence of the agent.

A special, pertinent case evaluated by Linteris and co-workers was that of a potential new fire suppressant that could be inert at storage temperature and release an effective fire suppressant via decomposition or evaporation when added to a fire.[85] This would be analogous to the commonly used powder $NaHCO_3$, which decomposes to release the active scavenging species into the gas phase. To simulate such a system, they used a step function perturbation (as opposed to the impulse function in the previous section). The shape of the B_i function is illustrated in Figure 3-120c. Below the "activation temperature," the inhibition reactions were turned off, and above the activation temperature, the inhibition reactions were turned on. For ease of calculation, they used the perfect inhibitor model (with inhibitor volume fraction of $4.0 \cdot 10^{-5}$).

The curve labeled "activation" in Figure 3-126 shows the flame speed resulting from inhibitor activation at different temperatures between 300 K and 2200 K. The flame speed was fairly constant up to about 1700 K, but then started to increase. The location of the increase coincided with the peak radical concentration. As the activation occurred later in the flame, the inhibitor had less time to scavenge radicals.

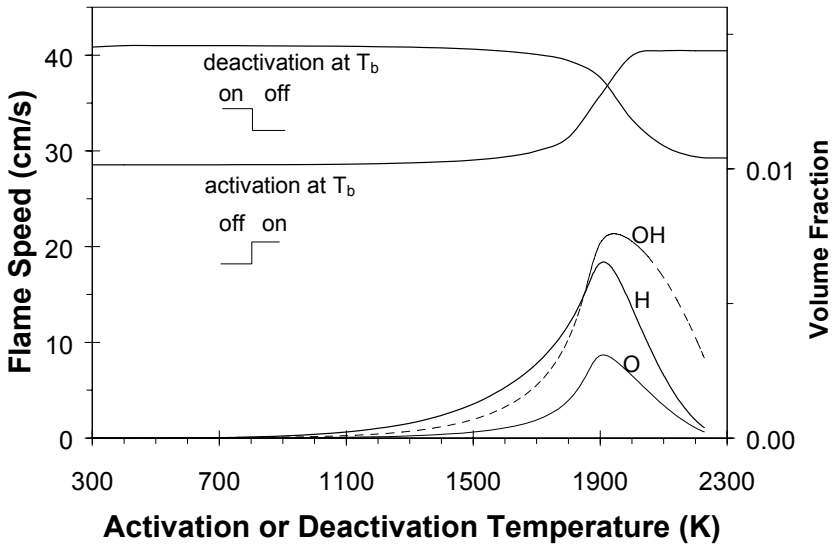

Figure 3-126. Variation of Flame Speed for Stepwise Inhibitor Activation or Deactivation for a Stoichiometric Methane-air Mixture. Also shown are calculated volume fractions of OH, H, and O in an uninhibited stoichiometric methane-air flame.

A second special case was that of an active inhibitor that decomposed at a certain temperature and lost its inhibition power. This was exemplified by $Fe(CO)_5$ inhibition, in which the active gas phase species were lost because of condensation to particles at some point in the flame. Since the particle formation was related to the residence time, the deactivation might occur over a range of temperatures. The stepwise deactivation was simulated with a band in which the B_i function (Figure 3-120d) was a mirror image of the previous example. Above the "deactivation" temperature, the inhibition reactions were turned off, and below the deactivation temperature, the inhibition reactions were turned on. As in the stepwise activation calculations, the effect of the inhibitor was more or less constant until about 1700 K. The very small reduction in flame speed when the inhibitor is active between 300 K and 1700 K reaffirmed the importance of the high temperature reactions. The most important region for the perfect inhibitor was above 1700 K for a strong effect on the flame speed; hence, particle formation for $Fe(CO)_5$ inhibition must be retarded until after the active species have reached the region of about 1700 K.

Conclusions

Numerical simulations of perturbed, premixed CH_4-air flames using model inhibitors with reaction rates spatially varied in the flame demonstrated the following:

- For agents which catalytically recombine radicals, the flame speed was most reduced when the inhibitor was allowed to act near (a) the region of maximum radical volume fraction or (b) the region of maximum rates of the radical scavenging reactions, depending upon the kinetic mechanism of the particular inhibitor.

- For CF_3Br-inhibited flames, the temperature of maximum influence was near 1750 K, significantly higher than previously suggested. The perturbations had a negligible effect in the region of the flame temperature below 1200 K.
- Inhibition in a relatively small portion of the flame caused a significant reduction in flame speed. In some cases, inhibition in a band spanning only 300 K caused nearly as much reduction in flame speed as when the inhibiting reactions were turned on everywhere.
- Perturbation of the $H+O_2 \leftrightarrow OH+O$ reaction rate or addition of the perfect inhibitor had a maximum burning velocity reduction in a temperature region which followed the relative position of the peak H-atom volume fraction. This was independent of whether the flame was rich, stoichiometric, or lean.
- The effect of sudden activation and deactivation of the perfect inhibitor was small when the activation or deactivation temperature was above or below 1700 K, respectively. Hence, new inhibitors that may be developed need not become active until near 1700 K, and must not lose their effectiveness until about 2150 K if they are to retain their maximum potential effectiveness.

It is important to note that these conclusions might be different for other fuels, inhibitors, or flame types.

3.6 INSIGHTS ON FLAME INHIBITION

Flame inhibition research has been conducted for more than 50 years, providing a technical base on which the NGP was able to build. As a result, the NGP has generated a unified view of chemical flame inhibition.

- Efficient chemical inhibition and suppression of flames results from reduction of the concentrations of flame propagating radicals (H, O, and OH) toward their equilibrium concentrations. This can result from (a) reaction of the inhibitor breakdown products with the radicals, forming stable product species which are relatively inert in the flame, and/or (b) catalytic radical recombination, in which intermediate species formed from the inhibitor breakdown products form more stable molecules from the radicals in a gas phase catalytic cycle.
- An effective catalytic inhibitor must:
    - Break down in the flame with a relatively low activation energy so that the proper intermediates for the catalytic cycle can be present with sufficient time to interact with the radical pool. NGP research has shown that alternate forms of parent molecules can be used as long as they readily breakdown and form the same intermediate species.
    - Form intermediates that regenerate themselves in the catalytic cycle and undergo reactions that are nearly thermally neutral and fast.
    - Break down to intermediate species which can then make it to the right part of the flame, which is the location of the peak chain branching reactions (and hence, peak radical volume fractions). This is generally in the temperature regime between 1700 K and 2100 K.
- Fuels with larger radical pools will be less affected by addition of a catalytic inhibitor.

- Flow-field effects can limit effectiveness, for example through the formation of a condensed phase, followed by entrainment or thermophoresis which limit the agent's transport to the radical pool location.
- Thermodynamic constraints can keep the active moiety from forming the necessary intermediates at the radical pool location by:
    - Driving the active moiety into less active chemical forms, or creating an imbalance in the distribution of species in the catalytic cycle.
    - Causing the intermediates to form a less active condensed form, such as liquid NaOH, or particles of metal oxides.
    - Forming non-active stable species, such as the conversion of Fe to iron fluorides.

NGP research has also developed solid understanding of the flame quenching activity of chemicals built around certain highly effective atoms.

- Extinction measurement and OH reduction were equivalent markers of agent effectiveness.
- Compounds of iron, manganese, chromium, antimony, lead, and tin were very effective at reducing the rates of the chemical reactions that propagate flames.
- Additional metals whose compounds are likely to be effective at low concentrations, but which had not been suggested in previous reviews of metal flame inhibition, are tungsten, molybdenum, and cobalt.
- Phosphorus-containing compounds can be 40 times more effective than nitrogen and 2 to 4 times more effective than CF_3Br at quenching non-premixed hydrocarbon flames.
- DMMP and TMP were roughly equivalent in suppression efficiency, independent of the differences in their ligands. PN was decidedly less effective, likely due to the resonant bonding of the phosphorus atoms in the parent molecule.
- Catalytic inhibitors in general have a strong temperature dependence, with lower effectiveness at higher adiabatic flame temperatures.
- Current computational models adequately (but somewhat under-) predicted the effect of DMMP on flame extinguishment. This may have been due to the significant uncertainties in several of the reaction rate coefficients in the phosphorus mechanism.

3.7 REFERENCES

1. Battin-Leclerc, F., Walravens, B., Come, G.M., Baronnet, F., Sanogo, O., Delfau, J.L., and Vovelle, C., "The Chemical Inhibiting Effect of Some Fluorocarbons and Hydrofluorocarbons Proposed As Substitutes for Halons," in Miziolek, A.W. and Tsang, W., eds., *Halon Replacements: Technology and Science* ACS Symposium Series 611, American Chemical Society, Washington, D.C., 1995.

2. Li, K., Kennedy, E.M., Moghtaderi, B., and Dlugogorski, B.Z., "Experimental and Computational Studies on the Gas-Phase Reaction of CF_3Br With Hydrogen," *Environmental Science & Technology* **34,** 584-590 (2000).

3. Simmons, R.F. and Wolfhard, H.G., "The Influence of Methyl Bromide on Flames, Part 1.-Pre-Mixed Flames ," *Combustion and Flame* **1,** 155-161 (1957).

4. Wilson, W.E., "Structure, Kinetics, and Mechanism of a Methane-Oxygen Flame Inhibited With Methyl Bromide ," *Proceedings of the Combustion Institute* **10,** 47-54 (1965).

5. Biordi, J.C., Lazzara, C.P., and Papp, J.F., "Flame-Structure Studies of CF_3Br-Inhibited Methane Flames," *Proceedings of the Combustion Institute* **14,** 367-381 (1973).

6. Hayes, K.F. and Kaskan, W.E., "Inhibition by CH_3Br of CH_4-Air Flames Stabilized on a Porous Burner," *Combustion and Flame* **24,** 405-407 (1975).

7. Safieh, H.Y., Vandooren, J., and Van Tiggelen, P.J., "Experimental Study of Inhibition Induced by CF_3Br in a CO-H_2-O_2-Ar Flame," *Proceedings of the Combustion Institute* **19,** 117-126 (1982).

8. Westbrook, C.K., "Inhibition of Hydrocarbon Oxidation in Laminar Flames and Detonations by Halogenated Compounds," *Proceedings of the Combustion Institute* **19,** 127-141 (1982).

9. Reynolds, W.C., *"The Element Potential Method for Chemical Equilibrium Analysis: Implementation in the Interactive Program STANJAN,"* ME 270 HO no 7, *Stanford University* , Stanford, CA, (1986).

10. Sanogo, O., Delfau, J.L., Akrich, R., and Vovelle, C., "A Comparative Study of the Structure of CF_3Br- and CF_3I-Doped Methane Flames," *Journal De Chimie Physique Et De Physico-Chimie Biologique* **93,** 1939-1957 (1996).

11. Kim, C.H., Kwon, O.C., and Faeth, G.M., "Effects of Halons and Halon Replacements on Hydrogen-Fueled Laminar Premixed Flames," *Journal of Propulsion and Power* **18,** 1059-1067 (2002).

12. Simmons, R.F. and Wolfhard, H.G., "The Influence of Methyl Bromide on Flames, Part 2.-Diffusion Flames," *Transactions of the Faraday Society* **52,** 53-59 (1956).

13. Sheinson, R.S., Penner-Hahn, J.E., and Indritz, D., "The Physical and Chemical Action of Fire Suppressants," *Fire Safety Journal* **15,** 437-450 (1989).

14. Lott, J.L., Christian, S.D., Sliepcevich, C.M., and Tucker, E.E., "Synergism Between Chemical and Physical Fire-Suppressant Agents," *Fire Technology* **32,** 260-271 (1996).

15. Friedman, R. and Levy, J.B., "Inhibition of Opposed-Jet Methane-Air Diffusion Flame. The Effects of Alkali Metal Vapours and Organic Halides," *Combustion and Flame* **7,** 195 (1963).

16. Milne, T.A., Green, C.L., and Benson, D.K., "The Use of the Counter-Flow Diffusion Flame in Studies of Inhibition Effectiveness of Gaseous and Powdered Agents," *Combustion and Flame* **15,** 255-264 (1970).

17. Kent, J.H. and Williams, F.A., "Effect of CF_3Br on Stagnation-Point Combustion of a Heptane Pool," *Proceedings of the Western States Section Meeting*, pp. 73-24, Combustion Institute, Pittsburgh, PA, 1973.

18. Seshadri, K. and Williams, F.A., "Effect of CF_3Br on Counterflow Combustion of Liquid Fuel With Diluted Oxygen," in Gann, R.G., ed., *Halogenated Fire Suppressants* ACS Symposium Series 16, American Chemical Society, Washington, D.C., 1975.

19. Marolewski, T.A. and Weil, E.D., "A Review of Phosphate Ester Fire Resistance Mechanisms and Their Relevance to Fluid Testing, Vol. ASTM STP 1284," in Totten, G.E. and Jürgen, R., Eds., *Fire Resistance of Industrial Fluids* American Society for Testing and Materials, Philadelphia, 1996.

20. Babushok, V., Noto, T., Burgess, D.R.F., Hamins, A., and Tsang, W., "Influence of CF_3I, CF_3Br, and CF_3H on the High-Temperature Combustion of Methane," *Combustion and Flame* **107,** 351-367 (1996).

21. Grosshandler, W.L., Gann, R.G., and Pitts, W.M., *"Evaluation of Alternative In-Flight Fire Suppressants for Full-Scale Testing in Simulated Aircraft Engine Nacelles and Dry Bays,"* NIST SP 861, National Institute of Standards and Technology, Gaithersburg, MD, (1994).

22. Gann, R.G., *"Fire Suppression System Performance of Alternative Agents in Aircraft Engines and Dry Bay Laboratory Simulations,"* NIST SP 890, vols. I and II, National Institute of Standards and Technology, Gaithersburg MD, (1995).

23. Gann, R.G., *" FY2003 Annual Report -- Next Generation Fire Suppression Technology Program (NGP),"* NIST Technical Note 1457, National Institute of Standards and Technology, Gaithersburg, MD, (2004).

24. Saso, Y., "Roles of Inhibitors in Global Gas-Phase Combustion Kinetics," *Proceedings of the Combustion Institute* **29,** 337-344 (2003).

25. Vora, N. and Laurendeau, N.M., "Analysis of CF_3Br Flame Suppression Activity Using Quantitative Laser-Induced Fluorescence Measurements of the Hydroxyl Radical," *Combustion Science and Technology* **166,** 15-39 (2001).

26. Williams, B.A. and Fleming, J.W., "CF_3Br and Other Suppressants: Differences in Effects on Flame Structure," *Proceedings of the Combustion Institute* **29,** 345-351 (2003).

27. Bundy, M., Hamins, A., and Lee, K.Y., "Suppression Limits of Low Strain Rate Non-Premixed Methane Flames," *Combustion and Flame* **133,** 299-310 (2003).

28. Williams, F.A., "A Unified View of Fire Suppression," *Journal of Fire and Flammability* **5,** 54-63 (1974).

29. Burgoyne, J.H. and Williams-Lier, G., "The Influence of Incombustible Vapours on the Limits of Inflammability of Gases and Vapours in Air," *Proceedings of the Royal Society* **A193,** 525-539 (1948).

30. Belles, F.E. and O'Neal, C., Jr., "Effects of Halogenated Extinguishing Agents on Flame Quenching and a Chemical Interpretation of Their Action," *Proceedings of the Combustion Institute* **6,** 806-813 (1957).

31. Butlin, R.N. and Simmons, R.F., "The Inhibition of Hydrogen-Air Flames by Hydrogen Bromide," *Combustion and Flame* **12,** 447-456 (1968).

32. Garner, F.H., Long, R., Graham, A.J., and Badakhshan, A., "Effect of Certain Halogenated Methanes on Premixed and Diffusion Flames," *Proceedings of the Combustion Institute* **6,** 802 (1957).

33. Rosser, W.A., Wise, H., and Miller, J., "Mechanism of Combustion Inhibition by Compounds Containing Halogen," *Proceedings of the Combustion Institute* **7,** 175-182 (1959).

34. Lask, G. and Wagner, H.G., "Influence of Additives on the Velocity of Laminar Flames," *Proceedings of the Combustion Institute* **8,** 432-438 (1962).

35. Edmondson, H. and Heap, M.P., "The Burning Velocity of Methane-Air Flames Inhibited by Methyl Bromide," *Combustion and Flame* **13,** 472-478 (1969).

36. Niioka, T., Mitani, T., and Takahashi, M., "Experimental Study on Inhibited Diffusion and Premixed Flames in a Counterflow System," *Combustion and Flame* **50,** 89-97 (1983).

37. Mitani, T., "Flame-Retardant Effects of CF_3Br and $NaHCO_3$," *Combustion and Flame* **50,** 177-188 (1983).

38. Levy, A., Droege, J.W., Tighe, J.J., and Foster, J.F., "The Inhibition of Lean Methane Flames," *Proceedings of the Combustion Institute* **8,** 524-533 (1960).

39. Wilson, W.E., O'Donavan, J.T., and Fristrom, R.M., "Flame Inhibition by Halogen Compounds," *Proceedings of the Combustion Institute* **12,** 929-942 (1969).

40. Biordi, J.C., Lazzara, C.P., and Papp, J.F., R.G. Gann, "The Effect of CF_3Br on a $CO-H_2-O_2$-Ar Diffusion Flame," *Halogenated Fire Suppressants,* American Chemical Society, Washington, D.C., 256-294 (1975).

41. Day, M.J., Stamp, D.V., Thompson, K., and Dixon-Lewis, G., "Inhibition of Hydrogen-Air and Hydrogen-Nitrous Oxide Flames by Halogen Compounds," *Proceedings of the Combustion Institute* **13,** 705-712 (1971).

42. Dixon-Lewis, G. and Simpson, R.J., "Aspects of Flame Inhibition by Halogen Compounds," *Proceedings of the Combustion Institute* **16,** 1111-1119 (1977).

43. Westbrook, C.K., "Numerical Modeling of Flame Inhibition by CF_3Br," *Combustion Science and Technology* **34,** 201-225 (1983).

44. Creitz, E.C., "Inhibition of Diffusion Flames by Methyl Bromide and Trifluoromethyl Bromide Applied to the Fuel and Oxygen Sides of the Reaction Zone," *Journal of Research of the National Bureau of Standards A. Physics and Chemistry* **65A,** 389-396 (1961).

45. Masri, A.R., "Chemical Inhibition of Nonpremixed Flames of Hydrocarbon Fuels With CF_3Br," *Combustion Science and Technology* **96,** 189-212 (1994).

46. Masri, A.R. and Clarke, T.C., "Lifted Flames and the Effects of Inhibitors," *Combustion Science and Technology* **105,** 345-355 (1995).

47. Ibiricu, M.M. and Gaydon, A.G., "Spectroscopic Studies of the Effect of Inhibitors on Counterflow Diffusion Flames," *Combustion and Flame* **8,** 51-61 (1964).

48. Kent, J.H. and Williams, F.A., "Extinction of Laminar Diffusion Flames for Liquid Fuels," *Proceedings of the Combustion Institute* **15,** 315-325 (1974).

49. Seshadri, K. and Williams, F.A., "Effect of CF_3Br on Counterflow Combustion of Liquid Fuel With Diluted Oxygen," in Gann, R.G., ed., *Halogenated Fire Suppressants* ACS Symposium Series 16, American Chemical Society, Washington, D.C., 1975.

50. Hamins, A., Trees, D., Seshadri, K., and Chelliah, H.K., "Extinction of Nonpremixed Flames With Halogenated Fire Suppressants," *Combustion and Flame* **99,** 221-230 (1994).

51. Smyth, K.C. and Everest, D.A., "The Effect of CF_3I Compared to CF_3Br on OH Soot Concentrations in Co-Flowing Propane/Air Diffusion Flames," *Proceedings of the Combustion Institute*, 1385-1393, The Combustion Institute, Pittsburgh, 1996.

52. Noto, T., Babushok, V., Burgess Jr., D.R., Hamins, A., Tsang, W., and Miziolek, A.W., "Effect of Halogenated Flame Inhibitors on C1-C2 Organic Flames," *Proceedings of the Combustion Institute* **26,** 1377-1383 (1996).

53. Miziolek, A.W. and Tsang, W., eds., *Halon Replacements*, ACS Symposium Series 611, American Chemical Society, Washington, D.C., 1995.

54. Westmoreland, P.R., Burgess, D.R.F. Jr., Zachariah, M.R., and Tsang, W., "Fluoromethane Chemistry and Its Role in Flame Suppression," *Proceedings of the Combustion Institute* **25,** 1505 (1994).

55. Hynes, R.G., Mackie, J.C., and Masri, A.R., "Inhibition of Premixed Hydrogen-Air Flames by 2-H Heptafluoropropane," *Combustion and Flame* **113,** 554-565 (1998).

56. Hynes, R.G., Mackie, J.C., and Masri, A.R., "Shock-Tube Study of the Pyrolysis of the Halon Replacement Molecule CF_3CHFCF_3," *Journal of Physical Chemistry a* **103,** 54-61 (1999).

57. Linteris, G.T. and Truett, L., "Inhibition of Premixed Methane-Air Flames by Fluoromethanes," *Combustion and Flame* **105,** 15-27 (1996).

58. Linteris, G.T., Burgess, D.R., Babushok, V., Zachariah, M., Tsang, W., and Westmoreland, P., "Inhibition of Premixed Methane-Air Flames by Fluoroethanes and Fluoropropanes," *Combustion and Flame* **113,** 164-180 (1998).

59. Sanogo, O., Delfau, J.L., Akrich, R., and Vovelle, C., "Experimental and Computational Study of the Effect of C_2F_6 on Premixed Methane Flames," *Proceedings of the Combustion Institute* **25,** 1489 (1994).

60. Vandooren, J., da Cruz, F.N., and Van Tiggelen, P.J., "The Inhibiting Effect of CF_3H on the Structure of a Stoichiometric $H_2/CO/O_2/Ar$ Flame," *Proceedings of the Combustion Institute* **22,** 1587-1595 (1988).

61. L'esperance, D., Williams, B.A., and Fleming, J.W., "Intermediate Species Profiles in Low Pressure Premixed Flames Inhibited by Fluoromethanes," *Combustion and Flame* **117,** 709-731 (1999).

62. Zegers, E.J.P., Williams, B.A., Fisher, E.M., Fleming, J.W., and Sheinson, R.S., "Suppression of Nonpremixed Flames by Fluorinated Ethanes and Propanes," *Combustion and Flame* **121,** 471-487 (2000).

63. Papas, P., Fleming, J.W., and Sheinson, R.S., "Extinction of Non-Premixed Methane- and Propane-Air Counterflow Flames Inhibited With CF_4, CF_3H, and CF_3Br," *Proceedings of the Combustion Institute* **26,** 1405-1411 (1996).

64. Huber, M., Gallagher, J., McLinden, M., and Morrison, G., NIST Thermodynamic Properties of Refrigerants and Refrigerant Mixtures Database (REFPROP), National Institute of Standards and Technology, Gaithersburg, MD, 1996.

65. Wagman, D.D., Evans, W.H., Parker, V.B., Schumm, R.H., Halow, I., Bailey, S.M., Churney, K.L., and Nuttall, R.L., "The NBS Tables of Chemical Thermodynamic Properties: Selected Values for Inorganic and C1 and C2 Organic Substances in SI Units.," *Journal of Physical Chemistry Reference Data* **11,** 1982).

66. Booth, K., Melia, B.J., and Hirst, R., *"Critical Concentration Measurements for Flame Extinguishment of Diffusion Flames Using Laboratory "Cup Burner" Apparatus,"* ICI Mond Division, Winnington Laboratory, (1973).

67. Chelliah, H.K., Law, C.K., Ueda, T., Smooke, M.D., and Williams, F.A., "An Experimental and Theoretical Investigation of the Dilution, Pressure and Flow-Field Effects on the Extinction Condition of Methane-Air-Nitrogen Diffusion Flames," *Proceedings of the Combustion Institute* **23,** 503-511 (1991).

68. Saso, Y., Saito, N., Liao, C.H., and Ogawa, Y., "Extinction of Counterflow Diffusion Flames With Halon Replacements," *Fire Safety Journal* **26,** 303-326 (1996).

69. Tucker, D.M., Drysdale, D.D., and Rasbash, D.J., "The Extinction of Diffusion Flames Burning in Various Oxygen Concentrations by Inert-Gases and Bromotrifluoromethane," *Combustion and Flame* **41,** 293-300 (1981).

70. Tanoff, M.A., Dobbins, R.R., Smooke, M.D., Burgess, D.R., Jr., Zachariah, M.R., Tsang, W., and Westmoreland, P.R., "C1 and C2 Fluorinated Hydrocarbon Effects on the Extinction Characteristics of

Methane Vs. Air Counterflow Diffusion Flames," in Gann, R.G., Burgess, S.R., Whisner, K.C., and Reneke, P.A., eds., *Papers From 1991-2006 Halon Options Technical Working Conferences (HOTWC)*, CD-ROM, NIST SP 984-4, National Institute of Standards and Technology, Gaithersburg, MD, (2006).

71. Potter, A.E., Jr. and Butler, J.N., "A Novel Combustion Measurement Based on the Extinguishment of Diffusion Flames," *American Rocket Society Journal* **29,** 54-56 (1959).

72. Konnov, A.A., Idir, M., Delfau, J.L., and Vovelle, C., "Experimental Study of Extinction of Nonadiabatic Counterflow Premixed Flames," *Combustion and Flame* **105,** 308-320 (1996).

73. Fallon, G.S., Chelliah, H.K., and Linteris, G.T., "Chemical Effects of CF_3H in Extinguishing Counterflow CO/Air/H_2 Diffusion Flames," *Proceedings of the Combustion Institute* **26,** 1395-1403 (1996).

74. Balakrishnan, G., Trees, D., and Williams, F.A., "An Experimental Investigation of Strain-Induced Extinction of Diluted Hydrogen-Air Counterflow Diffusion Flames," *Combustion and Flame* **98,** 123-126 (1994).

75. Rolon, J.C., Veynante, D., Martin, J.P., and Durst, F., "Counter Jet Stagnation Flows," *Experiments in Fluids* **11,** 313-324 (1991).

76. Seshadri, K. and Williams, F.A., "Laminar Flow Between Parallel Plates With Injection of Reactant at High Reynolds Number," *Int. J. of Heat and Mass Transfer* **21,** 137-150 (1978).

77. Pellett, G.L., Isaac, K.M., Humphreys, W.M., Gartrell, L.R., Roberts, W.L., Dancey, C.L., and Northam, G.B., "Velocity and Thermal Structure, and Strain-Induced Extinction of 14 to 100% Hydrogen-Air Counterflow Diffusion Flames," *Combustion and Flame* **112,** 575-592 (1998).

78. Yang, G.S. and Kennedy, I.A., "The Effect of Strain on Laminar Diffusion Flames of Chlorinated Hydrocarbons," *Combustion and Flame* **92,** 187-192 (1993).

79. Macdonald, M.A., Jayaweera, T.M., Fisher, E.M., and Gouldin, F.C., "Inhibition of Nonpremixed Flames by Phosphorus-Containing Compounds," *Combustion and Flame* **116,** 166-176 (1999).

80. Puri, I.K. and Seshadri, K., "Extinction of Diffusion Flames Burning Diluted Methane and Diluted Propane in Diluted Air ," *Combustion and Flame* **65,** 137-150 (1986).

81. Yang, M.H., Hamins, A., and Puri, I.K., "The Structure of Inhibited Counterflowing Nonpremixed Flames," *Combustion and Flame* **98,** 107-122 (1994).

82. Grosshandler, W., Donnelly, M., and Womeldorf, C., *"Lean Flammability Limit As a Fundamental Refrigerant Property. Final Technical Report,"* Report No. DOE/CE/23810-98, US Department of Energy, Washington, DC, (1998).

83. Burgess, D.R., Zachariah, M.R., Tsang, W., and Westmoreland, P.R., *"Thermochemical and Chemical Kinetic Data for Fluorinated Hydrocarbons,"* NIST TN 1412, National Institute of Standards and Technology, Gaithersburg, MD, (1995).

84. Williams, B.A., L'esperance, D.M., and Fleming, J.W., "Intermediate Species Profiles in Low-Pressure Methane/Oxygen Flames Inhibited by 2-H Heptafluoropropane: Comparison of Experimental Data With Kinetic Modeling," *Combustion and Flame* **120,** 160-172 (2000).

85. Linteris, G.T. and Chelliah, H.K., *"Powder-Matrix Systems for Safer Handling and Storage of Suppression Agents,"* NISTIR 6766, National Institute of Standards and Technology, Gaithersburg, MD, (2001).

86. Linteris, G.T., Rumminger, M.D., Babushok, V., Chelliah, H., Lazzarini, A.K., and Wanigarathne, P., *"Effective Non-Toxic Metallic Fire Suppressants,"* NISTIR 6875, National Institute of Standards and Technology, Gaithersburg MD, (2002).

87. Linteris, G.T., *"Limits to the Effectiveness of Metal-Containing Fire Suppressants,"* NISTIR 7177, National Institute of Standards and Technology, Gaithersburg MD, (2004).

88. Jost, W., Bonne, U., and Wagner, H.G., "Iron Carbonyl Found to Be Powerful Flame Inhibitor," *Chemical & Engineering News* **39,** 76 (1961).

89. Bonne, U., Jost, W., and Wagner, H.G., "Iron Pentacarbonyl in Methane-Oxygen (or Air) Flames," *Fire Research Abstracts and Reviews* **4,** 6-18 (1962).

90. Kimmel, E.C., Smith, E.A., Reboulet, J.E., Black, B.H., Sheinson, R.S., and Carpenter, R.L., "Physical and Chemical Characteristics of SFE Fire Suppressant Atmospheres: Comparison of Small- With Large-Scale Laboratory Atmospheres," in Gann, R.G., Burgess, S.R., Whisner, K.C., and Reneke, P.A., eds., *Papers From 1991-2006 Halon Options Technical Working Conferences (HOTWC)*, CD-ROM, NIST SP 984-4, National Institute of Standards and Technology, Gaithersburg, MD, (2006).

91. Rosser, W.A., Inami, S.H., and Wise, H., "The Effect of Metal Salts on Premixed Hydrocarbon-Air Flames," *Combustion and Flame* **7,** 107-119 (1963).

92. Vanpee, M. and Shirodkar, P., "A Study of Flame Inhibition by Metal Compounds," *Proceedings of the Combustion Institute* **17,** 787-795 (1979).

93. Skaggs, R.R., Daniel, R.G., Miziolek, A.W., McNesby, K.L., Babushok, V.I., Tsang, W., and Smooke, M.D., "Spectroscopic Studies of Inhibited Opposed-Flow Propane-Air Flames," in Gann, R.G., Burgess, S.R., Whisner, K.C., and Reneke, P.A., eds., *Papers From 1991-2006 Halon Options Technical Working Conferences (HOTWC)*, CD-ROM, NIST SP 984-4, National Institute of Standards and Technology, Gaithersburg, MD, (2006).

94. Kovarik, B., "Charles F. Kettering and the Development of Tetraethyl Lead in the Context of Alternative Fuel Technologies," *Fuels and Lubricants*, Society of Automotive Engineers, New York, 1994.

95. Walsh, A.D., "The Mode of Action of Tetraethyllead As an Antiknock," in *Six Lectures on the Basic Combustion Process* Ethyl Corp., New York, NY, 1954.

96. Erhard, K.H.L. and Norrish, R.G.W., "Studies of Knock and Antiknock by Kinetic Spectroscopy," *Proceedings of the Royal Society (London) A* **234,** 178-191 (1956).

97. Muraour, H., "La Theorie Des Anti-Detonants," *Chem. et Industr.* **14,** 1911 (1925).

98. Chamberlain, G.H.N. and Walsh, A.D., "The Inhibiting Effect of Lead Tetraethyl. 1. The Effect of Lead Compounds on the Vapour Phase Slow Oxidation of Diisopropyl Ether and on the Ignition of Diethyl Ether.," *Proceedings of the Royal Society A* **215,** 175-186 (1952).

99. Cheaney, D.E., Davies, D.A., Davis, A., Hoare, D.E., Protheroe, J., and Walsh, A.D., "Effects of Surfaces on Combustion of Methane and Mode of Action of Anti-Knock Containing Metals," *Proceedings of the Combustion Institute* **7,** 183-187 (1959).

100. Richardson, W.L., Ryason, P.R., Kautsky, G.J., and Barusch, M.R., "Organolead Antiknock Agents-Their Performance and Mode of Action ," *Proceedings of the Combustion Institute* **9,** 1023-1033 (1962).

101. Zimpel, C.F. and Graiff, L.B., "An Electron Microscopic Study of Tetraethyllead Decomposition in an Internal Combustion Engine," *Proceedings of the Combustion Institute* **11,** 1015-1025 (1967).

102. Rumminger, M.D. and Linteris, G.T., "The Role of Particles in the Inhibition of Premixed Flames by Iron Pentacarbonyl," *Combustion and Flame* **123,** 82-94 (2000).

103. Reinelt, D. and Linteris, G.T., "Experimental Study of the Inhibition of Premixed and Diffusion Flames by Iron Pentacarbonyl," *Proceedings of the Combustion Institute* **26,** 1421-1428 (1996).

104. Rumminger, M.D., Reinelt, D., Babushok, V.I., and Linteris, G.T., "Numerical Study of the Inhibition of Premixed and Diffusion Flames by Iron Pentacarbonyl," *Combustion and Flame* **116,** 207-219 (1999).

105. Rumminger, M.D. and Linteris, G.T., "Numerical Modeling of Counterflow Diffusion Flames Inhibited by Iron Pentacarbonyl," *Fire Safety Science: Proceedings of the Sixth International Symposium*, 289-300, Int. Assoc. for Fire Safety Science, Marne-La-Vallee, France, 2000.

106. Linteris, G.T., Rumminger, M.D., Babushok, V.I., and Tsang, W., "Flame Inhibition by Ferrocene and Blends of Inert and Catalytic Agents," *Proceedings of the Combustion Institute* **28,** 2965-2972 (2000).

107. Linteris, G.T., Knyazev, V.D., and Babushok, V.I., "Inhibition of Premixed Methane Flames by Manganese and Tin Compounds," *Combustion and Flame* **129,** 221-238 (2002).

108. Rumminger, M.D. and Linteris, G.T., "The Role of Particles in the Inhibition of Counterflow Diffusion Flames by Iron Pentacarbonyl," *Combustion and Flame* **128,** 145-164 (2002).

109. Kuppu Rao, V. and Prasad, C.R., "Knock Suppression in Petrol Engines," *Combustion and Flame* **18,** 167-172 (1972).

110. Linteris, G.T. and Rumminger, M.D., "Particle Formation in Laminar Flames Inhibited by Metals," *Proceedings of the Western States Section Meeting*, Paper 030, Combustion Institute, Pittsburgh, PA, 2002.

111. Morrison, M.E. and Scheller, K., "The Effect of Burning Velocity Inhibitors on the Ignition of Hydrocarbon-Oxygen-Nitrogen Mixtures," *Combustion and Flame* **18,** 3-12 (1972).

112. Miller, D.R., Evers, R.L., and Skinner, G.B., "Effects of Various Inhibitors on Hydrogen-Air Flame Speeds," *Combustion and Flame* **7,** 137-142 (1963).

113. Miller, W.J., "Inhibition of Low Pressure Flames," *Combustion and Flame* **13,** 210-212 (1969).

114. Cotton, D.H. and Jenkins, D.R., "Catalysis of Radical-Recombination Reactions in Flames by Alkaline Earth Metals," *Transactions of the Faraday Society* **67,** 730-739 (1971).

115. Bulewicz, E.M., Padley, P.J., Cotton, D.H., and Jenkins, D.R., "Metal-Additive-Catalysed Radical-Recombination Rates in Flames," *Chemical Physics Letters* **9,** 467-468 (1971).

116. Bulewicz, E.M. and Padley, P.J., "Catalytic Effect of Metal Additives on Free Radical Recombination Rates in H_2+O_2+N_2 Flames," *Proceedings of the Combustion Institute* **13,** 73-80 (1971).

117. deWitte, M., Vrebosch, J., and van Tiggelen, A., "Inhibition and Extinction of Premixed Flames by Dust Particles," *Combustion and Flame* **9,** 257-266 (1964).

118. Rumminger, M.D. and Linteris, G.T., "Inhibition of Premixed Carbon Monoxide-Hydrogen-Oxygen-Nitrogen Flames by Iron Pentacarbonyl," *Combustion and Flame* **120,** 451-464 (2000).

119. Macdonald, M.A., Gouldin, F.C., and Fisher, E.M., "Temperature Dependence of Phosphorus-Based Flame Inhibition," *Combustion and Flame* **124,** 668-683 (2001).

120. MacDonald, M.A., Jayaweera, T.M., Fisher, E.M., and Gouldin, F.C., "Variation of Chemically Active and Inert Flame-Suppression Effectiveness With Stoichiometric Mixture Fraction," *Proceedings of the Combustion Institute* **27,** 2749-2756 (1998).

121. Babushok, V.I. and Tsang, W., "Inhibitor Rankings for Hydrocarbon Combustion," *Combustion and Flame* **123,** 488-506 (2000).

122. James, C.G. and Sugden, T.M., "Photometric Investigations of Alkali Metals in Hydrogen Flame Gases. 3. The Source of the Alkali Metal Continuum," *Proceedings of the Royal Society A* **248,** 238-247 (1958).

123. Bulewicz, E.M., James, C.G., and Sugden, T.M., "Photometric Investigations of Alkali Metals in Hydrogen Flame Gases. 2. The Study of Excess Concentrations of Hydrogen Atoms in Burnt Gas Mixtures," *Proceedings of the Royal Society A* **235,** 89-106 (1956).

124. Bulewicz, E.M. and Sugden, T.M., "Determination of the Dissociation Constants and Heats of Formation of Molecules by Flame Photometry; Part 3.-Stability of Gaseous Cuprous Hydroxide," *Transactions of the Faraday Society* **52,** 1481-1488 (1956).

125. Bulewicz, E.M. and Sugden, T.M., "Determination of the Dissociation Constants and Heats of Formation of Molecules by Flame Photometry; Part 2.-Heat of Formation of Gaseous Cuprous Hydroxide," *Transactions of the Faraday Society* **52,** 1475-1480 (1956).

126. Bulewicz, E.M. and Padley, P.J., "Photometric Investigations of the Behavior of Chromium Additives in Premixed H_2+O_2+N_2 Flames," *Proceedings of the Royal Society London A*. **323,** 377-400 (1971).

127. Howard, J.B. and Kausch, W.J., "Soot Control by Fuel Additives," *Progress in Energy and Combustion Science* **6,** 263-276 (1980).

128. Cotton, D.H., Friswell, N.J., and Jenkins, "The Suppression of Soot Emission From Flames by Metal Additives.," *Combustion and Flame* **17,** 87-98 (1971).

129. Bulewicz, E.M., Jones, G., and Padley, P.J., "Temperature of Metal Oxide Particles in Flames," *Combustion and Flame* **13,** 409-412 (1969).

130. Tischer, R.L. and Scheller, K., "The Behavior of Uranium Oxide Particles in Reducing Flames," *Combustion and Flame* **15,** 199-202 (1970).

131. Jensen, D.E. and Jones, G.A., "Mass-Spectrometric Tracer and Photometric Studies of Catalyzed Radical Recombination in Flames," *Journal of the Chemical Society-Faraday Transactions I* **71,** 149-160 (1975).

132. Jensen, D.E. and Jones, G.A., "Catalysis of Radical Recombination in Flames by Iron," *Journal of Chemical Physics* **60,** 3421 (1974).

133. Jensen, D.E. and Jones, G.A., "Aspects of Flame Chemistry of Cobalt," *Journal of the Chemical Society-Faraday Transactions I* **72,** 2618-2630 (1976).

134. Fenimore, C.P. and Martin, F.J., "Flammability of Polymers," *Combustion and Flame* **10,** 135-139 (1966).

135. Fenimore, C.P. and Jones, G.W., "Modes of Inhibiting Polymer Flammability," *Combustion and Flame* **10,** 295-301 (1966).

136. Fenimore, C.P. and Martin, F.J., "Candle-Type Test for Flammability of Polymers," *Modern Plastics* **12,** 141-192 (1966).

137. Fenimore, C.P. and Martin, F.J., "Burning of Polymers," in Wall, L.A., Ed., *The Mechanisms of Pyrolysis, Oxidation and Burning of Organic Materials* National Bureau of Standards, Washington, D.C., 1972.

138. Martin, F.J. and Price, K.R., "Flammability of Epoxy Resins," *Journal of Applied Polymer Science* **12,** 143 (1968).

139. Hastie, J.W., "Molecular Basis of Flame Inhibition," *Journal of Research of the National Bureau of Standards - A. Physics and Chemistry* **77A,** 733-754 (1973).

140. Hastie, J.W. and McBee, C.L., "Mechanistic Studies of Halogenated Flame Retardants: The Antimony-Halogen System," in Gann, R.G., ed., *Halogenated Fire Suppressants* American Chemical Society , Washington, DC, 1975.

141. Hastie, J.W., "Mass Spectroscopic Studies of Flame Inhibition: Analysis of Antimony Trihalides in Flames," *Combustion and Flame* **21,** 49-54 (1973).

142. Dolan, J.E. and Dempster, P.B., "The Suppression of Methane-Air Ignitions by Fine Powders," *Journal of Applied Chemistry* **5,** 510-517 (1955).

143. Matsuda, S. and Gutman, D., "Shock-Tube Study of C_2H_2-O_2 Reaction. Acceleration of Reaction in the Presence of Trace Amounts of $Cr(CO)_6$," *Journal of Physical Chemistry* **75,** 2402-2404 (1971).

144. Matsuda, S., "Gas Phase Homogeneous Catalysis in Shock Waves. II. The Oxidation of Carbon Monoxide by Oxygen in the Presence of Iron Pentacarbonyl," *Journal of Physical Chemistry* **57,** 807-812 (1972).

145. Linteris, G.T., Rumminger, M.D., and Babushok, V.I., "Premixed Carbon Monoxide-Nitrous Oxide-Hydrogen Flames: Measured and Calculated Burning Velocities With and Without Fe(CO)5," *Combustion and Flame* **122,** 58-75 (2000).

146. Park, K., Bae, G.T., and Shin, K.S., "The Addition Effect of $Fe(CO)_5$ on Methane Ignition," *Bulletin of the Korean Chemical Society* **23,** 175-176 (2002).

147. Jensen, D.E. and Webb, B.C., "Afterburning Predictions for Metal-Modified Propellant Motor Exhausts," *AIAA Journal* **14,** 947-954 (1976).

148. Westblom, U., Fernandezalonso, F., Mahon, C.R., Smith, G.P., Jeffries, J.B., and Crosley, D.R., "Laser-Induced Fluorescence Diagnostics of a Propane Air Flame With a Manganese Fuel Additive," *Combustion and Flame* **99,** 261-268 (1994).

149. Suyuan Y., Jones, A.D., Chang, D.P.Y., Kelly, P.B., and Kennedy, I.M., "The Transformation of Chromium in a Laminar Premixed Hydrogen-Air Flame," *Proceedings of the Combustion Institute* **27,** 1639-1645 (1998).

150. Kennedy, I.M., Zhang, Y., Jones, A.D., Chang, D.P.Y., Kelly, P.B., and Yoon, Y., "Morphology of Chromium Emissions From a Laminar Hydrogen Diffusion Flame," *Combustion and Flame* **116,** 233-242 (1999).

151. Kellogg, C.B. and Irikura, K.K., "Gas-Phase Thermochemistry of Iron Oxides and Hydroxides:Portrait of a Super-Efficient Flame Suppressant," *Journal of Physical Chemistry a* **103,** 1150-1159 (1999).

152. Tapscott, R.E., Sheinson, R.S., Babushok, V., Nyden, M.R., and Gann, R.G., *"Alternative Fire Suppressant Chemicals: a Research Review With Recommendations,"* NIST TN 1443, National Institute of Standards and Technology, Gaithersburg MD, (2001).

153. Linteris, G.T., Katta, V.R., and Takahashi, F., "Experimental and Numerical Evaluation of Metallic Compounds for Suppressing Cup-Burner Flames," *Combustion and Flame* **138,** 78-96 (2004).

154. Katta, V.R., Takahashi, F., and Linteris, G.T., "Numerical Investigations of CO_2 As Fire Suppressing Agent," *Fire Safety Science: Proceeding of the Seventh International Symposium*, 531-542, Int. Assoc. for Fire Safety Science, Boston, MA, 2003.

155. Fallis, S., Holland, G.F., McCormick, J.L., Reed, R., and Wilson, K.A., "Advanced Propellant/Additive Development for Fire Suppressing Gas Generators: Hybrid Systems," in Gann, R.G., Burgess, S.R., Whisner, K.C., and Reneke, P.A., eds., *Papers From 1991-2006 Halon Options Technical Working Conferences (HOTWC)*, CD-ROM, NIST SP 984-4, National Institute of Standards and Technology, Gaithersburg, MD, (2006).

156. Masri, A.R., Dally, B.B., Barlow, R.S., and Carter, C.D., "The Structure of Laminar Diffusion Flames Inhibited With CF_3Br," *Combustion Science and Technology* **114,** 17-34 (1996).

157. Skaggs, R.R., McNesby, K.L., Daniel, R.G., Homan, B., and Miziolek, A.W., "Spectroscopic Studies of Low-Pressure Opposed Flow Methane/Air Flames Inhibited by $Fe(CO)_5$, CF_3Br, or N_2," *Combustion Science and Technology* **162,** 1-17 (2001).

158. Chidsey, I.L. and Crosley, D.R., "Calculated Rotational Transition Probabilities for the A-X System of OH ," *Journal of Quantitative Spectroscopy and Radiative Transfer* **23,** 187 (1980).

159. Dieke, G.H. and Croswhite, H.M., "The Ultraviolet Bands of OH Fundamental Data," *Journal of Quantitative Spectroscopy and Radiative Transfer* **2,** 97 (1962).

160. Kotlar, A., Personal Communication, 1998.

161. Eckbreth, A.C., *Laser Diagnostics for Combustion Temperatures and Species*, Abacus Press, Cambridge MA, 1998.

162. Smooke, M.D., Yale University, Personal Communication, 1997.

163. Babushok, V., NIST, Personal Communication, 1999.

164. Rumminger, M.D., Reinelt, D., Babushok, V., and Linteris, G.T., "Inhibition of Flames by Iron Pentacarbonyl," in Gann, R.G., Burgess, S.R., Whisner, K.C., and Reneke, P.A., eds., *Papers From 1991-2006 Halon Options Technical Working Conferences (HOTWC)*, CD-ROM, NIST SP 984-4, National Institute of Standards and Technology, Gaithersburg, MD, (2006).

165. Daniel, R.G., McNesby, K.L., Skaggs, R.R., Sagear, P., and Miziolek, A.W., "Spectroscopy of Inhibited Counterflow Diffusion Flames Proceedings," *1997 JANNAF Combustion Subcommittee Meeting*, 1997.

166. Gaydon, A.G., *The Spectroscopy of Flames*, John Wiley and Sons, New York, NY, 1972.

167. Babushok, V.I., Tsang, W., Linteris, G.T., and Reinelt, D., "Chemical Limits to Flame Inhibition," *Combustion and Flame* **115,** 551-560 (1998).

168. Peters, N., "Local Quenching Due to Flame Stretch and Non-Premixed Turbulent Combustion," *Combustion Science and Technology* **30,** 1-17 (1983).

169. Liew, S.K., Bray, K.N.C., and Moss, J.B., "A Stretched Laminar Flamelet Model of Turbulent Non-Premixed Combustion ," *Combustion and Flame* **56,** 199 (1984).

170. Haworth, D.C., Drake, M.C., and Blint, R.J., "Stretched Laminar Flamelet Modeling of a Turbulent Jet Diffusion Flame," *Combustion Science and Technology* **60,** 287-318 (1988).

171. Bilger, R.W., "The Structure of Turbulent Non-Premixed Flames," *Proceedings of the Combustion Institute* **22,** 450-488 (1988).

172. Roberts, W.L., Driscoll, J.F., Drake, M.C., and Ratcliffe, J.W., "OH Fluorescence Images of The Quenching of a Premixed Flame During an Interaction With a Vortex 169.," *Proceedings of the Combustion Institute* **24,** 169 (1992).

173. Miller, J.H., "Applications of Conserved Scalars to Combustion Chemistry," *Proceedings of the Eastern States Section Meeting*, pp. 1-10, Combustion Institute, Pittsburgh, PA, 1996.

174. Reinelt, D., Babushok, V., and Linteris, G.T., "Numerical Study of the Inhibition of Premixed and Diffusion Flames by Iron Pentacarbonyl," *Proceedings of the Eastern States Section Meeting* , pp. 273-276, Combustion Institute, Pittsburgh, PA, 1996.

175. Noto, T., Babushok, V., Hamins, A., and Tsang, W., "Inhibition Effectiveness of Halogenated Compounds," *Combustion and Flame* **112,** 147-160 (1998).

176. Fallis, S., Reed, R., Lu, Y.-C., Wierenga, P.H., and Holland, G.F., "Advanced Propellant/Additive Development for Fire Suppressing Gas Generators," *Halon Options Technical Working Conference*, 361-370, Albuquerque, NM, 2000.

177. Rosser, W.A., Inami, S.H., and Wise, H., *"Study of the Mechanisms of Fire Extinguishment of Liquid Rocket Propellants,"* WADC Technical Report 59-206, ASTIA Document No. AD 216355, 1959).

178. Lippincott, E.S. and Tobin, M.C.J., "The Vibrational Spectra and Thermodynamic Functions of Lead Tetramethyl, Tin Tetramethyl and Germanium Tetramethyl," *Journal of the American Chemical Society* **75,** 4141-4147 (1953).

179. Katta, V.R., Takahashi, F., and Linteris, G.T., "Extinction Characteristics of Cup-Burner Flame in Microgravity," *41st Aerospace Sciences Meeting and Exhibit,* AIAA Paper No. 2003-1150, AIAA, 2003.

180. Linteris, G.T., "Extinction of Cup-Burner Diffusion Flames by Catalytic and Inert Inhibitors," *Second NRIFD Symposium - Science, Technology and Standards for Fire Suppression Systems*, Tokyo, Japan, 2002.

181. Cusack, P.A. and Killmeyer, A.J., "Inorganic Tin-Compounds As Flame, Smoke, and Carbon-Monoxide Suppressants for Synthetic-Polymers," in Nelson, G.L., ed., *Fire and Polymers, Hazards Identification and Prevention* ACS Symposium Series 425, American Chemical Society, Washington, DC, 1990.

182. Hornsby, P.R., Mitchell, P.A., and Cusack, P.A., "Flame Retardation and Smoke Suppression of Polychloroprene Containing Inorganic Tin-Compounds," *Polymer Degradation and Stability* **32,** 299-312 (1991).

183. Pitts, W.M., Nyden, M.R., Gann, R.G., Mallard, W.G., and Tsang, W., *"Construction of an Exploratory List of Chemicals to Initiate the Search for Halon Alternatives,"* NIST Technical Note 1279, National Institute of Standards and Technology, Gaithersburg MD, (1990).

184. Nesmeyanov, A.N., Ed., *Manganese containing antiknock compounds*, Nauka, Moscow, 1971.

185. Tapscott, R.E., Heinonen, E.W., and Brabson, G.D., *"Advanced Agent Identification and Preliminary Assessment,"* NMERI 95/38/32350, NMERI, University of New Mexico, Albuquerque, NM, (1996).

186. Chao, B.H., Egolfopoulos, F.N., and Law, C.K., "Structure and Propagation of Premixed Flame in Nozzle-Generated Counterflow," *Combustion and Flame* **109,** 620-638 (1997).

187. Andrews, G.E. and Bradley, D., "Determination of Burning Velocities: a Critical Review," *Combustion and Flame* **18,** 133-153 (1972).

188. Gilbert, A.G. and Sulzmann, K.G.P., "The Vapor Pressure of Iron Pentacarbonyl," *Journal of the Electrochemical Society* **121,** 832 (1974).

189. Stull, D.R., "Vapor Pressure of Pure Substances Organic Compounds," *Industrial Engineering Chemistry* **39,** 517-540 (1947).

190. Hollrah, D., Ethyl Corp., Personal Communication, 2001

191. Bulewicz, E.M. and Padley, P.J., "Photometric Observations on the Behaviour of Tin in Premixed H_2-O_2-N_2 Flames," *Transactions of the Faraday Society* **67,** 2337-2347 (1971).

192. Goodings, J.M. and Chen, Q.-F., "Chemical Kinetics and Thermodynamics of Tin Ionization in H_2-O_2-N_2 Flames and the Proton Affinity of SnO," *Canadian Journal of Chemistry* **76,** 1437-1446 (1998).

193. Taylor, J.E. and Milazzo, T.S., "Synthesis of Nanoscale Metal-Oxide Particles Using Laser Vaporization Condensation in a Diffusion Cloud Chamber," *Journal of Physical Chemistry* **82,** 847-852 (1978).

194. Gurvich, L.V., Karachevtsev, G.V., Kondratiev, V.N., Lebedev, Yu., A., Medvedev, V.A., Potapov, V.K., and Hodeev, Ya.S., *Bond energies. Ionization Potentials and Electron Affinities* , Nauka, Moscow, 1974.

195. Fontijn, A. and Bajaj, P.N., "Kinetics of the SN(P-3(0)) Reactions With CO_2 and O_2 Over Wide Temperature Ranges," *Journal of Physical Chemistry* **100,** 7085-7089 (1996).

196. Husain, D., Plane, J.M., and Xiang, C.C., "A Direct Kinetic Study of the Reaction K + OH + He =3D KOH + He by Time-Resolved Molecular Resonance-Fluorescence Spectroscopy, OH(A2=ABSIGMA=BB+-X 2=ABPI=BB), Coupled With Steady Atomic Fluorescence Spectroscopy, K(5 2PJ-4 2S1/2)," *Journal of the Chemical Society, Faraday Transactions II* **80,** 1465-1483 (1984).

197. Gurvich, L.V. and Glushkov, V.P., *"Thermodynamic Properties of Individual Substances,"* NIST special database 5, IVTHANTHERMO-PC, National Institute of Standards and Technology, Gaithersburg, MD, (1998).

198. Smith, G.P., SRI, Personal Communication, 1999

199. J.A. Martinho Simões, "Organometallic Thermochemistry Data," in Mallard, W.G. and Linstrom, P.J., Eds., *NIST Chemistry WebBook, NIST Standard Reference Database Number 69* National Institute of Standards and Technology, Gaithersburg, MD 20899 (http://webbook.nist.gov), 2000.

200. Hildenbrand, D.L. and Lau, K.H., "Thermochemistry of Gaseous Manganese Oxides and Hydroxides," *Journal of Chemical Physics* **100,** 8377-8380 (1994).

201. Babushok, V.I. and Tsang, W., "Influence of Phosphorus-Containing Additives on Methane Flames," *Proceedings of the Joint Meeting of the United States Sections*, pp. 587-590, The Combustion Institute, Pittsburgh, PA, 1999.

202. Jensen, D.E., "Condensation Modeling for Highly Supersaturated Vapours: Application to Iron," *Journal of the Chemical Society, Faraday Transactions* **76,** 1494 (1980).

203. Kee, R.J., Grcar, J.F., Smooke, M.D., and Miller, J.A., *"A Fortran Computer Program for Modeling Steady Laminar One-Dimensional Premixed Flames,"* SAND85-8240, Sandia National Laboratories, Livermore, CA, (1991).

204. Kee, R.J., Rupley, F.M., and Miller, J.A., *"CHEMKIN-II: A Fortran Chemical Kinetics Package for the Analysis of Gas Phase Chemical Kinetics,"* SAND89-8009B, Sandia National Laboratories, Livermore, CA, (1989).

205. Kee, R.J., Dixon-Lewis, G., Warnatz, J., Coltrin, R.E., and Miller, J.A., *"A Fortran Computer Package for the Evaluation of Gas-Phase, Multicomponent Transport Properties,"* SAND86-8246, Sandia National Laboratories, Livermore, CA, (1986).

206. Smith, G.P., Golden, D.M., Frenklach, M., Moriarty, N.W., Eiteneer, B., Goldenberg, M., Bowman, C.T., Hanson, R.K., Song, S., Gardiner, Jr., W.C., Lissianski, V.V., and Qin, Z., "GRI Mech 3.0," 2000.

207. Linteris, G.T., "Effect of Inhibitor Concentration on the Inhibition Mechanism of Fluoromethanes in Premixed Methane-Air Flames," in Miziolek, A.W. and Tsang, W., eds., *Halon Replacements* ACS Symposium Series 611, American Chemical Society, Washington, D.C., 1995.

208. Breck, D.W., "Correlations of Calculated Intracrystalline Void Volumes and Limiting Absorption Volumes in Zeolite," in Meier, W.M. and Uytterhoeven, J.B., Eds., *Molecular Sieves* American Chemical Society, Washington, D.C., 1973.

209. Andersen, S.O., "Halons and the Stratospheric Ozone Issue," *Fire Journal* **81,** 56-62 (1987).

210. Reed, M.D., Williams, B.A., Sheinson, R.S., and Fleming, J.W., "Behavior of Bicarbonate Powders in Counterflow Diffusion Flames," *Proceedings of the Eastern States Section Meeting*, pp. 83-86, Combustion Institute, Pittsburgh, PA, 1997.

211. Lutz, A.E., Kee, R.J., Grcar, J.F., and Rupley, F.M., *"OPPDIF: A Fortran Computer Program for Computing Opposed-Flow Diffusion Flames,"* SAND96-8243, Sandia National Labs., Albuquerque, NM, (1996).

212. Chelliah, H.K., Yu, G., Hahn, T.O., and Law, C.K., "An Experimental and Numerical Study on the Global and Detailed Kinetics of Premixed and Nonpremixed Flames of Chloromethane, Methane, Oxygen and Nitrogen," *Proceeding of the Combustion Institute* **24,** 1083-1090 (1993).

213. Zhang, J. and Megaridis, C.M., "Iron/Soot Interaction in a Laminar Ethylene Nonpremixed Flame," *Proceedings of the Combustion Institute* **25,** 593-600 (1994).

214. Zhang, J. and Megaridis, C.M., "Soot Suppression by Ferrocene in Laminar Ethylene/Air Nonpremixed Flames," *Combustion and Flame* **105,** 528-540 (1996).

215. Carty, P., Grant, J., and Metcalfe, E., "Flame-Retardancy and Smoke-Suppression Studies on Ferrocene Derivatives in PVC," *Applied Organometallic Chemistry* **10,** 101-111 (1996).

216. Kasper, M. and Siegmann, K., "The Influence of Ferrocene on PAH Synthesis in Acetylene and Methane Diffusion Flames," *Combustion Science and Technology* **140,** 333-350 (1998).

217. Kasper, M., Sattler, K., Siegmann, K., Matter, U., and Siegmann, H.C., "The Influence of Fuel Additives on the Formation of Carbon During Combustion," *Journal of Aerosol Science* **30,** 217-225 (1999).

218. Kishore, K., Kannan, P., and Iyanar, K., "Synthesis, Characterization, and Fire Retardancy of Ferrocene Containing Polyphosphate Esters," *Journal of Polymer Science Part a-Polymer Chemistry* **29,** 1039-1044 (1991).

219. Zheng, R., Bray, K.N.C., and Rogg, B., "Effect of Sprays of Water and NaCl-Water Solution on the Extinction of Laminar Premixed Methane-Air Counterflow Flames," *Combustion Science and Technology* **126,** 389-401 (1997).

220. Pelino, M., Tomassetti, M., Piacente, V., and D'Ascenzo, G., "Vapor Pressure Measurements of Ferrocene, Mono- and 1,1 Di-Acetyl Ferrocene," *Thermochimica Acta* **44,** 89-99 (1981).

221. Lewis, K.E. and Smith, G.P., "Bond Dissociation Energies in Ferrocene," *Journal of the American Chemical Society* **106,** 4650-4651 (1984).

222. Turnbull, A.G., "Thermochemistry of Biscyclopentadienyl Metal Compounds. 1.) Preparation and Thermal Stability," *Australian Journal of Chemistry* **20,** 2059-2067 (1967).

223. Sabbah, R. and Perez, J.A.G., "Contribution a L'Etude Thermochique De Ferrocene," *Thermochemica Acta* **297,** 17-32 (1997).

224. Reid, R.C., Prausnitz, Y.M., and Sherwood, T.K., *The Properties of Gases and Liquids*, McGraw-Hill, New York, 1987.

225. Wang, H. and Frenklach, M., "Transport Properties of Polycyclic Aromatic Hydrocarbons," *Combustion and Flame* **96,** 163-170 (1994).

226. Sung, C.J., Li, B., Law, C.K., and Wang, H., "Structure and Sooting Limits in Counterflow Methane/Air and Propane/Air Diffusion Flames From 1 to 5 Atmospheres," *Proceedings of the Combustion Institute* **27,** 1523-1529 (1998).

227. Zachariah, M.R., Westmoreland, P.R., Burgess, D.R., and Tsang, W., "BAC-MP4 Predictions of Thermochemical Data for C-1 and C-2 Stable and Radical Hydrofluorocarbons and Oxidized Hydrofluorocarbons," *Journal of Physical Chemistry* **100,** 8737-8747 (1996).

228. Tsang, W., NIST, Personal Communication, 1999

229. Burgess, D.R., Zachariah, M.R., Tsang, W., and Westmoreland, P.R., "Thermochemical and Chemical Kinetic Data for Fluorinatedhydrocarbons," *Progress in Energy and Combustion Science* **21,** 453-529 (1995).

230. Fristrom, R.M. and Sawyer, R.F., "Flame Inhibition Chemistry," *AGARD Conference Proceedings No. 84 on Aircraft Fuels, Lubricants, and Fire Safety, AGARD-CP 84-71*, 12-2 to 12-17, North Atlantic Treaty Organization, Neuilly-sur-Seine, France, 1971.

231. Nesmeianov, A.N., *Vapour Pressure of the Elements.*, New York, Academic Press, 1963.

232. Grimley, R.T., Burns, R.P., and Inghram, M.G., "Thermodynamics of the Vaporization of Cr_2O_3: Dissociation Energies of CrO, CrO_2, and CrO_3," *Journal of Chemical Physics* **34,** 664-667 (1961).

233. Barin, I. and Knacke, O., *Thermochemical Properties of Inorganic Substances*, Springer-Verlag, Berlin, New York, 1973.

234. Barin, I., Knacke, O., and Kubaschewski, O., *Thermochemical Properties of Inorganic Substances*, Springer-Verlag, Berlin, New York , 1977.

235. Tapscott, R.E., Mather, J.D., Heinonen, E.W., Lifke, J.L., and Moore, T.A., *"Identification and Proof Testing of New Total Flooding Agents: Combustion Suppression Chemistry and Cup-Burner Testing,"* NMERI 97/6/33010, Albuquerque, NM, (1998).

236. Fay, J.A., "The Distributions of Concentration and Temperature in a Laminar Jet Diffusion Flame," *Journal of Aeronautical Sciences* **21,** 681-689 (1954).

237. Staendeke, H. and Scharf, D.J., "Halogen-Free Flame-Retardant Based on Phosphorus-Compounds," *Kunststoffe-German Plastics* **79,** 1200-1204 (1989).

238. Avondo, G., Vovelle, C., and Delbourgo, R., "Role of Phosphorus and Bromine in Flame Retardancy," *Combustion and Flame* **31,** 7-16 (1978).

239. Sherman, L.M., "Flame Retardants Update: Phosphorus Expands Its Niche," *Plastics Technology* **38,** 102-105 (1992).

240. Shelley, S., "Keeping Fire at Bay," *Chemical Engineering* **100,** 71-73 (1993).

241. Brauman, S.K., "Phosphorus Fire retardance in Polymers. I. General Mode of Action," *Journal of Fire Retardant Chemistry* **4,** 18-37 (1977).

242. Green, J., "Mechanisms for Flame Retardancy and Smoke Suppression: A Review," *Journal of Fire Sciences* **14,** 426-442, 1996).

243. Kashiwagi, T., Gilman, J.W., McGrath, J.E., and Wan, I.-Y., "Flammability Properties of Phosphine Oxide Copolymers and of Commodity Polymers With New Flame Retardant Additives," *1996 FRCA Fall Meeting*, 1996.

244. Peters, E.N., "Flame-Retardant Thermoplastics .1. Polyethylene-Red Phosphorus," *Journal of Applied Polymer Science* **24,** 1457-1464 (1979).

245. Haessler, W., "Dry Chemical Agents and Application Systems," in Cote, A.E. and Linville, J.L., Eds., *Fire Protection Handbook* National Fire Protection Association, Quincy, MA, 1986.

246. Kordylewski, W. and Amrogowicz, J., "Comparison of $NaHCO_3$ and $NH_4H_2PO_4$ Effectiveness As Dust Explosion Suppressants," *Combustion and Flame* **90,** 344-345 (1992).

247. Amrogowicz, J. and Kordylewski, W., "Effectiveness of Dust Explosion Suppression by Carbonates and Phosphates," *Combustion and Flame* **85,** 520-522 (1991).

248. Song, C. E., Kim, I. O., Lee, J. K., Kim, T. K., and Lee, S. G., "Liquid Fire Extinguishing Composition," U.S. Patent 5219474 (1990).

249. Kaizerman, J.A. and Tapscott, R.E., *"Advanced Streaming Agent Development, Volume II: Phosphorus Compounds,"* NMERI 96/5/32540, New Mexico Engineering Research Institute, Albuquerque, NM, (1996).

250. Lifke, J. L., Moore, T. A., and Tapscott, R. E., *"Advanced Streaming Agent Development, Volume V: Laboratory-Scale Streaming Tests,"* NMERI 96/2/32540, New Mexico Engineering Research Institute, Albuquerque, NM, (1996).

251. Jordan, T.E., "Metal Organic Compounds," in *Vapor Pressure of Organic Compounds, 1st Ed.* Interscience Publishers, New York, 1954.

252. Weil, E.D., "Phosphorus-Based Flame Retardants," in Engel, R., Ed., *Handbook of Organophosphorus Chemistry* Marcel Dekker, Inc., New York, 1992.

253. Korobeinichev, O.P., Chernov, A.A., and Shvartsberg, V.M., " Destruction Chemistry of Trimethyl Phosphate in H_2/O_2/Ar Flame Studied by Molecular Beam Mass-Spectrometry," *3rd Asia-Pacific International Symposium on Combustion and Energy Utilization*, 1995.

254. Korobeinichev, O.P., Ilyin, S.B., Mokrushin, V.V., and Shmakov, A.G., "Destruction Chemistry of Dimethyl Methylphosphonate in H_2/O_2/Ar Flames Studied by Molecular-Beam Mass Spectrometry," *Combustion Science and Technology* **116,** 51-67 (1996).

255. Fenimore, C.P. and Jones, G.W., "Phosphorus in the Burnt Gas From Fuel-Rich Hydrogen-Oxygen Flames," *Combustion and Flame* **8,** 133-137 (1964).

256. Hastie, J.W. and Bonnell, D.W., *"Molecular Chemistry of Inhibited Combustion Systems. Final Report.,"* NBSIR 80-2169, National Bureau of Standards, Gaithersburg, MD, (1980).

257. Babushok, V.I. and Tsang, W., "Influence of Phosphorus-Containing Fire Suppressants on Flame Propagation," *International Conference on Fire Research and Engineering, Third*, 257-267, Society of Fire Protection Engineers, Boston, MA, 1999.

258. Twarowski, A., "Reduction of a Phosphorus Oxide and Acid Reaction Set," *Combustion and Flame* **102,** 41-54 (1995).

259. Twarowski, A., "The Effect of Phosphorus Chemistry on Recombination Losses in a Supersonic Nozzle," *Combustion and Flame* **102,** 55-63 (1995).

260. Twarowski, A., "Photometric-Determination of the Rate of H_2O Formation From Hand OH in the Presence of Phosphine Combustion Products," *Combustion and Flame* **94,** 341-348 (1993).

261. Trees, D., Grudno, A., and Seshadri, K., "Experimental and Numerical Studies on Chemical Inhibition of Nonpremixed Methane Flames by CF_3Br," *Combustion Science and Technology* **124,** 311-& (1997).

262. Saso, Y., Zhu, D.L., Wang, H., Law, C.K., and Saito, N., "Laminar Burning Velocities of Trifluoromethane-Methane Mixtures: Experiment and Numerical Simulation," *Combustion and Flame* **114,** 457-468 (1998).

263. Zegers, E.J.P. and Fisher, E.M., "Gas-Phase Pyrolysis of Diethyl Methylphosphonate," *Combustion Science and Technology* **116,** 69-89 (1996).

264. Zegers, E.J., *"Flow Reactor Pyrolysis of Alkyl Phosphates and Phosphonates, Ph.D. Thesis, Mechanical Engineering,"* Cornell University, Ithaca, NY, 1997.

265. Beaud, P., Radi, P.P., Franzke, D., Frey, H.M., Mischler, B., Tzannis, A.P., and Gerber, T., "Picosecond Investigation of the Collisional Deactivation of OH A(2)Sigma(+)(V ' = 1, N ' = 4, 12) in an Atmospheric-Pressure Flame," *Applied Optics* **37,** 3354-3367 (1998).

266. Smith, G.P. and Crosley, D.R., "Vibrational-Energy Transfer in A2-Sigma+ OH in Flames," *Applied Optics* **22,** 1428-1430 (1983).

267. Allen, M.G., McManus, K.R., Sonnenfroh, D.M., and Paul, P.H., "Planar Laser-Induced-Fluorescence Imaging Measurements of OH and Hydrocarbon Fuel Fragments in High-Pressure Spray-Fame Combustion," *Applied Optics* **34,** 6287-6300 (1995).

268. Puri, R., Moser, M., Santoro, R.J., and Smyth, K.C., "Laser-Induced Fluorescence Measurements of OH Concentration in the Oxidation Region of Laminar, Hydrocarbon Diffusion Flames," *Proceedings of the Combustion Institute* **24,** 1015-1022 (1996).

269. Arnold, A., Bombach, R., Kappeli, B., and Schlegel, A., "Quantitative Measurements of OH Concentration Fields by Two-Dimensional Laser-Induced Fluorescence," *Applied Physics B-Lasers and Optics* **64,** 579-583 (1997).

270. Kelman, J.B. and Masri, A.R., "Quantitative Imaging of Temperature and OH in Turbulent-Diffusion Flames by Using a Single Laser Source," *Applied Optics* **33,** 3992-3999 (1994).

271. Barlow, R.S. and Collignon, A., "Linear LIF Measurements of OH in Nonpremixed Methane-Air Flames: When Are Quenching Corrections Unnecessary," *29th Aerospace Sciences Meeting*, AIAA 91-0179 , Reno, 1991.

272. Kollner, M. and Monkhouse, P., "Time-Resolved LIF of OH in the Flame Front of Premixed and Diffusion Flames at Atmospheric Pressure," *Applied Physics B-Lasers and Optics* **61,** 499-503 (1995).

273. Norton, T.S., Smyth, K.C., Miller, J.H., and Smooke, M.D., "Comparison of Experimental and Computed Species Concentration and Temperature Profiles in Laminar, 2-Dimensional Methane Air Diffusion Flames," *Combustion Science and Technology* **90,** 1-34 (1993).

274. Luque, J. and Crosley, D.R., *"LIFBASE: Database and Simulation Program (v 1.6),"* SRI International Report MP 99-009, 1999).

275. Paul, P.H., "Vibrational-Energy Transfer and Quenching of OH A(2)Sigma(+)(V'=1) Measured at High Temperatures in a Shock Tube," *Journal of Physical Chemistry* **99,** 8472-8476 (1995).

276. Paul, P.H., "A Model for Temperature-Dependent Collisional Quenching of OH A(2)Sigma+," *Journal of Quantitative Spectroscopy & Radiative Transfer* **51,** 511-524 (1994).

277. Tamura, M., Berg, P.A., Harrington, J.E., Luque, J., Jeffries, J.B., Smith, G.P., and Crosley, D.R., "Collisional Quenching of CH(a), OH(a), and NO(a) in Low-Pressure Hydrocarbon Flames," *Combustion and Flame* **114,** 502-514 (1998).

278. Carrier, G.F., Fendell, F.E., and Marble, F.E., "Effect of Strain Rate on Diffusion Flames," *Siam Journal on Applied Mathematics* **28,** 463-500 (1975).

279. Linan, A., "The Asymptotic Structure of Counterflow Diffusion Flames for Large Activation Energy," *Acta Astronautica* **1,** 1007-1039 (1974).

280. Grudno, A. and Seshadri, K., "Characteristic Residence Times of Laminar Nonpremixed Flames at Extinction," *Combustion Science and Technology* **112,** 199-210 (1996).

281. Fisher, E.M., Williams, B.A., and Fleming, J.W., "Determination of the Strain in Counterflow Diffusion Flames From Flow Conditions," *Proceedings of the Eastern States Section Meeting*, pp. 191-194, Combustion Institute, Pittsburgh, PA, 1997.

282. Nishioka, M., Law, C.K., and Takeno, T., "A Flame-Controlling Continuation Method for Generating S-Curve Responses With Detailed Chemistry," *Combustion and Flame* **104,** 328-342 (1996).

283. Otsuka, Y. and Niioka, T., " *Combustion and Flame* **21,** 163-176 (1973).

284. Trees, D., Seshadri, K., and Hamins, A., "Experimental Studies of Diffusion Flame Extinction With Halogenated and Inert Fire Suppressants," in Miziolek, A.W. and Tsang, W., eds., *Halon Replacements: Technology and Science* ACS Symposium Series 611, American Chemical Society, Washington, D.C., 1995.

285. MacDonald, M.A., Jayaweera, T.M., Fisher, E.M., and Gouldin, F.C., "Inhibited Counterflow Non-Premixed Flames With Variable Stoichiometric Mixture Fractions," *Proceedings of the Eastern States Section*, pp. 91-94, Combustion Institute, Pittsburgh, PA, 1997.

286. Baldwin, R.R., Hopkins, D.E., and Walker, R.W., "Addition of Ethane to Slowly Reacting Mixtures of Hydrogen and Oxygen at 500°C," *Transaction of the Faraday Society* **66,** 189-203 (1970).

287. Yetter, R.A. and Dryer, F.L., "Inhibition of Moist CO Oxidation by Trace Amounts of Hydrocarbons," *Proceedings of the Combustion Institute* **24,** 757 (1992).

288. Grudno, A. and Seshadri, K., "Rate-Ratio Asymptotic Analysis of Inhibition of Nonpremixed Methane-Air Flames by CF_3Br," *Combustion and Flame* **112,** 418-437 (1998).

289. Bowman, C.T., Hanson, R.K., Davidson, D.F., Gardiner, W.C., Lissianski, V., Smith, G.P., Golden, D.M., Frenklach, M., and Goldenberg, M., *"GRI-MECH: Ver. 2.11 - an Optimized Detailed Chemical Reaction Mechanism for Methane Combustion and NO Formation and Reburning,"* No. GRI-95/0058, http://www.me.berkeley.edu/gri_mech, The Gas Research Institute, Chicago, IL, (1995).

290. Li, S.C., Libby, P.A., and Williams, F.A., "Experimental and Theoretical Studies of Counterflow Diffusion Flames," *Proceedings of the Combustion Institute* **24,** 1503-1512 (1996).

291. Kim, J.S. and Williams, F.A., "Structures of Flow and Mixture-Fraction Fields for Counterflow Diffusion Flames With Small Stoichiometric Mixture Fractions," *Siam Journal on Applied Mathematics* **53,** 1551-1566 (1993).

292. Brown, T.M., Tanoff, M.A., Osborne, R.J., Pitz, R.W., and Smooke, M.D., "Experimental and Numerical Investigation of Laminar Hydrogen-Air Counterflow Diffusion Flames," *Combustion Science and Technology* **129,** 71-88 (1997).

293. Arnold, A., Becker, H., Hemberger, R., Hentschel, W., Ketterle, W., Kollner, M., Meienburg, W., Monkhouse, P., Neckel, H., Schafer, M., Schindler, K.P., Sick, V., Suntz, R., and Wolfrum, J., "Laser in-Situ Monitoring of Combustion Processes," *Applied Optics* **29,** 4860-4872 (1990).

294. Wainner, R.T., McNesby, K.L., Daniel, R.G., Miziolek, A.W., and Babushok, V.I., "Experimental and Mechanistic Investigation of Opposed-Flow Propane/Air Flames by Phosphorus-Containing Compounds," in Gann, R.G., Burgess, S.R., Whisner, K.C., and Reneke, P.A., eds., *Papers From 1991-2006 Halon Options Technical Working Conferences (HOTWC)*, CD-ROM, NIST SP 984-4, National Institute of Standards and Technology, Gaithersburg, MD, (2006).

295. Skaggs, R.R., Daniel, R.G., Miziolek, A.W., and McNesby, K., "Spectroscopic Studies of Inhibited Opposed Flow Propane/Air Flames," *Proceedings of the First Joint Meeting of the U.S. Sections*, pp. 575-578, Combustion Institute, Pittsburgh, PA, 1999.

296. Kee, R.J., Rupley, F.M., and Miller, J.A., CHEMKIN Collection, Release 3.5, Reaction Design, Inc., San Diego, CA, 1999.

297. Sung, C.J., Liu, J.B., and Law, C.K., "Structural Response of Counterflow Diffusion Flames to Strain-Rate Variations," *Combustion and Flame* **102,** 481-492 (1995).

298. Ravikrishna, R.V. and Laurendeau, N.M., "Laser-Induced Fluorescence Measurements and Modeling of Nitric Oxide in Methane-Air and Ethane-Air Counterflow Diffusion Flames," *Combustion and Flame* **120,** 372-382 (2000).

299. Magre, P., Aguerre, F., Collin, G., Versaevel, P., Lacas, F., and Rolon, J.C., "Temperature and Concentration Measurements by Cars in Counterflow Laminar Diffusion Flames," *Experiments in Fluids* **18,** 376-382 (1995).

300. Werner, J.H. and Cool, T.A., "Kinetic Model for the Decomposition of DMMP in a Hydrogen/Oxygen Flame," *Combustion and Flame* **117,** 78-98 (1999).

301. Mokrushin, V.V., Bol'shova, T.A., and Korobeinichev, O.P., "A Kinetic Model for the Decomposition of DMMP in a Hydrogen/Oxygen Flame", Personal Communication, 1998.

302. Babushok, V., NIST, Personal Communication, 2000

303. Twarowski, A., "The Influence of Phosphorus Oxides and Acids on the Rate of H+OH Recombination," *Combustion and Flame* **94,** 91-107 (1993).

304. Linstrom, P.J. and Mallard, W.G., Eds., *NIST Chemistry WebBook, NIST Standard Reference Database Number 69* National Institute of Standards and Technology, Gaithersburg MD, 20899 (http://webbook.nist.gov), 2001.

305. MacDonald, M.A., *" Inhibition of Non-Premixed Flames by Phosphorus-Containing Compounds,"* , Ph.D. Dissertation, Cornell University, Ithaca, NY, 2000.

306. Smyth, K.C., Tjossem, P.J.H., Hamins, A., and Miller, J.H., "Concentration Measurements of OH. and Equilibrium Analysis in a Laminar Methane Air Diffusion Flame," *Combustion and Flame* **79,** 366-380 (1990).

307. Glaude, P.A., Curran, H.J., Pitz, W.J., and Westbrook, C.K., "Kinetic Study of the Combustion of Organophosphorus Compounds," *Proceedings of the Combustion Institute* **28,** 1749-1756 (2000).

308. Korobeinichev, O.P., Ilyin, S.B., Shvartsberg, V.M., and Chernov, A.A., "The Destruction Chemistry of Organophosphorus Compounds in Flames - I: Quantitative Determination of Final Phosphorus-Containing Species in Hydrogen-Oxygen Flames," *Combustion and Flame* **118,** 718-726 (1999).

309. Korobeinichev, O.P., Bolshova, T.A., Shvartsberg, V.M., and Chernov, A.A., "Inhibition and Promotion of Combustion by Organophosphorus Compounds Added to Flames of CH_4 or H_2 in O_2 and Ar," *Combustion and Flame* **125,** 744-751 (2001).

310. Korobeinichev, O.P., Shvartsberg, V.M., Chernov, A.A., and Mokrushin, V.V., "Hydrogen-Oxygen Flame Doped With Trimethyl Phosphate, Its Structure and Trimethyl Phosphate Destruction Chemistry.," *Proceedings of the Combustion Institute* **26,** 1035-1042 (1996).

311. Korobeinichev, O.P., Shvartsberg, V.M., and Chernov, A.A., "The Destruction Chemistry of Organophosphorus Compounds in Flames - II: Structure of a Hydrogen-Oxygen Flame Doped With Trimethyl Phosphate," *Combustion and Flame* **118,** 727-732 (1999).

312. Riches, J., Grant, K., and Knutsen, L., "Laboratory Testing of Some Phosphorus-Containing Compounds As Flame Suppressants," in Gann, R.G., Burgess, S.R., Whisner, K.C., and Reneke, P.A., eds., *Papers From 1991-2006 Halon Options Technical Working Conferences (HOTWC)*, CD-ROM, NIST SP 984-4, National Institute of Standards and Technology, Gaithersburg, MD, (2006).

313. Nogueira, M.F.M. and Fisher, E.M., "Effects of Dimethyl Methylphosphonate on Premixed Methane Flames," *Combustion and Flame* **132,** 352-363 (2003).

314. Korobeinichev, O.P., Ilyin, S.B., Bolshova, T.A., Shvartsberg, V.M., and Chernov, A.A., "The Chemistry of the Destruction of Organophosphorus Compounds in Flames - III: The Destruction of DMMP and TMP in a Flame of Hydrogen and Oxygen," *Combustion and Flame* **121,** 593-609 (2000).

315. Korobeinichev, O.P., Chernov, A.A., and Bolshova, T.A., "The Chemistry of the Destruction of Organophosphorus Compounds in Flames - IV: Destruction of DIMP in a Flame of H_2+O_2+Ar," *Combustion and Flame* **123,** 412-420 (2000).

316. Zegers, E.J.P. and Fisher, E.M., "Pyrolysis of Triethyl Phosphate," *Combustion Science and Technology* **138,** 85-103 (1998).

317. Zegers, E.J.P. and Fisher, E.M., "Gas-Phase Pyrolysis of Diisopropyl Methylphosphonate," *Combustion and Flame* **115,** 230-240 (1998).

318. Yi, A.C. and Knuth, E.L., "Probe-Induced Concentration Distortions in Molecular-Beam Mass-Spectrometer Sampling," *Combustion and Flame* **63,** 369-379 (1986).

319. Kaiser, E.W., Rothschild, W.G., and Lavoie, G.A., "Effect of Fuel-Air Equivalence Ratio and Temperature on the Structure of Laminar Propane-Air Flames," *Combustion Science and Technology* **33,** 123-134 (1983).

320. Nogueira, M.F.M., *"Effects of Dimethyl Methylphosphonate of Premixed Methane Flames, Ph.D. Thesis, Mechanical Engineering,"* Cornell University, Ithaca, NY, 2001.

321. Kaiser, E.W., Wailington, T.J., Hurley, M.D., Platz, J., Curran, H.J., Pitz, W.J., and Westbrook, C.K., "Experimental and Modeling Study of Premixed Atmospheric-Pressure Dimethyl Ether-Air Flames," *Journal of Physical Chemistry a* **104,** 8194-8206 (2000).

322. Karbach, V. and Warnatz, J., "Http://Nathan.Ca.Sandia.Gov/Tdf/3rdWorkshop/Ch4mech. Html. " *Proceedings of the 3rd International Workshop on Measurement and Computation of Turbulent Nonpremixed Flames*, Boulder, CO, 1998.

323. Williams, B.A. and Fleming, J.W., "Extinction Studies of Hydrocarbons in Methane/Air and Propane/Air Counterflow Diffusion Flames: The Role of the CF_3 Radical," in Gann, R.G. , Burgess, S.R., Whisner, K.C., and Reneke, P.A., eds., *Papers From 1991-2006 Halon Options Technical Working Conferences (HOTWC)*, CD-ROM, NIST SP 984-4, National Institute of Standards and Technology, Gaithersburg, MD, (2006).

324. Fisher, E.M., Gouldin, F.C., Jayaweera, T.M., and MacDonald, M.A., *"Flame Inhibition by Phosphorus-Containing Compounds,"* Final Technical Report Distributed by the Defense Advanced Research Projects Agency, Arlington, VA, (1998).

325. *Cup Burner Flame Extinguishment Concentrations,"* NMERI/CGET Technical Update Series (CGET-a) 1995 20/a, 1998).

326. Gann, R.G., NIST, Personal Communication, 1999

327. Brabson, G.D., Walters, E.A., Gennuso, A.R., Owen, J.P., and Tapscott, R.E., "Molecular Beam Mass Spectroscopy of Low-Pressure Flames Seeded With Iron Pentacarbonyl," *Journal of Physical Chemistry* (submitted), 1998).

328. Marinov, N.M., Castaldi, M.J., Melius, C.F., and Tsang, W., "Aromatic and Polycyclic Aromatic Hydrocarbon Formation in a Premixed Propane Flame," *Combustion Science and Technology* **128,** 295-342 (1997).

329. Marinov, N.M., Pitz, W.J., Westbrook, C.K., Castaldi, M.J., and Senkan, S.M., "Modeling of Aromatic and Polycyclic Aromatic Hydrocarbon Formation in Premixed Methane and Ethane Flames," *Combustion Science and Technology* **116,** 211-287 (1996).

330. Marinov, N.M., Pitz, W.J., Westbrook, C.K., Vincitore, A.M., Castaldi, M.J., Senkan, S.M., and Melius, C.F., "Aromatic and Polycyclic Aromatic Hydrocarbon Formation in a Laminar Premixed N-Butane Flame," *Combustion and Flame* **114,** 192-213 (1998).

331. Ewing, C.T., Hughes, J.T., and Carhart, H.W., "The Extinction of Hydrocarbon Flames Based on the Heat-Absorption Processes Which Occur in Them," *Fire and Materials* **8,** 148-156 (1984).

332. Westbrook, C.K., "Inhibition of Methane-Air and Methanol-Air Flames by HBr," *Combustion Science and Technology* **23,** 191-202 (1980).

333. Simmons, R.F. and Wolfhard, H.G., "The Influence of Methyl Bromide on Flames, Part 1.-Pre-Mixed Flames ," *Transactions of the Faraday Society* **1,** 1211-1217 (1955).

334. Frenklach, M., Wang, H., Yu, C.-L., Goldenberg, M., Bowman, C.T., Hanson, R.K., Davidson, D.F., Chang, E.J., Smith, G.P., Golden, D.M., Gardiner, W.C., and Lissianski, V., *"GRI-MECH: an Optimized Detailed Chemical Reaction Mechanism for Methane Combustion,"* Gas Research Institute Topical Report No. GRI-95/0058, http://www.me.berkeley.edu/gri_mech, The Gas Research Institute, Chicago, IL, (1995).

335. Zamansky, V.M., Lissianski, V.V., Maly, P.M., Ho, L., Rusli, D., and Gardiner, W.C., "Reactions of Sodium Species in the Promoted SNCR Process," *Combustion and Flame* **117,** 821-831 (1999).

336. Babushok, V., Tsang, W., and Noto, T., "Propargyl Type Radicals As Precursors for Polychlorinated Aromatic Hydrocarbons During Incineration," *Proceedings of the Combustion Institute, Vol. 28*, (to appear), The Combustion Institute, Pittsburgh, PA, 2000.

337. Saso, Y., Ogawa, Y., Saito, N., and Wang, H., "Binary CF_3Br- and CHF_3-Inert Flame Suppressants: Effect of Temperature on the Flame Inhibition Effectiveness of CF_3Br and CHF_3," *Combustion and Flame* **118,** 489-499 (1999).

338. Padley, P.J. and Sugden, T.M., "Chemiluminescence and Radical Re-Combination in Hydrogen Flames," *Proceedings of the Combustion Institute* **7,** 235-244 (1959).

339. Kim, C.H., Kwon, O.C., and Faeth, G.M., "Effects of Fire Suppressants on Hydrogen-Fueled Laminar Premixed Flames," *Proceedings of the Joint Meeting of the U.S. Sections*, paper #219, Combustion Institute, Pittsburgh, PA, 2001.

340. Westbrook, C.K., "Numerical Modeling of Flame Inhibition by CF_3Br," *Combustion Science and Technology* **34,** 201-225 (1983).

341. Hamins, A., "Flame Extinction by Sodium Bicarbonate Powder in a Cup Burner.," *Proceedings of the Combustion Institute* **29,** 2857-2864 (1998).

342. Fristrom, R.M. and Van Tiggelen, P., "An Interpretation of the Inhibition of C-H-O Flames by C-H-X Compounds," *Proceedings of the Combustion Institute* **17,** 773-785 (1978).

343. Williams, B.A. and Fleming, J.W., *"Influence of Bond Energies on Catalytic Flame Inhibition: Implications for the Search for New Fire Suppressants,"* NRL/MR/618003-8728, Naval Research Laboratory, 2003).

344. Griffiths, J.F. and Barnard, J.A., *Flame and Combustion, 3rd Edition*, Blackie Academic and Professional, Glasgow, 1995.

345. Glassman, I., *Combustion*, Academic Press, Orlando, FL, 1987.

346. Casias, C.R. and McKinnon, J.T., "A Modeling Study of the Mechanisms of Flame Inhibition by CF_3Br Fire Suppressant Agent," *Proceedings of the Combustion Institute* **27,** 2731-2739 (1998).

347. Jensen, D.E. and Jones, G.A., "Kinetics of Flame Inhibition by Sodium," *Journal of the Chemical Society-Faraday Transactions I* **78,** 2843-2850 (1982).

348. Baulch, D.L., Duxbury, J., Grant, S.J., and Montague, D.C., "Evaluated Kinetic Data for High-Temperature Reactions, Vol. 4, - Homogeneous Gas-Phase Reactions of Halogen-Containing and Cyanide-Containing Species," *Journal of Physical and Chemical Reference Data* **10,** 1-721 (1981).

349. Atkinson, R., Baulch, D.L., Cox, R.A., Hampson, R.F., Kerr, J.A., Rossi, M.J., and Troe, J., "Evaluated Kinetic, Photochemical and Heterogeneous Data for Atmospheric Chemistry .5. IUPAC Subcommittee on Gas Kinetic Data Evaluation for Atmospheric Chemistry," *Journal of Physical and Chemical Reference Data* **26,** 521-1011 (1997).

350. Poulet, G., Laverdet, G., and Lebras, G., "Kinetics of the Reactions of Atomic Bromine With HO_2 and HCO at 298 K," *Journal of Chemical Physics* **80,** 1922-1928 (1984).

351. DeMore, W.B., Sander, S.P., Golden, D.M., Hampson, R.F., Kurylo, M.J., Howard, C.J., Ravishankara, A.R., Kolb, C.E., and Molina, M.J., *"Chemical Kinetics and Photochemical Data for Use in Stratospheric Modeling. Evaluation Number 12,"* JPL Publication 97-4, 1997).

352. Helmer, M. and Plane, J.M.C., "Experimental and Theoretical Study of the Reaction $Fe+O_2+N_2=FeO_2+N_2$," *Journal of the Chemical Society, Faraday Transactions* **90,** 395-401 (1994).

353. Akhmadov, U.S., Zaslonko, I.S., and Smirnov, V.N., " Mechanism and Kinetics of Interaction of Fe, Cr, Mo, and Mn Atoms With Molecular-Oxygen," *Kinetics and Catalysis* **29,** 251-257 (1988).

354. Fuss, S.P. and Hamins, A., "Determination of Planck Mean Absorption Coefficients for HBr, HCl, and HF," *Journal of Heat Transfer-Transactions of the ASME* **124,** 26-29 (2002).

355. Williams, B.A. and Fleming, J.W., "On the Suitability of CF_3Br As a Benchmark for Replacement Fire Suppressants.," in Gann, R.G., Burgess, S.R., Whisner, K.C., and Reneke, P.A., eds., *Papers From 1991-2006 Halon Options Technical Working Conferences (HOTWC)*, CD-ROM, NIST SP 984-4, National Institute of Standards and Technology, Gaithersburg, MD, (2006).

356. Fristrom, R.M. and Westenberg, A.A. , *Flame Structure*, McGraw-Hill, New York, 1965.

357. Glassman, I., *Combustion*, Academic Press, New York, NY, 1977.

358. Westbrook, C.K. and Dryer, F.L., "Chemical Kinetic Modeling of Hydrocarbon Combustion," *Progress in Energy and Combustion Science* **10,** 1-57 (1984).

359. Williams, F.A., *Combustion Theory*, Benjamin/Cummings Publishing Company, Menlo Park, California, 1985.

360. Pownall, C. and Simmons, R.F., "The Effect of Hydrogen Bromide on the Structure of Propane-Oxygen Flames Diluted With Argon.," *Proceedings of the Combustion Institute* **13,** 585-592 (1971).

361. Rumminger, M.D., Babushok, V.I., and Linteris, G.T., "Temperature Regions of Optimal Chemical Inhibition of Premixed Flames," *Proceedings of the Combustion Institute* **29,** 329–336 (2002).

362. Burgess, D.R., *XSenkplot, an Interactive, Graphics Postprocessor for Numerical Simulations of Chemical Kinetics*, http://Www.Nist.Gov/Cstl/Div836/Xsenkplot, National Institute of Standards and Technology, Gaithersburg, MD, 1997.